SCUOLA DI DOTTORATO
Università degli Studi di Milano Bicocca

Dipartimento di Fisica "Giuseppe Occhialini"
Dottorato di ricerca in Fisica e Astronomia - XXXVI Ciclo
Curriculum in Fisica Teorica

High precision for colour singlet processes: double Higgs boson production in GENEVA and Drell-Yan threshold resummation for rapidity distributions

Tutor:
Prof. Simone Alioli
Co-tutor:
Dr. Davide Napoletano
Coordinator:
Prof. Stefano Ragazzi

Candidate:
Giulia Marinelli
Registration Number:
868625

ANNO ACCADEMICO 2022/2023

Declaration

The content of this thesis is original and the outcome of my Ph.D. research projects.
It is based on the following publications:

- [1] for the first part of this thesis; based on joint research conducted within the GENEVA collaborations in the university of Milano-Bicocca;
- [2] for the second part of this thesis; based on joint research conducted with Dr. Marco Bonvini.

I hereby declare that no part of this dissertation has been submitted elsewhere for any other degree or qualification in this or in any other university.

Date: 30/10/2023 Giulia Marinelli

Abstract

With the High Luminosity (HL-LHC) program scheduled for the years to come, the integrated luminosity will be increased by a factor of 10 beyond the LHC's default value providing a wealth of new data for observing rare phenomena and to test the SM to high accuracy. Due to the increasing precision of LHC data, theoretical predictions should also improve in precision, as the current state of experimental analyses is constrained by theoretical uncertainties. Therefore, theoretical predictions play a central role for the interpretation of these collider data.

In this thesis, we address two different but related topics towards high-energy and precision physics. Firstly, we present the implementation of the double Higgs boson production within the GENEVA Monte Carlo event generator framework. These generators are essential tools for both theorists and experimentalists, enabling increasingly precise particle level predictions for collider experiments. The double Higgs boson production, moreover, allows for the direct measurement of the trilinear coupling, which is linked to many open questions about particle physics and cosmology. However, it is a rare and challenging process to study, demanding substantial effort from both experimentalists and theorists. For this project, we consider the infinite top mass limit, where the top quark is treated as infinitely heavy and its mass is integrated out. This approximation simplifies the implementation of the calculation, while allowing the study of the new interface for the three different parton showers available in the GENEVA framework. Being a gluon-gluon initiated process, the effects of the shower have been found to be different and more pronunced compared to other processes already implemented in our generator, but still compatible with the associated theoretical uncertainties.

In the second part of this work, we discuss the threshold resummation for rapidity distributions in the Drell-Yan process. Such logarithms, in the limit in which the invariant mass of the tagged final state is close to the centre-of-mass energy of the initial state, invalidate the calculation of the cross section by means of a perturbative expansion in the strong coupling, and need to be resummed. We review the threshold resummation approaches available in the literature for this particular case, discussing their primary differences and levels of accuracy. We propose a new proof for two of these approaches which have been questioned. We also study in detail their accuracy under various choices of the form of threshold logarithms, concluding with a comparison between all the various approaches to this type of resummation.

Contents

1 Introduction **5**

2 Theoretical tools **8**
2.1 Fixed-order prediction . . . 9
2.2 Resummation in perturbative QCD . . . 10
2.2.1 Soft Collinear Effective Theory . . . 12
2.3 Parton Shower . . . 14

I Double Higgs production in the GENEVA framework **16**

3 GENEVA framework **17**
3.1 Resummation of the zero-jettiness . . . 18
3.2 GENEVA formulas . . . 19
3.3 Shower interface in GENEVA . . . 23

4 Double Higgs boson production **28**

5 Higgs boson pair production in GENEVA **32**
5.1 Choice of the resolution cutoff in $\mathcal{T}_0$ . . . 32
5.2 Choice of resummation scales . . . 35
5.3 Resummation parameters . . . 38
5.3.1 One-jettiness resummation . . . 38
5.4 Numerical effect of $\mathcal{T}_0$ resummation . . . 39

6 Parton showers for double Higgs boson production **41**
6.1 PYTHIA8 . . . 41
6.2 SHERPA . . . 42
6.3 DIRE . . . 43
6.4 Comparison between parton showers . . . 44

7 Phenomenological results **46**
7.1 Physical parameters . . . 46
7.2 Validation of NNLO results . . . 47
7.3 Showered results . . . 50

II On the approaches to threshold resummation of rapidity distributions for the Drell-Yan process **53**

8 Threshold resummation of Drell-Yan rapidity distributions **54**
8.1 Genesis of threshold logarithms . . . 55
8.2 Factorisation for rapidity distributions . . . 56
8.3 Threshold resummation approaches for rapidity distributions . . . 61

9 Validation of the BNX and BFR approaches **64**
9.1 New proof of BNX and BFR . . . 64
9.2 Validity of the threshold expansion in the integrand . . . 67
9.3 Other objections to BNX and BFR . . . 72

10 Accuracies estimations of BNX and BFR approaches **77**
10.1 z-soft approximation . . . 78
10.2 N-soft approximation . . . 79
10.3 ψ-soft$_1$ approximation . . . 80
10.4 Numerical validation at NLO and NNLO . . . 82

11 Phenomenological comparison **86**
11.1 All-order resummed results for BFR . . . 89

Conclusions **92**

A SCET factorisation formula for double Higgs boson production **94**

B Hard function for $gg \to HH$ in the $\overline{\text{MS}}$ scheme **101**

C Distribution identities **106**
C.1 Convolutions in Mellin space . . . 109

D Analytical expressions for threshold resummation approaches **111**
D.1 Coefficient function for BNX/BFR approximations . . . 111
D.2 Coefficient function for BDDR/AMRST approximations . . . 113
D.3 Coefficient function for LMT approximation . . . 116

Bibliography **119**

Acknowledgements **130**

Chapter 1

Introduction

The discovery of the Higgs boson [3,4] at the Large Hadron Collider (LHC) has established the Standard Model (SM) as a successful theory of fundamental particles and their interactions. The continuous and intricate collaboration between experimental and theoretical physicists has propelled our understanding of the universe to unprecedented levels. The LHC, with its immense energies and precise detectors, continues to be at the forefront of this quest of knowledge, pushing the boundaries of human understanding. From one side, experimental measurements at the LHC are a cornerstone of high-energy physics. The detectors surrounding the LHC collision points, such as ATLAS and CMS, meticulously record the outcomes of these collisions, capturing a torrent of data that holds the key to understanding the universe's fundamental particles and their interactions. These experiments have not only confirmed the existence of the Higgs boson, but have also unveiled groundbreaking discoveries, including the measurement of the Yukawa coupling of the Higgs boson with fermions of the third generation and the observation of rare particle decays. From the other side, high-energy physics is not solely confined to the experimental realm. Theoretical measurements and models play an equally crucial role in this field, predicting the behavior of particles, studying the fundamental forces and exploring the limits of the SM. These theoretical measurements are essential for guiding experimental design and interpreting the results.

Despite all the discoveries and confirmations of the SM predictions, a number of experimental observations such as the neutrino masses, the dark matter and energy, call for the existence of new physics beyond the SM or extensions of it. Moreover, the SM describes three of the four fundamental forces of the universe leaving outside gravity, and there are many open questions related both to particle physics and cosmology. Many of these questions regard the Higgs self-interaction and the shape of the scalar potential. The LHC offers a unique opportunity to look for new physics beyond the SM: the high centre-of-mass energy of the collisions allows to search for new heavy particles directly, but new physics effects can also be discovered indirectly, by performing precise measurements and looking for deviations from the SM expectations.

Since LHC is a proton-proton collider, Quantum CromoDynamics (QCD) plays a central role in the computation of theoretical predictions, determining the structure of the cross section

formulas. Tipically, scattering processes occur at low energy and are predominantly elastic, while at high energy they are inelastic. These inelastic processes can be studied through perturbation theory, nameley as an expansion of the cross section in the strong coupling α_S. In addition to that, it is important to account for background contributions originating from other processes that produce the same final state as the process under investigation. These backgrounds introduce uncertainties which are also enhanced by the limited theoretical knowledge of higher-order corrections. One of the main efforts into this direction is the attempt to reducing the theoretical uncertainties on the SM predictions to a size comparable with the experimental ones. Achieving this goal involves techniques like the calculation of fixed-order corrections at higher orders. Moreover, it necessitates addressing the presence of large logarithmic terms in specific kinematic regions, which have to be resummed to all orders not to spoil the perturbative expansion of the cross section. Depending on the physical observables and kinematic regions considered, various types of logarithmic terms may arise, such as threshold logarithms, high-energy logarithms and tranverse momentum logarithms. Resummation of these terms can be done through classical methods like the Mellin transform of the physical observable [5–8], or innovative approaches like the Soft Collinear Effective Theory (SCET) [9–13], which is able to resum a wide range of logarithmic terms. Another effect that can improve the understanding of the QCD background is the study of multiparticle interactions (MPI), meaning the simultaneous interactions of the costituents from one proton with those from another proton.

Monte Carlo event generators represent indispensable tools for achieving precise theoretical predictions, incorporating various effects described above. These generators simulate the production of particle sets within scattering processes. Several methods have been employed in constructing Monte Carlo event generators. Historically, generators described QCD emissions via parton showers, primarily in the collinear and/or soft limit. Later, the predictions were obtained by matching the showers to the tree-level matrix elements of the process considered, improving the description also away from the soft and collinear limit. This is usually done matching the leading-order (LO) matrix elements directly to some generators provider such as Herwig [14], Pythia8 [15, 16] and Sherpa [17–19]. Similar matching approaches, but with increased accuracy, are used such as Powheg [20–22], which combines the QCD next-to leading order (NLO) prediction with the shower. There are other different methods in order to do so, such the MiNLO [23, 24] and MEPS@NLO [25] ones. In recent years, a significant leap has been made by extending partonic event generators to next-to-next-to leading order (NNLO) in QCD, matched to a parton shower. Notable examples include Geneva [26–28] and MiNNLOPS [29, 30].

The main arguments of this thesis, which drive the division into two parts, concern the implementation of a new process, the double Higgs boson production, in the Geneva framework, and the study of the threshold resummation approaches to rapidity distribution for the Drell-Yan process.

The outline of this thesis is the following. The starting point is the review of the fundamental theoretical tools used to described theoretical predictions: the fixed-order, the resummed and the parton shower results. This allows us to introduce the notation used in the following. The first part of this thesis regard the implementation of the double Higgs boson production process within the Geneva framework. Therefore, we first discuss the Geneva Monte Carlo

event generator method. In particular, we describe in detail the resummation of the resolution variable chosen for such event generator, the formulas to obtain the differential cross section in the N jet-regions required by GENEVA and the interface to the parton shower. We then specialise to the case of the double Higgs boson production, listing all the motivations to look at a such rare and challenging process. We also discuss and explain all the GENEVA parameters that have to be tuned in order to describe optimally the double Higgs boson production. The main discussion is driven by the choice of the resolution cutoffs and the energy scales for the resummation of the resolution variable. We briefly discuss the expected effects of the three different showers available in GENEVA on the double Higgs boson production and, finally, we present our phenomenological results.

The second part of this thesis deals with the threshold resummation for rapidity distribution in the Drell-Yan process. After a brief reminder on the genesis of threshold logarithms, we establish our notation for the rapidity distribution case. We briefly discuss the threshold resummation approaches that are available in the literature, highlighting their main differences and their accuracies. We then concentrate on two specific approaches: the Becher, Neubert, Xu (BNX henceforth) [31] and the Bonvini-Forte-Ridolfi (BFR henceforth) [32], which validity has been questioned. We propose a new proof for such approaches, discussing in detail its validity. We address all the possible limitations of the BNX/BFR approach, defining the specif limit of validity and presenting also numerical results to support our conclusions. We then move to the study of the accuracy of these approaches, which can be improved depending on the form of threshold logarithms that is chosen, with the support of numerical results for both approaches and for various form of threshold logarithms. Finally, we show the comparison at fixed-order with all the other approaches available in the literature. We add also some representative results for the BFR resummation only, since the all orders resummation for other approaches is not available in public codes. All the supplement material for both the parts of the thesis is reported in the appendices.

Chapter 2

Theoretical tools

Theoretical predictions for collider processes involving strongly interacting particles are a fundamental tool in describing experimental data. There are several methods to achieve this, namely using the fixed-order (FO) perturbation theory, the resummed perturbation theory and the predictions coming from a parton shower (PS). Each of these descriptions provides the most accurate prediction in a specific limit, but none of them can fully describe a physical process alone. The FO perturbation theory, for which the expansion parameter is the strong coupling α_S, becomes unreliable when large ratios of physical scales appear in the calculation. Usually the large scales ratio appears as a logarithmic term, and at each order in α_S there can be up to two powers of such logarithms. In such cases, the logarithms have to be resummed to all orders in α_S to provide precise perturbative predictions. Both the FO and resummed predictions, however, cannot predict the collision and the production of hadrons. This is due to the asympotic freedom of QCD, which allows only the interaction of their constituents, the partons, to be described through perturbation theory. Moreover, the higher-order resummation is applied to observables that are sensitive to a small number of physical scales, and that are sufficiently inclusive. To describe the final state that is fully exclusive in all emissions, parton showers are needed. The parton shower approach allows the evolution of partons from their production scales down to the hadronisation scale, providing a bridge between the perturbative QCD calculations and the non-perturbative effects that dominate at low energies, described by the hadronisation model which can be attached directly to parton showers. Monte Carlo event generators can combine these three descriptions to obtain a fully exclusive hadronised event with the perturbative accuracy of a higher-order calculation. As experimental results become more precise, it is crucial for all these three components to be as accurate as possible.

In this chapter, we review all the three different descriptions for theoretical predictions, considering a hadron-hadron collision at Large Hadron Collider (LHC) as a specific case, highlighting their features and the main topics of this thesis.

2.1 Fixed-order prediction

Each proton-proton collision at LHC can be described using the collinear factorisation theorem, as a generalization of the Deep Inelastic Scattering (DIS) case. The collision can be schematized as the interaction between the constituents of the protons, namely quark and gluons, referred to as partons. Considering two protons of momentum p_1 and p_2, the parton i has a fraction x_1 of the momentum p_1 of the proton, and its total momentum will be given by $x_1 p_1$. Similarly for the other parton j, its total momentum is given by $x_2 p_2$. The hadronic cross section, due to the collinear factorisation theorem, can be written as a convolution in the momentum fractions of the partonic cross section, the perturbative term, and in the parton distribution functions (PDFs), which are the non-perturbative part. Such cross section is given by

$$\sigma(\tau, Q^2) = \sum_{a,b} \int_{\frac{\tau}{x_1}}^{1} \mathrm{d}x_1 \int_{\frac{\tau}{x_2}}^{1} \mathrm{d}x_2 \, f_a\left(x_1, \mu^2\right) f_b\left(x_2, \mu^2\right) \times \hat{\sigma}_{ab}\left(\frac{\tau}{x_1 x_2}, \alpha_S(\mu^2), \frac{\mu^2}{Q^2}\right) + \mathcal{O}\left(\frac{\Lambda_{\mathrm{QCD}}}{Q}\right), \tag{2.1}$$

where Q^2 is the hard scale of the process, $\tau = \frac{Q^2}{S}$ with S the collider centre-of-mass energy, μ^2 the energy chosen for the renormalisation and a, b the flavour indices. This formulation is supposed to be valid up to corrections that are suppressed with powers of $\frac{\Lambda_{\mathrm{QCD}}}{Q}$, known as higher twist, where Λ_{QCD} is the hadronisation scale. Although a formal proof does not exist for the general case of a LHC process, this theorem holds for the most important production modes.

The perturbative part is represented by the partonic cross section, which can be written as an expansion in α_S as

$$\hat{\sigma}_{ab}\left(\frac{\tau}{x_1 x_2}, \alpha_S(\mu^2), \frac{\mu^2}{Q^2}\right) = \sum_k \alpha_S^{(k)}(\mu) \hat{\sigma}_{ab}\left(\frac{\tau}{x_1 x_2}, \frac{\mu_F^2}{Q^2}, \frac{\mu_R^2}{Q^2}\right), \tag{2.2}$$

where μ_F and μ_R are the factorisation and renormalisation scales, respectively.[1] The perturbative expansion is obtained by expanding up to a fixed k-th order Eq. (2.2). The fully differential cross section at lowest order, called leading order (LO), is given by

$$\mathrm{d}\hat{\sigma}_{ab}\left(\frac{\tau}{x_1 x_2}, \alpha_S(\mu^2), \frac{\mu^2}{Q^2}\right) = \mathcal{B}\left(p_1, p_2, q_1, ..., q_N\right) \mathrm{d}\Phi_N\left(q_1, ..., q_N\right), \tag{2.3}$$

where $\mathcal{B}\left(p_1, p_2, q_1, ..., q_N\right)$ is the Born term containing the matrix element squared relative to the process considered, dependent on the initial-state proton momenta and on the N final-state partons ones. The usual N body phase space is represented by $\mathrm{d}\Phi_N$.

In order to have meaningful predictions to be compared with experimental data, the perturbative expansion in Eq. (2.2) has to be computed with the highest possible accuracy. Since the expansion parameter is the strong coupling α_S, going beyond the LO can be seen

[1] Note that any physical observable is independent of the factorisation and renormalisation scales, they are just an artifact of the theory.

as adding extra vertices to the Born matrix element, and, effectively, as including an extra particle. Depending on how this additional particle is added to the Born level, it can be classified as a real correction $\mathcal{R}$, if it appears in the final state, or a virtual one $\mathcal{V}$, if it is absorbed in a loop. In the first case, the particles are resolved, meaning that extra particles are emitted or absorbed during the interaction being considered, and they represent actual radiation in the process. As a consequence, the phase space for a real correction will be different from the one at the Born level, since extra particles have to be counted. Virtual corrections, instead, arise from the exchange of virtual particles in the interaction. These particles are not directly resolved, and thus observed, as they are involed in loops in Feynman diagrams. When integrating over the phase space of these corrections, singular contributions can arise from the calculation, when the extra particles are either soft or collinear to one of the other particles involved in the process. Thanks to the Kinoshita-Lee-Nauenberg theorem [33, 34], these singularities are always cancelled when virtual terms are combined with real emission terms. To prove that the real emission term and the virtual one have the same exact value, but with a different sign, the phase space integrals have to be regularised, typically using dimensional regularisation ($d = 4 - 2\epsilon$). In this way the singularities are represented as poles in ϵ. Moreover, due to the non-abelian nature of QCD, ultraviolet divergences also appear, which can be effectively addressed through renormalisation.

The idea of iteratively adding an extra vertex to the LO cross section can be extended arbitrarily, but the number of diagrams to be computed grows factorially, making the evaluation of matrix elements time-consuming. Additionally, the virtual and real contributions belong to different phase spaces, posing a challenge when implementing a Monte Carlo event generator that typically deals with one phase space at a time. To address these issues, one can subtract divergences at the integrand level, using the so-called subtraction methods. To show how the subtraction methods work, consider computing a next-to-leading order (NLO) cross section (one extra power of α_S to the Born level). A counterterm $\mathcal{C}$ is introduced to subtract and reproduce the exact soft and collinear divergences arising from the real term $\mathcal{R}$. Basically, the cross section at NLO can be written as

$$\sigma_{\text{NLO}} = \int \mathcal{B}\left(\Phi_N\right) \mathrm{d}\Phi_N + \lim_{d\to 4-2\epsilon} \int \left[\mathcal{V}\left(\Phi_N\right) + \int \mathcal{C}\left(\Phi_{N+1}\right) \frac{\mathrm{d}\Phi_{N+1}^{(d)}}{\mathrm{d}\Phi_N}\right] \mathrm{d}\Phi_N + \int \left[\mathcal{R}\left(\Phi_{N+1}\right) - \mathcal{C}\left(\Phi_{N+1}\right)\right] \mathrm{d}\Phi_{N+1}\,. \tag{2.4}$$

The introduction of $\mathcal{C}\left(\Phi_{N+1}\right)$, requires the existence of a mapping between the Φ_{N+1} and Φ_N phase space. This mapping is needed to project the Φ_{N+1} configurations close to the soft and collinear limits onto the Φ_N configuration, for which the virtual poles and the real ones cancel. The most commonly used subtraction methods are the Catani-Seymour dipole formalism [35] and the Frixione-Kunszt-Signer method [36].

2.2 Resummation in perturbative QCD

Any physical observable, such as the cross section, can be described using perturbation theory. Depending on which observable and kinematic region are considered, certain contributions in

the perturbative coefficient of a generic expansion, like the one in Eq. (2.2), can appear, leading to large corrections to all orders in α_S. These potentially large terms appear at each order in perturbation theory, spoiling the convergence of the perturbative series, usually guaranteed by the small value of the strong coupling. The form of these contributions is typically expressed as the logarithm of the ratio of two energy scales $\log\left(\mu_1^2/\mu_2^2\right)$. When μ_1^2 and μ_2^2 are very different, the logarithms can become large. If the power of these logarithms grows with the power of α_S, then the effective expansion parameter becomes

$$\alpha_S^n \log^k\left(\frac{\mu_1^2}{\mu_2^2}\right) \sim 1\,, \qquad k \leq n\,, \tag{2.5}$$

and all the terms in the perturbative series are of the same order. In these cases, the resummation of the logarithms to all orders in α_S is needed.

Depending on the physical observable chosen, there can be many different logarithmic terms that require resummation. In the particular case of the cross section, the logarithms that need to be resummed are typically associated with large or small values of the momentum transfer, or the energy scale in the scattering process. Thus, there are at least three different families of logarithms to consider: the threshold logarithms, the high-energy logarithms and the transverse momentum logarithms. Each of these families has been widely studied in literature, and their resummation is relevant in a specific kinematic limit. The first topology of logarithms named, the threshold logarithms, will be the subject of the second part of this thesis, introduced in chapter 8. Concerning Monte Carlo event generators, one has to deal with the logarithms arising when partons are emitted nearly collinear to the direction of the parent parton, and they depend on the resolution variable chosen for that particular event generator. The resummation to all orders can be done analytically or by numerical methods using a parton shower Monte Carlo. In this thesis, we are interesting in the analytical method. In QCD, this typically involves the use of techniques from renormalisation group theory and factorisation theorems to systematically organize and sum up the logarithmic terms to all orders in perturbation theory. A classic way to organize such logarithms is in terms of the Mellin transform, defined in Sec. C.1, of the partonic cross section [5–8], which can then be written as

$$\mathrm{d}\hat{\sigma}_{ab}(N,\alpha_S) = \exp\left[\frac{1}{\alpha_S} g_1(\alpha_S \log N) + g_2(\alpha_S \log N) + \alpha_S\, g_3(\alpha_S \log N) + ...\right] + \mathcal{O}\left(\frac{1}{N}\right). \tag{2.6}$$

The functions g_i only depend on $\alpha_S \log N$, and each of them corresponds to a different order: g_1 gives the leading logarithmic (LL) accurate term, g_2 contains the next-to-leading logarithmic (NLL) accurate contribution and so on so forth for the others g_i. This expression is obtained in Mellin (N) space, and the g_i values determines a whole tower of logarithms to all orders in perturbation theory. In order to obtain the physical cross section, it is necessary to compute the inverse Mellin transform of Eq. (2.6) taking into account the branch cut in the complex N-plane due to the Landau pole.[2] To achieve this, different solutions have been proposed: the

[2]The running of the strong coupling α_S can be represented as

$$\alpha_S(\mu^2) = \frac{1}{\beta_0 \log\frac{\mu^2}{\Lambda^2}}\,, \tag{2.7}$$

Minimal Prescription (MP) [37], and the Borel Prescription (BP) [38].

There are, however, other approaches to this resummation, as for example with the introduction of an effective field theory to describe QCD in the soft and collinear regime, called Soft Collinear Effective Theory (SCET). SCET allows to separate the full QCD theory into different sectors introducing new fields and symmetries to describe the dynamics of soft and collinear particles separately and achieving resummation of these large logarithms. This last approach will be widely used in this thesis, for this reason we discuss the SCET formalism in the following section.

2.2.1 Soft Collinear Effective Theory

Soft Collinear Effective field Theory (SCET) [9–11] is a low-energy field theory of the Standard Model, widely used for high-energy processes involving light particles. It is particularly relevant for collider physics and heavy-quark physics.

Effective field theories (EFTs) are used to expand a physical observable in the ratio of two disparate scales, usually an high-energy scale (Λ_{high}) and a lower one (Λ_{low}). Thanks to the expansion, it becomes possible to separate the low-energy contributions from the high-energy ones. For QCD processes involving initial-state hadrons, there is always a low-energy part that is non-perturbative, represented by the parton distribution functions, and a high-energy part that is computed perturbatively. Moreover, the perturbative part can further depend on more than one scale, leading to large logarithms of the scale ratios that appear order by order in the strong coupling α_S. In the case of SCET, similar to what has already been said, these logarithms can be represented by

$$\alpha_S^n \log^{2n}\left(\frac{\Lambda_{\text{high}}}{\Lambda_{\text{low}}}\right), \qquad n \in \mathbb{N}\,. \tag{2.8}$$

The basic idea behind SCET is to split the momenta of particles involved in a scattering process into different components, each corresponding to different energy scales. The most useful coordinate system for this purpose is the light-cone coordinates one: introducing two light-like vectors $n_\mu = (1,0,0,1)$ and $\bar{n}_\mu = (1,0,0,-1)$ in the directions of the momenta of the particles, any four momenta p^μ can be decomposed as

$$p^\mu = (n\cdot p)\frac{\bar{n}^\mu}{2} + (\bar{n}\cdot p)\frac{n^\mu}{2} + p_\perp^\mu \equiv p_+^\mu + p_-^\mu + p_\perp^\mu, \tag{2.9}$$

resulting in a sum of two collinear terms and a perpendicular one. This allows for the analysis of interactions of these particles by isolating the dominant contributions at each energy scale. This separation is performed in SCET by introducing different sets of fields corresponding to different energy regimes. The starting point is the expansion of the Feynman diagrams through the strategy of regions. The strategy of regions, based on dimensional regularisation, allows to carry out asymptotic expansions of loop integrals by splitting the integration into different regions, and expanding the integrand in each of them. The expansion parameter used, λ, is

where μ is the scale at which the corresponding value of the strong coupling is computed, $\Lambda \approx 200$ MeV is the Landau pole and $\beta_0 = \frac{11C_A - 2n_f}{12\pi}$ with $C_A = 3$ and n_f the number of light quarks. The Landau pole marks the energy scale at which the strong coupling becomes infinite.

usually defined as the ratio of a hard scale Q and another energy scale involved in the process at hand. Once these regions have been identified, an effective Lagrangian is constructed, which produces the different terms contributing to the expanded diagrams. Moreover, the regions can be integrated out in sequence performing an integral over the field of the particles. All the different pieces can be connected through a matching process, which allows to relate the parameters of one effective region to the parameters of another region at higher or lower energy scale. This matching process is done at a given renormalisation scale, and it is represented by a coefficient called the Wilson coefficient. The Wilson coefficient satisfies the renormalisation group equation (RGE) on that renormalisation scale considered.

The expansion of the loop integrals is performed in four different regions,[3] separated according to how the components of the integration momentum k^μ scales:

1. **Soft region:** $k^\mu \sim (\lambda^2, \lambda^2, \lambda^2)Q$
   dealing with particles that carry energy much smaller than the hard scale of the process. In this region, soft interactions are described by soft Wilson lines, which encode the long-range interactions of soft gluons;

2. **Hard region:** $k^\mu \sim (1, 1, 1)Q$
   involving particles that carry energy at the highest scale in the process. This region is described by the usual perturbative QCD calculations;

3. **Collinear region:** $k^\mu \sim (\lambda^2, 1, \lambda)Q$
   dealing with particles that carry energy much smaller than the hard scale, but larger than the soft one. These particles move along specific directions closely aligned to the parent particle's direction. In this region, collinear interactions are described by collinear Wilson lines, which encode the interactions of collinear gluons and quarks;

4. **Anticollinear region:** $k^\mu \sim (1, \lambda^2, \lambda)Q$
   similar to the collinear region, but the particles move in directions nearly opposite to the parent particle's direction.

For some particular applications, such as exclusive B-mesons decays or some observables sensitive to small transverse momenta, it is possible to have also the ultra-soft region characterized by the λ^4 scaling.

This procedure in the SCET formalism allows to write the cross section in a factorise form. For the particular case of colour singlet production κ, which will be the subject of this thesis, the differential hadronic cross section can be written, pictorially, as

$$\frac{\mathrm{d}\sigma_\kappa}{\mathrm{d}\rho} = \sum_{a,b} H_\kappa(\mu_H)\, U_H(\mu_H, \mu)\, [B_a(\mu_B, \rho) \otimes U_B(\mu_B, \mu)][B_b(\mu_B, \rho) \otimes U_B(\mu_B, \mu)] \otimes [S_\kappa(\mu_S, \rho) \otimes U_S(\mu_S, \mu)] + \mathcal{O}(\rho)\,. \tag{2.10}$$

Here, ρ represents any resolution variable sensitive to the soft or collinear radiation. This factorised formula is valid up to power corrections in the resolution variable chosen. H,

[3] It can be proven that all of the other possible scalings for the integration do not contribute to the final result, since they give rise to scaleless integrals only.

$B_{a,b}$ and S are the hard, beam and soft functions, respectively. The hard function H is process-dependent, and it encodes the part of the calculation coming from the hard region. The beam functions $B_{a,b}$ depend on whether the process is gluon- or quark-initiated, and they are directly linked to the collinear and anticollinear regions. Lastly, the soft function S, for the production of colour singlet processes, only depends on whether the Born process is quark- or gluon-initiated. The convolution of these functions is schematically represented by the symbol $\otimes$, and each of them is computed at a suitable scale $\mu_{H,B,S}$ in such a way that no large logarithmic corrections are present in their fixed-order perturbative expansions. They are then evaluated at a single common scale μ, through the evolution factors $U_{H,B,S}$ from their own characteristic scale to the common one, resumming all the large logarithms generated by the ratio of the two scales.

2.3 Parton Shower

A parton shower is the simulation of the evolution of a high-energy particle collision that incorporates a sequence of parton branchings. It is a fundamental tool for performing fully differential calculations at higher multiplicities, by adding extra radiation to a partonic event. The emission process involves a parton emitting a gluon or a quark, and it is often referred to as branching, as the parton branches into multiple partons. The parton shower evolves sequentially, where each emitted parton in a branching can subsequently undergo further emissions. This cascade-like process generates a series of successive parton emissions. Emissions are ordered based on a specific evolution variable, ensuring that each emission is softer and more collinear than the previous one. Parton showers respect unitarity, meaning that a parton can either split into two partons, or not split at all. Moreover, it conserves locally flavour and four momentum. The emissions can occur at different stages of a particle collision, resulting in two types of radiation: initial-state radiation (ISR) and final-state radiation (FSR). Both types of radiations are governed by the same Dokshitzer-Gribov-Lipatov-Altarelli-Parisi (DGLAP) equations.

Let's consider the case of a radiation in the final state (FSR) where a mother parton a splits into two daughter partons b and c. The differential probability for this branching to occur at a virtuality scale t is given by

$$\mathrm{d}\mathcal{P}_a(z,t) = \sum_{b,c} \frac{\mathrm{d}t}{t} \frac{\alpha_S}{2\pi} P_{a\to bc}(z)\,\mathrm{d}z\,, \tag{2.11}$$

where z is the fraction of the mother energy taken by b and $1-z$ is the one taken by c, and $P_{a\to bc}(z)$ are the splitting kernels. This equation accounts for an infinite number of partons emissions. The emissions continue until a shower cutoff Λ is reached. It usually coincides with the hadronisation scale (~ 1 GeV). It is then convenient to express the probability that no emission occurs between the initial maximum scale $t_{\max}$ and a given t, called the Sudakov form factor

$$\mathcal{P}_a^{\mathrm{no}}(t_{\max},t) = \exp\left(-\sum_{b,c}\int_t^{t_{\max}}\int_{z_{\min}}^{z_{\max}} \mathrm{d}\mathcal{P}_a(z',t')\right)\,, \tag{2.12}$$

where the limits of integration on z depend on the kinematics and the Λ cutoff. The probability of the first branching occuring at $t = t_a$ is then given by $\mathrm{d}\mathcal{P}_a(z, t_a)\mathcal{P}_a^{\mathrm{no}}(t_{\max}, t_a)$. Subsequently, the daughters b and c can branch, with their $t_{\max}$ given by the scale at which the mother made its branching, $t_{\max} = t_a$. This can continue iteratively until the Λ cutoff is reached and the shower stops.

The same structure of Eqs. (2.11) and (2.12) can be used to describe ISR, but this case is usually treated with the backwards evolution, also called reverse evolution. In this approach, the order of the shower described above is reversed. The initial-state shower starts from the hard scattering process, where partons resulting from the collision are generated, and evolves towards the initial state, simulating the emission of increasingly energetic partons. The probability that a parton a resolves into two partons b and c is defined based on the DGLAP equation as

$$\mathrm{d}f_b(x,t) = \sum_{a=q,g} \frac{\mathrm{d}t}{t}\frac{\alpha_S}{2\pi}\int \frac{\mathrm{d}y}{y} f_a(y,t) P_{a\to bc}\left(\frac{x}{y}\right) . \tag{2.13}$$

More specifically, the equation above, where $f_{a,b}$ are the parton densities, describes the probability that a parton a with momentum y is resolved into a parton b at $x = zy$ and another parton c at $y - x = (1 - z)y$. Similarly, a parton b can be unresolved into a parton a, and the relative probability is given by the ratio $\mathrm{d}f_b/f_b$, which leads to

$$\mathrm{d}\mathcal{P}_b(x,t) = \sum_{a=q,g} \frac{\mathrm{d}t}{t}\frac{\alpha_S}{2\pi}\int \mathrm{d}z \frac{y f_a(y,t)}{x f_b(x,t)} P_{a\to bc}(z) . \tag{2.14}$$

As already done for the FSR case, the no-emission probability $\mathcal{P}_b^{\mathrm{no}}(x, t_{\max}, t)$ can be defined as in Eq. (2.12), exponentiating Eq. (2.14). As they are defined, considering the structure of the Sudakov form factor, parton showers are leading logarithmic accurate. There are various studies on how to improve their accuracy, but we will not discuss them and we only consider a leading logarithmic accurate parton shower.

Another important point to note is that partons carry momentum, flavour, spin and colour, and all these quantum numbers have to be handled correctly. In particular, the treatment of colour does not fit properly in the event generator formalism, since the interference between different colour states is significant. In all the parton showers considered in this work, the leading colour approximation is used, which means that the number of colors $N_c = 3$ is fixed and all the contributions to the probability to obtain a partonic final state suppressed by powers of $1/N_c^2$ are neglected.

Part I

Double Higgs production in the GENEVA framework

Chapter 3

GENEVA framework

GENEVA, GENerate EVents Analytically, is a Monte Carlo event generator that combines the three theoretical predictions used to describe collider processes: the fixed-order perturbation theory, the resummed perturbation theory and the predictions from parton shower. The aim of GENEVA is to combine these three descriptions obtaining fully exclusive hadronised events with the perturbative accuracy of a higher-order calculation. Moreover, including the higher-order resummation in an appropriate resolution variable, the FO and PS regimes are separated and only connected through the resummation itself. This allows to have an event-by-event systematic estimate of the theoretical perturbative uncertainties, and to improve the perturbative accuracy away from the FO regions. Currently, in GENEVA most of the processes implemented are colour singlet production, but also final states with heavy coloured partons and jets have started to be studied.

The GENEVA method is based on the definition of physical and infrared-safe (IR safe) events at a given perturbative accuracy, with the requirement that the IR singularities cancel on an event-by-event basis. Events are discriminated according to the value of N-jet resolution variables which divides the phase space into 0-, 1- or 2-jets. In order to match the resummation to the fixed-order prediction, moreover, the resummation of such IR safe variable has to be known. In principle, hence, GENEVA can be used with any resolution variable which satisfies these two requirements. One optimal choise is the N-jettiness, but in the past also the transverse momenutum of a colour singlet system has been chosen as a resolution variable [39].

In this thesis we are going to use only the N-jettiness [40], defined as

$$\mathcal{T}_N = \sum_{i=1}^{N} \min_{q_1,...q_N} \left(q_a \cdot \hat{p}_i, q_b \cdot \hat{p}_i, q_1 \cdot \hat{p}_i, ..., q_N \cdot \hat{p}_i\right), \tag{3.1}$$

where $q_a = (1, 0, 0, 1)$, $q_b = (1, 0, 0, -1)$ are the beam directions, and $q_1, ..., q_N$ can be any jet direction. Note that $\hat{p}_i$ is the longitudinally boosted momenta from the laboratory frame to the one in which the colour singlet has zero rapidity.

The N-jettiness can be thought as a variable which measures the degree to which the final state is N-jet-like for a given value of N, and automatically clusters the final state into N-jet

and beam regions. Basically, any configuration with a number of final state partons that is equal or lower than N has $\mathcal{T}_N = 0$. Instead, any configuration with additional emission that is not soft nor collinear gives a nonzero value of $\mathcal{T}_N$.

Among the various properties of this observable, two are particularly useful for GENEVA. It is an IR-safe variables, which means that $\mathcal{T}_N \to 0$ in presence of soft or almost collinear partons to the beam. Moreover, its resummation is known up to next-to-next-to-next-to-leading logarithmic ($\mathrm{N^3LL}$) accuracy for $N = 0$ (zero-jettiness, $\mathcal{T}_0$) in the Soft Collinear Effective Theory (SCET) formalism. For $N = 1$ (one-jettiness, $\mathcal{T}_1$) all the ingredients required are available up to next-to-next-to-leading logarithmic (NNLL) accuracy. For our purposes, we will consider the resummation of the one-jettiness up to NLL. As it will be shown, these two variables will be used to divide the events into the aforementioned jet-regions. For colour singlet production processes, these resummed predictions are matched with the next-to-next-to-leading order (NNLO) calculations, and then are interfaced to a parton shower. Currently, three different showers are available: PYTHIA8, DIRE and SHERPA. Even though the accuracy known for the resummation of the zero-jettiness is $\mathrm{N^3LL}$, we will consider only the $\mathrm{NNLL'}$[1] accuracy not to spoil it when interfacing with the parton shower.

In this chapter, we discuss in detail the separation into jet-regions, reporting the differential cross section formulas used. We also summarize the ingredients needed for the resummation of the zero-jettiness in the SCET formalism and, lastly, we present the interface to the parton shower for GENEVA.

3.1 Resummation of the zero-jettiness

In the GENEVA framework, we are interested in the production of a colour singlet from the scattering of two hadrons, and we perform the zero-jettiness resummation in the SCET formalism, already introduced in Sec 2.2.1.

We can express the $\mathcal{T}_0$ in the light-cone coordinate, as

$$\mathcal{T}_0 = \sum_{i=1}^{N} \min(\hat{p}_i^+, \hat{p}_i^-), \tag{3.2}$$

where $\hat{p}_i^{\pm} = \hat{p}_i^0 \mp \hat{p}_i^3$ and p_i is the momentum of the partons in the process considered. The SCET factorisation theorem [41, 42] gives us the resummed, differential in the Born phase space, cross section

$$\frac{\mathrm{d}\sigma^{\mathrm{resum}}}{\mathrm{d}\Phi_0\, \mathrm{d}\mathcal{T}_0} = H_\kappa(Q^2, \mu) \int B_{k_a}(t_a, x_a, \mu) B_{k_b}(t_b, x_b, \mu) S_\kappa\left(\mathcal{T}_0 - \frac{t_a + t_b}{Q}, \mu\right) \mathrm{d}t_a\, \mathrm{d}t_b, \tag{3.3}$$

where κ is the production channel of a generic colour singlet coming from the scattering of two hadrons a, b and $x_{a,b}$ are the fractions of momenta of the partons $k_{a,b}$. Here we have introduced the hard function H_κ, the beam functions $B_{a,b}$ and the soft function S_κ, each of these is dependent on the resummation scale μ. Their main features have already been introduced in Sec. 2.2.1, we just remark here that the hard function, being process dependent,

[1] The prime means that we are including contributions proportional to $\delta(\mathcal{T}_N)$.

contains the corresponding Born and virtual matrix elements. Moreover, the beam functions also depend on the transverse virtualities $t_{a,b}$, and for $t_{a,b} \gg \Lambda_{\rm QCD}$ they satisfy an operator product expansion (OPE) in terms of the perturbative collinear matching coefficients and standard parton distribution functions. Each of these three functions admits a perturbative expansion in powers of the strong coupling, and it manifests a logarithmic dependence on a single characteristic scale. This choice of scales is made in order to remove the large logarithms in the perturbative expansion of H, B and S. But since the factorisation formula requires all the components to be evaluated at a single common scale μ, the RGE operator has to act on each function, resulting

$$\begin{aligned}\frac{\mathrm{d}\sigma^{\mathrm{NNLL}'}}{\mathrm{d}\Phi_0\,\mathrm{d}\mathcal{T}_0} &= H_\kappa(Q^2,\mu_H)U_H(\mu_H,\mu)\\ &\times\int[B_{k_a}(t_a,x_a,\mu_B)\otimes U_B(\mu_B,\mu)][B_{k_b}(t_b,x_b,\mu_B)\otimes U_B(\mu_B,\mu)]dt_a\,dt_b\\ &\times\left[S_\kappa\left(\mathcal{T}_0-\frac{t_a+t_b}{Q},\mu_S\right)\right].\end{aligned}\tag{3.4}$$

We abbreviated the convolution over internal variables using the symbol $\otimes$. In the formula above the large logarithms arising from ratios of disparate scales have been resummed by RGE factors $U_i(\mu_i,\mu)$.

3.2 GENEVA formulas

In this section we will describe the general formulas for the matching between FO predictions and resummation. All these details can be found in Refs. [1, 39, 43–47].

As previously mentioned, GENEVA employs the infrared-safe resolution variables $\mathcal{T}_0$ and $\mathcal{T}_1$ to discriminate between events which are classified as having 0- (Φ_0), 1- (Φ_1) or 2- (Φ_2) jets. This is done by comparing the value of the resolution variables with two cutoffs, $\mathcal{T}_0^{\rm cut}$ and $\mathcal{T}_1^{\rm cut}$, for each configuration generated. In practice, emissions below the resolution cutoff $\mathcal{T}_N < \mathcal{T}_N^{\rm cut}$ are considered unresolved and are integrated over. According to Ref. [28], the cutoff on the zero-jettiness allows the discrimination between 0- and 1-partons in the final state, while the cutoff on the one-jettiness discriminates between 1- and 2-partons. Each generated event is distributed according to the following Monte Carlo (MC) cross sections

$$\begin{aligned}\Phi_0 \text{ events}: &\quad \frac{\mathrm{d}\sigma_0^{\rm MC}}{\mathrm{d}\Phi_0}(\mathcal{T}_0^{\rm cut})\\ \Phi_1 \text{ events}: &\quad \frac{\mathrm{d}\sigma_1^{\rm MC}}{\mathrm{d}\Phi_1}(\mathcal{T}_0>\mathcal{T}_0^{\rm cut};\mathcal{T}_1^{\rm cut})\\ \Phi_2 \text{ events}: &\quad \frac{\mathrm{d}\sigma_2^{\rm MC}}{\mathrm{d}\Phi_2}(\mathcal{T}_0>\mathcal{T}_0^{\rm cut};\mathcal{T}_1>\mathcal{T}_1^{\rm cut})\,.\end{aligned}\tag{3.5}$$

Within this framework, the IR safety of each event at each perturbative order is ensured. In the Φ_1 events, configurations with two partons in the final state that do not satisfy the condition $\mathcal{T}_1 > \mathcal{T}_1^{\rm cut}$ are also considered. These configurations have to be projected onto the

phase space with one parton less, which can be achieved using a mapping from Φ_2 to Φ_1. Similarly, the Φ_0 events contain also the configurations with one parton in the final state that have $\mathcal{T}_0 < \mathcal{T}_0^{\text{cut}}$. These configurations are projected through a mapping from Φ_1 to Φ_0. Also the two-partons configurations with $\mathcal{T}_0 < \mathcal{T}_0^{\text{cut}}$ and $\mathcal{T}_1 < \mathcal{T}_1^{\text{cut}}$ are considered Φ_0 events, and they are projected through a composition of the $\Phi_2 \to \Phi_1$ and $\Phi_1 \to \Phi_0$ mappings. Not all the Φ_{N+1} configurations can be projected onto the phase space with one parton less, i.e. can be mapped to a valid Φ_N configuration. Therefore, the Φ_1 and Φ_2 configurations can be divided into projectable and non-projectable ones. Since the mapping has to be infrared-safe, all the configurations close to an infrared limit must be projectable, while the non-projectable ones are free from QCD singularities. By these projections, we ensure that the NNLO accuracy is reached for the cross section with Φ_0 events, the NLO one for the cross section with Φ_1 events and, lastly, the LO one for the cross section with Φ_2 events. In general, the cross section for any observable X will be defined as

$$\begin{aligned}\sigma(X) = &\int \frac{\mathrm{d}\sigma_0^{\text{MC}}}{\mathrm{d}\Phi_0}(\mathcal{T}_0^{\text{cut}})\mathcal{O}(\Phi_0)\,\mathrm{d}\Phi_0 + \int \frac{\mathrm{d}\sigma_1^{\text{MC}}}{\mathrm{d}\Phi_1}(\mathcal{T}_0 > \mathcal{T}_0^{\text{cut}}; \mathcal{T}_1^{\text{cut}})\mathcal{O}(\Phi_1)\,\mathrm{d}\Phi_1 \\ &+ \int \frac{\mathrm{d}\sigma_2^{\text{MC}}}{\mathrm{d}\Phi_2}(\mathcal{T}_0 > \mathcal{T}_0^{\text{cut}}; \mathcal{T}_1 > \mathcal{T}_1^{\text{cut}})\mathcal{O}(\Phi_2)\,\mathrm{d}\Phi_2\,, \end{aligned} \tag{3.6}$$

where $\mathcal{O}(\Phi_N)$ is the function that computes the observable X for the N-parton final state Φ_N. Note that this cross section is not exactly equal to the fixed-order result. This is due to the unresolved emissions for which the observable is computed on the projected phase space points instead of the exact phase space points. This difference vanishes in the limit $\mathcal{T}_N^{\text{cut}} \to 0$, so its value should be as small as possible. Small values of $\mathcal{T}_N^{\text{cut}}$ are directly linked to the appearance of large logarithms of the ratio of $\mathcal{T}_N$ and $\mathcal{T}_N^{\text{cut}}$, which are then resummed in GENEVA.

We can now give the differential cross section implemented in our generator. Considering the exclusive 0-jet cross section, we can write it as

$$\frac{\mathrm{d}\sigma_0^{\text{MC}}}{\mathrm{d}\Phi_0}(\mathcal{T}_0^{\text{cut}}) = \frac{\mathrm{d}\sigma^{\text{NNLL}'}}{\mathrm{d}\Phi_0}(\mathcal{T}_0^{\text{cut}}) + \frac{\mathrm{d}\sigma^{\text{nons}}}{\mathrm{d}\Phi_0}(\mathcal{T}_0^{\text{cut}}), \tag{3.7}$$

where the first term is the resummed contribution introduced in Eq. (3.4) integrated in $\mathcal{T}_0$, the second represents the nonsingular term containing contributions that vanish as $\mathcal{T}_0^{\text{cut}} \to 0$. In order to get NNLO_0[2] accuracy, the nonsingular matching contribution has to be

$$\frac{\mathrm{d}\sigma^{\text{nons}}}{\mathrm{d}\Phi_0}(\mathcal{T}_0^{\text{cut}}) = \frac{\mathrm{d}\sigma^{\text{NNLO}_0}}{\mathrm{d}\Phi_0}(\mathcal{T}_0^{\text{cut}}) - \left[\frac{\mathrm{d}\sigma^{\text{NNLL}'}}{\mathrm{d}\Phi_0}(\mathcal{T}_0^{\text{cut}})\right]_{\text{NNLO}_0}. \tag{3.8}$$

The first contribution is the FO, while the second is the FO expansion to $\mathcal{O}(\alpha_S^2)$ of the resummed cumulant. One can think of move as much of the nonsingular contributions as possible into the resolved region of the phase space, while maintaining the IR safety requirements. In this way the phase space can be better described with the full event kinematics. Therefore, in GENEVA is possible to replace the cut on the zero-jettiness with two separate cuts: $\mathcal{T}_{0,\text{re}}^{\text{cut}}$ acting only on the resummed singular contribution, and $\mathcal{T}_{0,\text{ns}}^{\text{cut}}$ acting on the nonsingular term. The idea

[2]With N^kLO_l we refer to the FO calculation at k-th order in QCD for the final state with l resolved jets.

is to chose $\mathcal{T}_{0,\mathrm{ns}}^{\mathrm{cut}}$ smaller than $\mathcal{T}_{0,\mathrm{re}}^{\mathrm{cut}}$, in order to push down the calculation of the nonsingular contributions to lower values. Note, however, that the result should be independent of the exact choice of $\mathcal{T}_{0,\mathrm{re}}^{\mathrm{cut}}$, modulo higher-order corrections. We are going to show this later, for the particular case of the double Higgs boson production.

Having said that, the exclusive 0-jet cross section is defined as

$$\begin{aligned}\frac{\mathrm{d}\sigma_0^{\mathrm{MC}}}{\mathrm{d}\Phi_0}(\mathcal{T}_{0,\mathrm{re}}^{\mathrm{cut}},\mathcal{T}_{0,\mathrm{ns}}^{\mathrm{cut}}) = \frac{\mathrm{d}\sigma^{\mathrm{NNLL'}}}{\mathrm{d}\Phi_0}(\mathcal{T}_{0,\mathrm{re}}^{\mathrm{cut}}) - \frac{\mathrm{d}\sigma^{\mathrm{NNLL'}}}{\mathrm{d}\Phi_0}(\mathcal{T}_{0,\mathrm{ns}}^{\mathrm{cut}})\Big|_{\mathrm{NNLO}_0} \\ + (B_0+V_0+W_0)(\Phi_0) + \int \frac{\mathrm{d}\Phi_1}{\mathrm{d}\Phi_0}(B_1+V_1)(\Phi_1)\,\theta\big(\mathcal{T}_0(\Phi_1)<\mathcal{T}_{0,\mathrm{ns}}^{\mathrm{cut}}\big) \\ + \int \frac{\mathrm{d}\Phi_2}{\mathrm{d}\Phi_0}\,B_2(\Phi_2)\,\theta\big(\mathcal{T}_0(\Phi_2)<\mathcal{T}_{0,\mathrm{ns}}^{\mathrm{cut}}\big)\,, \end{aligned} \tag{3.9}$$

where, from now on, B_N defines the N-parton tree-level contributions, V_N is the N-parton one-loop contributions and W_0 is the two-loop contributions. We have introduced the notation

$$\frac{\mathrm{d}\Phi_M}{\mathrm{d}\Phi_N} = \mathrm{d}\Phi_M\,\delta[\Phi_N-\Phi_N(\Phi_M)], \qquad N\le M\,, \tag{3.10}$$

to denote the radiation phase space Φ_M limited to those configurations that are projected onto the Φ_N phase space.
Moving to the 1-jet cross section, we can repeat the same strategy used for the 0-jet cross section and write

$$\begin{aligned}\frac{\mathrm{d}\sigma_1^{\mathrm{MC}}}{\mathrm{d}\Phi_1}(\mathcal{T}_0>\mathcal{T}_{0,\mathrm{ns}}^{\mathrm{cut}};\mathcal{T}_{0,\mathrm{re}}^{\mathrm{cut}};\mathcal{T}_1^{\mathrm{cut}}) = \Bigg\{\frac{\mathrm{d}\sigma^{\mathrm{NNLL'}}}{\mathrm{d}\Phi_0\mathrm{d}\mathcal{T}_0}\mathcal{P}(\Phi_1)\,\theta(\mathcal{T}_0>\mathcal{T}_{0,\mathrm{re}}^{\mathrm{cut}}) \\ + \Bigg[(B_1+V_1^C)(\Phi_1) - \frac{\mathrm{d}\sigma^{\mathrm{NNLL'}}}{\mathrm{d}\Phi_0\mathrm{d}\mathcal{T}_0}\Big|_{\mathrm{NLO}_1}\mathcal{P}(\Phi_1)\Bigg]\theta(\mathcal{T}_0>\mathcal{T}_{0,\mathrm{ns}}^{\mathrm{cut}})\Bigg\}\times U_1(\Phi_1,\mathcal{T}_1^{\mathrm{cut}}) \\ + \int\Bigg[\frac{\mathrm{d}\Phi_2}{\mathrm{d}\Phi_1^{\mathcal{T}}}\,B_2(\Phi_2)\,\theta\big(\mathcal{T}_0(\Phi_2)>\mathcal{T}_{0,\mathrm{ns}}^{\mathrm{cut}}\big)\;\theta(\mathcal{T}_1<\mathcal{T}_1^{\mathrm{cut}}) - \frac{\mathrm{d}\Phi_2}{\mathrm{d}\Phi_1^{C}}\,C_2(\Phi_2)\,\theta(\mathcal{T}_0>\mathcal{T}_{0,\mathrm{ns}}^{\mathrm{cut}})\Bigg] \\ - B_1(\Phi_1)\,U_1^{(1)}(\Phi_1,\mathcal{T}_1^{\mathrm{cut}})\,\theta(\mathcal{T}_0>\mathcal{T}_{0,\mathrm{ns}}^{\mathrm{cut}})\,. \end{aligned} \tag{3.11}$$

We have introduced a new shorthand notation

$$\frac{\mathrm{d}\Phi_M}{\mathrm{d}\Phi_N^{\mathcal{T}}} = \mathrm{d}\Phi_M\,\delta[\Phi_N-\Phi_N^{\mathcal{T}}(\Phi_M)]\,\Theta^{\mathcal{T}}(\Phi_M), \qquad N\le M\,, \tag{3.12}$$

to indicate that the integration over a region of the M-body phase space is done keeping the N-body phase space and the value of the observable $\mathcal{T}$ fixed. The $\Theta^{\mathcal{T}}(\Phi_N)$ term limits the integration region to the phase space points included in the singular contribution for the observable $\mathcal{T}$. The V_1^C term includes contributions of soft and collinear origin and it is defined as

$$V_1^C(\Phi_1) = V_1(\Phi_1) + \int\frac{\mathrm{d}\Phi_2}{\mathrm{d}\Phi_1^C}\,C_2(\Phi_2)\,, \tag{3.13}$$

where C_2 acts as a local NLO subtraction counterterm that reproduces the singular behaviour of B_2. The subtraction counterterms are integrated over the radiation variables $\frac{\mathrm{d}\Phi_2}{\mathrm{d}\Phi_1^C}$ considering the singular limit C of the phase space mapping.
Note also that in Eq. (3.11) the resummed and resummed expanded contributions are multiplied by a normalized splitting function $\mathcal{P}(\Phi_1)$. This function has been introduced to make the resummed $\mathcal{T}_0$ spectrum fully differential in Φ_1. In general, these splitting functions $\mathcal{P}(\Phi_{N+1})$ are normalized such that

$$\int \mathcal{P}(\Phi_{N+1}) \frac{\mathrm{d}\Phi_{N+1}}{\mathrm{d}\Phi_N \, \mathrm{d}\mathcal{T}_N} = 1, \tag{3.14}$$

where, besides $\mathcal{T}_N$, the energy ratio z and the azimuthal angle ϕ are needed to define the $\Phi_N \to \Phi_{N+1}$ splitting. Its definition is given by

$$\mathcal{P}\left(\Phi_{N+1}\right) = \frac{f_{kj}\left(\Phi_N, \mathcal{T}_N, z\right)}{\sum\limits_{k'=1}^{N+2} \int_{z_{\min}^{k'}(\Phi_N,\mathcal{T}_N)}^{z_{\max}^{k'}(\Phi_N,\mathcal{T}_N)} \mathrm{d}z' J_{k'}\left(\Phi_N, \mathcal{T}_N, z'\right) I_\phi^{k'}\left(\Phi_N, \mathcal{T}_N, z'\right) \sum\limits_{j'=1}^{n_{\text{split}}^{k'}} f_{k'j'}\left(\Phi_N, \mathcal{T}_N, z'\right)}, \tag{3.15}$$

where

$$I_\phi^k\left(\Phi_N, \mathcal{T}_N, z\right) = \phi_{\max}^k\left(\Phi_N, \mathcal{T}_N, z\right) - \phi_{\min}^k\left(\Phi_N, \mathcal{T}_N, z\right). \tag{3.16}$$

In the formula above $f_{kj}\left(\Phi_N, \mathcal{T}_N, z\right)$ are generic functions based on the Altarelli-Parisi splitting functions, depending if the radiation is in the initial (ISR) or final (FSR) state

$$\begin{aligned} f_{kj}\left(\Phi_N, \mathcal{T}_N, z\right) &= \frac{f(x_M/z, \mu)}{f(x_S, \mu)} \qquad \text{for ISR}, \\ f_{kj}\left(\Phi_N, \mathcal{T}_N, z\right) &= \mathrm{AP}_{\mathrm{sp}}(z, \phi) \qquad \text{for FSR}, \end{aligned} \tag{3.17}$$

where $f(x, \mu)$ are the standard parton distribution functions (considering a $M \to DS$ splitting, with M the mother and S the sister) and $\mathrm{AP}_{\mathrm{sp}}$ are the unregularised Altarelli-Parisi splitting function. In Eq. (3.15) we introduced $z_{\min,\max}(\Phi_N, \mathcal{T}_N, z)$, $\phi_{\min,\max}(\Phi_N, \mathcal{T}_N, z)$ that are the integration limits, respectively, in z and ϕ and $J\left(\Phi_N, \mathcal{T}_N, z\right)$ the Jacobian related to the change of variable. One of the latest novelties in the GENEVA framework is the new implementation of these splitting functions. All the details about this new implementation can be found in Refs. [47,48], but the idea is to compute the integral appearing in the denominator of Eq. (3.15) for each configuration generated. In order to do this, the integration limits on z and ϕ and the Jacobian $J\left(\Phi_N, \mathcal{T}_N, z\right)$ need to be computed both for the $0 \to 1$ and $1 \to 2$ mappings. We just want to stress that for the $0 \to 1$ splitting, the PDFs are evaluated at the exact momentum fractions $x_{a,b}(z)$ of the real emission phase space Φ_1, reproducing the correct soft and collinear limit. In the $1 \to 2$ splitting case, instead, $x_{a,b}$ also depend on ϕ, and they are approximated dropping this additional dependence, representing an improvement with respect to the strict collinear limit.

Last element in Eq. (3.11) to be introduced is $U_1(\Phi_1, \mathcal{T}_0^{\mathrm{cut}})$. This is the Sudakov factor which resums the dependence of $\mathcal{T}_1^{\mathrm{cut}}$ to next-to-leading-logarithmic (NLL) accuracy. The symbol $U_1^{(1)}$ represents its $\mathcal{O}(\alpha_S)$ expansion.

The remain cross section to be define is the 2-jet one, given by

$$\begin{aligned}
&\frac{\mathrm{d}\sigma^{\mathrm{MC}}_{\geq 2}}{\mathrm{d}\Phi_2}(\mathcal{T}_0 > \mathcal{T}^{\mathrm{cut}}_{0,\mathrm{ns}}; \mathcal{T}^{\mathrm{cut}}_{0,\mathrm{re}}; \mathcal{T}_1 > \mathcal{T}^{\mathrm{cut}}_1) = \qquad (3.18)\\
&\quad \left\{ \left[(B_1 + V_1^C)(\Phi_1) - \frac{\mathrm{d}\sigma^{\mathrm{NNLL}'}}{\mathrm{d}\Phi_0 \mathrm{d}\mathcal{T}_0}\Big|_{\mathrm{NLO}_1} \mathcal{P}(\Phi_1) \right] \theta(\mathcal{T}_0 > \mathcal{T}^{\mathrm{cut}}_{0,\mathrm{ns}})\Big|_{\Phi_1 = \Phi_1^{\mathcal{T}}(\Phi_2)} \right]\\
&\quad + \frac{\mathrm{d}\sigma^{\mathrm{NNLL}'}}{\mathrm{d}\Phi_0 \mathrm{d}\mathcal{T}_0}\, \mathcal{P}(\Phi_1)\, \theta(\mathcal{T}_0 > \mathcal{T}^{\mathrm{cut}}_{0,\mathrm{re}})\Big|_{\Phi_1 = \Phi_1^{\mathcal{T}}(\Phi_2)} \Bigg\} U_1'(\Phi_1, \mathcal{T}_1)\, \mathcal{P}(\Phi_2)\, \theta(\mathcal{T}_1 > \mathcal{T}^{\mathrm{cut}}_1)\\
&\quad + B_2(\Phi_2)\, \theta(\mathcal{T}_1 > \mathcal{T}^{\mathrm{cut}}_1) \theta\left(\mathcal{T}_0(\Phi_2) > \mathcal{T}^{\mathrm{cut}}_{0,\mathrm{ns}}\right)\\
&\quad - B_1(\Phi_1^{\mathcal{T}})\, U_1^{(1)'}\left(\Phi_1, \mathcal{T}_1\right) \mathcal{P}(\Phi_2)\, \Theta(\mathcal{T}_1 > \mathcal{T}^{\mathrm{cut}}_1)\, \theta\left(\mathcal{T}_0(\Phi_2) > \mathcal{T}^{\mathrm{cut}}_{0,\mathrm{ns}}\right) .
\end{aligned}$$

Here U_1' is the first derivative of $U_1(\Phi_1, \mathcal{T}_1)$ with respect to $\mathcal{T}_1$, and $U_1'^{(1)}$ its $\mathcal{O}(\alpha_S)$ expansions.

We can assign a cross section to all the non-projectable Φ_1 and Φ_2 events. These can be due to an invalid flavour projection or come from points in the phase space not covered by the $\mathcal{T}_0$-preserving mapping. Their cross section is defined as

$$\frac{\mathrm{d}\sigma^{\mathrm{MC}}_1}{\mathrm{d}\Phi_1}(\mathcal{T}_0 \leq \mathcal{T}^{\mathrm{cut}}_{0,\mathrm{ns}}; \mathcal{T}^{\mathrm{cut}}_1) = (B_1 + V_1)(\Phi_1)\, \overline{\Theta}^{\mathrm{FKS}}_{\mathrm{map}}(\Phi_1)\, \theta(\mathcal{T}_0 < \mathcal{T}^{\mathrm{cut}}_{0,\mathrm{ns}}) , \qquad (3.19)$$

$$\frac{\mathrm{d}\sigma^{\mathrm{MC}}_{\geq 2}}{\mathrm{d}\Phi_2}(\mathcal{T}_0 > \mathcal{T}^{\mathrm{cut}}_{0,\mathrm{ns}}; \mathcal{T}_1 \leq \mathcal{T}^{\mathrm{cut}}_1) = B_2(\Phi_2)\, \overline{\Theta}^{\mathcal{T}}_{\mathrm{map}}(\Phi_2)\, \theta(\mathcal{T}_1 < \mathcal{T}^{\mathrm{cut}}_1)\, \theta\left(\mathcal{T}_0(\Phi_2) > \mathcal{T}^{\mathrm{cut}}_{0,\mathrm{ns}}\right) . \qquad (3.20)$$

With $\Theta^{\mathrm{X}}_{\mathrm{map}}$ we define the constraints due to the projections in the two mappings: the FKS map in the case of the $\Phi_1 \to \Phi_0$ projection and the $\mathcal{T}_0$-preserving map for the $\Phi_2 \to \Phi_1$ projection. The overlined versions represent their complements.

3.3 Shower interface in GENEVA

Before describing the actual interface to the parton shower in GENEVA, let's examine the specific case of a parton shower ordered in N-jettiness. Given that the resummation in GENEVA is performed in $\mathcal{T}_N$, this case represents the simplest case to match the resummed prediction with the shower. The interface to a parton shower plays a crucial role, as it must ensure a smooth transition between the hard scattering process and the subsequent parton shower evolution, preventing any compromise to the accuracy of both calculations. In order to understand how this can be achieved, consider the specific case where the parton shower is ordered using the same variable as the one employed for resummation in the GENEVA framework, a parton shower organized in N-jettiness.

As already mentioned, the N-jettiness represents the hardness of the emission, and in the singular limit we can assume that the direction of the axes needed in the definition of $\mathcal{T}_N$ is aligned to the direction of the N hard partons. Calling $\mathcal{T}_{N-1}$ the N-jettiness after N emissions and $\mathcal{T}_N$ the $(N+1)$-jettiness after one emission, the single emission can be expressed using

the probability of branching and no-branching and incorporating a Sudakov factor Δ_N and the splitting probability $\mathcal{P}$, as

$$S^{(1)} = \Delta_N(\mathcal{T}_N^{\max}, \Lambda) + \Delta'_N(\mathcal{T}_N^{\max}, \mathcal{T}_N)\, \frac{\mathrm{d}\Phi_{N+1}}{\mathrm{d}\Phi_N}\, \mathcal{P}(\Phi_{N+1})\, \theta(\mathcal{T}_N^{\max} > \mathcal{T}_N > \Lambda)\,. \tag{3.21}$$

Here, $\mathcal{T}_N^{\max}$ is the maximum possible allowed value of $\mathcal{T}_N$ limited by the hardness of the configuration before the emission (hence $\mathcal{T}_N^{\max} \sim \mathcal{T}_{N-1}$) and Λ is the shower cutoff. In Eq. (3.21), Δ'_N denotes the derivative of the Sudakov form factor with respect to $\mathcal{T}_N$, and $\Delta'_N(\mathcal{T}_N^{\max}, \mathcal{T}_N)\, \mathcal{P}(\Phi_{N+1})$ gives the probability of an additional emission with respect to the one already considered. Since the N-jettiness is the resolution scale considered for now, we have assumed the following strong ordering

$$\mathcal{T}_{N+1} \ll \mathcal{T}_N\,. \tag{3.22}$$

This condition ensures that emissions coming from the shower will not interfere with the Sudakov of the resummation. The generalization of Eq. (3.21) with the ordering specified in Eq. (3.22) will allow to construct a shower in the N-jettiness variable. However, in the GENEVA framework we have to face that the three showers to which we interface our results use a different resolution scale, namely, the transverse momentum of the emission, and we have also to ensure that the accuracy of our resummation and the accuracy of the shower are both preserved. Therefore, matching our GENEVA results to a parton shower ordered by transverse momentum is not a straightforward process. Let's see in detail how it can be done.

In our Monte Carlo event generator, the resummation is performed in $\mathcal{T}_N$, starting from a hard scale Q down to a lower scale $\mathcal{T}_N^c$. A graphical illustration of this can be seen in Fig. 3.1, where the Lund plane (ACD triangle) represents all the kinematic space available for possible emissions. Each emission is represented as a point, with the central region of the plane occupied by soft and collinear emissions, the region near the $z = 1$ line populated by hard-collinear emissions, and the vertical line housing soft large-angle emissions.

GENEVA produces events with 0, 1 or 2 final-state partonic jets, and for each of them, different lower scales for the resummation are set, corresponding to $\mathcal{T}_{0,\mathrm{re}}^{\mathrm{cut}}$, $\mathcal{T}_1^{\mathrm{cut}}$ and $\mathcal{T}_1(\Phi_2)$, respectively. These three scales corresponds to a diagonal line on the Lund Plane, dividing it into two parts. The ACE triangle represents the resummation region, where emissions are prohibited. At leading logarithmic accuracy, the integral over this region corresponds to the Sudakov form factor of the shower, as it gives the probability of no-emission.

Since the showers considered are ordered in transverse momentum, we need to translate the lower scales for the resummation into this variable. For each N-partonic jets, their intersection with the maximum available energy fraction that an emission can have (E) determines the maximum relative transverse momentum of the emission ($k_T(\mathcal{T}_N^c)$).[3] This delineates the shower region, forming the BCDE trapezium. However, the BCE triangle is shared by both the

[3]The maximum allowed value for the transverse momentum of the hardest emission can be computed as

$$k_T = \sqrt{\hat{k}_0^2 - \hat{k}_3^2} = \sqrt{\mathcal{T}_N(\hat{k}_0 + \hat{k}_3)} \leq \sqrt{\mathcal{T}_N \sqrt{s}} < \sqrt{\mathcal{T}_N^{\mathrm{hard}} \sqrt{s}}\,, \tag{3.23}$$

having used $\mathcal{T}_N = \hat{k}_0 - \hat{k}_3$.

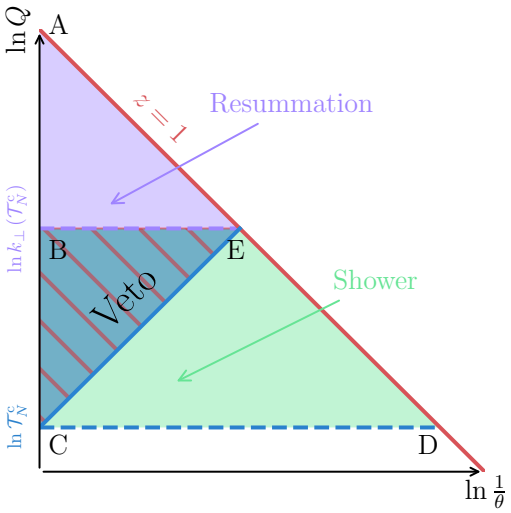

Figure 3.1: Lund Plane representation of shower emissions after the first two performed by GENEVA, taken from [1].

resummation and shower regions, implying that the shower could potentially produce emissions in the resummation region, thereby spoiling its accuracy. To address this issue, we introduce a veto procedure. Any event for which, after the shower,

$$\mathcal{T}_N > \mathcal{T}_N^c \tag{3.24}$$

is discarded and retried.

Let's examine in detail how the shower affects each of the GENEVA jet-regions. In the case of Φ_0 events, they are showered with the requirement that the emission has $\mathcal{T}_0 < \mathcal{T}_{0,\mathrm{re}}^{\mathrm{cut}}$. For these events GENEVA only predicts the normalization and not the distribution in $\mathcal{T}_0$. The shower will provide the missing $\mathcal{T}_0$ shape below the cutoff, and due to the unitarity constraint, it will not change the normalization of these events. For $N \geq 1$ final-state partons, the zero-jettiness at the partonic level is spoiled by the shower by an amount of $\mathcal{T}_N \ll \mathcal{T}_0$. Typically, this variation is small enough to be ignored, but for Φ_1 events, it can lead to large numerical deviations. Therefore, the first shower emission $\Phi_1 \to \Phi_2$ is performed by hand in GENEVA using a $\mathcal{T}_0$-preserving mapping. Lastly, for Φ_2 events, emissions are vetoed by Eq. (3.22) and it will be shown later that the parton shower only affects the $\mathcal{T}_0$ spectrum beyond NNLL′. With that in mind, and following Eq. (3.21), we decompose the N-jet differential cross sections events into two pieces, adding emissions up to two partons. For the 0-jet region we get

$$\frac{\mathrm{d}\sigma_0^{\mathrm{MC}}}{\mathrm{d}\Phi_0}(\mathcal{T}_{0,\mathrm{re}}^{\mathrm{cut}};\, \Lambda_0) = \frac{\mathrm{d}\sigma_0^{\mathrm{MC}}}{\mathrm{d}\Phi_0}(\mathcal{T}_{0,\mathrm{re}}^{\mathrm{cut}})\, U_0(\mathcal{T}_{0,\mathrm{re}}^{\mathrm{cut}}, \Lambda_0)\,, \tag{3.25}$$

where U_0 represents the Sudakov factor associated with the shower emissions. For Φ_1 events

we have

$$\frac{\mathrm{d}\sigma_1^{\mathrm{MC}}}{\mathrm{d}\Phi_1}(\mathcal{T}_0 > \Lambda_0, \mathcal{T}_{0,\mathrm{re}}^{\mathrm{cut}}; \mathcal{T}_1^{\mathrm{cut}}; \Lambda_1) = \frac{\mathrm{d}\sigma_1}{\mathrm{d}\Phi_1}(\mathcal{T}_0 > \mathcal{T}_{0,\mathrm{re}}^{\mathrm{cut}}, \mathcal{T}_1^{\mathrm{cut}})\, U_1(\mathcal{T}_1^{\mathrm{cut}}, \Lambda_1) + \frac{\mathrm{d}}{\mathrm{d}\mathcal{T}_0}\frac{\mathrm{d}\sigma_0^{\mathrm{MC}}}{\mathrm{d}\Phi_0}(\mathcal{T}_{0,\mathrm{re}}^{\mathrm{cut}}; \mathcal{T}_0)\, \mathcal{P}(\Phi_1)\, \theta(\mathcal{T}_{0,\mathrm{re}}^{\mathrm{cut}} > \mathcal{T}_0 > \Lambda_0)\, U_1(\mathcal{T}_1^{\mathrm{max}}, \Lambda_1)\,, \tag{3.26}$$

where the first term corresponds to the emission of a single parton with $\mathcal{T}_0$ and $\mathcal{T}_1$ satisfying the cutoff conditions, and the second term accounts for additional emissions from Φ_0 events. For Φ_2 events, instead, we have

$$\frac{\mathrm{d}\sigma_{\geq 2}^{\mathrm{MC}}}{\mathrm{d}\Phi_2}(\mathcal{T}_0 > \Lambda_0, \mathcal{T}_1 > \Lambda_1, \mathcal{T}_{0,\mathrm{re}}^{\mathrm{cut}}, \mathcal{T}_1^{\mathrm{cut}}) = \frac{\mathrm{d}\sigma_{\geq 2}^{\mathrm{MC}}}{\mathrm{d}\Phi_2}(\mathcal{T}_0 > \mathcal{T}_{0,\mathrm{re}}^{\mathrm{cut}}, \mathcal{T}_1^{\mathrm{cut}}) + \frac{\mathrm{d}}{\mathrm{d}\mathcal{T}_1}\frac{\mathrm{d}\sigma_1^{\mathrm{MC}}}{\mathrm{d}\Phi_1}(\mathcal{T}_0 > \Lambda_0, \mathcal{T}_{0,\mathrm{re}}^{\mathrm{cut}}, \mathcal{T}_1^{\mathrm{cut}}, \mathcal{T}_1)\, \mathcal{P}(\Phi_2)\, \theta(\tilde{\mathcal{T}}_1^{\mathrm{max}} > \mathcal{T}_1 > \Lambda_1)\,, \tag{3.27}$$

where the first term corresponds to events with at least two partons emitted with $\mathcal{T}_0$ and $\mathcal{T}_1$ satisfying the cutoff conditions, and the second term accounts for additional emissions from Φ_1 events. $\tilde{\mathcal{T}}_1^{\mathrm{max}}$ can be equal to $\mathcal{T}_1^{\mathrm{cut}}$ or $\mathcal{T}_1^{\mathrm{max}}$ depending on wheter the derivative is on the first or second term of Eq. (3.26). In the above equations, Λ_N for $N = 0, 1$ is a jet resolution parameter.

In the remainder of this section we give an argument to show that no single shower emission can end up in the vetoed region, and consequently that the parton shower acting on the jet events does not affect the NNLL′ accuracy of the $\mathcal{T}_0$ spectrum. Recalling that for any given final-state multiplicity N, $\mathcal{T}_M(\Phi_N) = 0$ for any $M \leq N$ and that for any one emission from the parton shower that produces a final state with $N+1$ partons $\mathcal{T}_M(\Phi_{N+1}) = \mathcal{T}$, we apply the shower to a configuration with two partons Φ_2. For this particular case, the starting scale of the shower will be determined by the hardness of the configuration itself, so $\mathcal{T}_N^c = \mathcal{T}_1(\Phi_2)$ and the starting scale will be $k_T(\mathcal{T}_1(\Phi_2))$. One additional emission of the shower will have a hardness of $\mathcal{T} = \mathcal{T}_2(\Phi_3)$ which will be smaller than $\mathcal{T}_N^c$ for the veto condition. Considering a second emission, its hardness will be $\mathcal{T} = \mathcal{T}_3(\Phi_4) \leq \mathcal{T}_2(\Phi_4)$ which has to be smaller than $\mathcal{T}_1(\Phi_2)$ to satisfy the veto. The relation $\mathcal{T}_3(\Phi_4) \leq \mathcal{T}_2(\Phi_4)$ follows because the N-jettiness is an additive variable of strictly positive terms, so more in general we can write

$$\mathcal{T}_N(\Phi_M) \geq \mathcal{T}_{N+1}(\Phi_M)\,. \tag{3.28}$$

Basically we have constructed the following chain of inequalities[4]

$$\mathcal{T}_3(\Phi_4) \leq \mathcal{T}_2(\Phi_4) \leq \mathcal{T}_N^c = \mathcal{T}_1(\Phi_2)\,. \tag{3.29}$$

We can generalize this chain iterating the same procedure for k additional shower emissions, obtaining

$$\mathcal{T}_{N+k-1}(\Phi_{N+k}) \leq \mathcal{T}_{N+k-2}(\Phi_{N+k}) \leq \cdots \leq \mathcal{T}_N(\Phi_{N+k}) \leq \mathcal{T}_N^c\,. \tag{3.30}$$

[4]This argument does not impose any ordering between the hardness of the two emissions, $\mathcal{T}_2(\Phi_3)$ and $\mathcal{T}_3(\Phi_4)$, it just implies that they are both lower than $\mathcal{T}_N^c = \mathcal{T}_1(\Phi_2)$.

This implies that also the hardness of each of the k-th emissions has to be smaller than $\mathcal{T}_N^c$. This means that the final events accepted after the veto could always be generated via a sequence of $\mathcal{T}$-ordered emissions. Moreover, since the N-jettiness is additive, the hardness of the first emission is constrained by the veto to be lower than the lower resummation scale. Note also that the resummation region has a higher accuracy than that of the shower, and in the shower region there is no double-counted contribution. Therefore the accuracy of any observable computed with this matching is at least as accurate as the parton shower is.

Chapter 4

Double Higgs boson production

In this chapter we present the double Higgs boson production, describing its production modes and the current state of the calculation in the literature, both in the Standard Model and in the effective theory approach. We highlight the potential implications given by the study of such process for the understanding of fundamental physics.

One of the main goal of the forthcoming runs at LHC is to explore all the properties of the Higgs boson and, in particular, to access to its self-interactions. This would enable us to reconstruct the scalar potential of the Higgs doublet field Φ, which is responsible for the spontaneous electroweak symmetry breaking. The potential is defined as

$$V_H = \mu^2 \, \Phi^\dagger \, \Phi + \frac{1}{2} \lambda \, (\Phi^\dagger \, \Phi)^2 \, , \tag{4.1}$$

where $\lambda = \frac{m_H^2}{v^2}$, $\mu^2 = -\frac{1}{2} m_H^2$, m_H the mass of the Higgs boson and $v = 246$ GeV the vacuum expectation value (VEV). Introducing a physical Higgs boson field in the potential leads to the trilinear Higgs self-coupling λ_{HHH}, given by

$$\lambda_{HHH} = \frac{3 \, m_H^2}{v} \, . \tag{4.2}$$

It is important to note that the trilinear coupling only depends on the Higgs boson mass and the VEV. Its value is directly linked to the shape of the scalar potential, and consequently, it raises various open questions about cosmology and particle physics, such as the nature of the Higgs boson (whether it is an elementary particle or not). Additionally, an improved knowledge of the Higgs coupling will be relevant for single Higgs measurements and the exploration of Beyond the Standard Model (BSM) physics.

The trilinear coupling can be directly measured in the production of two Higgs bosons. There are also indirect methods of estimating the self-coupling by exploiting electroweak corrections in high precision observables, as shown in Refs. [49–51]. Unfortunately, the cross section for the double Higgs boson production is significantly smaller (around a thousand times) than the cross section for single Higgs boson production. Therefore, it is a rare and challenging process to study. At hadron colliders, several production channels exist for this

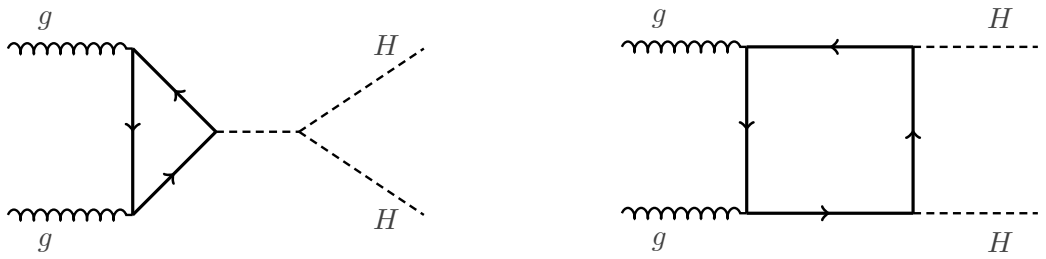

Figure 4.1: Leading order diagrams for the production of a Higgs boson pair with full top-quark mass dependence. On the left the triangle diagram, on the right the box one.

process, including gluon fusion, vector boson fusion (VBF), the top-quark associated channel and Higgsstrahlung. The gluon fusion channel contributes the most to the process, accounting for over 90% of the total inclusive cross section, which is approximately 35 fb at the collider energy $\sqrt{S} = 13$ TeV. At the same energy, the VBF channel contributes around 1.7 fb, the production of a pair of Higgs bosons in association with the W boson is approximately 0.50 fb, while in association with the Z boson it is about 0.36 fb. Finally, the top-quark associated channel contributes around 0.8 fb [52]. For the rest of this thesis, we will focus only on the gluon fusion mode being the dominant production mode for such process.

Since the Higgs boson does not have colour charge and it is not massless, it couples to gluons only through a quark loop, both top-quark and bottom-quark loops. However, the case with a bottom-quark loop can be neglected due to its small percentage of the total cross section.[1]

In gluon fusion, the production of two Higgs bosons through a top-quark loop [53] at tree level is represented by the two diagrams shown in Fig. 4.1. The diagram on the left is known as the triangle diagram, providing access to the trilinear Higgs coupling, while the one on the right is the box diagram. Although these diagrams have different topologies and contribute differently to the amplitude, the colour structure of the initial state gluons is the same. As can be seen from the figure, already at leading order we have to face a one-loop calculation [53–55], which makes the inclusion of higher-order terms particularly difficult. In the Standard Model, considering the full top-quark mass dependence, this process is known up to next-to-leading order (NLO) in QCD [56–59]. Some resummed results in the transverse momentum of the pair up to next-to-leading logarithmic (NLL) accuracy have been matched to the NLO prediction [60, 61], and a soft-gluon resummation to NLL was performed in Ref. [62]. Exact NLO results matched to the parton shower appeared in Refs. [63–65], and techniques to systematically include finite-mass effects have been studied [66–68] before the exact NLO results became available. Futhermore, several approaches towards analytical results for the two-loop amplitudes with full top-mass dependence based on different expansions, are available

[1] Also remember that, in the Standard Model, the interaction between the Higgs boson and the bottom-quark is relatively weak compared to other interactions. The strength of the interaction is proportional to the mass of the particle involved and since the bottom-quark is much lighter compared to the top-quark, the bottom-quark's contribution is relatively small.

Figure 4.2: Leading order diagrams for the production of a Higgs boson pair in the infinite top mass limit. On the left the triangle typology, on the right the box one.

see [69–80].

A simpler way to study this process is to consider the limit where the top-quark mass is much larger than the hard scale of the process, known as the infinite top mass limit ($m_t \to \infty$). In this approximation, the gluons directly couple with the Higgs bosons through an effective gluon-gluon-Higgs vertex [53] and the relative LO Feynman diagrams can be seen in Fig. 4.2. In the infinite top mass limit, NLO accuracy in QCD have been computed in Ref. [81], at next-to-next-to-leading order (NNLO) in Refs. [82, 83], and at next-to-next-to-next-to-leading order (N^3LO) in Refs. [84, 85]. Threshold resummation approximations at next-to-next-leading-logarithmic accuracy (NNLL) matched to NLO have been studied in Ref. [86], and matched to NNLO in Ref. [87].

It is important to note that the infinite top mass limit is not the optimal approximation for the double Higgs boson production process, although it simplifies the study of the production itself. This approximation is known to be less accurate for the double Higgs boson production compared to the single Higgs boson production [56, 64, 88]. One of the main issue is that this approximation receives correction of the order $\mathcal{O}\left(Q^2/m_t^2\right)$, where Q is the momentum transfer. When its value is around the peak of the invariant mass of the Higgs boson pair, M_{HH}, which is much larger than the Higgs boson mass, these corrections can be three to four times larger with respect to the single Higgs boson production. To be precise, the invariant mass of the Higgs boson pair spectrum has a wide distribution, this implies that the average M_{HH} value is much larger than the position of the peak, so the magnitude of these corrections can be even worse. Moreover, the diagrams in Fig. 4.1 interfere with each other, and this interference is large and negative causing a large overall cancellation. The same net result cannot be reached in the infinite top mass limit, because neither the box or the triangle diagrams are well approximated. This effect is due to the large energy scale (M_{HH}) that probes the top-quark loop in both the typology of diagrams, which undermines the approximation. This issue particularly affects the Higgs boson pair transverse momentum around $p_T \sim 2m_t$, where the invariant mass of the Higgs boson pair is larger than the top-quark mass and the approximation starts to break down.

To address this problem, a slightly different approximation called Heavy Top Limit (HTL) has been proposed in Ref. [89]. In the HTL approximation, higher-order terms are computed in the infinite top mass limit but properly reweighted with the exact LO cross section that includes the full top-quark mass dependence. This approach improves upon the infinite top mass limit, making it more accurate. Anyway, in order to have a realistic event generator for

the double Higgs boson production, heavy-quark mass effects need to be included, and ways to include them order-by-order using approximants have been studied [90]. However, for the purpose of this thesis, we will only consider the infinite top mass limit leaving as a future work the inclusion of the top-quark mass correction in the GENEVA framework.

Lastly, it is worth mentioning that the study of the double Higgs boson production can be extended to the context of New Physics and Effective Field Theories (EFT). Modifications to the Standard Model couplings, including the trilinear Higgs self-coupling, and the presence of novel couplings not present in the Standard Model can be explored. NLO QCD corrections including dimension 6 operators in the limit of large top-quark masses have been published in Ref. [91], as well as within the framework of a non-linearly effective field theory in Ref. [92]. NNLO QCD corrections including effects of new physics beyond the Standard Model with relevant dimension 6 operators have also been investigated in Ref. [93]. NLO predictions with full top-quark mass dependence with approximate NNLO predictions in a non-linear EFT framework are presented in Ref. [94].

Chapter 5

Higgs boson pair production in GENEVA

In this chapter we describe in detail all the GENEVA parameters set for the double Higgs boson production implementation. In particular, we discuss the choice of the resolution cutoffs, the procedure used to set all the scales entering in the GENEVA calculation, and all the ingredients needed for the resummation in the SCET formalism.

5.1 Choice of the resolution cutoff in $\mathcal{T}_0$

As discussed in Sec. 3.2, we consider two different cutoffs on the zero-jettiness, $\mathcal{T}_{0,\mathrm{ns}}^{\mathrm{cut}}$ and $\mathcal{T}_{0,\mathrm{re}}^{\mathrm{cut}}$. The first one is acting only on the nonsingular term, while the second on the resummed singular contribution. The role of $\mathcal{T}_{0,\mathrm{re}}^{\mathrm{cut}}$ is the same of the usual $\mathcal{T}_0^{\mathrm{cut}}$ previously used for all the processes implemented in GENEVA, while $\mathcal{T}_{0,\mathrm{ns}}^{\mathrm{cut}}$ is chosen much smaller in order to push down the calculation of these nonsingular contributions. It is fundamental to study how the value set for the two cutoffs affects the final theoretical prediction.

In the GENEVA framework, all the contributions below the cut on the 0-jet resolution variable are given in Eq. (3.9). This expression is NNLO accurate and fully differential in the Φ_0 phase space. To implement such term, and regulate the IR divergences appearing in the calculation, one could use a local NNLO subtraction. Given the lack of a local NNLO subtraction, the expression in Eq. (3.9) can be approximated, up to power corrections in $\mathcal{T}_{0,\mathrm{ns}}^{\mathrm{cut}}$, with

$$\begin{aligned}\widetilde{\frac{\mathrm{d}\sigma_0^{\mathrm{MC}}}{\mathrm{d}\Phi_0}}(\mathcal{T}_{0,\mathrm{re}}^{\mathrm{cut}},\mathcal{T}_{0,\mathrm{ns}}^{\mathrm{cut}}) = \frac{\mathrm{d}\sigma^{\mathrm{NNLL'}}}{\mathrm{d}\Phi_0}(\mathcal{T}_{0,\mathrm{re}}^{\mathrm{cut}}) - \frac{\mathrm{d}\sigma^{\mathrm{NNLL'}}}{\mathrm{d}\Phi_0}(\mathcal{T}_{0,\mathrm{ns}}^{\mathrm{cut}})\bigg|_{\mathrm{NLO}_0} + (B_0+V_0)(\Phi_0) \\ + \int B_1(\Phi_1)\,\theta(\mathcal{T}_0(\Phi_1)<\mathcal{T}_{0,\mathrm{ns}}^{\mathrm{cut}})\,\frac{\mathrm{d}\Phi_1}{\mathrm{d}\Phi_0}\,. \end{aligned} \tag{5.1}$$

With this replacement, only a local NLO subtraction and the expansion of the resummed term at $\mathcal{O}(\alpha_S)$ are needed. Eq. (5.1) is based on the fact that the singular and FO contributions cancel up to power corrections below the resolution cutoff at $\mathcal{O}(\alpha_S^2)$. The cancellation between these two terms as a function of the resolution cutoff $\mathcal{T}_0$ is shown in Fig. 5.1 by plotting the

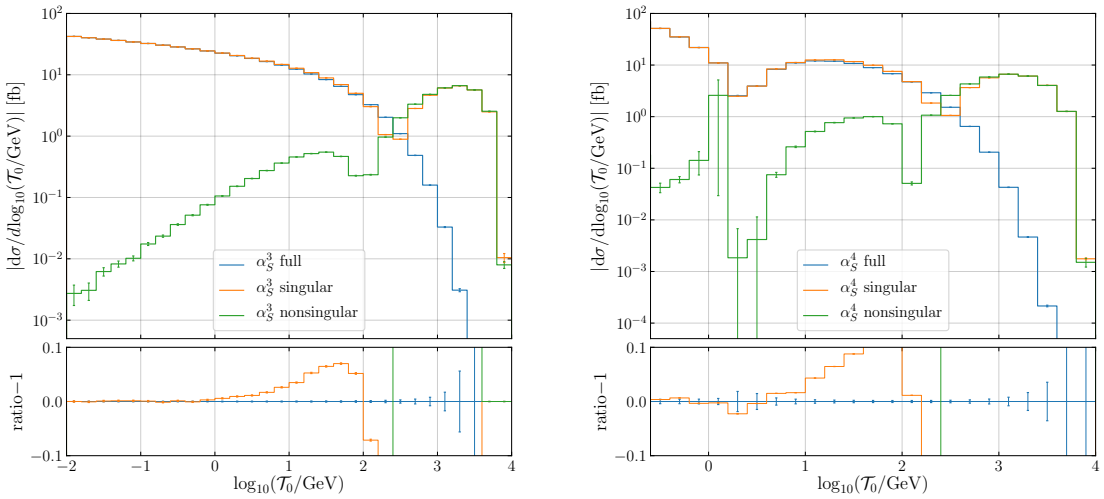

Figure 5.1: Singular and nonsingular contributions to the double Higgs boson production cross section as a function of $\mathcal{T}_0$ at NLO (left) and NNLO (right).

absolute values of their central predictions, both at LO_1, which is of absolute order α_S^3, on the left and at NLO_1,[1] the pure α_S^4 contribution on the right. We notice that the nonsingular distribution correctly approaches zero while the separate FO and singular contributions are diverging, both at order α_S^3 and α_S^4. This is despite the appearance of numerical instabilities in the region where the α_S^4 nonsingular changes sign, around $\mathcal{T}_0 \sim 1.5$ GeV. However, for any finite choice of $\mathcal{T}_{0,\mathrm{ns}}^{\mathrm{cut}}$, there are always remaining nonsingular power corrections below the cutoff, identified by the difference between Eq. (3.9) and (5.1), which reads

$$\begin{aligned}\frac{\mathrm{d}\Sigma_{\mathrm{ns}}^{(2)}}{\mathrm{d}\Phi_0}(\mathcal{T}_{0,\mathrm{ns}}^{\mathrm{cut}}) = &- \frac{\mathrm{d}\sigma^{\mathrm{NNLL'}}}{\mathrm{d}\Phi_0}(\mathcal{T}_{0,\mathrm{ns}}^{\mathrm{cut}})\bigg|_{\mathrm{NNLO}_0} + \frac{\mathrm{d}\sigma^{\mathrm{NNLL'}}}{\mathrm{d}\Phi_0}(\mathcal{T}_{0,\mathrm{ns}}^{\mathrm{cut}})\bigg|_{\mathrm{NLO}_0} + W_0(\Phi_0) \\ &+ \int V_1(\Phi_1)\,\theta(\mathcal{T}_0(\Phi_1) < \mathcal{T}_{0,\mathrm{ns}}^{\mathrm{cut}})\,\frac{\mathrm{d}\Phi_1}{\mathrm{d}\Phi_0} \\ &+ \int B_2(\Phi_2)\,\theta(\mathcal{T}_0(\Phi_2) < \mathcal{T}_{0,\mathrm{ns}}^{\mathrm{cut}})\,\frac{\mathrm{d}\Phi_2}{\mathrm{d}\Phi_0}. \end{aligned} \tag{5.2}$$

We show its absolute size as a function of $\mathcal{T}_{0,\mathrm{ns}}^{\mathrm{cut}}$ in Fig. 5.2, as well as its relative size as a fraction of the NNLO cross section computed by MATRIX [83, 95] on the right axis.

For the results presented in this work we choose $\mathcal{T}_{0,\mathrm{ns}}^{\mathrm{cut}} = 0.5$ GeV. The size of the missing corrections associated to that value is around 1.2% of the total cross section. These missing contributions only affect events below the cutoff, and we can recover the exact NNLO cross section by reweighting these events by this difference. Note that, while we could have chosen smaller values of $\mathcal{T}_{0,\mathrm{ns}}^{\mathrm{cut}}$ to further minimise the impact of power corrections, lowering this value has shown to cause instabilities in the matrix elements used for our calculation.

[1] Here LO_1 and NLO_1 refer to the order relative to the partonic phase space with one extra emission.

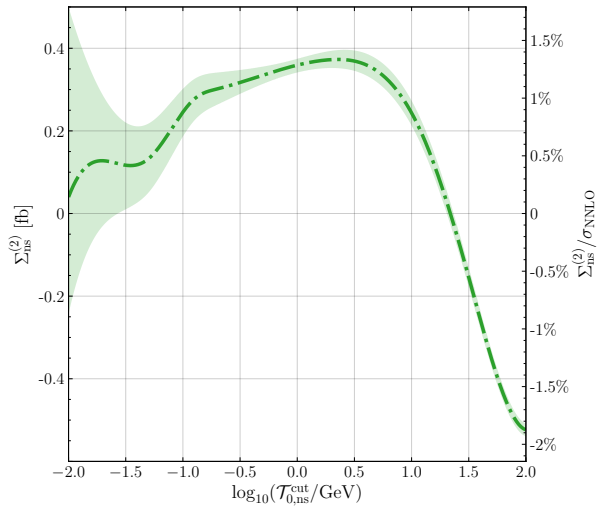

Figure 5.2: The neglected $\mathcal{O}(\alpha_S^2)$ nonsingular contribution to the $\mathcal{T}_0$ cumulant $\Sigma^{(2)}_{\rm NS}$ as a function of $\mathcal{T}^{\rm cut}_{0,\rm ns}$. The green band represents the statistical uncertainty.

Another important check to do is to ensure that the final result is independent of the exact choice of $\mathcal{T}^{\rm cut}_{0,\rm re}$, modulo higher-order corrections. We remark that a variation in the value of $\mathcal{T}^{\rm cut}_{0,\rm re}$ only amounts to shifting part of the resummed contribution from the 0-jet bin to the spectrum, and vice versa. In general, the resummed calculation might be problematic when the soft and beam scales reach small values of the order $\Lambda_{\rm QCD}$, due to the running of the strong coupling. The introduction of profile scales that smoothly turn off the divergence, freezing the soft scale and preventing it from approaching $\Lambda_{\rm QCD}$, partially solves this problem, but renders the perturbative resummed calculation unreliable in that extreme region. Moreover, $\mathcal{T}^{\rm cut}_{0,\rm re}$ is eventually tied to the starting scale of the parton shower inside the 0-jet bin. Therefore, for both of the previous reasons, it is advisable not to push the $\mathcal{T}^{\rm cut}_{0,\rm re}$ to too small values. In Fig. 5.3 we study the dependence of the GENEVA partonic results on the choice of $\mathcal{T}^{\rm cut}_{0,\rm re} = 1$ GeV (the default value) and $\mathcal{T}^{\rm cut}_{0,\rm re} = 2$ GeV for a fixed $\mathcal{T}^{\rm cut}_{0,\rm ns} = 0.5$ GeV. As expected, this choice does not impact in a statistically significant way the distributions shown, which are the transverse momentum of the Higgs boson pair p_T^{HH}, the transverse momentum of the hardest Higgs boson $p_T^{H_1}$ and the zero-jettiness, respectively.

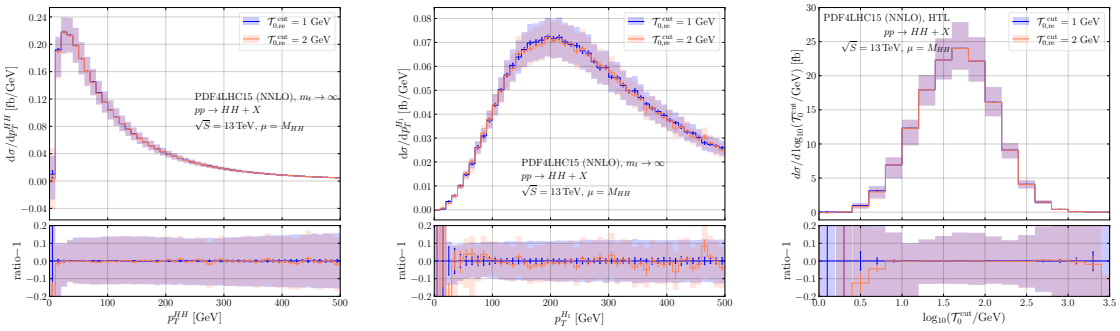

Figure 5.3: Comparison between $\mathcal{T}_{0,\mathrm{re}}^{\mathrm{cut}} = 1,\ 2$ GeV at fixed $\mathcal{T}_{0,\mathrm{ns}}^{\mathrm{cut}} = 0.5$ GeV for p_T^{HH} (left), $p_T^{H_1}$ (centre) and $\mathcal{T}_0$ (right) distributions.

5.2 Choice of resummation scales

The factorisation theorem of the SCET formalism in Eq. (3.4) allows to write the resummed cross section as a convolution of three functions. These three functions admit a perturbative expansion in powers of the strong coupling and manifest a logarithmic dependence on a single characteristic scale. The canonical choice of the energy scales that minimises these logarithmic terms is

$$\mu_H = Q\,, \qquad \mu_B = \sqrt{Q\mathcal{T}_0}\,, \qquad \mu_S = \mathcal{T}_0\,, \tag{5.3}$$

where Q is a hard scale of the process. With this choice, there are no large logarithms in the perturbative expansion of H, B and S. The variable on which we have control for the resummation is $\tau = \mathcal{T}_0/Q$ and the canonical scales are appropriate only in the resummation region ($\mathcal{T}_0 < Q$), where the singular contribution dominates. When approaching the fixed-order region ($\mathcal{T}_0 \sim Q$), the resummation must be turned off since the singular contribution, being resummed, becomes meaningless and the subsequent cancellation between singular and nonsingular terms must be preserved. This matching of the resummed and fixed-order region can be done interpolating between the canonical scales and the FO ones, using profile scales.

We choose Q to be equal to the FO scale, that is set to the invariant mass of the Higgs boson pair M_{HH}. We then have to evolve the soft and beam functions to the same common nonsingular scale $\mu_{\mathrm{NS}} = M_{HH}$, that is always the same scale for the hard function. The renormalisation group evolution (RGE) is then used to evolve each function from their characteristic scale to a common scale. The evolution of the soft and beam functions is done by using profile scales $\mu_S(\mathcal{T}_0)$ and $\mu_B(\mathcal{T}_0)$. These conventions have been introduced in Ref. [96], and are given by

$$\begin{aligned} \mu_S(\mathcal{T}_0) &= \mu_{\mathrm{NS}}\, f_{\mathrm{run}}(\mathcal{T}_0/Q), \\ \mu_B(\mathcal{T}_0) &= \mu_{\mathrm{NS}}\, \sqrt{f_{\mathrm{run}}(\mathcal{T}_0/Q)}, \end{aligned} \tag{5.4}$$

where $f_{\rm run}$ is defined as

$$f_{\rm run}(x) = \begin{cases} x_0[1+(x/(2x_0))^2] & x \le 2x_0, \\ x & 2x_0 < x \le x_1, \\ x + \frac{(2-x_1-x_2)(x-x_1)^2}{2(x_2-x_1)(x_3-x_1)} & x_1 < x \le x_2, \\ 1 - \frac{(2-x_1-x_2)(x-x_3)^2}{2(x_3-x_1)(x_3-x_2)} & x_2 < x \le x_3, \\ 1 & x_3 < x. \end{cases} \tag{5.5}$$

This functional form ensures the canonical scaling, given by Eq. (5.3), between x_0 and x_1 and switches off the resummation above x_3. The region below $2x_0$ corresponds to the region where we freeze the running of all couplings to avoid the Landau pole. The point x_2 corresponds to an inflection point in the profile function $f_{\rm run}$. In Fig. 5.4 we compare the absolute sizes of the singular and nonsingular contributions to the cross section as functions of τ at LO_1 and NLO_1 accuracy. We set the profile parameters to

$$x_0 = \frac{1\ \mathrm{GeV}}{Q}, \qquad \{x_1, x_2, x_3\} = \{0.2, 0.275, 0.35\}. \tag{5.6}$$

The values of x_1 and x_3 are chosen at the points where FO and singular contributions are of similar size and where the nonsingular contribution becomes dominant, respectively.

The theoretical uncertainties for the FO prediction are obtained by varying the central scale $\mu_{\rm NS}$ up and down by a factor of two and taking the maximal absolute deviation from the central value as a measure of uncertainty. For the resummed case we vary the central choices for the profile scales μ_S and μ_B independently, as e.g. detailed in Ref. [44], keeping $\mu_H = \mu_{\rm NS}$ fixed. We include also two more profiles where all the x_i are varied by ± 0.05 simultaneously, while keeping all the other scales at their central values. In total we get six profile variations and take the maximal absolute deviation in the result from the central value as the resummation uncertainty. The total uncertainty is then given by the quadrature sum of the resummation and FO uncertainties.

Due to the dependence on $\mathcal{T}_0$ of the profile scale μ, and the fact that integrating the factorisation theorem and choosing the scales do not commute with each other, the integral over the spectrum is not equal to the cumulant

$$\int_0^{\mathcal{T}_0^{\rm max}} \frac{\mathrm{d}\sigma^{\rm NNLL'}}{\mathrm{d}\Phi_0 \mathrm{d}\mathcal{T}_0}(\mu(\mathcal{T}_0))\,\mathrm{d}\mathcal{T}_0 = \frac{\mathrm{d}\sigma^{\rm NNLL'}}{\mathrm{d}\Phi_0}(\mathcal{T}_0^{\rm max}, \mu(\mathcal{T}_0^{\rm max})) + \mathcal{O}(\mathrm{N^3LL}), \tag{5.7}$$

where $\mathcal{T}_0^{\rm max}$ is the upper kinematical limit. Even if this difference is of higher order, it can be numerically relevant and it can cause a sizeable difference between the total matched cumulant and a purely fixed-order NNLO cross section. To obviate this problem, in GENEVA we add an additional higher-order term to our spectrum,

$$\begin{aligned} \frac{\mathrm{d}\sigma^{\rm improvedXS}}{\mathrm{d}\Phi_0 \mathrm{d}\mathcal{T}_0}(\mu(\mathcal{T}_0)) &= \frac{\mathrm{d}\sigma^{\rm NNLL'}}{\mathrm{d}\Phi_0 \mathrm{d}\mathcal{T}_0}(\mu(\mathcal{T}_0)) \\ &\quad + p\,\mathcal{K}(\mathcal{T}_0, \Phi_0)\left[\frac{\mathrm{d}}{\mathrm{d}\mathcal{T}_0}\frac{\mathrm{d}\sigma^{\rm NNLL'}}{\mathrm{d}\Phi_0}(\mathcal{T}_0, \mu_h(\mathcal{T}_0)) - \frac{\mathrm{d}\sigma^{\rm NNLL'}}{\mathrm{d}\Phi_0 \mathrm{d}\mathcal{T}_0}(\mu_h(\mathcal{T}_0))\right], \end{aligned} \tag{5.8}$$

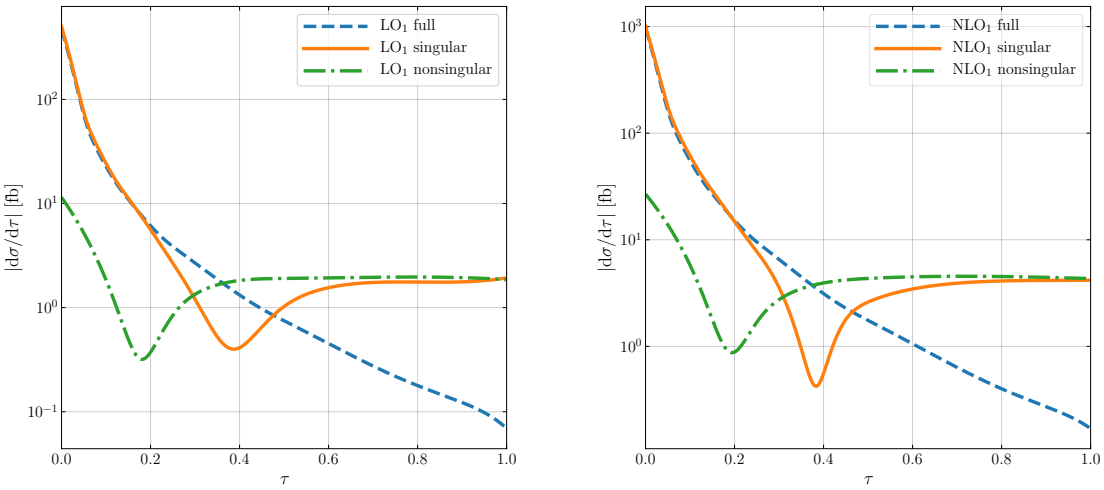

Figure 5.4: Comparison between the absolute values of the fixed-order distribution, of the expansion of the resummed contribution up to $\mathcal{O}(\alpha_S^2)$ (singular) and of their difference (nonsingular), as a function of τ at LO$_1$ (left) and NLO$_1$ (right).

where $\mu_h(\mathcal{T}_0)$ is a dedicated profile scale and $\mathcal{K}(\mathcal{T}_0, \Phi_0)$ is a smooth function defined as

$$\mathcal{K}(\mathcal{T}_0, \Phi_0) = \frac{1}{2} - \frac{1}{2}\tanh\left[32\left(\frac{\mathcal{T}_0}{M_{HH}} - \frac{1}{4}\right)\right]. \tag{5.9}$$

Note that by construction the additional term in Eq. (5.8) is of higher order, consequently the NNLL$'$ accuracy of the spectrum is not spoiled. Moreover, its effects are limited to the resummation region, since $\mu_h(\mathcal{T}_0) = Q$ in the FO region so that the difference in the square brackets of Eq. (5.8) vanishes. The function $\mathcal{K}(\mathcal{T}_0, \Phi_0)$ is chosen such that it tends to zero for large values of $\mathcal{T}_0$, and that the effects of the induced higher-order terms are compatible with the scale uncertainties of the original spectrum in the peak region. Consequently, the additional higher-order terms induced by this procedure contribute mostly in the peak and transition regions, where they are expected to be larger. Also the p value is tuned to ensure that the total inclusive cross section is recovered upon integration. In order to do so, the value of p is fixed by requiring that the integral over this modified version of the spectrum is equal to that of the cumulant,

$$p = \frac{\int \mathrm{d}\Phi_0 \int \mathrm{d}\mathcal{T}_0 \left[\frac{\mathrm{d}}{\mathrm{d}\mathcal{T}_0}\frac{\mathrm{d}\sigma^{\mathrm{NNLL}'}}{\mathrm{d}\Phi_0}(\mathcal{T}_0, \mu_h(\mathcal{T}_0)) - \frac{\mathrm{d}\sigma^{\mathrm{NNLL}'}}{\mathrm{d}\Phi_0 \mathrm{d}\mathcal{T}_0}(\mu_h(\mathcal{T}_0))\right]}{\int \mathrm{d}\Phi_0 \int \mathrm{d}\mathcal{T}_0 \left[\frac{\mathrm{d}}{\mathrm{d}\mathcal{T}_0}\frac{\mathrm{d}\sigma^{\mathrm{NNLL}'}}{\mathrm{d}\Phi_0}(\mathcal{T}_0, \mu_h(\mathcal{T}_0)) - \frac{\mathrm{d}\sigma^{\mathrm{NNLL}'}}{\mathrm{d}\Phi_0 \mathrm{d}\mathcal{T}_0}(\mu_h(\mathcal{T}_0))\right] \mathcal{K}(\mathcal{T}_0, \Phi_0)}. \tag{5.10}$$

One must however pay attention to the fact that both the value of p in Eq. (5.10) and the $\mathcal{K}(\mathcal{T}_0, \Phi_0)$ factor in Eq. (5.9) are obtained integrating over the Born variables Φ_0. In particular,

there is a nontrivial interplay between the Higgs boson pair invariant mass M_{HH} and the definition of $\mathcal{K}(\mathcal{T}_0, \Phi_0)$. Since the M_{HH} distribution spans over a wide range, using a single value of p across all the possible values of M_{HH} has a sizable effect on the predicted M_{HH} differential distribution, despite the fact that the correct inclusive cross section is obtained by construction. In Sec. 7 we are going to show the actual effect of such implementation in the validation against the NNLO result.

5.3 Resummation parameters

The SCET factorisation theorem for the double Higgs boson production was firstly introduced in Eq. (3.4). The calculation of such theorem for this process is reported in appendix A. The resummation of the zero-jettiness is carried out up to NNLL′ accuracy, therefore, the hard, beam and soft functions are computed at 2-loop order. The soft function has been computed at 2-loops in Refs. [97, 98]. The beam function are known up to 3-loops [99, 100] and, finally, the hard function is taken from Refs. [101] and [70], translating the result from the Catani scheme to the $\overline{\text{MS}}$ scheme. The details of this calculation can be found in appendix B. To reach the accuracy needed, the anomalous dimensions appearing in the evolution factors has to be known at 2- and 3-loop order for the noncusp [96] and cusp terms [102–104], respectively. Similarly, the QCD beta function [105, 106] is required to be known at 3-loop order.

The resummation accuracy of GENEVA is also extended to N^{3}LL, including at one order higher the noncusp and cusp anomalous dimensions [96, 107, 108], the QCD beta function [107] and the running of the strong coupling. At the moment, this is not the default accuracy chosen, because we are still studying its interface to the parton shower. The shower can, in principle, modify the distributions at order α_S^3, and consequently could spoil the resummation accuracy. Moreover, as we are going to show, N^{3}LL predictions can be used as a cross-check to quantify the effects of the shower.

5.3.1 One-jettiness resummation

In Eq. (3.11), we introduced the Sudakov factor needed for the resummation of the one-jettiness. Here, we report all the ingredients needed for such resummation for the specific case of gluons-initiated process, as the double Higgs boson production.

The Sudakov factor for the gluon channels is given by

$$U_1^{ggg}(\Phi_1, \mathcal{T}_1^{\text{cut}}) = \frac{U}{\Gamma\Big(1 + 6\, C_A\, \eta_{\text{cusp}}^{\text{NLL}}(\mu_S, \mu_H)\Big)}\,, \tag{5.11}$$

with Γ the Euler gamma function and

$$\begin{aligned}
\ln U = {} & 6\, C_A \Big[2\, K_{\Gamma_{\text{cusp}}}^{\text{NLL}}(\mu_J, \mu_H) - K_{\Gamma_{\text{cusp}}}^{\text{NLL}}(\mu_S, \mu_H) \Big] \\
& + C_A \Big[- \ln\left(\frac{Q_a^2 Q_b^2 Q_J^2}{\mu_H^6}\right) \eta_{\Gamma_{\text{cusp}}}^{\text{NLL}}(\mu_J, \mu_H) + \ln\left(\frac{Q_a^2 Q_b^2 Q_J^2}{stu}\right) \eta_{\Gamma_{\text{cusp}}}^{\text{NLL}}(\mu_S, \mu_H) \Big] \\
& - 6\, \gamma_E\, C_A\, \eta_{\Gamma_{\text{cusp}}}^{\text{NLL}}(\mu_S, \mu_J) + 3\, K_{\gamma_J^g}^{\text{NLL}}(\mu_J, \mu_H).
\end{aligned} \tag{5.12}$$

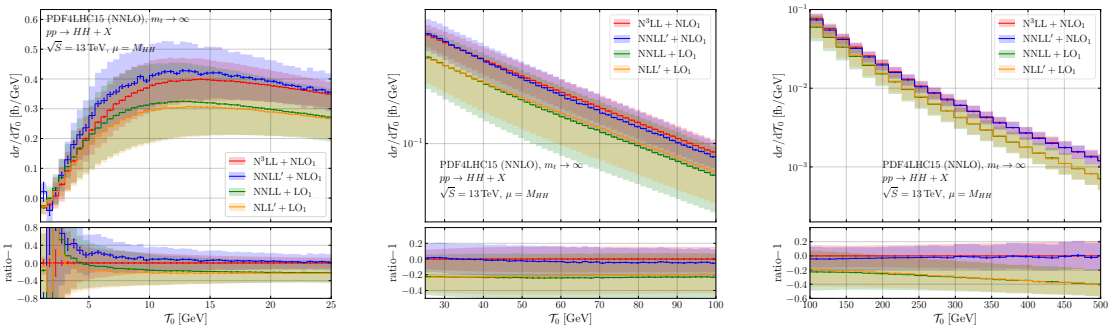

Figure 5.5: Resummed predictions matched to the appropriate fixed-order results at different accuracies for the $\mathcal{T}_0$ distribution in the peak (left), transition (centre) and tail (right) region.

The functions appearing in the formula above are common in the SCET literature, see e.g. Ref. [96], and are given by

$$\begin{aligned}
K^{\mathrm{NLL}}_{\Gamma_{\mathrm{cusp}}}(\mu_1,\mu_2) &= -\frac{\Gamma_0}{4\beta_0^2}\left[\frac{4\pi}{\alpha_S(\mu_1)}\left(1-\frac{1}{r}-\ln r\right)+\left(\frac{\Gamma_1}{\Gamma_0}-\frac{\beta_1}{\beta_0}\right)(1-r\ln r)+\frac{1}{2}\frac{\beta_1}{\beta_0}\ln^2 r\right],\\
\eta^{\mathrm{NLL}}_{\Gamma_{\mathrm{cusp}}}(\mu_1,\mu_2) &= -\frac{1}{2}\frac{\Gamma_0}{\beta_0}\left[\ln r+\frac{\alpha_S(\mu_1)}{4\pi}\left(\frac{\Gamma_1}{\Gamma_0}-\frac{\beta_1}{\beta_0}\right)(r-1)\right],\\
K^{\mathrm{NLL}}_{\gamma_J} &= -\frac{1}{2}\frac{\gamma_0}{\beta_0}\ln r\,,
\end{aligned} \tag{5.13}$$

with $r = \frac{\alpha_S(\mu_2)}{\alpha_S(\mu_1)}$, the scales $\mu_H = \mathcal{T}_1^{\max}$, $\mu_S = \mathcal{T}_1^{\mathrm{cut}}$ and $\mu_J = \sqrt{\mu_H \mu_S}$. The kinematics-dependent terms are given by

$$Q_a = p_a\, M_{HH}\, e^{Y_{HH}}, \qquad Q_b = p_b\, M_{HH}\, e^{-Y_{HH}}, \qquad Q_J = 2\, p_J\, E_J\,, \tag{5.14}$$

where Y_{HH} is the rapidity of the Higgs boson pair, $p_{a,b}$ are the incoming momenta, p_J is the momentum and E_J the energy of the jet in the final state (in the frame in which the Higgs boson pair system has $Y_{HH} = 0$). The cusp and noncusp anomalous dimensions are given by

$$\begin{aligned}
&\Gamma_0 = 4\,, \qquad \Gamma_1 = 4\left[\left(\frac{67}{9}-\frac{\pi^2}{3}\right)C_A - \frac{20}{9}T_F n_f\right],\\
&\gamma_0 = 12 C_F + 2\beta_0\,, \qquad \beta_0 = \frac{11}{3}C_A - \frac{4}{3}T_F n_f\,,\\
&\beta_1 = \frac{34}{3}C_A^2 - \frac{10}{3}C_A n_f - 2 C_F n_f\,.
\end{aligned} \tag{5.15}$$

5.4 Numerical effect of $\mathcal{T}_0$ resummation

To study the effect of the $\mathcal{T}_0$ resummation, in Fig. 5.5 we show the resummed predictions across the whole spectrum. In particular, we present the resummed predictions at various resummation orders matched to the appropriate fixed-order calculations: NLL$'$+LO$_1$, NNLL+LO$_1$,

NNLL′+NLO$_1$ and N^{3}LL + NLO$_1$. We report also the statistical errors due to the Monte Carlo integration, which appear as vertical bars, as well as the scale variation band, obtained by the procedure previously discussed. The lower insets of the plots show instead the normalised relative ratios between the curves. In the peak region (small $\mathcal{T}_0$), where resummation effects are most important, we observe a large spread among the predictions at different resummation accuracies. In the transition and tail region, the difference between the various predictions is driven by the FO accuracy, with LO$_1$ results being consistently smaller than the NLO$_1$ ones across the whole range. The scale variations at N^{3}LL + NLO$_1$ and NNLL′ + NLO$_1$ are smaller than those at lower orders, especially in the peak and transition regions, showing a reasonable convergence of the perturbative predictions. We notice however that resummation effects are still visible up to values of $\mathcal{T}_0 \lesssim 300$ GeV in the small difference between the N^{3}LL and the NNLL′ results, at the order of a few percent. This can be explained by the fact that the actual resummed variable is $\tau_0 = \mathcal{T}_0/M_{HH}$, which, in this particular process, can be small even for relatively large values of $\mathcal{T}_0$, when M_{HH} becomes very large, as already discussed above.

Chapter 6

Parton showers for double Higgs boson production

In this chapter we present the different showers with which GENEVA interfaces, paying particular attention to their effects in the case of the double Higgs boson production. We will only discuss the main differences, as additional information can be found in the relative references.

The double Higgs boson production is one of the first gluon-initiated processes implemented in GENEVA. Compared to other colour singlet production processes already studied within the GENEVA framework, the impact of the parton shower to this processes is significant. Two main reasons contribute to this behaviour. Firstly, the process is dominated by the gluon channel, hence the gluon emissions are more abundant than those from quarks (or antiquarks), and this difference is determined by the colour factor of the splitting, roughly speaking the emissions are scaled by a factor $C_A/C_F \sim 2$. Secondly, as mentioned in the previous sections, this process has a large hard scale, defined by the invariant mass of the Higgs boson pair M_{HH}. Unlike the case of the single Higgs boson production, where the hard scale is simply given by the mass of the Higgs boson, resulting in a well-defined sharp distribution, the invariant mass for double Higgs boson production spans over a wide range of values, starting from $2m_H$ up to the centre-of-mass energy $\sqrt{S}$ considered. The choice of the evolution variable t, which usually depends on the hard scale, and the choice of the starting scale of the shower define how much of the phase space is available for the shower emissions. Since the hard scale is set to M_{HH}, this feature will play a visible role in the effect of the shower.

Having said that, we will briefly comment on the main features of the parton showers considered in the GENEVA framework, emphasizing their nature as dipole showers, and discussing their evolution variables and the structure of the splitting evolutions.

6.1 PYTHIA8

The first shower used in the GENEVA framework is PYTHIA8 [15, 16]. Considering a generic splitting $a \to b+c$, each coloured parton a is assigned a recoiler r that carries the corresponding anticolour. This branching can be split in two steps: $a + r \to a^* + r' \to b + c + r'$, where a^*

is an intermediate off-shell parton of virtuality Q^2 and r' its recoiler. The evolution variable used is a modified transverse momentum, defined as

$$\begin{aligned} t^{\text{FSR}}_{\text{PYTHIA8}} &= z(1-z)Q^2 \text{ for FSR}\,, \\ t^{\text{ISR}}_{\text{PYTHIA8}} &= (1-z)Q^2 \quad \text{for ISR}\,, \end{aligned} \tag{6.1}$$

for final-state radiation and initial state radiation, respectively. Here Q^2 is the virtuality of the off-shell parton, z is related to the kinematics in the dipole rest frame. It represents the energy sharing between daughters in the rest frame of the radiator + recoiler system (specifically, $E_b = zE_a$ and $E_c = (1-z)E_a$). In this description, the colour does not flow between initial and final states, meaning that PYTHIA8 does not include interference between initial-final (IF) and final-initial (FI) emissions, treating the evolution of partons in the initial and final state independently. Moreover, it uses a collinear evolution, represented by the following DGLAP splitting kernels

$$\begin{aligned} P_{q\to qg}(z) &= C_F \frac{1+z^2}{1-z}\,, \\ P_{g\to gg}(z) &= C_A \frac{(1-z(1-z))^2}{z(1-z)}\,, \\ P_{g\to q\bar{q}}(z) &= T_R(z^2+(1-z)^2)\,, \end{aligned} \tag{6.2}$$

and satisfying the symmetry relations $P_{a\to cb}(z) = P_{a\to bc}(1-z)$. Here $C_F = 4/3$, $C_A = 3$ and $T_R = 1/2$ are the colour factors.

6.2 SHERPA

The parton shower implemented in SHERPA [17–19] is based on the Catani-Seymour dipole formalism. This formalism incorporates collinear evolution and the splitting of colour dipoles, ensuring energy-momentum conservation and proper treatment of colour flow in the shower evolution. It accurately simulates the probabilities and kinematics of collinear parton splittings. Considering the following splitting $\widetilde{aj} + \tilde{b} \to a + j + b$, the evolution variable is a modified transverse momentum which can be defined as

$$t_{\text{SHERPA}} = \frac{Q^2}{2}\left[\delta_{jg}(1-z) + \delta_{jq}\right]. \tag{6.3}$$

Here z is defined differently depending on whether we are considering an ISR or FSR, in particular

$$\begin{aligned} z^{\text{ISR}} &= \frac{(p_a - p_j + p_b)^2}{(p_a + p_b)^2}\,, \\ z^{\text{FSR}} &= \frac{(p_a + p_j + p_b)^2}{(p_a + p_b)^2}\,. \end{aligned} \tag{6.4}$$

The only difference is in the z variable, where all the momenta acquire a plus sign since we are considering a fully final state splitting. The expression for the splitting kernels are not

provided here, as their definition depends on the type of radiation (ISR or FSR) and whether the spectator is initial- or final-state. The common feature that they share is their dependence on the transverse momentum of the emitted parton, p_T, and on the hard scale Q^2. Also the definition of these two variables depends on the radiation considered, all the possible cases can be found in Ref. [17]. Compared to the splitting kernels of Eq. (6.2), the z in the denominator is scaled by a factor $\sim p_T^2/Q^2$ for each configuration considered.

6.3 DIRE

The DIRE [109] shower is baseds on the Catani-Seymour dipole shower formalism. It describes the parton shower evolution through the splitting of colour dipoles, focusing on the colour connections between partons. To address the issue of the soft radiation outside the collinear region, the DIRE shower introduces a t-dependence in the splitting functions, which restores the correct soft anomalous dimension.

For instance, consider an initial-state parton splitting process $\widetilde{ab} \to a + b \to j$, where a is the splitting parton and j the spectator in the initial state. The soft-enhanced terms are replaced by a partial fraction of the soft eikonal for the colour dipole

$$\frac{1}{1-z} \to \frac{1}{1-z+v}\,, \qquad 1-z = \frac{p_j p_b}{p_a p_b}\,, \quad v = \frac{p_j p_a}{p_a p_b}\,. \tag{6.5}$$

This replacement introduces a scaled transverse momentum t as the evolution variable, allowing for the correct description of soft radiation, defined as $t^{\text{ISR},i}_{\text{DIRE}} = (z-v)p_T^2$. The soft-enhanced term now reads

$$\frac{1-z}{(1-z)^2+\kappa^2}\,, \qquad \kappa^2 = \frac{t}{Q^2}\,, \qquad Q^2 = 2p_a p_b - 2(p_a+p_b)p_j\,. \tag{6.6}$$

If the spectator for the considered initial-state splitting is in the final state, the variables are slightly modified as follows

$$\begin{aligned} 1-z &= \frac{p_b p_j}{p_a p_b + p_a p_j}\,, \qquad u = \frac{p_b p_a}{p_a p_b + p_a p_j}\,, \\ t^{\text{ISR},f}_{\text{DIRE}} &= Q^2 u(1-z)\,, \qquad \kappa^2 = \frac{t}{Q^2}\,, \qquad Q^2 = 2p_a(p_b+p_j) - 2p_b p_j\,. \end{aligned} \tag{6.7}$$

Lastly, for final-state splittings with final-state spectator, we have

$$\begin{aligned} y &= \frac{2p_a p_b}{Q^2}\,, \qquad \tilde{z} = \frac{p_a p_j}{p_a p_j + p_b p_j}\,, \qquad Q^2 = 2p_a p_j + 2(p_a+p_k)p_b\,, \\ t^{\text{FSR},f}_{\text{DIRE}} &= Q^2 y(1-y)(1-\tilde{z})\,, \qquad 1-z = (1-\tilde{z})(1-y)\,. \end{aligned} \tag{6.8}$$

The case of final-state splitting with initial-state spectator can be reconstructed by symmetry.

With these replacements, the leading order splitting functions can be written as

$$
\begin{aligned}
P_{qq}(z,\kappa^2) &= 2C_F\left[\left(\frac{1-z}{(1-z)+\kappa^2}\right)_+ - \frac{1+z}{2}\right] + \frac{3}{2}C_F\delta(1-z)\,,\\
P_{gg}(z,\kappa^2) &= 2C_A\left[\left(\frac{1-z}{(1-z)+\kappa^2}\right)_+ + \frac{z}{z^2+\kappa^2} - 2 + z(1-z)\right] + \delta(1-z)\left(\frac{11}{6}C_A - \frac{10}{3}T_R\right)\,,\\
P_{qg}(z,\kappa^2) &= 2C_F\left[\frac{z}{z^2+\kappa^2} - \frac{2-z}{2}\right]\,,\\
P_{gq}(z,\kappa^2) &= T_R\left[z^2+(1-z)^2\right]\,.
\end{aligned}
\tag{6.9}
$$

6.4 Comparison between parton showers

The main difference between the three considered showers lies in the choice of the evolution variable t. Typically, the physical constraint implemented for the phase space is given by

$$t < \mu^2_{\rm PS}\,, \tag{6.10}$$

where μ_{PS} is the starting scale of the parton shower. Consequently, the available phase space in which the shower can generate emissions is limited by the evolution variable. To simplify the discussion and following Ref. [64], consider only the first hardest emission done by the shower for the specif case of the double Higgs boson production. In this scenario, a pair of Higgs bosons, along with a final state with momentum p_j, is produced from the collision between two massless partons of momenta p_a and p_b. In the centre-of-mass where the Higgs bosons are at rest, the hard scale is set to the invariant mass of the Higgs bosons, i.e. $Q^2 = M_{HH}$. Introducing the Mandelstam variables

$$
\begin{aligned}
s &= (p_a + p_b)^2 = 2\,p_a\,p_b\,,\\
t &= (p_a - p_j)^2 = -2\,p_a\,p_k\,,\\
u &= (p_b - p_j)^2 = -2\,p_b\,p_j\,,
\end{aligned}
\tag{6.11}
$$

we can define two variables linked to them, given by

$$v = \frac{2\,p_a\,p_j}{2\,p_a\,p_b} = -\frac{t}{s} \qquad w = \frac{2\,p_b\,p_j}{2\,p_a\,p_b} = -\frac{u}{s}\,. \tag{6.12}$$

The kinematics of the partons can be schematized as

$$
\begin{aligned}
p_a^\mu &= E(1,0,0,1)\,,\\
p_b^\mu &= E(1,0,0,-1)\,,\\
p_j^\mu &= E(1,0,\sin\theta,\cos\theta)
\end{aligned}
\tag{6.13}
$$

with θ the angle between the parton in the final state and the beam direction, and the momentum conservation imposes that $s+t+u = Q^2 = 4E^2$. This implies that

$$v + w = \left(1 - \frac{Q^2}{s}\right) < 1\,, \tag{6.14}$$

since the kinematic limits on s are given by the energy of the collider S and the hard scale Q^2, as $Q^2 < s < S$. We can also define

$$vw = \frac{t}{s} \cdot \frac{u}{s} = \frac{1}{2}\left(1 + \cos\theta\right) \cdot \frac{1}{2}\left(1 - \cos\theta\right) = \frac{1}{4}\sin^2\theta < \frac{1}{4}\,. \tag{6.15}$$

This product is useful to define the DIRE evolution variable, already defined in Eq. (6.6) as

$$\kappa^2 = \frac{t_{\text{DIRE}}}{Q^2} = vw = \frac{(p_a\, p_j)\;(p_b\, p_j)}{(p_a\, p_b)^2}\,. \tag{6.16}$$

From Eq. (6.15), we obtain $t_{\text{DIRE}} < \frac{Q^2}{4}$. Basically the DIRE shower satisfy Eq. (6.10) and it populates the full phase space under this condition. Exploiting the v and w variables, we can also rewrite the SHERPA evolution variable as

$$\frac{t_{\text{SHERPA}}}{Q^2} = \frac{vw}{1 - (v + w)}\,. \tag{6.17}$$

The t_{SHERPA} is larger than t_{DIRE} by construction, meaning that for a given value of the starting scale of the shower, the emission phase space of the SHERPA shower is more restricted than that of DIRE.

Another important differences between the showers arises from the large invariant mass of the double Higgs boson production process. Since it is a gluon-initiated process, when the pair of Higgs boson is associated with n-jets, in the t-channel, the partons can generate dipoles due to their colour connection. These dipoles carry a significant amount of energy, which is driven by the invariant mass of the boson pair. This results in a substantial energy budget available for gluon splittings, and since gluons have a large colour factor C_A compared to quarks, they have a more significant impact on the shower evolution.

In addition to that, the choice of splitting functions used by the showers also play a crucial role in describing gluon branchings. The parameterisation of the splitting function by PYTHIA8 and SHERPA describes correctly the collinear emission, but does not describe soft emissions as effectively. In the gluon splitting function, the leading dependence for soft emissions is given by the factor $1/z$. However, in the showers that uses Catani-Seymour-like dipoles, as mentioned in Sec. 6.2, the z variable is scaled by a term proportional to p_T^2/Q^2. In the collinear limit, the extra term appearing in the denominator is irrelevant since $p_T^2 = 0$. In the soft limit, where $p_T^2 \neq 0$, it leads to an overestimation of the gluon emission probability and, consequently, of the Sudakov form factor. The DIRE approach addresses this problem by introducing a different parameterisation for the dipoles, taking into account the inverse of the eikonal factor, as already seen. Consequently, the DIRE shower is better suited to handle gluons splittings, especially in the soft emission regime, compared to other showers.

Chapter 7

Phenomenological results

In this chapter, we present our results for the double Higgs production process. We begin by describing our physical setup and then proceed to validate our results by comparing them to a fixed-order NNLO calculation provided by an independent code. Finally, we present the showered results. Note that, for the showered results, we ignore any effects arising from hadronisation and fragmentation of hadrons in the shower, as well as those coming from multi-parton scattering. This choice is motivated by the lack of available experimental data and, more importantly, by the necessity of incorporating top-quark mass effects to ensure the reliability of Monte Carlo event generator.

7.1 Physical parameters

We consider proton-proton collisions at a hadronic centre-of-mass energy $\sqrt{S} = 13$ TeV. The process of interest is $p\,p \to H\,H + X$, where we work in the limit of infinite top-quark mass, requiring two on-shell Higgs bosons in the final state. We consider only the gluon fusion production channel. We use the `PDF4LHC15_nnlo_100` PDF set [110] from LHAPDF 6 [111], including the corresponding value of $\alpha_S(M_Z)$. The input parameters used are

$$\begin{aligned} m_H &= 125.06\ \text{GeV}\,, \qquad v = 246.32\ \text{GeV}\,, \qquad m_t = 173.1\ \text{GeV}\,, \\ \mathcal{T}_{0,\text{re}}^{\text{cut}} &= 1\ \text{GeV}\,, \qquad \mathcal{T}_{0,\text{ns}}^{\text{cut}} = 0.5\ \text{GeV}\,, \qquad \mathcal{T}_{1}^{\text{cut}} = 1\ \text{GeV}\,. \end{aligned} \tag{7.1}$$

This choice of cutoffs provides a reasonable compromise between the size of the neglected power-suppressed terms and the stability of the singular-nonsingular cancellation. We set both the factorisation (μ_F) and renormalisation (μ_R) scales to the invariant mass M_{HH} of the Higgs boson pair. The phase space for the process is generated by the Monte Carlo integrator MUNICH. To evaluate the beam functions we use the `beamfunc` module of `scetlib` [112, 113]. All tree-level matrix elements are calculated using RECOLA [114, 115] through a custom-built interface to GENEVA, while all the one-loop terms are calculated through the standard OPENLOOPS [116] interface already used for processes previously implemented, in both cases we are working in the complex-mass scheme. For the validation of the NNLO accuracy of the

GENEVA results, we compare to an independent calculation implemented in MATRIX [83,95], and we use the three-loop running of α_S for both the predictions.

7.2 Validation of NNLO results

The comparison between MATRIX and GENEVA predictions is performed at the partonic level, before interfacing to the parton shower. The theoretical uncertainties of both calculations are obtained with the 3-point μ_R and μ_F variations (by multipling and dividing the scales by a factor 2, the minimum and the maximum results are taken as the envelope of the uncertainties). In the comparison plots, the MATRIX result is presented in red, while the GENEVA one in blue.

We first show the inclusive distributions in Fig. 7.1, i.e. the invariant mass of the Higgs boson pair M_{HH} (on the left panel) and the Higgs boson pair rapidity y_{HH} (on the right one). For the comparison of M_{HH}, we also include the GENEVA result obtained using Eq. (5.10), in green, while the blue curve is obtained by Eq. (5.8). These implementations have been discussed in Sec. 5.2. The green and blue lines differ only by higher orders, which play a significant role for the invariant mass distribution of the Higgs boson pair. Precisely, the blue default GENEVA line is obtained by computing the value p in Eqs. (5.10) and (5.9) in different bins of M_{HH}. We have combined various runs in different M_{HH} bins, with a denser distribution in the peak region where the cross section is larger. This effect arises from the resummation performed by GENEVA, which is carried out in terms of the variable $\tau_0 = \mathcal{T}_0/M_{HH}$. Consequently, large resummation effects can be observed at large values of $\mathcal{T}_0$ and M_{HH} as long as their ratio is small. This effect is enlarge also by the fact that the invariant mass distribution of the Higgs boson pair spans to a wide range of values, and the peak region itself is large and not sharped around a specific value. As can be seen from the figure, the difference between these two curves spans a range from -5% to roughly $+10\%$, but only the blue line shows perfect agreement with the MATRIX result, as expected.

In Fig. 7.2, we show some exclusive distributions including the transverse momentum of the softest of the two Higgs bosons $p_T^{H_2}$ (left panel) and the hyperbolic tangent of the rapidity difference between the two Higgs bosons χ (right panel). This variable is defined as

$$\chi = \tanh\left(\frac{|y_{H_1} - y_{H_2}|}{2}\right), \tag{7.2}$$

where y_{H_1,H_2} are the rapidities of each Higgs boson. In Fig. 7.3, instead, we report the transverse momentum of the hardest of the two Higgs bosons $p_T^{H_1}$. These exclusive distributions exhibit good agreement between MATRIX and GENEVA, except in regions of small transverse momentum for both H_1 and H_2, as well as in the region of large χ. These differences are expected, since GENEVA provides not only a fixed-order prediction, as done by MATRIX, but also includes resummation effects. Consequently, the GENEVA results incorporate higher-order effects and power-suppressed corrections, which can account for these discrepancies. For example, in the region of small p_T, the transverse momentum of both the hardest and softest Higgs boson is small (due to their back-to-back nature), which coincides with the region of small transverse momentum of the Higgs boson pair. This region is problematic for MATRIX since the fixed-order is diverging and therefore the resummation is needed. We investigated the

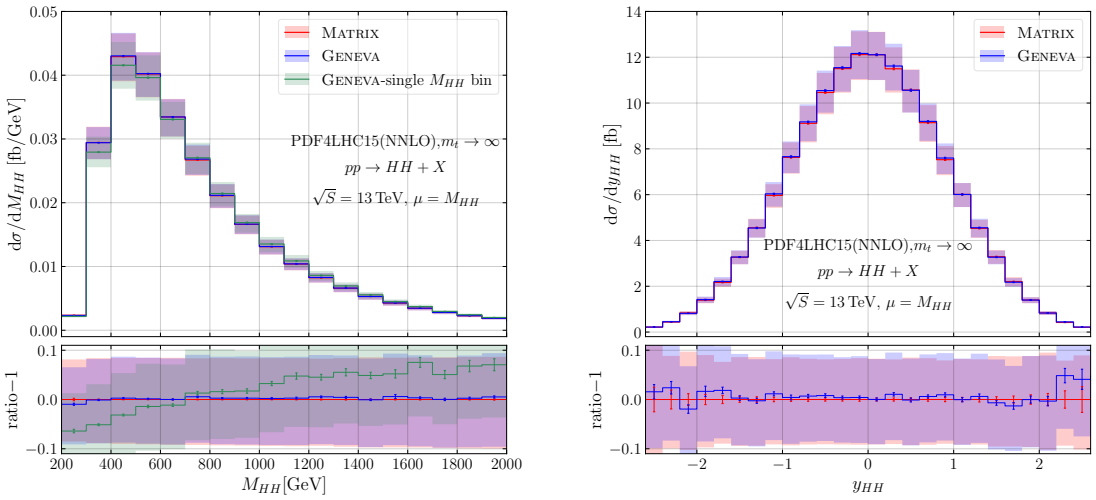

Figure 7.1: Comparison between MATRIX (in red) and GENEVA (in blue) for the invariant mass of the Higgs boson pair, on the left, and the rapidity, on the right.

discrepancies observed in the transverse momentum distribution of the hardest Higgs boson, where these effects are largest. In this region, the discrepancy can reach up to 100%, which is considerably larger than that observed in the p_T of the softest Higgs boson. In Fig. 7.3, we provide a breakdown of all possible sources contributing to the differences between a purely FO calculation, such as that obtained with MATRIX, and the GENEVA partonic prediction. Each subpanel displays the relative size of the respective quantity compared to the total distribution obtained with MATRIX, and we explain each of them below. The first source of discrepancy is denoted as A_1, and is defined as

$$A_1 \equiv \frac{\frac{\mathrm{d}\sigma^{\mathrm{NNLL}'}}{\mathrm{d}p_T^{H_1}} - \frac{\mathrm{d}\sigma^{\mathrm{NNLL}'}}{\mathrm{d}p_T^{H_1}}\Big|_{\alpha_S^2}}{\frac{\mathrm{d}\sigma^{\mathrm{MATRIX}}}{\mathrm{d}p_T^{H_1}}}, \tag{7.3}$$

which represents the difference between the resummed contribution and the resummed expanded up to $\mathcal{O}(\alpha_S^2)$ coming from GENEVA, normalised to the MATRIX NNLO result. As shown in the figure, this difference, which arises from logarithmic terms beyond NNLO, leads to a large positive effect in the region of interest. In the second ratio plot, we consider contributions from projectable configurations with $\mathcal{T}_0 < \mathcal{T}_{0,\mathrm{ns}}^{\mathrm{cut}}$ at relative $\mathcal{O}(\alpha_S)$, defined as

$$A_2 \equiv \frac{\frac{\mathrm{d}\sigma_{diff}^{\mathrm{NLO}_0}}{\mathrm{d}p_T^{H_1}}}{\frac{\mathrm{d}\sigma^{\mathrm{MATRIX}}}{\mathrm{d}p_T^{H_1}}}\,. \tag{7.4}$$

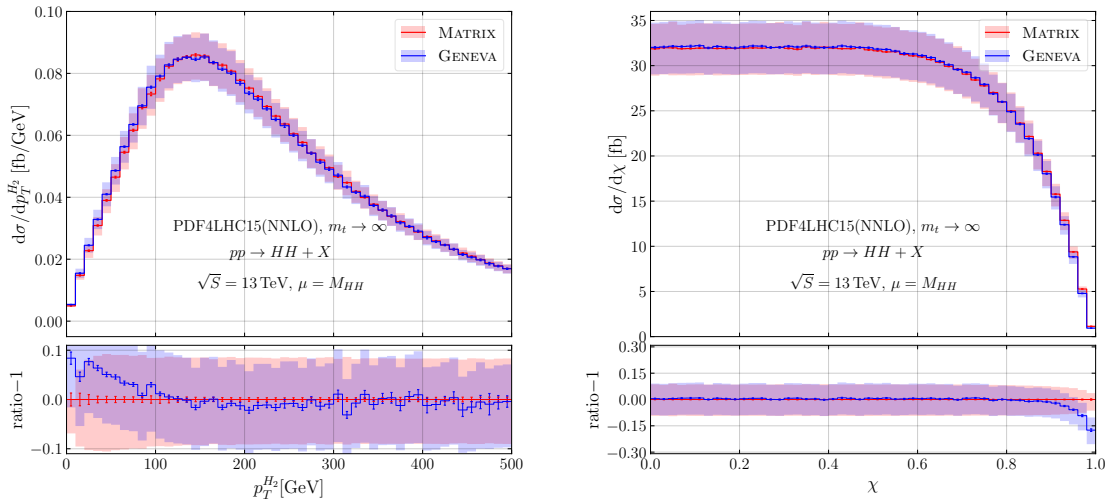

Figure 7.2: Comparison between MATRIX (in red) and GENEVA (in blue) for the transverse momentum of the softest Higgs boson, on the left, and the hyperbolic tangent of the rapidity difference of the two Higgs bosons, on the right.

The third ratio plot represents the contributions from projectable configurations with $\mathcal{T}_0 > \mathcal{T}_{0,\text{ns}}^{\text{cut}}$ and $\mathcal{T}_1 < \mathcal{T}_1^{\text{cut}}$ at relative $\mathcal{O}(\alpha_S^2)$, given by

$$A_3 \equiv \frac{\frac{d\sigma_{diff}^{\text{NLO}_1}}{dp_T^{H_1}}\theta(\mathcal{T}_0 > \mathcal{T}_{0,\text{ns}}^{\text{cut}})}{\frac{d\sigma^{\text{MATRIX}}}{dp_T^{H_1}}}\,. \tag{7.5}$$

In both cases the subscript *diff* refers to the difference between the observables evaluated on exact kinematical configurations and those evaluated on projected kinematics below the respective resolution cutoffs. These terms capture the effects of power corrections arising from the projections used in GENEVA to assign event kinematics below the resolution cutoffs. As shown in the figure, both contributions are large and positive. Lastly, we examine the following quantity,

$$A_4 \equiv \frac{\frac{d\sigma_{\alpha_S^2}^{\text{nonSing}}}{dp_T^{H_1}}\theta(\mathcal{T}_0 < \mathcal{T}_{0,\text{ns}}^{\text{cut}})}{\frac{d\sigma^{\text{MATRIX}}}{dp_T^{H_1}}}, \tag{7.6}$$

which represents the difference between the pure $\mathcal{O}(\alpha_S^2)$ contributions of GENEVA and MATRIX below $\mathcal{T}_{0,\text{ns}}^{\text{cut}}$, normalised to the same value as before. This term corresponds to the contribution in Eq. (5.2), projected onto $p_T^{H_1}$. To compute this quantity, one needs to subtract the $\mathcal{O}(\alpha_S^2)$ contribution from MATRIX and the resummed-expanded GENEVA result at the same order. This difference is negative and significantly larger than the previously considered terms, making

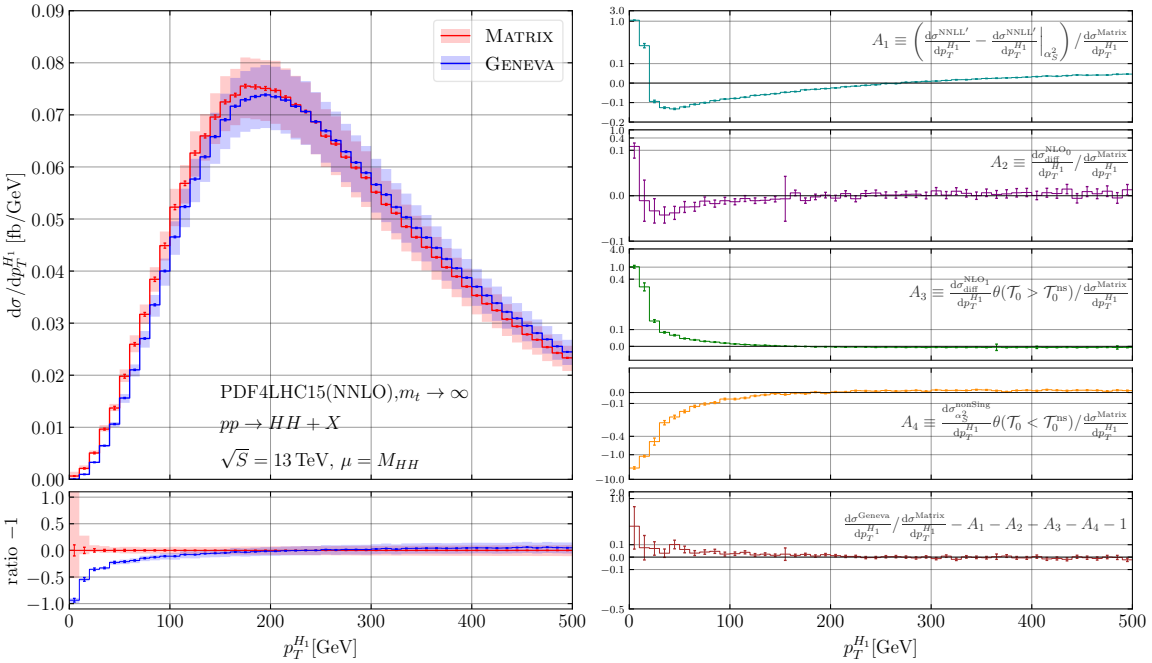

Figure 7.3: Comparison between MATRIX (in red) and GENEVA (in blue) for the transverse momentum of the hardest Higgs boson. On the left, all the possible sources of discrepancy between the two results.

it the primary driver of the discrepancy. To conclude and to demonstrate that there are no other possible sources of differences between GENEVA and MATRIX, we present, in the last panel, the difference between the partonic GENEVA result and MATRIX, subtracted of all the A_i contributions. As expected, this difference is compatible with zero, indicating agreement between the two calculations.

7.3 Showered results

To further study the impact of parton showers, we extend GENEVA's default shower interface to PYTHIA8 to both DIRE, as implemented in PYTHIA8, and the default shower in SHERPA. In order to validate the matching with the shower, we compare the GENEVA partonic result (in blue) with the three different showers available in our framework: PYTHIA8 (in red), DIRE (in green) and SHERPA (in yellow).

The study of the shower effects on double Higgs boson production is particularly interesting due to two main differences compared to other processes already implemented in GENEVA [39, 44, 46, 117]. As widely discussed in Sec. 6.4, since the process is dominated by gluon channel, we expect effects due to gluon emissions to be scaled by a factor $C_A/C_F \sim 2$. Due to the large value of the hard scale, M_{HH}, and considering the scale we have controll over is $\tau_0 = \mathcal{T}_0/M_{HH}$, even at relatively large values of $\mathcal{T}_0$, τ_0 can be small while M_{HH} remains large. As a result,

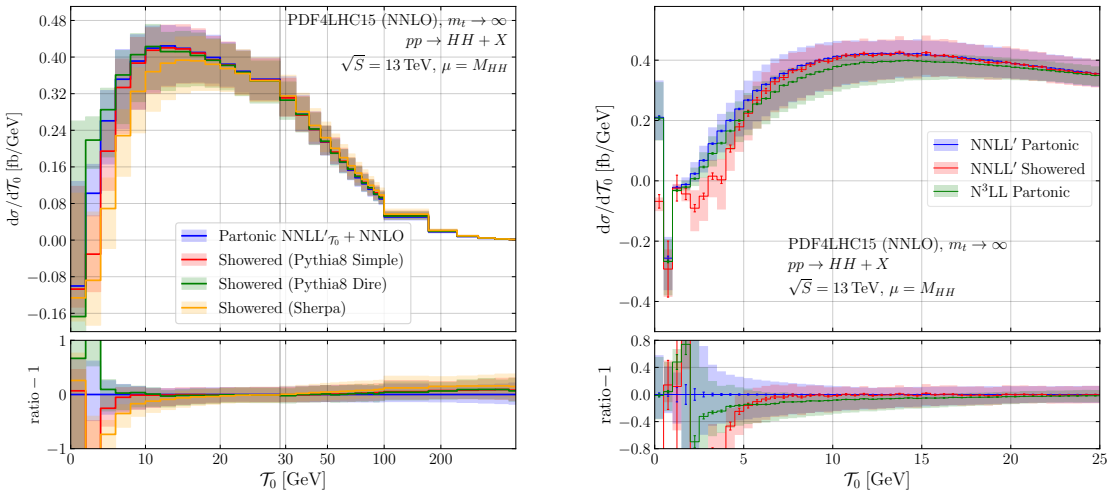

Figure 7.4: Comparison between the partonic and showered $\mathcal{T}_0$ in GENEVA, GENEVA +PYTHIA8, GENEVA +DIRE, GENEVA +SHERPA, on the left, and comparison of the effects of the shower and the effects of the N^{3}LL resummation, on the right.

for any fixed value of $\mathcal{T}_0$, the large logarithmic terms associated to this Higgs boson pair production can be significantly larger than the corresponding terms for the same value of $\mathcal{T}_0$ in other processes. This can be observed, for example, in Fig. 7.4 where we show the $\mathcal{T}_0$-showered spectrum on the left panel. The choice of the parton shower can have a relatively large impact, especially for small ($\leq$ 10 GeV) values of $\mathcal{T}_0$. While all three showers show deviations from the partonic result of roughly the same magnitude, they differ significantly among each other, which can be approximately viewed as a shower matching uncertainty. The net result is that, for the default choice of the evolution variable, the Catani-Seymour based shower as implemented in SHERPA has an evolution variable t on average larger than that of DIRE, leading to its phase space reach being more constrained. This is reflected in the suppression in the small $\mathcal{T}_0$ region. Moreover, the argument presented in Sec. 3.3 does not imply the numerical preservation of the resummed variable $\mathcal{T}_0$. As shown in Fig. 7.4 in the right panel, the parton shower induces a shift in the spectrum of similar size to that obtained by including higher-order effects in the resummation (N^{3}LL at partonic level in green).

In Fig. 7.5, we show how the shower correctly preserves the spectrum of fully inclusive variables such as the invariant mass of the Higgs boson pair, on the left, and the rapidity of the Higgs bosons, on the right. This indicates that the total inclusive cross section is also preserved by the shower. Lastly, in Fig. 7.6 we show how the different showers affect the transverse momentum of the Higgs boson pair system and that of the hardest Higgs boson. While the parton shower is not necessarily expected to preserve these observables, we obseve that all shower predictions are in good agreement with each other and with the partonic result, except for the first bin where they agree within uncertainties. This is likely due to the fact

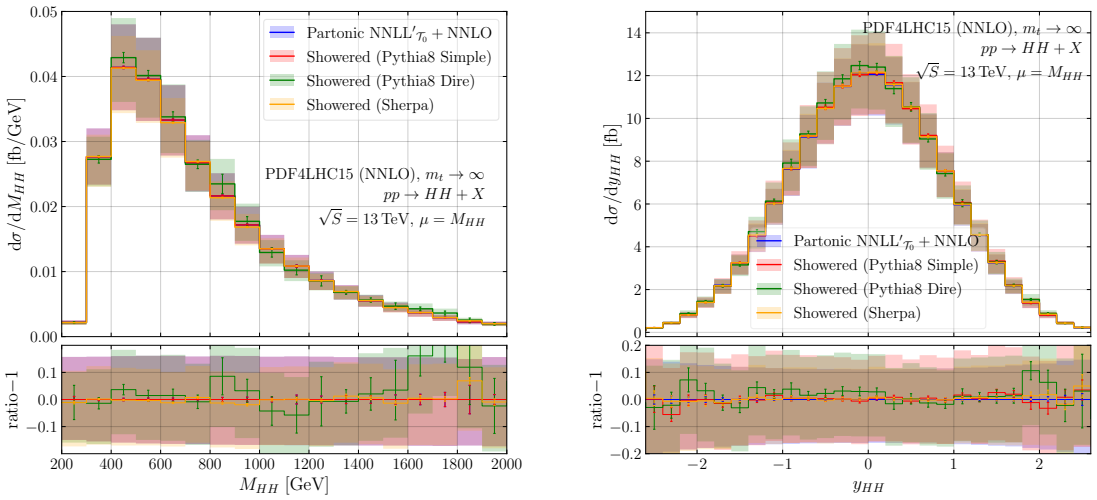

Figure 7.5: Comparison between the partonic and showered invariant mass of the Higgs boson pair, on the left, and their rapidity, on the right.

that partonic events produced by GENEVA already feature both a $\mathcal{T}_0$ and a $\mathcal{T}_1$ resummation, both of which have a non-trivial interplay with the transverse momentum distribution of the colour-singlet system.

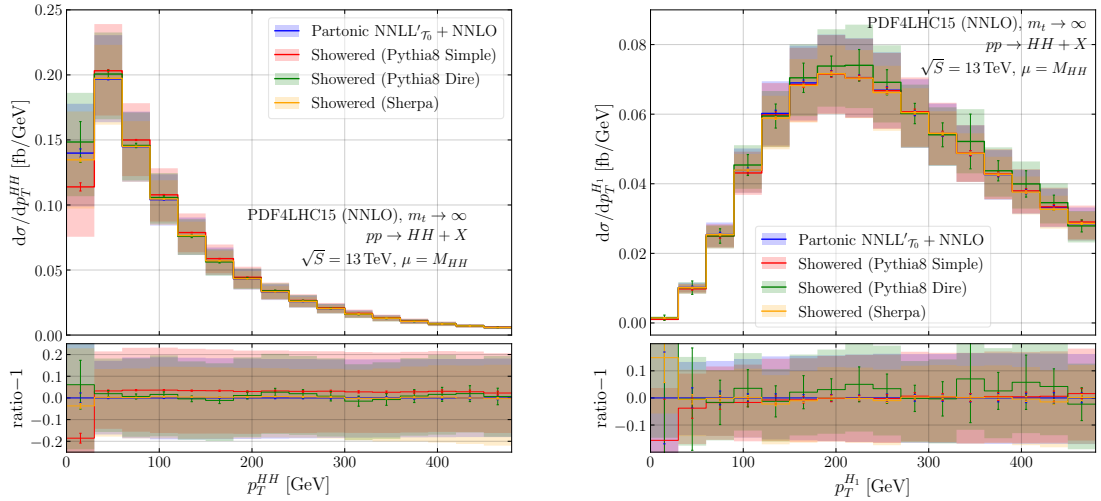

Figure 7.6: Comparison between the partonic and showered transverse momentum of the Higgs boson pair, on the left, and the transverse momentum of the hardest Higgs boson, on the right.

Part II

On the approaches to threshold resummation of rapidity distributions for the Drell-Yan process

Chapter 8

Threshold resummation of Drell-Yan rapidity distributions

The Drell-Yan (DY) process is a fundamental process to study to test the Standard Model to a high accuracy, but also to probe physics beyond this model. It is one of the cleanest processes in high-energy physics due to several reasons. The DY process involves the annihilation of a quark and an antiquark, from the collision of two hadrons, to produce a lepton-antilepton pair and a system of hadrons X. This can be done through the exchange of a virtual photon or a Z boson. When considering interactions involving charged leptons and neutrinos, the exchange of a W boson can also contribute to the DY process. This simplicity of initial and final states makes it easier to identify and reconstruct the particles in the detector. Moreover, the theoretical predictions for such process are well-developed, allowing for accurate estimates of the expected cross section and kinematic distributions. Together with the clean signatures, this allows to use the DY process as a calibration tool for particle detectors and event generators. In addition, the well-understood theoretical background leads to reduced systematic uncertainties in the measurements.

When one is interested in precision in a less inclusive scenario of the total cross section, the best observable are the rapidity distributions, for both experimental and theoretical reasons. One of the most significant advantages of rapidity is its boost-invariance under relativistic transformations. In high-energy collisions, particles are often produced with a wide range of velocities. Rapidities allow to study particle production independently of the energy of the collision. This is crucial because different particles have different masses and momenta, leading to different velocity distributions. Moreover, measuring rapidity distributions is often simpler than measuring momentum or energy distributions, especially when considering that particle detectors are designed to measure particle trajectories and tracks, which are closely related to rapidity.

The study of the rapidity distribution in the DY process, therefore, constitutes a solid testing ground for Standard Model physics and new physics too. The DY process has been study very carefully in perturbative QCD both for inclusive and differential distributions, such as the rapidity distributions which are considered in this work. At present, fixed-order perturbative

predictions in QCD for the cross section and rapidity distributions of this process are available up to next-to-next-to-next-leading order (N^3LO) [118–121]. Fixed order predictions, on their own, are unable to accurately reproduce all the kinematic regions of the phase space. Therefore, they cannot be considered reliable theoretical predictions.

In this chapter we introduce the threshold logarithms, discussing their appearance for rapidity distributions in the specif case of the DY process, establishing our notation. We also discuss in detail the threshold limits and the threshold resummation approaches available in the literature.

8.1 Genesis of threshold logarithms

During high-energy collisions, a large number of partons can be produced. Consider for simplicity a quark parton line that emits n gluons. At each emission, the gluon carries a fraction of the emitted quark energy denoted as $1 - z_n$. Thus, the quark energy decreases with each emission, ultimately amounting to a fraction $z = z_1 z_2 ... z_n$ of its initial energy. In the limit in which the corresponding z_n of the emitted gluon approaches one, the integration over the phase spaces of all the emitted gluons at order α_S^n generates a sequence of terms of the form

$$\alpha_S^n \frac{\log^k(1-z)}{1-z} \qquad 0 \leq k \leq 2n-1\,. \tag{8.1}$$

It becomes evident that as z approaches one, these logarithms become large and require resummation. Physically, this limit implies that after emitting n gluons, the quark retains a substantial portion of its energy, causing the emitted gluon to become soft, with its energy diminishing towards zero. This is the main reason why, usually, the threshold resummation is also called the soft-gluon resummation.

To discuss in more detail the threshold region and the associated resummation, it is convenient to introduce two variables that will be used extensively in the following

$$\tau = \frac{Q^2}{S}\,, \qquad z = \frac{Q^2}{s}\,. \tag{8.2}$$

The first variable, τ, represents a hadronic quantity defined as the ratio of the invariant mass of the final state Q^2 and the hadronic centre-of-mass S. The second variable, z, can be seen as the partonic version of τ, defined as the ratio of Q^2 and the partonic centre-of-mass $s = x_1 x_2 S$. Here $x_{1,2}$ denotes the momentum fractions of the partons originating from each hadron.

The limit in which $\tau \to 1$[1] is called the *hadronic threshold limit*, and it is not very interesting phenomenologically because the cross section is small (indeed, at $\tau = 1$ it becomes identically zero). A more interesting limit is the so-called *partonic threshold limit*, where the parton-level s approaches Q^2, namely that $z \to 1$. The kinematic limit for the partonic variable is $\tau \leq z \leq 1$; consequently, if $\tau \to 1$, then z is forced to be close to 1, meaning that the hadronic threshold limit implies the partonic threshold limit. However, the converse is not true: even far from the hadronic threshold (which is the phenomenologically interesting region for the DY process),

[1] This limit has to be considered from below, $\tau \to 1^-$, since τ has to be smaller than one by construction.

there are always contributions from the partonic threshold region $z \to 1$, as the integral extends to $z = 1$. In this threshold region, tipically defined as the limit in which the invariant mass of the tagged final state is close to the centre-of-mass energy of the initial state, most of the available energy flows into the final state so that any extra radiation has to be soft. Moreover, this region often dominates the integral, due to the shape of the PDFs acting as a weight favouring large values of z even at small τ. This is a well-know phenomenon called dynamical threshold enhancement [31, 32, 122].

To be precise, the form of the threshold logarithms in Eq. (8.1) is not exactly the one that appears in the calculation. Considering Eq. (2.1), when the partonic cross section $\hat{\sigma}_{ab}$ is convolved with the PDFs and then integrated, the terms in Eq. (8.1) present a non-integrable singularity in $z = 1$. In the prediction of any IR-safe observable, this singularity must be combined with the divergence of loop diagrams, which gives rise to

$$\alpha_S^n \left(\frac{\log^k(1-z)}{1-z} \right)_+ , \qquad 0 \leq k \leq 2n-1 \,. \tag{8.3}$$

The + sign denotes the usual plus distribution, defined as

$$\int_0^1 \mathrm{d}y \, [f(y)]_+ \, g(y) = \int_0^1 \mathrm{d}y \, f(y)[g(y) - g(1)] \,,$$
$$[f(x)]_+ = f(x) - \delta(1-x) \int_0^1 f(y) \, \mathrm{d}y \,. \tag{8.4}$$

The highest power of these threshold logarithms grows with the order of the expansion in α_S, with two extra power for each extra order. For instance, in the case of $n = 1$ within the bulk of contributions from Eq. (8.3), the first term appearing in the integrated cross section will be of the form $\alpha_S \log^2(1-z)$. When z is such that this term is roughly of order 1, all terms in the perturbative series become of the same order, rendering it meaningless to truncate the series. Consequently, in the partonic threshold limit, these enhanced logarithms spoil the reliability of the fixed-order computation and call for resummation to all orders.

As already said in Sec. 2.2, also the resummation of threshold logarithms is historically done in Mellin (N) space. The key feature in N space is that the threshold limit translates into the large-N limit. In particular, the logarithms of the type (8.3) generate, in Mellin space, contributions proportional to powers of $\log N$. The logarithms in z space are divergent in the $z \to 1$ limit, which corresponds to the $N \to \infty$ limit or, briefly, the large-N limit. Although this approach for the threshold resummation is well proven, other approaches are largely used, such as the one of SCET. In fact, SCET formalism is able to resum also this type of contributions, as we are going to see in the following.

8.2 Factorisation for rapidity distributions

According to the factorisation theorem of QCD, as expressed in Eq. (2.1), the hadronic rapidity (Y) distribution for a generic LHC process of invariant mass Q^2 at a centre-of-mass energy

$\sqrt{S}$ can be defined as

$$\frac{1}{\tau\,\sigma_0}\frac{\mathrm{d}^2\sigma}{\mathrm{d}Q^2\,\mathrm{d}Y} = \sum_{a,b} c_{ab} \int_{x_1^0}^1 \frac{\mathrm{d}x_1}{x_1} \int_{x_2^0}^1 \frac{\mathrm{d}x_2}{x_2} f_a^{(1)}(x_1)\, f_b^{(2)}(x_2)\, C_{ab}\left(\frac{\tau}{x_1\,x_2}, y, \alpha_S\right), \tag{8.5}$$

where C_{ab} is the perturbative coefficient function (i.e. the partonic cross section differential in Q^2 and y), c_{ab} a constant dependent on the process considered and on the initial partons a, b and

$$x_1^0 = \sqrt{\tau} e^Y\,, \qquad x_2^0 = \sqrt{\tau} e^{-Y}\,, \qquad y = Y - \frac{1}{2}\log\frac{x_1}{x_2}\,, \tag{8.6}$$

with τ already defined in Eq. (8.2) and y the rapidity of the colour singlet in the partonic centre-of-mass frame. Since the arguments of the parton distribution functions have to be smaller than one ($x_{1,2} \leq 1$), the allowed range for the hadronic rapidity of the colour singlet is given by

$$|Y| \leq \log\left(\frac{1}{\sqrt{\tau}}\right). \tag{8.7}$$

A convenient parameterisation can be obtained using the variable u instead of the partonic rapidity y, being linked by the following equations

$$u = \frac{e^{-2y} - z}{(1-z)(1+e^{-2y})}\,, \qquad e^{2y} = \frac{1-(1-z)u}{z+(1-z)u}\,, \tag{8.8}$$

which show that the variable u ranges from 0 to 1, as a consequence of the physical constraint $ze^{2|y|} \leq 1$. Therefore, we can express Eq. (8.5) in terms of the variables z, u, and the cross section becomes

$$\frac{1}{\tau\,\sigma_0}\frac{\mathrm{d}^2\sigma}{\mathrm{d}Q^2\,\mathrm{d}Y} = \sum_{a,b} \int_\tau^1 \frac{\mathrm{d}z}{z} \int_0^1 \mathrm{d}u\, \mathscr{L}_{ab}(z,u)\, C_{ab}(z,u,\alpha_S)\,. \tag{8.9}$$

The change of variables is understood implicitly, and in particular

$$C_{ab}(z,u,\alpha_S) = \left|\frac{\partial(\log x_1, \log x_2)}{\partial(\log z, u)}\right| C_{ab}\left(\frac{\tau}{x_1\,x_2}, y, \alpha_S\right). \tag{8.10}$$

We have defined the non-perturbative parton luminosity $\mathscr{L}_{ab}(z,u)$ as the product of the two parton distribution functions

$$\mathscr{L}_{ab}(z,u) = c_{ab} f_a\left(x_1\right) f_b\left(x_2\right). \tag{8.11}$$

The momentum fractions $x_{1,2}$ are given in terms of z, u, τ and Y by

$$x_1 = \sqrt{\frac{\tau}{z}} e^{Y-y} = \sqrt{\frac{\tau}{z}} e^{Y} \sqrt{\frac{z+(1-z)u}{1-(1-z)u}}\,, \tag{8.12a}$$

$$x_2 = \sqrt{\frac{\tau}{z}} e^{y-Y} = \sqrt{\frac{\tau}{z}} e^{-Y} \sqrt{\frac{1-(1-z)u}{z+(1-z)u}}\,. \tag{8.12b}$$

Note that the physical constraint $x_{1,2} \leq 1$ restricts the actual integration range of u, giving effectively

$$\max\left[0, \frac{\tau e^{-2Y} - z^2}{(1-z)(\tau e^{-2Y} + z)}\right] \leq u \leq \min\left[1, \frac{z(1-\tau e^{2Y})}{(1-z)(\tau e^{2Y} + z)}\right]. \tag{8.13}$$

For a lighter notation, we are omitting the explicit dependence on Y, τ and on the factorisation scale μ_F of the luminosity, which is always implicitly understood. Similarly, we are not showing the dependence on the factorisation and renormalisation scales of the partonic coefficient function, as their dependence is not central in our discussion.

For the specific case of the Drell-Yan process, threshold logarithms only appear in the $q\bar{q}$ channel.[2] For this reason, in Eq. (8.9) (and in all the other related equations) we consider solely the $q\bar{q}$ contribution to the cross section. To keep the notation light, we remove the subscript $q\bar{q}$ from the coefficient function. In addition, once chosen the production channel and hence the value of a and b, the coefficient function does not explicitly depend anymore on the flavour of the initial partons. The cross section for the $q\bar{q}$ channel is then given by

$$\frac{1}{\tau\,\sigma_0}\frac{\mathrm{d}^2\sigma_{q\bar{q}}}{\mathrm{d}Q^2\,\mathrm{d}Y} = \int_\tau^1 \frac{\mathrm{d}z}{z}\int_0^1 \mathrm{d}u\,\mathscr{L}_{q\bar{q}}(z,u)\,C(z,u,\alpha_S)\,, \tag{8.14}$$

where we have defined the "total" $q\bar{q}$ luminosity as

$$\mathscr{L}_{q\bar{q}}(z,u) = \sum_q c_{q\bar{q}} f_q\left(x_1\right) f_{\bar{q}}\left(x_2\right)\,, \tag{8.15}$$

since it is the only function to directly depend on the initial partons flavour. The general expression for the coefficient $c_{q\bar{q}}$ appearing in Eq. (8.15), taking into account the exchange of both a photon and a Z boson, is given by [123]

$$c_{q\bar{q}} = [(v_q^\gamma)^2 + (a_q^\gamma)^2]\,N_\gamma + v_q^\gamma\,v_q^Z\,N_{\gamma Z} + [(v_q^Z)^2 + (a_q^Z)^2]\,N_Z\,, \tag{8.16}$$

where v_q and a_q are the vector and axial couplings for up- and down-type quarks. For simplicity, we are going to consider only the exchange of a virtual photon, for which these constants read

$$\begin{aligned} &v_u^\gamma = \frac{2}{3}\,, \qquad a_u^\gamma = a_d^\gamma = 0\,, \qquad v_d^\gamma = -\frac{1}{3}\,, \\ &N_\gamma = 1\,, \qquad N_{\gamma Z} = 0\,, \qquad N_Z = 0\,. \end{aligned} \tag{8.17}$$

When considering rapidity-integrated distributions, such as the invariant mass distribution or the total cross section, the definition of the threshold logarithm Eq. (8.3) is unique. However, it is possible to distinguish between the logarithms originating from each incoming quark. To achieve this distinction, it is more convenient to use a different set of variables: namely, z_a, z_b

[2] Contributions from other channels are suppressed by at least one power of $(1-z)$ with respect to the threshold logarithms as defined in Eq. (8.3).

related to z, u (or z, y) by the following equations

$$z_a = \sqrt{z}e^{y} = \sqrt{z}\sqrt{\frac{1-(1-z)u}{z+(1-z)u}}, \tag{8.18a}$$

$$z_b = \sqrt{z}e^{-y} = \sqrt{z}\sqrt{\frac{z+(1-z)u}{1-(1-z)u}}, \tag{8.18b}$$

which in turn gives $z = z_a z_b$. Each of these variables is related to each incoming parton. In particular, the momentum fractions $x_{1,2}$ defined in Eq. (8.12) are given by

$$x_1 = \frac{x_a}{z_a}, \qquad x_a = \sqrt{\tau}e^{Y}, \tag{8.19a}$$

$$x_2 = \frac{x_b}{z_b}, \qquad x_b = \sqrt{\tau}e^{-Y}, \tag{8.19b}$$

with $x_a x_b = \tau$. In terms of these variables, Eq. (8.14) takes the form of a double Mellin convolution

$$\frac{1}{\tau\,\sigma_0}\frac{\mathrm{d}^2\sigma_{q\bar{q}}}{\mathrm{d}Q^2\,\mathrm{d}Y} = \int_{x_a}^1 \frac{\mathrm{d}z_a}{z_a}\int_{x_b}^1 \frac{\mathrm{d}z_b}{z_b}\,\tilde{C}\left(z_a, z_b, \alpha_S\right)\sum_q c_{q\bar{q}}\, f_q\left(\frac{x_a}{z_a}\right) f_{\bar{q}}\left(\frac{x_b}{z_b}\right), \tag{8.20}$$

where

$$\tilde{C}\left(z_a, z_b, \alpha_S\right) = \frac{\mathrm{d}z\,\mathrm{d}u}{\mathrm{d}z_a\,\mathrm{d}z_b} C\left(z(z_a, z_b), u(z_a, z_b), \alpha_S\right). \tag{8.21}$$

The coefficient function in terms of these variables contains double logarithms of the form Eq. (8.3) but in the variables z_a and z_b separately:

$$\alpha_S^n\left(\frac{\log^k(1-z_a)}{1-z_a}\right)_+ \qquad \text{and} \qquad \alpha_S^n\left(\frac{\log^k(1-z_b)}{1-z_b}\right)_+, \qquad 0 \le k \le 2n-1\,. \tag{8.22}$$

These are related to the threshold logarithms in the variable z, but the conversion is not straightforward, as it involves also the u dependence. For completeness, we report in appendix C the conversions needed to write the coefficient function in the two sets of variables, taking the NLO coefficient function as a concrete example. Some conversions can also be found in Ref. [124].

When using these parton-specific variables, there are two regions that generate large logarithms: $z_a \to 1$ and $z_b \to 1$. The threshold region discussed before, $z \to 1$, coincides with the overlap of the two regions $z_a \to 1$ and $z_b \to 1$, because of the relation $z = z_a z_b$. This can be seen in Fig. 8.1, where we give a simple representation of the regions identified by these three variables. Considering the (z_a, z_b) plane, the limits $z_a \to 1$ and $z_b \to 1$ define the two light-blue shaded regions. These regions include the case in which just one of these two variables is large, say $z_a \to 1$, and the other is not large, $z_b \ll 1$. Since $z = z_a z_b$, z is not large and, consequently, in this particular case the threshold logarithms in Eq. (8.3) are harmless. However, there are large logarithms (8.22) in the coefficient functions (those from

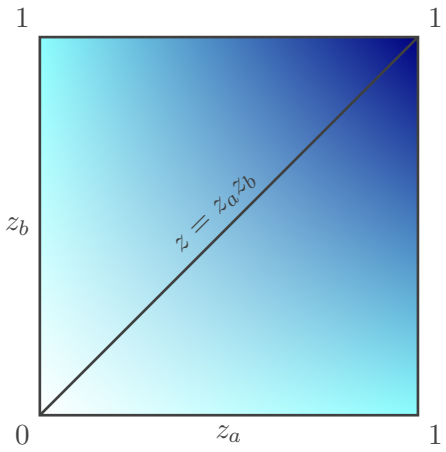

Figure 8.1: Graphic illustration of the threshold limits in the (z_a, z_b) plane. The light-blue regions, corresponding to $z_{a,b} \to 1$, define the generalized partonic threshold region. The blue region, given by the diagonal line $z = z_a z_b$, defines the partonic threshold limit.

z_a) which may spoil the perturbative convergence.[3] These considerations show that there is a region where these logarithms are large, bigger than the partonic threshold region previously defined, and adopting a notation introduced in Ref. [124], we may call it *generalized partonic threshold region*. In order to restore the partonic threshold limit, meaning $z \to 1$, both the partons have to be at threshold, $z_a \to 1$ and $z_b \to 1$. This is represented by the blue shaded region around the diagonal line in Fig. 8.1. The two light-blue shaded regions can be seen as the partonic version of the generalized hadronic threshold region of Ref. [124], identified by the condition $\tau e^{2|Y|} \to 1$ (or equivalently either x_a or x_b close to 1, depending on the sign of Y), which corresponds to the tails of the rapidity distribution irrespectively of the value of τ. This corresponds to the region in which the production of the Drell-Yan lepton pair is at threshold at a given value of the rapidity Y. In this region, either z_a or z_b is forced to be large, but the other variable can take any accessible value. Therefore, the generalized hadronic threshold limit implies the generalized partonic threshold limit. It is worth noting that in the stronger hadronic threshold limit $\tau \to 1$, both z_a and z_b are forced to be large, and therefore this generalized partonic threshold region coincides with the partonic threshold region $z \to 1$.

[3] This mechanism can be understood in terms of the z, u variables noting that there are other large contributions in the coefficient function coming from the u dependence. It is immediate to see from Eq. (8.18) that $z_a \to 1$ corresponds to $u \to 0$, and $z_b \to 1$ corresponds to $u \to 1$, as already pointed out in appendix C. These singular contributions from the u dependence are enhanced at the partonic rapidity endpoints, as one can see from Eq. (8.8), and are therefore relevant to describe the tails of the rapidity distribution.

8.3 Threshold resummation approaches for rapidity distributions

Depending on which parameterisation is used, if (8.12) or (8.19), there exist at least two families of threshold resummation approaches. The one using the parameterisation in z, u aims at resumming the logarithms in the z variable, while the one using the z_a, z_b variables aims at resumming the logarithms in the single $z_{a,b}$ variables. Concerning the first family, in the partonic threshold region $z \to 1$ the coefficient function can be expanded as

$$C(z,u) = C_{\text{thr}}(z,u)[1 + \mathcal{O}(1-z)]\,, \tag{8.23}$$

where we are omitting again the argument α_S to emphasise the dependence on the other variables. Here, $C_{\text{thr}}(z,u)$ contains all leading power threshold contributions, namely the plus distributions Eq. (8.3) and delta functions $\delta(1-z)$. With this parameterisation, there may be terms that are apparently singular in $z=1$ but multiply some u-dependent contribution that makes them integrable. In this case, the plus distribution is not needed, see e.g. the second term in the second line of Eq. (C.2).

To our knowledge, there exist four approaches to resum threshold logarithms in rapidity distribution for the Drell-Yan process. We present them in chronological order of appearance, briefly discussing their main differences:

1. The approach of Becher, Neubert, Xu (**BNX** henceforth) [31], using the z, u parameterisation. It is based on the observation that the u dependence in the PDF luminosity Eq. (8.15) is next-to-leading power at large z, Eq. (8.12), which allows to write the leading power contribution in terms of the rapidity-integrated coefficient function, whose resummation is well known. With respect to Eq. (8.23), the u dependence of the coefficient function at threshold is further approximated as

$$C_{\text{thr}}^{\text{BNX}}(z,u) \equiv \frac{\delta(1-u)+\delta(u)}{2}\, C_{\text{thr}}(z)\,, \tag{8.24}$$

   where $C_{\text{thr}}(z)$ is the rapidity-integrated coefficient function at threshold.[4] This structure, due to the subleading nature of the u dependence in the PDFs, is proposed to all orders. The resummation of the coefficient function $C_{\text{thr}}^{\text{BNX}}(z)$ is computed through SCET, and the hadronic cross section is given by

$$\frac{1}{\tau\,\sigma_0}\frac{\mathrm{d}^2\sigma_{q\bar{q}}^{\text{res,BNX}}}{\mathrm{d}Q^2\,\mathrm{d}Y} = \int_\tau^1 \frac{\mathrm{d}z}{z}\,\frac{\mathscr{L}_{q\bar{q}}(z,0)+\mathscr{L}_{q\bar{q}}(z,1)}{2}\, C_{\text{thr}}^{\text{res}}(z)\,, \tag{8.25}$$

   where the integration over the u variable has been performed.

2. The approach of Bonvini, Forte, Ridolfi (**BFR** henceforth) [32], using the z, u parameterisation. It is similar to the BNX approach, but the derivation is based on a different

[4] The expressions at NLO and NNLO for this coefficient are reported in appendix D.1 for completeness.

argument in Mellin-Fourier space [125], and extends the older result of Ref. [126]. The proposed factorisation reads

$$C_{\rm thr}^{\rm BFR}(z,u) \equiv \delta\left(u-\frac{1}{2}\right) C_{\rm thr}(z)\,, \tag{8.26}$$

leading to the following hadronic cross section

$$\frac{1}{\tau\,\sigma_0}\frac{{\rm d}^2\sigma_{q\bar{q}}^{\rm res,BFR}}{{\rm d}Q^2\,{\rm d}Y} = \int_\tau^1 \frac{{\rm d}z}{z}\,\mathscr{L}_{q\bar{q}}\left(z,\frac{1}{2}\right) C_{\rm thr}^{\rm res}(z)\,. \tag{8.27}$$

Note that the BFR and BNX results[5] are both based on factorising the u dependence in the threshold limit, but this is achieved in two different ways. Indeed, it can be shown that the two formulations are equivalent up to power suppressed contributions in the threshold limit. In particular, since the difference in the two formulations is in the structure of the parton luminosity, the equivalence is shown by providing that

$$\frac{\mathscr{L}_{q\bar{q}}(z,0)+\mathscr{L}_{q\bar{q}}(z,1)}{2} - \mathscr{L}_{q\bar{q}}\left(z,\frac{1}{2}\right) = \mathcal{O}[(1-z)^2]\,. \tag{8.28}$$

This fact does not mean that the accuracy of these two formulations is higher, it just tells that the two approaches are more similar than expected from the accuracy of the derivation.

3. The approach of Banerjee, Das, Dhani, Ravindran (**BDDR** henceforth) [128, 129], using the z_a, z_b parameterisation. It is a two-scale extension of the original approaches to rapidity-integrated resummation [5, 6], already introduced for x_F distributions in Ref. [6] and later converted to rapidity distributions in Refs. [130–134], where a double Mellin transform is taken with respect to the two variables z_a and z_b and logarithms of the product of the two Mellin conjugate variables are resummed to all orders. The novelty of this approach is in the resummed coefficient function, which is written as the sum of two contributions

$$C^{\rm res,BDDR}(z_a,z_b,Q^2) = C^{\rm hard}(z_a,z_b,Q^2) + C^{\rm SV}(z_a,z_b,Q^2)\,. \tag{8.29}$$

The first term is calculated through SCET and constitutes the hard part of the process (similarly to the hard function), while the second one is called the soft-plus-virtual (SV) term. It is the analogous of the threshold logarithms exponentiation but in N space. The $C^{\rm SV}$ coefficient, for the specific case of the DY process and only considering the $q\bar{q}$ channel, is computed doing a double Mellin transform of the individual contributions ($z_a \to N_a$ and $z_b \to N_b$, separately) and then the canonical exponentiated form is obtained, yielding to

$$\tilde{C}_{q\bar{q}}^{\rm SV}(w) = \int_0^1 {\rm d}z_a\, z_a^{N_a-1} \int_0^1 {\rm d}z_b\, z_b^{N_b-1}\, C_{q\bar{q}}^{\rm SV} = g_{q\bar{q}}^0(\alpha_S)\exp[g_{q\bar{q}}(\alpha_S,w)]\,, \tag{8.30}$$

[5] It is important also to stress that the integral over u of both (8.24) and (8.26) gives exactly $C_{\rm thr}(z)$. This coefficient function is then the threshold limit of the well known inclusive coefficient function, whose resummation has been studied for decades [5, 6, 8, 12, 37, 127].

with $w = \alpha_S \beta_0 \log(N_a N_b)$, where β_0 is the zeroth order coefficient of the beta function. The coefficients $g_{q\bar{q}}(\alpha_S, w)$ are process independent and contain purely logarithmically enhanced terms that can be expanded to the desired order.

4. The approach of Lustermans, Michel, Tackmann (**LMT** henceforth) [124], using the z_a, z_b parameterisation. It considers the SCET formalism to factorise the cross section in terms of beam and a soft functions, enabling the resummation of threshold logarithms after solving the renormalization group equations that they obey. As already said, it is designed to be valid in the generalized threshold region, thus enlarging its kinematic range of applicability. The generalized threshold factorisation theorem can be schematised as

$$\frac{\mathrm{d}^2\sigma}{\mathrm{d}Q^2\,\mathrm{d}Y} = \frac{1}{S}\,\mathbf{H}_{q\bar{q}}\left[f_q^{\mathrm{thr}} \otimes \mathbf{B}_q + \mathbf{B}_q \otimes f_{\bar{q}}^{\mathrm{thr}} - \mathbf{S} \otimes f_q^{\mathrm{thr}} f_{\bar{q}}^{\mathrm{thr}}\right], \tag{8.31}$$

where **H** is the hard function, **B** the beam function and **S** the soft function. The first term of such equation represents the limit $x_a \to 1$, while the second one $x_b \to 1$, meaning that these are two regions in which one of the two partons is at threshold while the other one can take any allowed value. The last term is the subtraction of the overlap between the two threshold limits considered.

To conclude this discussion, we want to stress that the BDDR approach has been recently extended [135–138] to resum next-to-leading power contributions to the dominant $q\bar{q}$ channel, specifically those suppressed by one power of $1 - z_a$ or $1 - z_b$ with respect to the leading power logarithms Eq. (8.22). This extension allows to enlarge the region where threshold contributions dominate, and is therefore very useful to obtain reliable predictions close to threshold and more precise predictions even far from threshold. However, achieving higher accuracy necessitates the inclusion of next-to-leading power contributions from other channels, such as the qg channel. It is important to note that the LMT approach already captures these subleading power contributions, predicting also the off-diagonal qg channel at leading power. This approach is constructed to resum the leading power terms in one variables while retaining full dependence on the other variable. Therefore, it contains contributions suppressed with any power of $1 - z_b$ which multiples the leading-power terms in z_a, and vice versa.[6] Although the LMT approach provides the best analytic structure for this resummation, and it is valid in a wider kinematic range, it currently does not implement all-order results in a numerical code.

[6] These towers of contributions are referred to as leading power in the generalized threshold limit ($\mathrm{LP}_{\mathrm{gen}}$) in Ref. [124].

Chapter 9

Validation of the BNX and BFR approaches

In this chapter, we focus on the BNX and BFR approaches introduced in Sec. 8.3, whose validity has been criticised in Ref. [124]. We present a new detailed proof that validates both approaches, while also addressing potential caveats and the reliability of this result. We also comment on other criticisms that are not directly linked to the proof of the two approaches.

Before moving on, we want to stress again that the original BNX and BFR approaches use different methods for resumming to all orders the coefficient $C_{\rm thr}(z)$, as briefly discussed in Sec. 8.3. For our purposes, the way in which $C_{\rm thr}(z)$ is resummed is irrelevant, and the quality of such resummation will be discussed later on.

In this section, the fundamental element is the factorisation of the luminosity in conjunction with the expanded coefficient function. Indeed, considering Eqs. (8.24) and (8.26), the u dependence of the coefficient function is distributional, and each equation cannot be seen as an approximation of the other. Thus, it is not correct to assert that $\delta(u) + \delta(1-u) \simeq 2\delta(u - \frac{1}{2})$. The meaning of such equations resides in the way they are convolved with the PDFs, and consequently in the way they appear in the cross section formula (8.14). We show this in detail.

9.1 New proof of BNX and BFR

In Ref. [124], one of the major objections is the fact that the original proof of the BFR approach [32] has a conceptual problem in one of the steps. In particular, the authors claim that it is not correct to assert that the Fourier transform of the coefficient function, $\tilde{C}(z, M)$, where M is the Fourier conjugate variable to the parton rapidity y, is independent from M. The proof is based on the expansion of the Fourier transform kernel e^{iMy} in powers of y, which is truncated at order 0 because y is a variable ranging in $|y| < \frac{1}{2}\log\frac{1}{z} \sim \frac{1}{2}(1-z)$, and so higher orders in y are effectively suppressed by powers of $(1-z)$. The objection is that the conjugate variable M has to be counted as of order $\frac{1}{1-z}$ according to the Fourier inversion theorem. Therefore, the expansion in powers of y is not legitimate, in the sense that the neglected terms are not really power suppressed. We agree with this criticism, and confirm that the proof of BFR in Ref. [32] is not satisfactory. For this reason, we now propose a

new derivation of the BFR approach, which is also valid for the BNX one, making use of the peculiar z, u dependence of the luminosity.

As already mentioned, the key element is the convolution of the PDFs and the coefficient function in (8.24) and (8.26). Looking at the argument of the luminosity in Eq. (8.12), we observe that in the threshold limit, $z \to 1$, the PDFs become independent of the u variable. This can be further seen by expanding the arguments of the PDFs, Eq. (8.12), in powers of $(1-z)$

$$x_1 = \sqrt{\tau} e^{Y} \left[1 + u(1-z) + \mathcal{O}((1-z)^2)\right], \tag{9.1a}$$

$$x_2 = \sqrt{\tau} e^{-Y} \left[1 + (1-u)(1-z) + \mathcal{O}((1-z)^2)\right]. \tag{9.1b}$$

Following the same line, also the luminosity (8.15) can be expanded as

$$\mathscr{L}_{q\bar{q}}(z,u) = \mathscr{L}_{q\bar{q}}(1,u) - \mathscr{L}'_{q\bar{q}}(1,u)(1-z) + \mathcal{O}[(1-z)^2]\,. \tag{9.2}$$

Here, $\mathscr{L}'_{q\bar{q}}$ is the derivative with respect the z variable, and the first term represents the luminosity computed in $z=1$ which is independent of u,

$$\mathscr{L}_{q\bar{q}}(1,u) = \sum_q c_{q\bar{q}} f_q\left(\sqrt{\tau}e^{Y}\right) f_{\bar{q}}\left(\sqrt{\tau}e^{-Y}\right), \tag{9.3}$$

where we are omitting again the dependence on the factorisation scale not to make the notation heavier. When we will want to emphasise the u independence, we will write it as $\mathscr{L}_{q\bar{q}}(1,\cdot)$.

The fact that the u dependence of the luminosity is power suppressed in the partonic threshold limit $z \to 1$ shows that the u dependence of the coefficient function can be integrated over at leading power.[1] To formally prove this, we consider the cross section formula Eq. (8.14) and we expand the luminosity at threshold, along the lines of Ref. [31]:

$$\begin{aligned}
\frac{1}{\tau\sigma_0}\frac{\mathrm{d}^2\sigma_{q\bar{q}}}{\mathrm{d}Q^2\,\mathrm{d}Y} &= \int_\tau^1 \frac{\mathrm{d}z}{z}\int_0^1 \mathrm{d}u\,\left[\mathscr{L}_{q\bar{q}}(1,\cdot) + \mathcal{O}(1-z)\right] C(z,u) \\
&= \mathscr{L}_{q\bar{q}}(1,\cdot)\int_\tau^1 \frac{\mathrm{d}z}{z}\int_0^1 \mathrm{d}u\, C(z,u)\left[1+\mathcal{O}(1-z)\right] \\
&= \mathscr{L}_{q\bar{q}}(1,\cdot)\int_\tau^1 \frac{\mathrm{d}z}{z}\, C(z)\left[1+\mathcal{O}(1-z)\right] \\
&= \int_\tau^1 \frac{\mathrm{d}z}{z}\,\mathscr{L}_{q\bar{q}}(z,\bar{u})\, C(z)\left[1+\mathcal{O}(1-z)\right] \\
&= \int_\tau^1 \frac{\mathrm{d}z}{z}\,\mathscr{L}_{q\bar{q}}(z,\bar{u})\, C_{\mathrm{thr}}(z)\left[1+\mathcal{O}(1-z)\right].
\end{aligned} \tag{9.4}$$

Here we have first used Eq. (9.2) to expand the luminosity at large z, then we used the u independence of the luminosity in $z=1$ to pull it out of the integral, we then computed the

[1] This is formally correct only at leading power, since the second term of Eq. (9.2) is suppressed by one power of $(1-z)$, constituting a next-to-leading power (NLP) contribution.

u integral to obtain the rapidity-integrated coefficient function $C(z)$.[2] In the penultimate line we restored the z dependence of the luminosity, which is again legitimate up to $\mathcal{O}(1-z)$ thanks to Eq. (9.2), but in doing so we also need to restore the u dependence in the second argument. As u has been integrated over, any value $\bar{u}$ between 0 and 1 is formally acceptable. Finally, in the last step we have further approximated $C(z)$ with its threshold limit. From this last equation, the BNX and BFR formulation can be obtained by choosing the value of $\bar{u}$. In particular, the BFR formulation is given by $\bar{u} = \frac{1}{2}$, while the BNX one corresponds to the average of the result with $\bar{u} = 0$ and $\bar{u} = 1$, already expressed in Eqs. (8.25) and (8.27). In order to use these equations for resummation, the function $C_{\rm thr}(z)$ needs to be resummed to all orders in the threshold limit. The resummed result should then be matched to fixed-order computations, which shall not be approximated. The quality of the resummed and matched result also depend on whether the resummed threshold logarithms are the dominant part of the higher orders or not: we will address this question in section 10.

One last remark is that BNX and BFR are just two of infinitely many possible alternative and equivalent formulations of resummation, which can be obtained by using different values of $\bar{u}$ and averages thereof. We notice however that not all combinations make physical sense. Indeed, the rapidity distribution for the Drell-Yan process in proton-proton collisions is forward-backward symmetric, but the luminosity $\mathscr{L}_{q\bar{q}}(z,u)$ is not symmetric for $Y \to 1-Y$ unless $u = 1/2$. More precisely, the luminosity Eq. (8.15) is symmetric under the exchange of x_1 and x_2, which can in turn be realised by changing $Y \to -Y$ and $u \to 1-u$ simultaneously, see Eq. (8.12). Therefore, only symmetric sums $\mathscr{L}_{q\bar{q}}(z,u) + \mathscr{L}_{q\bar{q}}(z,1-u)$ are symmetric in Y. Since the dependence on the rapidity Y of Eq. (9.4) only comes from the luminosity, the general physically acceptable resummed expression is given by

$$\frac{1}{\tau\sigma_0}\frac{\mathrm{d}^2\sigma^{\rm res}_{q\bar{q}}}{\mathrm{d}Q^2\,\mathrm{d}Y} = \int_\tau^1 \frac{\mathrm{d}z}{z}\,\frac{\mathscr{L}_{q\bar{q}}(z,\bar{u}) + \mathscr{L}_{q\bar{q}}(z,1-\bar{u})}{2} C_{\rm thr}(z)\,, \tag{9.5}$$

where any value of $\bar{u}$ in the allowed range $0 \le \bar{u} \le 1$ is acceptable. Also any weighted average of results with different $\bar{u}$ provides a valid formulation of resummation. It is easy to prove that any symmetric average of the form Eq. (9.5) with any value of $\bar{u}$ is equivalent to BFR and BNX up to $\mathcal{O}[(1-z)^2]$. Obviously, BNX and BFR are two (maximally different) special cases of Eq. (9.5).

In this derivation there are some delicate assumptions that needs to be clarify. Firstly, the second term of Eq. (9.2) can be considered as truly suppressed by a power of $(1-z)$ if $\mathscr{L}'_{q\bar{q}}(1,u)$ is of the same size of $\mathscr{L}_{q\bar{q}}(1,\cdot)$. Moreover, in Eq. (9.4), we are assuming that

$$\mathscr{L}_{q\bar{q}}(1,\cdot) + \mathcal{O}(1-z) = \mathscr{L}_{q\bar{q}}(1,\cdot)\left[1 + \mathcal{O}(1-z)\right]. \tag{9.6}$$

This assumption is not always valid and it can potentially be one limitation of our derivation. By comparing numerically the size of these two functions in section 9.2, we will study the

[2] Note that in this step we also used the fact that in the $z \to 1$ limit the whole region $0 \le u \le 1$ is kinematically allowed, as a consequence of the fact that the restriction imposed by the condition $x_{1,2} < 1$, expressed by the limits Eq. (8.13), are immaterial in the $z \to 1$ limit. This is also obvious from the fact that the restriction on u would be imposed by θ functions hidden in the luminosity, which in $z = 1$ no longer depends on u.

range of applicability of such approximation. We anticipate that keeping the parton luminosity unexpanded is certainly more natural and ensures for instance that kinematic constraints coming from the limits of PDF arguments are preserved by the resummed expression. However, from a formal point of view, it is allowed to also include the parton luminosity in the threshold expansion. The selection of terms that are expanded in Eq. (9.4) is obviously arbitrary but legitimate according to the power counting in $(1-z)$, and it is made in a way to reproduce BNX and BFR as we shall see. We also stress that in Eq. (9.4) we have expanded in powers of $(1-z)$ selected terms of the entire integrand. This is in contrast with the standard approach of threshold resummation [5, 6], where only the coefficient function is expanded. Note also that the contributions of $\mathcal{O}(1-z)$ in the integrand of Eq. (9.4) may be large, as the integral extends down to $z=\tau$ and if τ is small there is a part of the integration region in which these corrections are not suppressed. This fact does not invalidate the derivation of Eq. (9.4), but poses questions about the quality of an approximation obtained neglecting those subleading power terms. We will see in section 9.2 that the approximation for the dependence on the luminosity is rather good even for small values of τ.

9.2 Validity of the threshold expansion in the integrand

In this section, we address and clarify all the assumptions raised in the derivation of the new proof for the BNX and BFR approaches, which can be seen as a limitation of the final result. We are going to show that this is not the case and that BNX/BFR approaches are still valid in the phenomenologically relevant region.

One first problem can be given by the luminosity expansion in Eq. (9.2), which can be used in our derivation if the $\mathscr{L}'_{q\bar{q}}(1,u)$ term is of the same size of $\mathscr{L}_{q\bar{q}}(1,\cdot)$. This is directly linked to the equality in Eq. (9.6) that is used to obtain the final result of the BNX/BFR derivation in Eq. (9.4). This equality is almost always verified, the only problematic region is when $\tau e^{2|Y|}$ is close to 1, corresponding to the region where the PDFs are computed close to their endpoints $x=1$.

To study in detail this region, we focus on the case in which τ is close to 1, which is very similar to consider large values of rapidity but τ small. In this case, as already said, the identity Eq. (9.6) is no longer valid. We can see this analytically, by approximating the PDFs as

$$f(x,\mu_F^2) \simeq (1-x)^\alpha \tag{9.7}$$

for some positive value of α, which is a good approximation at large x. The luminosity is then defined as

$$\mathscr{L}_{q\bar{q}}(z,u) = \sum_q c_{q\bar{q}} (1-x_1)^\alpha (1-x_2)^\alpha \,, \tag{9.8}$$

and the $z=1$ case gives

$$\mathscr{L}_{q\bar{q}}(1,u) = \sum_q c_{q\bar{q}} \left(1-\sqrt{\tau}e^{Y}\right)^\alpha \left(1-\sqrt{\tau}e^{-Y}\right)^\alpha . \tag{9.9}$$

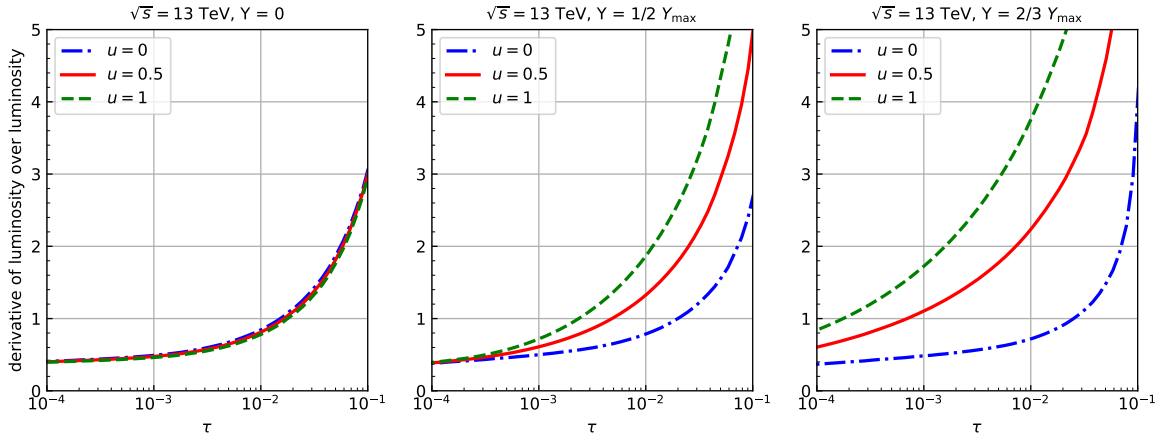

Figure 9.1: Ratio of the derivative of the luminosity over the luminosity in $z = 1$ as a function of τ for $Y = 0$ (left), $Y = 1/2$ (central) and $Y = 2Y_{\max}/3$ (right) for different values of u.

Assuming that the same value of α holds for all quark PDFs, the derivative of the luminosity can be written as

$$\mathscr{L}'_{q\bar{q}}(1,u) \simeq -\alpha\sqrt{\tau}\left(\frac{e^{Y}u}{1-\sqrt{\tau}e^{Y}}+\frac{e^{-Y}(1-u)}{1-\sqrt{\tau}e^{-Y}}\right)\mathscr{L}_{q\bar{q}}(1,\cdot)\,. \tag{9.10}$$

It is clear that at large $\tau e^{2|Y|} \to 1$ one of the two denominators becomes parametrically small, and thus for some values of u the derivative becomes parametrically larger than the luminosity. This becomes even clearer at central rapidity $Y = 0$,

$$\mathscr{L}'_{q\bar{q}}(1,u) \overset{Y=0}{\simeq} -\alpha\frac{\sqrt{\tau}+\tau}{1-\tau}\mathscr{L}_{q\bar{q}}(1,\cdot)\,, \tag{9.11}$$

where the denominator enhances the derivative with respect to the luminosity for any value of u in the $\tau \to 1$ limit. In the derivation of Eq. (9.4), therefore, when we assume that τ is close to 1 which in turn implies that $1 - z$ is of the same order as $1 - \tau$, the term $-\mathscr{L}'_{q\bar{q}}(1,u)(1-z)$ is not subleading power with respect to $\mathscr{L}_{q\bar{q}}(1,\cdot)$ in Eq. (9.2) and the expansion in Eq. (9.4) is not accurate.

This can be seen also numerically in figure 9.1, where we plot the ratio of the derivative of the true luminosity (not the approximated one of Eq. (9.8)) over the luminosity in $z = 1$ as a function of τ for different values of $Y = 0, Y_{\max}/2, 2Y_{\max}/3$, with $Y_{\max} = \frac{1}{2}\log\frac{1}{\tau}$, and $u = 0, 1/2, 1$, using the PDF4LHC21 NNLO PDF set [139] and assuming photon-mediated Drell-Yan production at LHC $\sqrt{S} = 13$ TeV. At central rapidity $Y = 0$, we see that the luminosity is almost independent of u, and we observe that for a wide range of τ values $10^{-4} < \tau < 10^{-1}$ this ratio is of $\mathcal{O}(1)$, making the proof of the previous section valid for these specific kinematics. We see however a clear growth of this ratio going towards large τ, confirming that the assumption Eq. (9.6) breaks down at some point when τ is too large. Increasing the rapidity, the situation gets worse and the ratio becomes larger at smaller values of τ for some values of u (in this case, having used positive rapidity, the largest effect is at

$u = 1$). Despite this deterioration, we notice that in the phenomenologically interesting region of mid-low τ this ratio remais of $\mathcal{O}(1)$ even at large rapidities.

We can thus conclude that the BNX and BFR approaches are formally valid in a restricted kinematical region. They are not supposed to be accurate at large τ and towards the rapidity endpoints, although these are precisely the regions identified by the hadronic threshold limit, where threshold resummation is certainly relevant. The point is that the BNX and BFR formulation are based on an approximation of the dependence of z and u of the coefficient function, and it is this particular approximation that is not valid in the hadronic threshold region. Far from it, the approximation is legitimate, and it allows to resum the partonic threshold logarithms in the cross section.

To further study in which kinematic region the BNX and BFR formulation are valid, we can consider a slightly different version of the BNX and BFR expression (8.25) and (8.27). To do so, instead of using the threshold expansion of the coefficient function $C_{\rm thr}(z)$, we replace it with the full $C(z)$

$$\frac{1}{\tau\sigma_0}\frac{\mathrm{d}^2\sigma^{\rm BNX}_{q\bar{q}}}{\mathrm{d}Q^2\,\mathrm{d}Y} \to \int_\tau^1 \frac{\mathrm{d}z}{z}\,\frac{\mathscr{L}_{q\bar{q}}(z,0)+\mathscr{L}_{q\bar{q}}(z,1)}{2}C(z)\,, \tag{9.12}$$

$$\frac{1}{\tau\sigma_0}\frac{\mathrm{d}^2\sigma^{\rm BFR}_{q\bar{q}}}{\mathrm{d}Q^2\,\mathrm{d}Y} \to \int_\tau^1 \frac{\mathrm{d}z}{z}\,\mathscr{L}_{q\bar{q}}\left(z,\frac{1}{2}\right)C(z)\,. \tag{9.13}$$

These expressions represent alternative formulations for the rapidity distribution where only the luminosity is approximated, and correspond to neglecting the $\mathcal{O}(1-z)$ contributions in the penultimate line of Eq. (9.4). These expression cannot be used for resummation, as the exact $C(z)$ is not know to all orders. As such, comparing them with the exact distribution at fixed order, we are able to judge the quality of the approximation of the luminosity, and thus the impact of the neglected derivative terms.

In figures 9.2 and 9.3, where we plot the exact contributions to the rapidity distribution at NLO and NNLO (in the $q\bar{q}$ channel only) along with the approximations of the luminosity dependence à la BNX and BFR, Eqs. (9.12), (9.13). In the first figure the distribution is shown as a function of τ and for different values of $Y = 0, Y_{\rm max}/2, 2Y_{\rm max}/3$, while the second figure shows the same distribution but as a function of Y for three values of $\tau = 10^{-4}, 10^{-2}, 10^{-1}$. The plots are obtained considering photon-mediated Drell-Yan production at LHC $\sqrt{S} = 13$ TeV, using again the PDF4LHC21 NNLO PDF set [139] and taking from it the value of the strong coupling. The exact NNLO result is taken from the `Vrap` code [123,140], selecting from it only the terms contributing to the $q\bar{q}$ channel.

We observe that at small τ and central rapidity, the quality of the approximation is excellent at NLO and NNLO, as in both cases the BNX/BFR curves are almost identical to the exact result. Note that while we expect a failure of the validity of the expansion in powers of $(1-z)$ at large τ and/or large rapidity, it is perhaps surprising to see such a good agreement at such small values of τ. Indeed, the neglected $\mathcal{O}(1-z)$ contributions, though geniunely subleading, are not necessarily small as the integration over z extends to values as small as τ. An explanation of this effect is the fact that the shape of the luminosity strongly favours large values of z in the integrand and suppresses the region of z close to τ, as a consequence of the small-x growth and the large-x suppression of the PDFs $f_i(x,\mu_f^2)$, respectively. Therefore, the

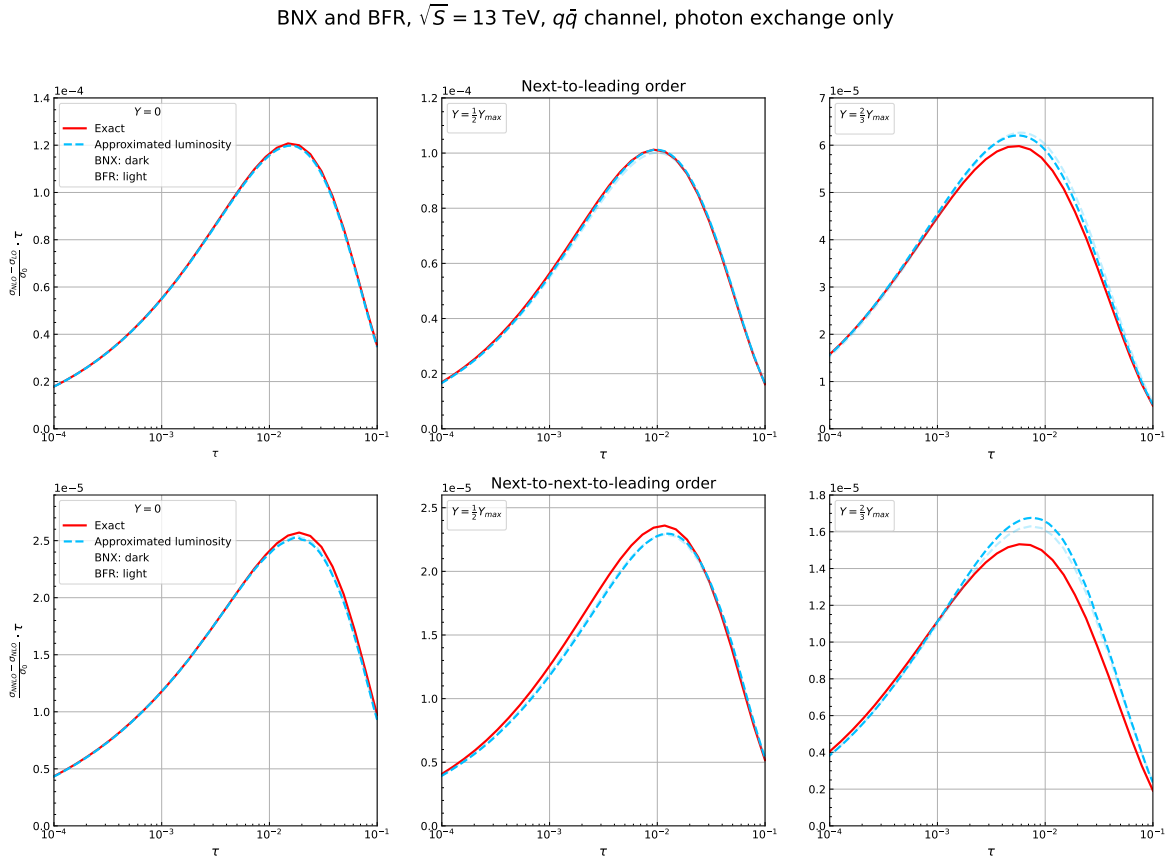

Figure 9.2: Rapidity distributions at NLO (up) and NNLO (down) as a function of τ for $Y = 0, Y_{\max}/2, 2Y_{\max}/3$. The approximations are obtained expanding the luminosity à la BNX (darker colour) and à la BFR (lighter colour), given by Eq. (9.12) and (9.13) respectively, where we use the full $C(z)$ instead of its threshold approximation $C_{\rm thr}(z)$.

integral over z is dominated by the large-z region, well described by a threshold approximation, while the contribution from medium-small z down to τ is a small correction. This phenomenon is the so-called dynamical threshold enhancement of Ref. [31], and it is responsible for the threshold dominance also at the rapidity-integrated level, see e.g. Ref. [141].

Moving towards larger values of Y and τ we see some deterioration of the agreement, more marked at NNLO. However, in the range of values of τ, Y considered here, the accuracy of the approximation remains very high, with discrepancies of the order of some percent. We can appreciate in particular a slight distorsion of the Y dependence of the distribution, clearly visible at NNLO in figure 9.3. We stress that, by construction, the integral in rapidity of all the curves in each plot is the same and coincides with the exact rapidity-integrated cross section, as we also verified numerically. This constraint also contributes to the high accuracy of the approximation.

The excellent quality of the approximation of the luminosity at the core of the BNX/BFR

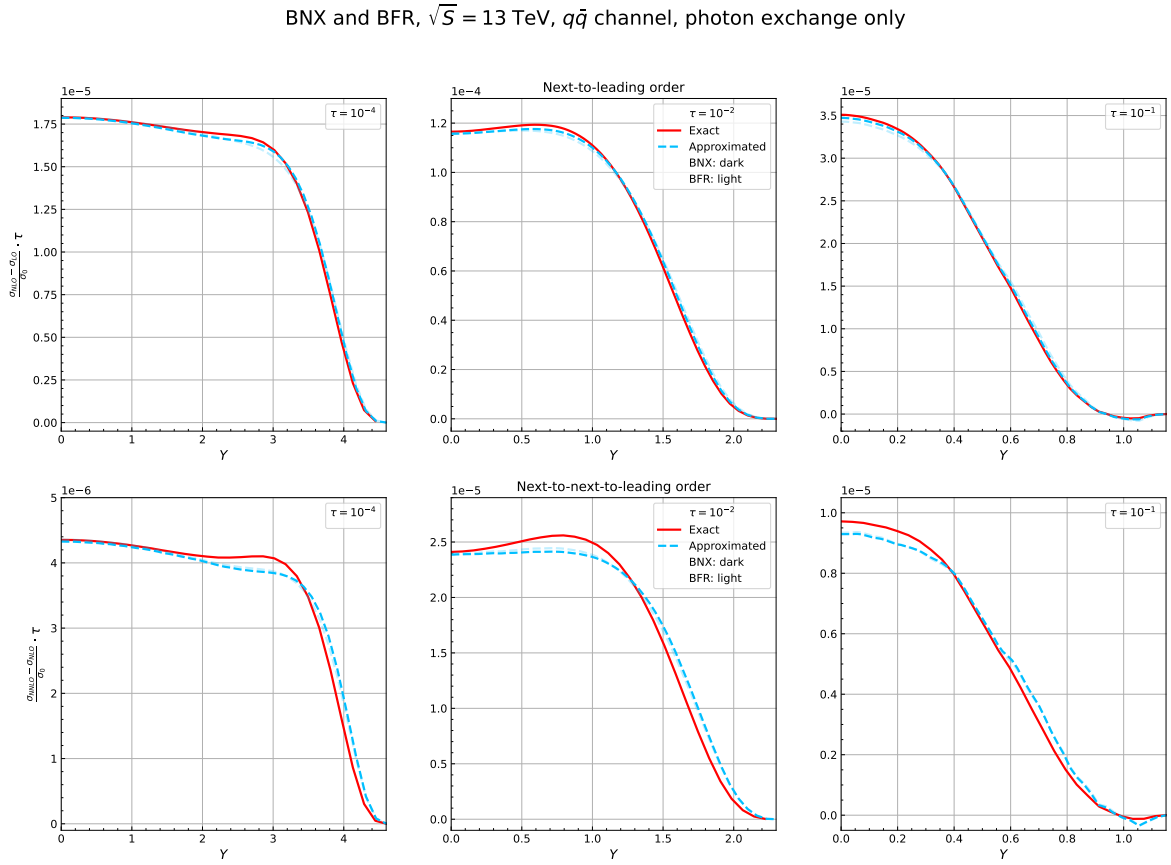

Figure 9.3: Rapidity distributions at NLO (up) and NNLO (down) as a function of Y for $\tau = 10^{-4}, 10^{-2}, 10^{-1}$. The approximations are obtained expanding the luminosity à la BNX (darker colour) and à la BFR (lighter colour), given by Eq. (9.12) and (9.13) respectively, where we use the full $C(z)$ instead of its threshold approximation $C_{\text{thr}}(z)$.

formulation can be understood analytically. By repeating the derivation of Eq. (9.4) keeping also the linear term in $(1-z)$ of the expansion of the luminosity Eq. (9.2), it is easy to find

$$\frac{1}{\tau\sigma_0}\frac{\mathrm{d}^2\sigma_{q\bar{q}}}{\mathrm{d}Q^2\,\mathrm{d}Y} = \int_\tau^1 \frac{\mathrm{d}z}{z}\Big[\mathscr{L}_{q\bar{q}}(z,\bar{u})\,C(z) + (1-z)\int_0^1 \mathrm{d}u\Big(\mathscr{L}'_{q\bar{q}}(1,\bar{u}) - \mathscr{L}'_{q\bar{q}}(1,u)\Big)C(z,u) + \mathcal{O}\left((1-z)^2\right)\Big] \tag{9.14}$$

where the term proportional to $\mathscr{L}'_{q\bar{q}}(1,\bar{u})$ appears when we replace $\mathscr{L}_{q\bar{q}}(1,\cdot)$ with $\mathscr{L}_{q\bar{q}}(z,\bar{u})$ in the fourth line of Eq. (9.4). We thus observe that the linear term in $(1-z)$ is not proportional to the entire derivative $\mathscr{L}'_{q\bar{q}}(1,u)$, but to the difference $\mathscr{L}'_{q\bar{q}}(1,\bar{u}) - \mathscr{L}'_{q\bar{q}}(1,u)$, which is obviously smaller. The same holds for higher derivative terms. In other words, restoring the z dependence in the luminosity, even if this introduces a dependence on the new, arbitrary variable $\bar{u}$, is beneficial as it allows to reduce the impact of the missing contributions at higher order in

$(1-z)$.

We thus conclude that the limitations coming from the growth of the derivative of the luminosity at large $\tau e^{2|Y|}$ is more formal than practical, and for all phenomenologically relevant values of these parameters the approximation of the luminosity leading to the BNX/BFR expressions is fully valid. In passing, we have also shown that the large-z approximation on the luminosity in Eq. (9.4) is of very high quality even when τ is small, despite the integral contains many values of z which are far from 1 and for which the threshold expansion is not formally accurate. The actual quality of threshold resummation based on Eq. (9.4), performed either à la BNX Eq. (8.25) or à la BFR Eq. (8.27), also depends on how well $C_{\rm thr}(z)$ approximates the exact $C(z)$, and we will discuss this in chapter 10.

9.3 Other objections to BNX and BFR

Here we analyse other objections raised in Ref. [124], claiming that the BNX and BFR approaches are not accurate at leading power in $(1-z)$. The main argument is that a class of terms apparently enhanced in the $z\to 1$ limit are missed in these approaches. Specifically, any term in $C(z,u)$ that vanishes after integration over u cannot be captured by the BNX and BFR approaches. One simple example can be extracted by the coefficient at NLO given in Eq. (C.2), in particular by the term of the form

$$F(z,u)=\frac{1}{1-z}\left[\left(\frac{1}{u}\right)_+ +\left(\frac{1}{1-u}\right)_+\right]. \tag{9.15}$$

This term is singular in $z=1$, but since it multiplies plus distributions in u it vanishes after integration over u. According to Ref. [124], this is a leading power contribution that is missing in BNX and BFR but it is correcly counted in their approach.

If we were to count powers of $(1-z)$ at the level of the coefficient function only, the term Eq. (9.15) is formally leading power, like the terms that are retained in BNX/BFR, and we will agree with the authors of Ref. [124]. However, our derivation of BNX/BFR in section 9.1 adopts a power counting in $(1-z)$ at the level of the full integrand of Eq. (8.14), thus including also the parton luminosity. What we are now going to show is that the term Eq. (9.15), because of its peculiar u dependence, contributes at next-to-leading power to the integral, and is thus consistently missing in the BNX/BFR leading power result.

The proof that the term Eq. (9.15) does not contribute at leading power relies again on the fact that the luminosity in $z=1$ is independent of u. To see this, we consider the u integral of that term multiplied by the luminosity,

$$\begin{aligned}\bar{F}(z)&\equiv\int_0^1 \mathrm{d}u\, F(z,u)\,\mathscr{L}_{q\bar{q}}(z,u)\\&=\frac{1}{1-z}\left[\int_0^1\frac{\mathrm{d}u}{u}\,\left(\mathscr{L}_{q\bar{q}}(z,u)-\mathscr{L}_{q\bar{q}}(z,0)\right)+\int_0^1\frac{\mathrm{d}u}{1-u}\,\left(\mathscr{L}_{q\bar{q}}(z,u)-\mathscr{L}\_q\bar{q}(z,1)\right)\right].\end{aligned} \tag{9.16}$$

Each difference of luminosities in the integrands can be expanded in powers of $(1-z)$,

$$\begin{aligned}\mathscr{L}_{q\bar{q}}(z,u)-\mathscr{L}_{q\bar{q}}(z,0) &= \cancel{\mathscr{L}_{q\bar{q}}(1,u)-\mathscr{L}_{q\bar{q}}(1,0)} \\ &\quad -\Big(\mathscr{L}'_{q\bar{q}}(1,u)-\mathscr{L}'_{q\bar{q}}(1,0)\Big)(1-z)+\mathcal{O}[(1-z)^2] \qquad (9.17a)\\ \mathscr{L}_{q\bar{q}}(z,u)-\mathscr{L}_{q\bar{q}}(z,1) &= \cancel{\mathscr{L}_{q\bar{q}}(1,u)-\mathscr{L}_{q\bar{q}}(1,1)} \\ &\quad -\Big(\mathscr{L}'_{q\bar{q}}(1,u)-\mathscr{L}'_{q\bar{q}}(1,1)\Big)(1-z)+\mathcal{O}[(1-z)^2]\,, \qquad (9.17b)\end{aligned}$$

and the zeroth-order contribution in each difference vanishes because the luminosity in $z=1$ does not depend on u. Therefore, each integral in the big rounded brackets in Eq. (9.16) is of order $(1-z)$, and thus cancels the singularity of the $\frac{1}{1-z}$ term in front. We conclude that this contribution behaves as a constant in the $z\to 1$ limit, and therefore counts as a next-to-leading power contribution. This is also the reason why there is no need to surround this term with a plus distribution, which would instead be needed if it counted as leading power.

We can verify this numerically, by plotting the function $\bar{F}(z)$ Eq. (9.16) to see that it does not diverge at $z=1$. We do this in figure 9.4, for different values of $\tau=10^{-4},10^{-2},10^{-1}$ and of the rapidity $Y=0,Y_{\rm max}/2,2Y_{\rm max}/3$, using the usual physical setup. Since there are some numerical oscillations at large z, probably due to the fact that the curve is the ratio of two small numbers, we also plot the PDF uncertainty band to make sure that the interpretation of the result is solid. It is clear that $\bar{F}(z)$ does not diverge in $z=1$, rather it is perfectly finite, showing explicitly that this term is next-to-leading power. We also show, without uncertainty, each of the two contributions to Eq. (9.16) coming from each integral in the rounded brackets, as they are separately regular. We see indeed that both of them do not diverge in $z=1$.

In fact, it is possible to note from the plots that the full function $\bar{F}(z)$ seems to go to zero at $z=1$. This is indeed the case, as we can verify analytically by noticing that the $\mathcal{O}(1-z)$ terms in the expansions Eq. (9.17) satisfy the relation

$$\frac{\mathscr{L}'_{q\bar{q}}(1,u)-\mathscr{L}'_{q\bar{q}}(1,0)}{u}+\frac{\mathscr{L}'_{q\bar{q}}(1,u)-\mathscr{L}'_{q\bar{q}}(1,1)}{1-u}=0\,, \qquad (9.18)$$

which is easy to prove using the general form of the derivative of the luminosity given by

$$\mathscr{L}'_{q\bar{q}}(1,u)=-\sum_q c_{q\bar{q}}\Big[u\sqrt{\tau}e^{Y}f'_q(\sqrt{\tau}e^{Y})f_{\bar{q}}(\sqrt{\tau}e^{-Y})+(1-u)\sqrt{\tau}e^{-Y}f_q(\sqrt{\tau}e^{Y})f'_{\bar{q}}(\sqrt{\tau}e^{-Y})\Big]\,. \qquad (9.19)$$

Therefore, the whole term contributes to the rapidity distribution at next-to-next-to-leading power, and it is thus more suppressed at threshold than naively expected. The same is true also for the individual integrals of Eq. (9.16) when $Y=0$, as a consequence of the fact that the luminosity is symmetric for the exchange $x_1\leftrightarrow x_2$, that at $Y=0$ corresponds to a symmetry for the exchange $u\leftrightarrow 1-u$.

More in general, the BNX and BFR approaches miss any term in $C(z,u)$ that vanishes after integration in u from 0 to 1. Consider a generic function $G(z,u)$ that may seem to be leading power

$$G(z,u)=\frac{\log^k(1-z)}{1-z}g(u)\,, \qquad (9.20)$$

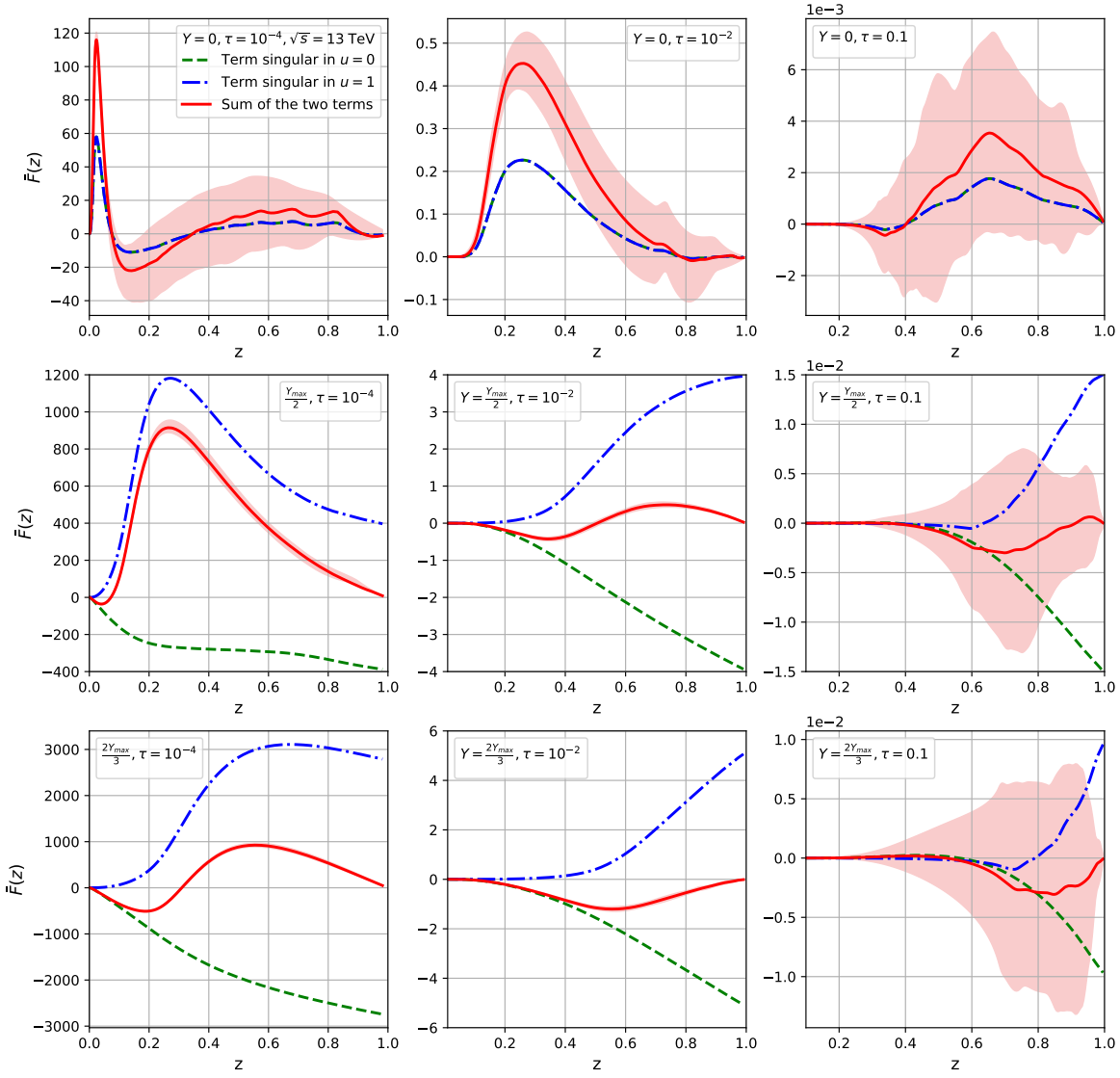

Figure 9.4: $\bar{F}(z)$ contribution in Eq. (9.16) as a function of z for $\tau = 10^{-4}, 10^{-2}, 10^{-1}$ and $Y = 0, Y_{\max}/2, 2Y_{\max}/3$.

for some integer value of k, and with $g(u)$ any function or distribution satisfying the constraint

$$\int_0^1 \mathrm{d}u\, g(u) = 0\,. \tag{9.21}$$

Expanding the luminosity in powers of $1-z$ we find

$$\int_0^1 \mathrm{d}u\, G(z,u)\mathscr{L}_{q\bar{q}}(z,u) = \frac{\log^k(1-z)}{1-z}\int_0^1 \mathrm{d}u\, g(u)\big[\mathscr{L}_{q\bar{q}}(1,\cdot) - \mathscr{L}'_{q\bar{q}}(1,u)(1-z) + \mathcal{O}[(1-z)^2]\big]$$
$$= \log^k(1-z)\int_0^1 \mathrm{d}u\, g(u)\big[-\mathscr{L}'_{q\bar{q}}(1,u) + \mathcal{O}(1-z)\big]\,, \tag{9.22}$$

where, thanks to the fact that the luminosity in $z=1$ is u independent, we could use Eq. (9.21) in the last step to show that the first term of the expansion vanishes. We thus conclude that any apparently leading power term of the general form Eq. (9.20) that vanishes after integration over u contributes effectively at next-to-leading power. Therefore, the fact that BNX and BFR miss these contributions does not represent a power-counting issue.

We observe that contributions of this kind are instead present in the approaches to threshold resummation that keep the separate dependence on z_a and z_b, e.g. Refs. [6, 128, 130–134]. These approaches are also supposed to be valid in the threshold $z\to 1$ limit, but since the limit is performed at the level of the coefficient function these contributions count as leading power and are thus preserved. For what we have shown, in the strict $z\to 1$ limit their inclusion does not increase the accuracy as they are suppressed with respect to the other leading power terms. However, if a threshold approximation/resummation is extended outside the threshold region, namely for values of z that are not large enough, these contributions may be relevant. Indeed, a term like Eq. (9.15) contains enhanced contributions in $u\to 0,1$, which are irrelevant at $z\to 1$ but not at generic z. To understand this, recall that $u\to 0,1$ corresponds to $z_a\to 1$ and $z_b\to 1$ respectively. Since $z=z_a z_b$, when $z\to 1$ both $z_a, z_b\to 1$ irrespectively of the value of u. But when z is not large, one among z_a and z_b can be large if u tends to 0 or 1. These non-threshold but enhanced contributions are captured by the aforementioned approaches, and improve the description of the tails of the rapidity distribution. Therefore, the fact that these contributions are missing in BNX and BFR makes them less accurate than other approaches when the process is far from threshold.

In Ref. [124] there are other arguments used to criticise the validity of the BNX and BFR approaches. One of them is an explicit calculation using the same toy PDF Eq. (9.7) showing that after integration in z and u the two functions

$$A(z,u) = \left(\frac{1}{1-z}\right)_+ \delta\left(u-\frac{1}{2}\right)\,, \qquad B(z,u) = \left(\frac{1}{1-z}\right)_+ \frac{\delta(u)+\delta(1-u)}{2}\,, \tag{9.23}$$

give rise to different leading power contributions. As these correspond to a BFR and a BNX implementation of the same term, if they are both correct at leading power, they should give the same leading power contributions. The problem here is that the computation of Ref. [124] assumes $1-x_a\sim 1-x_b\ll 1$, namely $\tau\to 1$. We have already commented in section 9.2 that in this limit the derivation of BNX and BFR of section 9.1 does not hold anymore, so this conclusion is not surprising. Moreover, the power counting is performed at hadron level, namely the terms identified in Ref. [124] are leading power in $1-x_a$ and $1-x_b$, which makes sense because they assume $\tau\to 1$ but it cannot be directly related to the leading power terms in $(1-z)$ when τ is not large.

Another objection of Ref. [124] regarding the BNX and BFR approaches is related to the expansion of the luminosity Eq. (9.2). In particular, LMT say that the expansion of the arguments $x_{1,2}$ of the PDFs, Eq. (9.1), to the zeroth order is too trivial because it does not depend on z. We believe that this is not a real issue: the expansion in powers of $(1-z)$ is legitimate at large z, and if the zeroth order of this expansion is independent of z it cannot represent a reason for expanding to one order higher. However, for completeness, we can consider an alternative expansion that overcomes the LMT objection, without affecting the proof Eq. (9.4). Specifically, we can expand in powers of $(1-z)$ not the full $x_{1,2}$ expression Eq. (8.12), but only the square root that depends on u:

$$x_1 = \sqrt{\frac{\tau}{z}} e^{Y} \left[1 + \left(u - \frac{1}{2} \right) (1-z) + \mathcal{O}((1-z)^2) \right], \tag{9.24a}$$

$$x_2 = \sqrt{\frac{\tau}{z}} e^{-Y} \left[1 + \left(\frac{1}{2} - u \right) (1-z) + \mathcal{O}((1-z)^2) \right]. \tag{9.24b}$$

Now the leading z dependence appears in the zeroth order term of the expansion, which is still u independent. Of course, this arbitrary expansion is equivalent to that of Eq. (9.1) up to the order at which it is truncated. We can write the luminosity as

$$\mathscr{L}_{q\bar{q}}(z,u) = \mathscr{L}^{(0)}_{q\bar{q}}(z) + \mathcal{O}(1-z) \tag{9.25}$$

with

$$\mathscr{L}^{(0)}_{q\bar{q}}(z) = \sum_q c_{q\bar{q}} f_q \left(\sqrt{\frac{\tau}{z}} e^{Y} \right) f_{\bar{q}} \left(\sqrt{\frac{\tau}{z}} e^{-Y} \right) = \mathscr{L}_{q\bar{q}} \left(z, \frac{1}{2} \right), \tag{9.26}$$

which is again u independent, thus making the rest of the proof identical to what discussed in section 9.1 (except for the fact that $\mathscr{L}^{(0)}_{q\bar{q}}(z)$ can be moved outside the u integral but not the z integral, but this is immaterial for the derivation of the final result).

Chapter 10

Accuracies estimations of BNX and BFR approaches

In this chapter, we analytically and numerically assess the quality of the BNX and BFR formulations by comparing the fixed-order truncation of the resummed result with the full fixed-order cross section. These approaches, despite their simplicity, remain compelling alternatives to more advanced resummation formalisms due to their reliance on the resummation of the rapidity-integrated coefficient function, which is available for a broader range of processes and with higher logarithmic accuracy.

The accuracy of any threshold approximation, and hence resummation, depends on the definition of the threshold logarithms that are used. Any definition of threshold logarithms that differs from Eq. (8.3) by subleading power contributions is formally equivalent and thus acceptable, but the result may differ significantly. This difference may be seen as a limitation of the threshold approximation, as it comes from sizeable contributions from next-to-leading power terms that are beyond the control of leading power threshold resummation. Recently, threshold resummation has been extended to next-to-leading power [135, 142–147], opening up the possibility of pushing the accuracy beyond that of traditional methods. Anyway, some of these subleading power contributions have a universal structure that can be incorporated in the definition of threshold logarithms, improving the quality of a threshold approximation [148–155].

In the following, we define and discuss different choices of threshold logarithms, giving the analytical expression both at NLO and NNLO, and compare their accuracies numerically. In order to do that, we consider the following pertubative expansion of the rapidity-integrated coefficient function

$$C(z,\alpha_S) = \sum_{n=0}^{\infty} \alpha_S^n \left[c_n \delta(1-z) + \sum_{k=0}^{2n-1} \left(c_{nk} \left(\frac{\log^k(1-z)}{1-z} \right)_+ + d_{nk} \log^k(1-z) \right) + ... \right], \tag{10.1}$$

which is the key ingredient of the BNX and BFR formulations. The series with the c_n and c_{nk} coefficients include the leading power (LP) singular terms. The d_{nk} coefficient, instead, multiplies a term that is suppressed by one power of $(1-z)$ and gives the next-to-leading power

(NLP) contribution. The leading logarithmic accuracy (LL) consists in the c_0 and $c_{n(2n-1)}$ coefficients, while including also the $d_{n(2n-1)}$ will give the NLP LL series of the coefficient function. To go beyond the LL accuracy, also the other terms with intermediate indices between 0 and $2n-1$ have to be included.

Since we are interesting in the fixed-order expansion of the coefficient function, we can rewrite the last equation as

$$C(z,\alpha_S) = C^{(0)}(z) + \frac{\alpha_S}{\pi} C^{(1)}(z) + \left(\frac{\alpha_S}{\pi}\right)^2 C^{(2)}(z) + \mathcal{O}(\alpha_S^3)\,, \tag{10.2}$$

with the perturbative coefficient given by

$$\begin{aligned}
C^{(0)}(z) &= c_0\,\delta(1-z) = \sigma_0\,,\\
C^{(1)}(z) &= c_1\,\delta(1-z) + \sum_{k=0}^{1}\left(c_{1k}\left(\frac{\log^k(1-z)}{1-z}\right)_+ + d_{1k}\log^k(1-z)\right)\,,\\
C^{(2)}(z) &= c_2\,\delta(1-z) + \sum_{k=0}^{3}\left(c_{2k}\left(\frac{\log^k(1-z)}{1-z}\right)_+ + d_{2k}\log^k(1-z)\right)\,.
\end{aligned} \tag{10.3}$$

The first coefficient is defined as the Born term, i.e. the LO contribution. The second and the third are the pure NLO and NNLO contributions, respectively.

10.1 z-soft approximation

The simplest choice for constructing a threshold approximation is to retain all contributions of the form of Eq. (8.3) and delta functions. In this case, the coefficient function is approximated at threshold, at order α_S^n, as

$$C^{(n)}_{\rm thr}(z) = c_n\delta(1-z) + \sum_{k=0}^{2n-1} c_{nk}\left(\frac{\log^k(1-z)}{1-z}\right)_+\,, \tag{10.4}$$

where c_n and c_{nk} are numerical coefficients and not functions of z. Extending the notation of Refs. [151, 152], we shall call the threshold approximation based on Eq. (10.4) z-soft approximation, meaning the natural threshold approximation in z space (to be precise, in Ref. [151] it was called soft-0).

The z-soft approximation is not particularly convenient and accurate, as we are going to show in the numerical comparison. From the analytical point of view, it is not easy to construct an all-order resummed result that contains all and only those contributions, although there are various approaches to reproduce the logarithms Eq. (10.4) such as Ref. [31] based on SCET and Ref. [152] based on the Borel prescription for resummation. From now on, we conveniently write the distributional terms in a compact form defined by

$$\mathcal{D}_k(z) \equiv \left(\frac{\log^k(1-z)}{1-z}\right)_+\,. \tag{10.5}$$

In appendix D.1, and in particular in Eqs. (D.2) and (D.3), we report the value of the pure NLO and NNLO coefficient function, respectively, using this approximation.

10.2 N-soft approximation

The most widespread definition of threshold logarithms that is used in resummed computation is done in Mellin conjugate space, where the phase space of the gluon emissions (responsible of threshold logarithms) factorises making possible the construction of an all-order expression in closed form. Such a definition is based on the expansion at large-N (corresponding to the threshold region in Mellin space) of the Mellin transform of z-space logarithmic terms [152,156]

$$\int_0^1 \mathrm{d}z\, z^{N-1} \left(\frac{\log^k(1-z)}{1-z}\right)_+ = \frac{1}{k+1}\sum_{j=0}^{k+1}\binom{k+1}{j}\Gamma^{(j)}(1)\log^{k+1-j}\frac{1}{N} + \mathcal{O}\left(\frac{1}{N}\right), \quad (10.6)$$

where $\Gamma^{(j)}(x)$ is the j-th derivative of the Euler gamma function $\Gamma(x)$. Neglecting the $\mathcal{O}(1/N)$ contributions (which are subleading power at threshold, $N \to \infty$), this expansion provides an alternative approximation at threshold, that we call N-soft according to the notation of Refs. [151, 152].

Defining the following distributions [152]

$$\mathcal{D}_k^{\log}(z) \equiv \left(\frac{\log^k \log\frac{1}{z}}{\log\frac{1}{z}}\right)_+, \quad (10.7)$$

the Mellin transform can be computed using the results of appendix B.4 of Ref. [156], and it is given by

$$\int_0^1 \mathrm{d}z\, z^{N-1}\left[\mathcal{D}_k^{\log}(z) + \frac{\Gamma^{(k+1)}(1)}{k+1}\delta(1-z)\right] = \frac{1}{k+1}\sum_{j=0}^{k+1}\binom{k+1}{j}\Gamma^{(j)}(1)\log^{k+1-j}\frac{1}{N}. \quad (10.8)$$

Eqs. (10.6) and (10.8) only differ for subleading terms ($\sim 1/N$), while the dominant term in the large-N limit is the same. This is a characteristic of logarithmically enhanced contribution in z space, which contain subleading terms when converted in N space and vice versa. This peculiarity suggests us a straight way to pass from z-soft to N-soft, simply using the following replacement

$$\mathcal{D}_k(z) \to \mathcal{D}_k^{\log}(z) + \frac{\Gamma^{(k+1)}(1)}{k+1}\delta(1-z). \quad (10.9)$$

For the specific case of the coefficient function at NLO and NNLO, Eq. (10.9) gives the following conversions

$$\begin{aligned}
\mathcal{D}_0(z) &\to \mathcal{D}_0^{\log}(z) - \gamma\delta(1-z),\\
\mathcal{D}_1(z) &\to \mathcal{D}_1^{\log}(z) + \frac{1}{2}\left(\gamma^2+\zeta_2\right)\delta(1-z),\\
\mathcal{D}_2(z) &\to \mathcal{D}_2^{\log}(z) - \frac{1}{3}\left(\gamma^3+3\gamma\zeta_2+2\zeta_3\right)\delta(1-z),\\
\mathcal{D}_3(z) &\to \mathcal{D}_3^{\log}(z) + \frac{1}{4}\left(\gamma^4+6\gamma^2\zeta_2+8\gamma\zeta_3+3\zeta_2^2+6\zeta_4\right)\delta(1-z),
\end{aligned} \quad (10.10)$$

where γ is the Euler-Mascheroni constant. Basically, the N-soft approximation involves shifting the coefficient function by a factor of $\sqrt{z}$. Details for the NLO and NNLO coefficient function are given in Eqs. (D.4) and (D.5) in appendix D.1. We also notice that we can write

$$\mathcal{D}_k^{\log}(z) + \frac{\Gamma^{(k+1)}(1)}{k+1}\delta(1-z) = \mathcal{D}_k(z) + \frac{\log^k \log \frac{1}{z}}{\log \frac{1}{z}} - \frac{\log^k(1-z)}{1-z}\,, \tag{10.11}$$

that provides an alternative, possibly simpler, implementation of N-soft.

10.3 ψ-soft$_1$ approximation

An alternative definition of threshold logarithms was proposed in Ref. [152], whereby $\log N$ is replaced by $\psi_0(N+1)$, where ψ_0 is the digamma function. In this case, the exact Mellin transform of the threshold logarithms is expressed in terms of polygamma functions $\psi_k(N)$, all of which go to zero at large N as N^{-k} with the exception of $\psi_0(N)$ which grows as $\log N$. To obtain a translation rule for ψ-soft, we introduce the distributions $\hat{\mathcal{D}}_k(z)$ already defined in Ref. [152]

$$\hat{\mathcal{D}}_k(z) = \mathcal{D}_k(z) + \frac{\log^k \frac{1-z}{\sqrt{z}}}{1-z} - \frac{\log^k(1-z)}{1-z}\,. \tag{10.12}$$

From an analytical point of view, this expression is equivalent to including a $\frac{1}{\sqrt{z}}$ factor in the argument of the threshold logarithm, although it is subleading. It has a kinematical origin and is thus universal [8, 31, 151]. This operation can be done in such a way that the Mellin transform of the $\hat{\mathcal{D}}_k(z)$ differ by that of $\mathcal{D}_k(z)$ by $1/N$ terms, thus providing at leading power an equivalent but possibly better definition of threshold logarithms. Using again the results of appendix B.4 of Ref. [156], we can write the Mellin trasform of the $\hat{\mathcal{D}}_k(z)$ distributions as

$$\int_0^1 \mathrm{d}z\, z^{N-1}\, \hat{\mathcal{D}}_k(z) = \frac{1}{k+1}\sum_{j=0}^{k+1}\binom{k+1}{j}\Gamma^{(j)}(1)\Upsilon_{k+1-j}(N,0)\,, \tag{10.13}$$

where

$$\Upsilon_0(N,\xi) = \frac{\Gamma(N-\xi/2)}{\Gamma(N+\xi/2)} \tag{10.14}$$

and $\Upsilon_n(N,\xi)$ is the n-th derivative of $\Upsilon_0(N,\xi)$ with respect to ξ. Always considering the coefficient function up to NNLO, the first few terms are given by

$$\begin{aligned}
\Upsilon_1(N,0) &= -\psi_0(N)\,,\\
\Upsilon_2(N,0) &= \psi_0^2(N)\,,\\
\Upsilon_3(N,0) &= -\psi_0^3(N) - \frac{1}{4}\psi_2(N)\,,\\
\Upsilon_4(N,0) &= \psi_0^4(N) + \psi_2(N)\psi_0(N)\,,
\end{aligned} \tag{10.15}$$

where $\psi_n(N) = \frac{\mathrm{d}^{n+1}}{\mathrm{d}N^{n+1}} \log\Gamma(N)$ is the polygamma function. As already pointed out in Ref. [152], we observe that

$$\Upsilon_k(N,0) = [-\psi_0(N)]^k \left[1 + \mathcal{O}\left(\frac{1}{N^2}\right)\right], \tag{10.16}$$

namely up to next-to-next-to-leading power corrections the use of $\hat{\mathcal{D}}_k(z)$ Eq. (10.12) can be obtained from a N-soft expression Eq. (10.8) with the replacement $\log N \to \psi_0(N)$. The ψ-soft formulation consists in using the distributions $\hat{\mathcal{D}}_k(z)$ for the threshold logarithms but ignoring these subleading $\mathcal{O}(1/N^2)$ contributions and retaining only the powers of $\psi_0(N)$, which is easy to implement to all orders in N space. A z-space analog would be implemented by a modified distribution $\hat{\mathcal{D}}_k^{\psi}(z)$ defined by

$$\int_0^1 \mathrm{d}z\, z^{N-1}\, \hat{\mathcal{D}}_k^{\psi}(z) = \frac{1}{k+1} \sum_{j=0}^{k+1} \binom{k+1}{j} \Gamma^{(j)}(1) \Big[-\psi_0(N)\Big]^{k+1-j}, \tag{10.17}$$

for which however we cannot find an easy closed form for any k. Up to the order we are interested in, we have that $\hat{\mathcal{D}}_0^{\psi}(z) = \hat{\mathcal{D}}_0(z)$ and $\hat{\mathcal{D}}_1^{\psi}(z) = \hat{\mathcal{D}}_1(z)$, while

$$\begin{aligned}
\int_0^1 \mathrm{d}z\, z^{N-1} \left[\hat{\mathcal{D}}_2^{\psi}(z) - \hat{\mathcal{D}}_2(z)\right] &= \frac{\psi_2(N)}{12}, \\
\int_0^1 \mathrm{d}z\, z^{N-1} \left[\hat{\mathcal{D}}_3^{\psi}(z) - \hat{\mathcal{D}}_3(z)\right] &= -\frac{\psi_2(N)}{4}(\psi_0(N) + \gamma).
\end{aligned} \tag{10.18}$$

The inverse Mellin transforms of these differences can be computed analytically, using e.g. the results of Refs. [156, 157]. We find

$$\begin{aligned}
\hat{\mathcal{D}}_2^{\psi}(z) &= \hat{\mathcal{D}}_2(z) - \frac{1}{12}\frac{\log^2(z)}{1-z}, \\
\hat{\mathcal{D}}_3^{\psi}(z) &= \hat{\mathcal{D}}_3(z) - \frac{\zeta_2}{2}\frac{\log(z)}{1-z} + \frac{1}{12}\frac{\log^3(z)}{1-z} - \frac{1}{2}\frac{\mathrm{Li}_2(z)\log(z)}{1-z} + \frac{\mathrm{Li}_3(z)}{1-z} - \frac{\zeta_3}{1-z} \\
&\quad - \frac{1}{4}\frac{\log(1-z)\log^2(z)}{1-z}.
\end{aligned} \tag{10.19}$$

The argument of $\psi_0(N)$ can be further shifted to $N+1$, which is still equivalent up to $\mathcal{O}(1/N)$. This choice, denoted ψ-soft$_1$ in Ref. [152], corresponds to the approximation obtained by neglecting the $\mathcal{O}(1/N)$ contributions in the expansion

$$\int_0^1 \mathrm{d}z\, z^{N-1} \left(\frac{\log^k(1-z)}{1-z}\right)_+ = \frac{1}{k+1} \sum_{j=0}^{k+1} \binom{k+1}{j} \Gamma^{(j)}(1) \Big[-\psi_0(N+1)\Big]^{k+1-j} + \mathcal{O}\left(\frac{1}{N}\right). \tag{10.20}$$

The use of $\psi_0(N+1)$ allows to include at the rapidity-integrated level subleading power contributions that have a kinematical origin and are thus universal [148–155]. In particular, the leading logarithmic terms at next-to-leading power in $(1-z)$ are predicted correctly to

all orders in ψ-soft$_1$ in the dominant flavour-diagonal channel for colour-singlet production processes such as Higgs and Drell-Yan, and subleading logarithmic contributions are also partially included. As a consequence, at the rapidity-integrated level, the ψ-soft$_1$ choice of logarithmic terms provides better numerical agreement with the exact result than z-soft or N-soft, and also leads to a better stabilisation of the scale dependence at resummed level. These results were obtained for Higgs production [151, 152], and they also hold for the Drell-Yan process. It is important to note, however, that this simple modification of the resummed logarithms is not able to predict subleading power contributions coming from the other channels, most importantly the qg channel, which would be needed for achieving a higher accuracy of the resummation.

The formal accuracy of this expression is equivalent to that of N-soft and z-soft, as they all differ among each other by subleading power contributions at threshold. However, the ψ-soft$_1$ approximation has some advantages that make its quality superior to other choices. This simple modification of the resummed logarithms is not able to predict subleading power contributions coming from the other channels, most importantly the qg channel, which would be needed for achieving a higher accuracy of the resummation. The ψ-soft$_1$ prescription mentioned in the main text uses $N+1$ rather than just N as the argument of the digamma function: $\psi_0(N+1)$. This is the simplest form of the "collinear improvement" introduced in Ref. [152] that includes subleading power contributions from universal splitting functions. In z space a shift $N \to N+1$ corresponds to multiplication by z, so the recipe for the conversion of Eqs. (D.2) and (D.3) to ψ-soft$_1$ is simply given by the replacement

$$\mathcal{D}_k(z) \to z\,\hat{\mathcal{D}}_k^{\psi}(z)\,. \tag{10.21}$$

Similarly to the N-soft case, the ψ-soft$_1$ approximation shifts the coefficient function of a factor z. We stress that any "traditional" Mellin-space resummation code that uses N-soft by default can be straightforwardly upgraded to ψ-soft$_1$ simply replacing $\log N$ with $\psi_0(N+1)$. The coefficient functions with this choice of threshold logarithms at NLO and NNLO are reported in Eqs. (D.6) and (D.7).

10.4 Numerical validation at NLO and NNLO

In this section we compare the exact NLO and NNLO contributions to the Drell-Yan rapidity distribution against threshold approximations based on the BNX and BFR formulations and for the three choices of threshold logarithms discussed above.

To do that, we consider neutral current Drell-Yan production at LHC with $\sqrt{S} = 13$ TeV, including only the contribution from the photon for simplicity (the extension to include also the Z boson case will be straightfoward, adapting the coefficient in Eq. (8.16) of the luminosity for this particular case). We use the PDF4LHC21 NNLO PDF set [139], and take from it the value of the strong coupling. We always fix the renormalisation and factorisation scales to the invariant mass of the lepton pair $Q = \sqrt{\tau S}$, $\mu_F = \mu_R = Q$. We only plot the $q\bar{q}$ contribution to the rapidity distribution. The exact NNLO result is taken from the `Vrap` code [123, 140]. In each figure, in the upper plots we always show the comparison at pure NLO and in the lower

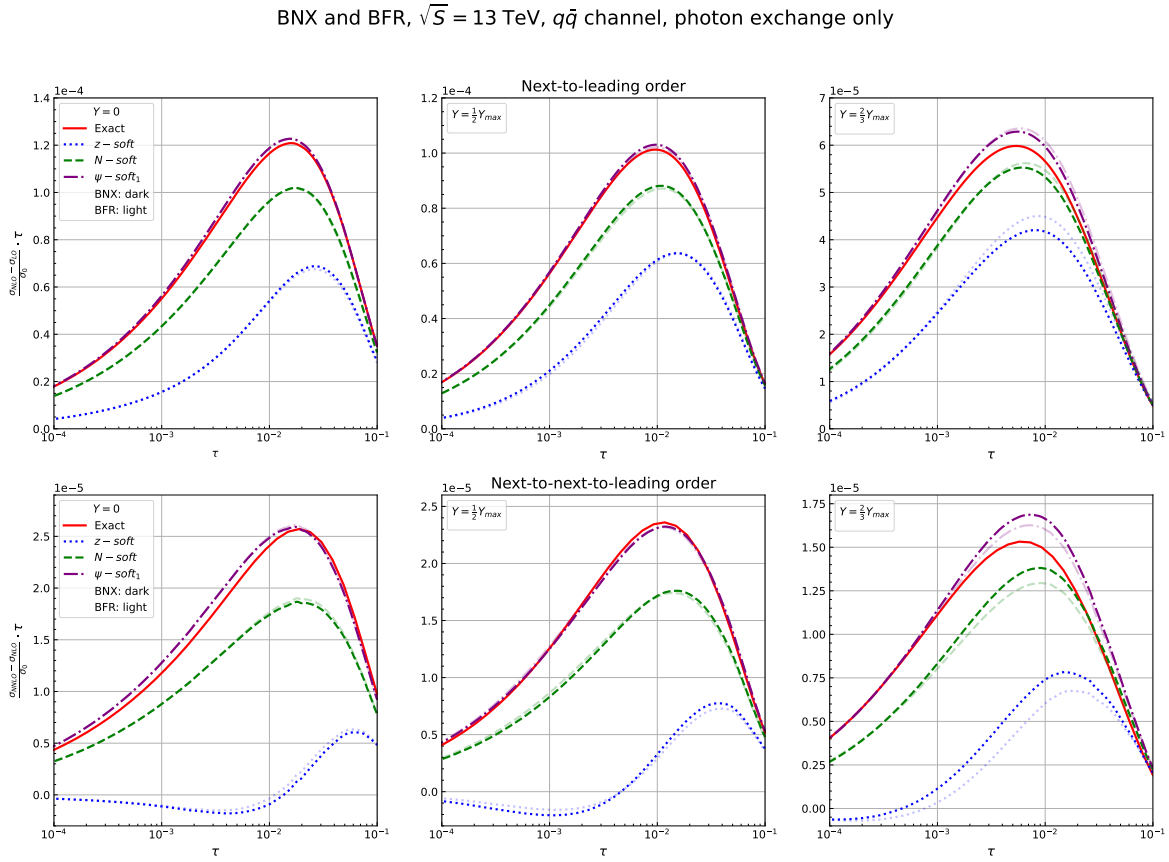

Figure 10.1: Rapidity distributions at NLO (up) and NNLO (down) as a function of τ for $Y = 0, Y_{\max}/2, 2Y_{\max}/3$. The approximations z-soft, N-soft and ψ-soft$_1$ are shown in darker colour for BNX and in lighter colour for BFR.

plots at pure NNLO. The choice of the three threshold logarithms is pictured both for BNX (darker curvers) and BFR (lighter curves) and we always show the exact result in solid red, the z-soft in dotted blue, the N-soft in dashed green and ψ-soft$_1$ in dot-dashed purple.

We start by showing plots of the rapidity distribution at fixed rapidity and as a function of τ, i.e. as a function of Q since we keep the collider energy fixed. These are shown in figure 10.1, where each plot corresponds to different values of rapidity, $Y = 0, Y_{\max}/2, 2Y_{\max}/3$ with $Y_{\max} = \frac{1}{2}\log\frac{1}{\tau}$. We observe that ψ-soft$_1$ is by far the best approximation, in most cases overshooting the exact result by a small amount. This is expected because integrating over rapidity Eq. (8.25) and Eq. (8.27) we obtain the correct rapidity-integrated distribution, for which ψ-soft$_1$ is known to perform well. Moreover, comparing with figure 9.2, we can observe that the ψ-soft$_1$ curve is very similar to the curves obtained with the exact $C(z)$, as a consequence of the aforementioned fact. The N-soft approximation is reasonably good but definitely worse than ψ-soft$_1$, and it always undershoots the exact by an amount that can reach 35%. Only at large rapidity the large-τ behaviour seems to be better for N-soft

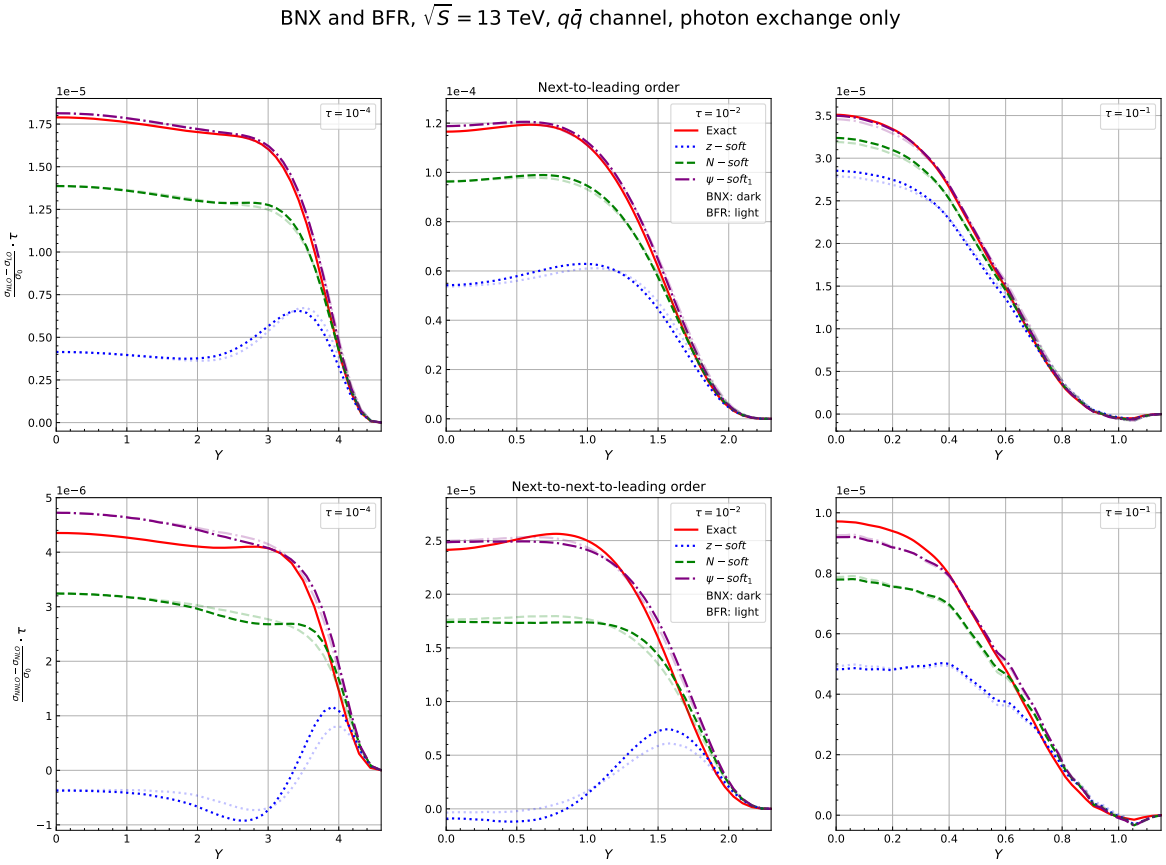

Figure 10.2: Rapidity distributions at NLO (up) and NNLO (down) as a function of Y for $\tau = 10^{-4}, 10^{-2}, 10^{-1}$. The approximations z-soft, N-soft and ψ-soft$_1$ are shown in darker colour for BNX and in lighter colour for BFR.

than for ψ-soft$_1$, but this is due to an accidental compensation of the deterioration of the approximation of the luminosity visible in figure 9.2 and the undershooting of N-soft. Finally, z-soft is the worst, especially at NNLO where it seems completely unrelated to the exact result, except at very large τ. This failure of the z-soft approximation is well known and expected at the rapidity-integrated level, and it has been studied in various works, mostly in the context of Higgs production [37, 151, 158–160].

In figure 10.2 we show the same differential distribution as a function of the rapidity Y for fixed values of $\tau = 10^{-4}, 10^{-2}, 10^{-1}$. We clearly see that at large rapidity the agreement of all the approximations is good, but moving towards smaller rapidity z-soft deviates soon and significantly, N-soft also deviates undershooting the exact result by a large amount, while ψ-soft$_1$ is closer to the exact result, typically overshooting it by a small amount. At NNLO for $\tau = 10^{-1}$, the BNX and BFR have some oscillations. Their presence is not due to numerical instabilities, but it depends on the PDF set used, as we verified. We note that, also for this case, the shape of ψ-soft$_1$ is very similar to the result obtained with the full $C(z)$, figure 9.3.

There is a slight deterioration of the accuracy of ψ-soft$_1$ at NNLO with respect to the NLO, with the shape at this order being somewhat distorted. However, reassuringly, the quality of all the approximations is generally similar at NLO and NNLO, showing that the procedure is stable and hopefully preserves its reliability at higher orders.

These considerations hold the same for both BNX and BFR. While the two approaches give very similar results, in these plots we can see a small difference between them, which is more marked at medium-small τ and in the less accurate approximations based on z-soft and N-soft. In particular, it seems that BNX is able to better reproduce the little bump present in the rapidity distribution at the transition between the central rapidity plateau and the large rapidity drop. However, the difference between BNX and BFR is so mild and in particular much smaller than the difference between exact and approximate, and between the different choices of threshold logarithms that it cannot be used to strongly favour one of the two approaches over the other.

In conclusion, the BNX and BFR approaches can describe well the fixed-order result, even far from threshold, provided a good choice of threshold logarithms is used. The ψ-soft$_1$ choice is more accurate than the others also for rapidity distributions, thereby providing the most convenient choice of threshold logarithms for an accurate resummation, and at the same time it is very easy to implement at resummed level.

Chapter 11

Phenomenological comparison

In this chapter we compare the BNX/BFR approaches to other approaches to threshold resummation available in the literature, namely BDDR [128] and LMT [124]. We also consider the AMRST [135] approach, which is the next-to-leading power extension of BDDR. This is not the first numerical comparison to have been done, indeed in Ref. [128] a comparison between BDDR and BFR was performed, but the choice of logarithms used for BFR was the one of the original paper [32] (z-soft).

For this comparison, we focus only on the BFR approach for simplicity, since BNX would lead to very similar results, and we choose the ψ-soft$_1$ version of threshold logarithms which we know is the most accurate, as shown in Sec. 10.4. In particular, for BDDR and AMRST, being them formulated in Mellin space, the logarithms are defined according to N-soft with two separate logarithms in the variables z_a, z_b, corresponding to logarithms in Mellin space of two distinct variables N_a and N_b. Expressions for BDDR at NLO and NNLO are given in N_a, N_b space in Ref. [128] and can be converted to z_a, z_b space using the results of appendix D.1. For AMRST, we have expanded the resummed formulas of Ref. [135] to order α_S and α_S^2. Explicit expressions for both BDDR and AMRST at NLO and NNLO are given in appendix D.2, both in Mellin space and in momentum space. For LMT, the logarithms used correspond to the z-soft definition. Despite it being a choice that gives inaccurate approximations at leading power, the fact that LMT includes subleading power contributions partially cures this deficiency. We stress that the LMT approximation corresponds to the full distributional part of the coefficient function when written in terms of the z_a, z_b variables. Explicit expressions at NLO and NNLO are given in appendix D.3.

For this comparison, we use the usual setup: we consider neutral current Drell-Yan production at LHC with $\sqrt{S} = 13$ TeV including only the exchange of a photon. The PDF set used is PDF4LHC21 NNLO, from which we take also the running of the strong coupling. The scales are set as $\mu_F = \mu_R = Q = \sqrt{\tau S}$, and we only plot the $q\bar{q}$ contribution to the rapidity distribution. The exact NNLO is taken from the `Vrap` code. In each figure, the upper plots show the pure NLO contribution, while the lower plots the NNLO one. The exact result is represented in solid red, the LMT result in dotted blue, the BDDR in dashed green, the BFR based on ψ-soft$_1$ in dot-dashed purple and, finally, the ARMST in dot-dot-dashed orange.

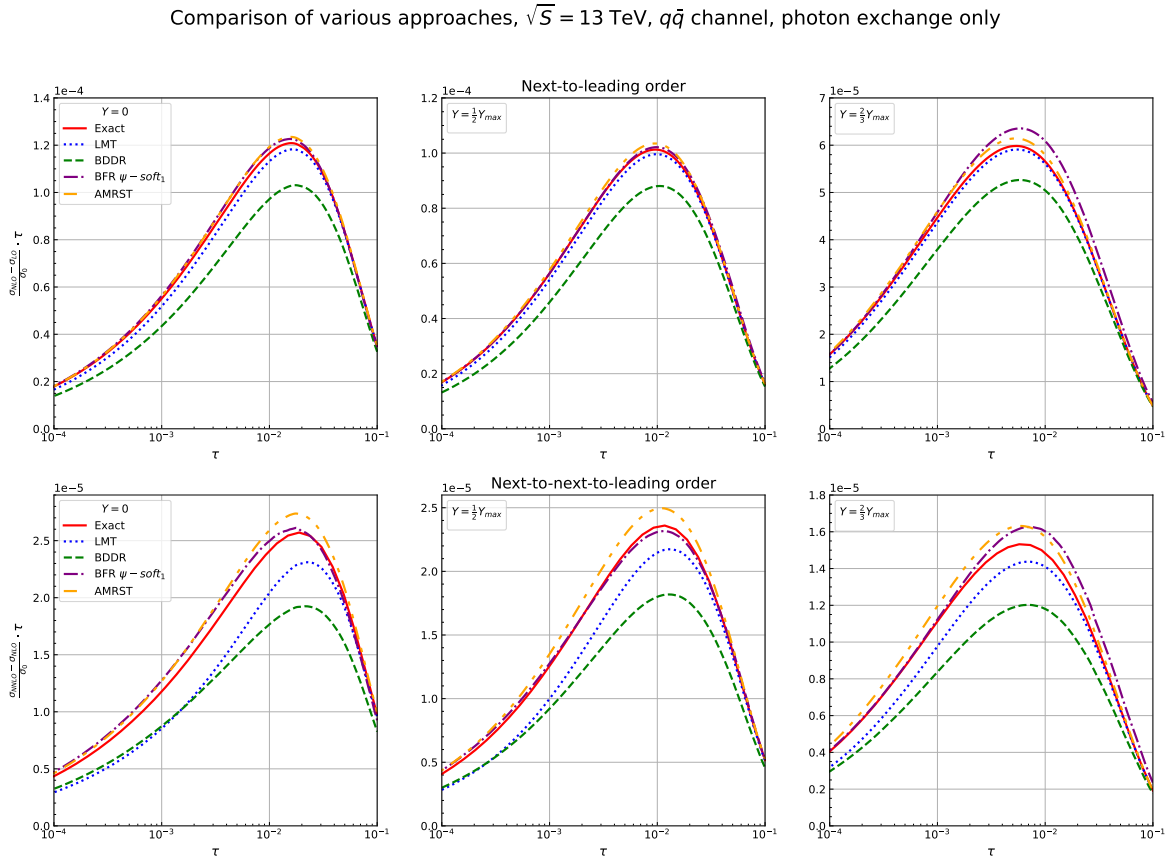

Figure 11.1: Rapidity distributions at NLO (up) and NNLO (down) as a function of τ for $Y = 0, Y_{\max}/2, 2Y_{\max}/3$, comparing the LMT, BDDR, BFR with ψ-soft$_1$ and AMRST results.

In figure 11.1 we plot the Drell-Yan rapidity distribution as a function of τ and in figure 11.2 as a function of Y. One of the first things that can be noticed is that BFR with ψ-soft$_1$ performs much better than BDDR both at NLO and NNLO, being much closer to the exact result. This effect can be due to the choice of the N-soft approximation for the threshold logarithms done in BDDR, which is not optimal as already explained. The BFR curve in rapidity, because of the approximate nature of the BFR approach itself, does not reproduce the shape of the exact result (e.g., the NNLO bump). However, it is overall close to the exact result thanks to the fact that the BFR approach (as the BNX one) is designed to reproduce the inclusive threshold result at the rapidity-integrated level, and it is also well approximated by ψ-soft$_1$.

Moving to the other approaches, the LMT result is generally more accurate than BDDR, in particular at large rapidity where it is very close to the exact result. Such agreement is very good especially at large τ, but the LMT accuracy deteriorates significantly at NNLO, being worse than BDDR at central rapidity for small τ. The reason is mainly due to the usage of the z-soft for threshold logarithms, and it can be noticed using a better choice of logarithms

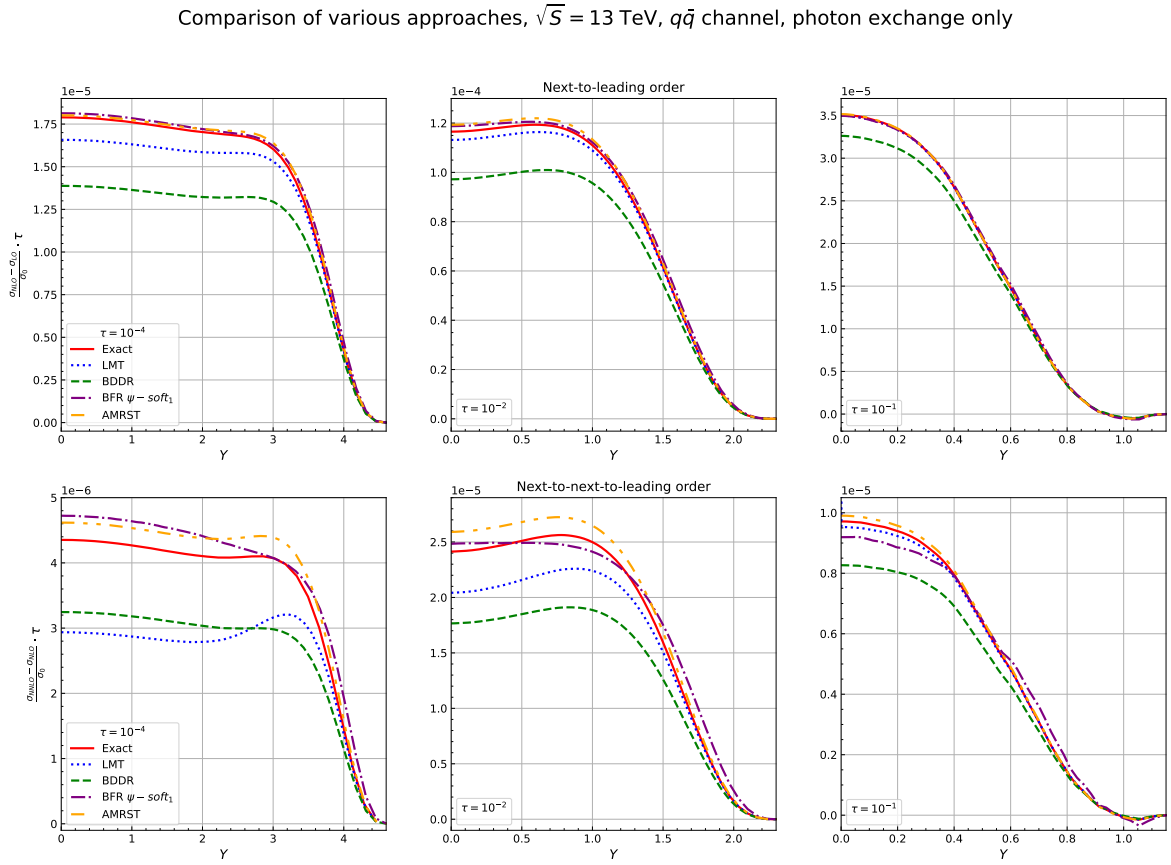

Figure 11.2: Rapidity distributions at NLO (up) and NNLO (down) as a function of Y for $\tau = 10^{-4}, 10^{-2}, 10^{-1}$, comparing the LMT, BDDR, BFR with ψ-soft$_1$ and AMRST results.

as demonstrated by the AMRST result discussed later. Indeed, the structure of the LMT result is such that the subleading power corrections in one variable (say z_a), which help the improvement of the accuracy of the resummation, are retained when multiplying only the leading power terms in the other variable (z_b). These are not accurate enough when using z-soft, unless the kinematics forces that variable to be large, i.e. at large rapidity.

The AMRST result, lastly, formally contains less information than the LMT one. Indeed, for each variable it only adds the next-to-leading power correction multiplied by the leading power term in the other variable, and not all subleading power corrections as it is done in LMT. However, the advantage of the AMRST result is that it uses the N-soft definition of the threshold logarithms, which is superior to the z-soft one as already discussed. Therefore, the AMRST result is the one that best approximates the exact results, being very close to it both at NLO and NNLO. It is also able to reproduce the shape in rapidity which is only vaguely approximated by BFR, as already commented.

Notably, BFR with ψ-soft$_1$ is closer to the exact result than BDDR and LMT, with the exception of the high rapidity region. In fact it is rather close to the AMRST result as well,

making BFR (and BNX) comparable even with the best approach on the market today. This comparison confirms once more that the BNX/BFR formulation of threshold resummation of rapidity distribution is legitimate and competitive with canonical, more complex approaches. Indeed, the BFR/BNX approaches are based on the leading-power resummation of the rapidity integrated cross section, which is available for a large variety of processes and to a high logarithmic accuracy, while the recent AMRST approach requires more ingredients and it is only available for a limited number of processes so far. We will demonstrate the value of the BFR approach by showing representative resummed results in section 11.1.

We conclude by stressing that the comparisons presented here are for the $q\bar{q}$ channel only, but at next-to-leading power also the other channels contribute. At the moment only the LMT approach can control the resummation in these subleading channels, which is a clear advantage for the goal of achieving the highest precision. It would thus be very interesting to understand if it is possible to modify the LMT approach by changing the form of the threshold logarithms to take advantage of other better definitions like N-soft or ψ-soft$_1$, in order to improve its quality, reaching and possibly surpassing AMRST. In this way one could achieve the best description of the dominant $q\bar{q}$ channel, supplemented by the important contributions from the other subleading channels.

11.1 All-order resummed results for BFR

Having established the accuracy of the BNX/BFR approaches to resummation comparing to fixed order, in this section we present some representative all-order results. We restrict our attention to BFR resummation with the ψ-soft$_1$ choice for threshold logarithms, as already done previously.

We perform the resummation using the public `TROLL` code [152, 161, 162], which implements the resummation up to next-to-next-to-next-to-leading logarithmic accuracy (N^{3}LL$'$), both for rapidity distributions and for rapidity-integrated cross sections. The ingredients for N^{3}LL$'$ resummation are all available in the literature [163–165], including the $\delta(1-z)$ term at N^{3}LO which is taken from Ref. [166] and the recent four-loop cusp anomalous dimension computed in Ref. [167]. Here, the prime notation [96, 168, 169] indicates that on top of the purely N^{k}LL contributions the constant term (in N space) at N^{k}LO is also included, despite it contributing formally at N^{k+1}LL in the resummed exponent. It is well known that this addition enables the prediction of one extra subleading power of the logarithms in the cross section and usually captures most of the next logarithmic order. While it is possible to exponentiate the constant terms in N space using `TROLL` [152, 162], we choose to adhere to a more conventional approach, as the impact on this process is relatively minor.

In figure 11.3 we show the rapidity distribution as a function of τ for $Y = 0, Y_{\max}/2, 2Y_{\max}/3$ at fixed LO (solid black), NLO (solid blue) and NNLO (solid red) along with the resummed results at NLO+NLL$'$ (dashed blue), NNLO+NNLL$'$ (dashed red), and NNLO+N^{3}LL$'$ (dotted green). We were not able to include in the plots the N^{3}LO curve [120] as to our knowledge there is no public code available out of which we can extract the $q\bar{q}$ contribution. Consequently, we could not show the N^{3}LO+N^{3}LL$'$ resummed result, but we consider the NNLO+N^{3}LL$'$ result, which should be equivalent to the former in the region of large τ and Y where the

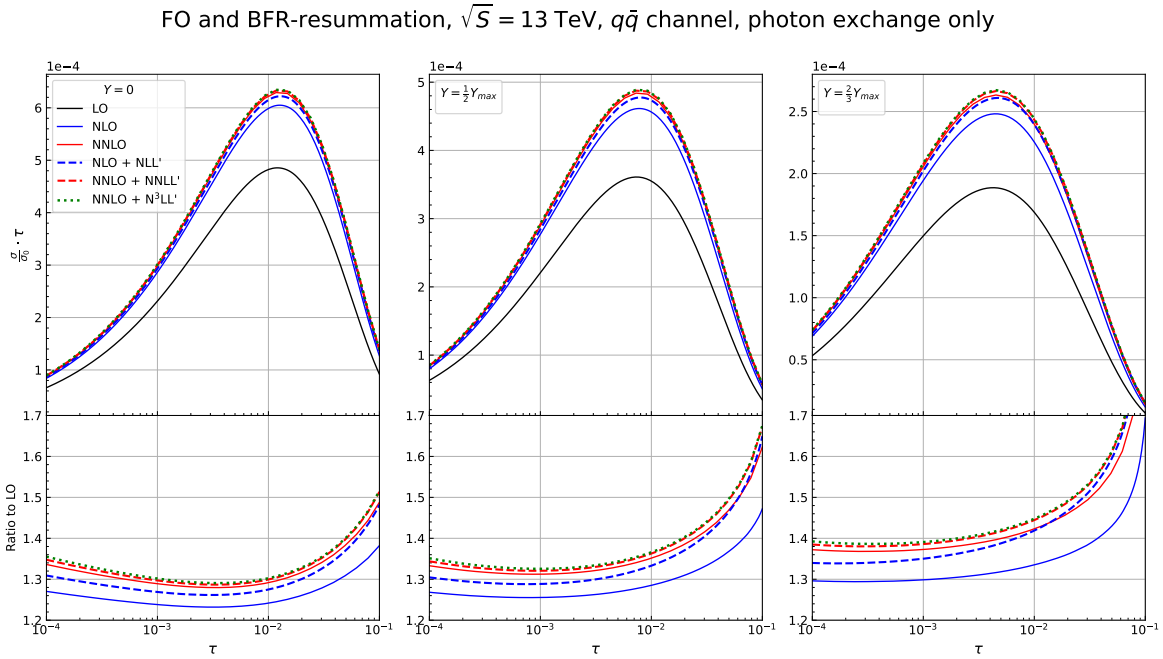

Figure 11.3: Rapidity distributions at fixed order (solid lines) and with resummation à la BFR (dashed/dotted lines) as a function of τ for $Y = 0, Y_{\max}/2, 2Y_{\max}/3$.

threshold logarithms dominate the distribution. Far from this region, the addition of the N^{3}LO result would instead improve the accuracy.

Similarly, in figure 11.4 we plot the rapidity distributions as a function of Y for $\tau = 10^{-4}, 10^{-2}, 10^{-1}$. In all plots we also show a lower panel with the ratio to the LO result, to better appreciate the relative size of the various perturbative corrections. As in the previous sections, we only plot the dominant $q\bar{q}$ channel.

We observe a good convergence of the resummed result, improved with respect to that of the fixed-order result especially at large τ and Y, where threshold logarithms are more dominant. Overall, we notice that the effect of adding resummation over the fixed order is small at NLO and very small at NNLO, which is a consequence of the fact that the Drell-Yan process exhibits a good perturbative convergence as long as we consider the NNLO fixed-order result, (as opposed for instance to the Higgs production process in gluon fusion, see e.g. [170, 171]). From the ratio plots,[1] it is apparent that going towards large rapidity or large τ all the resummed curves tend to overlap, while the fixed-order contributions get larger thus showing a perturbative instability. This is a consequence of the fact that in these regions the threshold logarithms are dominant and large, and resumming them the perturbative expansion stabilizes significantly and leads to reliable perturbatively-stable results.

In conclusion, we have demonstrated that the BNX/BFR formulations are available for

[1]The spike in the third ratio plot of figure 11.4 is due to the LO result becoming negative at large rapidity. This is clearly unphysical, and it is an annoying artefact of the PDFs used that are not very well behaved at large x.

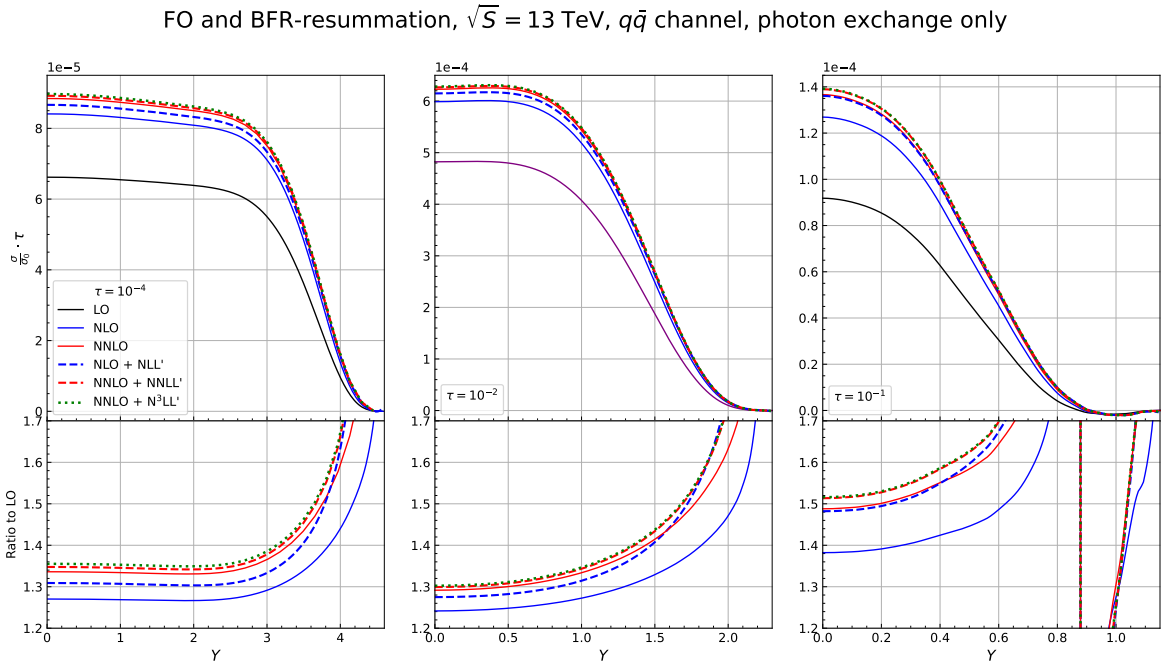

Figure 11.4: Rapidity distributions at fixed order (solid lines) and with resummation à la BFR (dashed/dotted lines) as a function of Y for $\tau = 10^{-4}, 10^{-2}, 10^{-1}$.

producing reliable resummed results for rapidity distributions at high logarithmic accuracy. The public TROLL code implements these results up to N^{3}LL$'$ accuracy, with the ψ-soft$_1$ choice of threshold logarithms (N-soft is also available). The results for ψ-soft$_1$ resummation for Drell-Yan rapidity distributions are presented here for the first time.

Conclusions

In this thesis, we have explored two distinct yet interconnected tools to achieve precise theoretical predictions for collider processes involving strongly interacting particles.

In the first part of this thesis, we delved into the implementation of the double Higgs boson production within the GENEVA Monte Carlo event generator. In chapter 3, we presented the GENEVA framework, emphasizing its main features, which allow to obtain theoretical predictions at least up to NNLO+NNLL$'$ accuracy for a wide range of colour singlet production processes as well as processes featuring heavy-coloured partons and jets in the final state. This achievement is made possible through the definition of physical and IR-safe events, obtained by employing a N-jet resolution variable which divides the phase space into 0-, 1- and 2-jet regions. In principle, GENEVA can be employed with any resolution variable that satisfies IR-safety and has a known resummation. Many of the implemented processes utilise the N-jettiness or the transverse momentum of the colour singlet system, which resummation is perfomed in the SCET framework. Another important feature connected to the GENEVA framework is the possibility of showering and hadronizing the generated events. One of the main novelties of GENEVA, introduced with this work, is the interface with three different parton showers: PYTHIA8 [15,16], DIRE [109] and SHERPA [17–19]. The study of any processes showered with different parton showers is particularly interesting in order to estimate indirectly the parton shower uncertainty. In chapter 4, we focused on the process chosen for this thesis, the double Higgs boson production, presenting the state of the art and outlining the primary motivations to look at this rare process. Considering the infinite top mass limit for simplicity, we demonstrated the SCET factorisation formula for this specific process and computed the hard function needed for the resummation, all the details can be found in appendix A and B. In chapter 5, we outlined all the GENEVA formulas required and parameters chosen for the implementation of such process. Alongside describing the general setup for our generator, we discussed the size of the missing nonsingular corrections due to configurations with $\mathcal{T}_0 < \mathcal{T}_0^{\text{cut}}$, for which is possible to recover the correct integrated cross section thanks to a reweighting from an independent NNLO fixed-order calculation. In chapter 6, we discussed the main properties of the three showers available in the GENEVA framework, also presented the expected differences for the double Higgs boson production results. Finally, in chapter 7, we show our final results both with and without the effect of the showers.

It is important to emphasize that this is the first time this process has been implemented in a Monte Carlo event generator with such accuracy, considering the infinite top mass limit. While this approximation may not be ideal for this specific process, as discussed earlier, these

results underscore the significance of the GENEVA event generator, being competitive with other approaches and giving a valid alternative to other event generators. The inclusion of the top-quark mass corrections is currently underway, which will be fundamental both from the theoretical and experimental point of view. In the first case, it will constitute the first theoretical prediction coming from a Monte Carlo event generator including the matching between the fixed-order and the resummed result, and studies regarding the result obtained with the full theory and the approximated one will be possible. In the second case, with the High-Luminosity LHC phase and the forthcoming project, the possibility of measuring such rare and challenging process becomes viable. Comparing these experimental observations with Standard Model expectations becomes essential.

The second part of this thesis is dedicated to the threshold resummation of rapidity distributions for the Drell-Yan process. In chapter 9, we proposed a new and detailed proof for the BNX [31] and BFR [32] approaches, addressing their limitation and affirming their correctness within their accuracy. We answered also to several criticisms raised by the LMT [124] authors regarding these two approaches. We also investigated the quality of the BNX and BFR resummation approach in chapter 10, studing the possible choices for the form of threshold logarithms. Selecting the ψ-soft$_1$ as the optimal choice, we validated such approaches against the exact and pure NLO and NNLO results, concluding that despite the approximate nature of the BNX and BFR approaches they perform rather well as they are able to reproduce to a good accuracy the exact NLO and NNLO result, even far from threshold. In chapter 11, we extended this comparison also to include other threshold resummation approaches available in the literature: BDDR [128], AMRST [135] and LMT. Although the best approximation is given by the AMRST result, the BNX /BFR approaches with the ψ-soft$_1$ choice of threshold logarithms lead to approximations that are comparable with the others, despite the latter are formally more accurate. We also showed representative results of BFR resummation up to N^{3}LL$'$ accuracy, using the public `TROLL` code.

Notably, this study confirms that the BNX/BFR approaches are rather good alternatives to more modern approaches, providing a good framework for fast implementation of threshold resummation in rapidity distributions at high logarithmic accuracy. Futhermore, a closer examination of the structure of the AMRST and LMT results reveals that the LMT result is more accurate than the AMRST one. The reason why AMRST results perform better is the different form of threshold logarithms used in the two approaches. As already discussed, the z-soft choice of threshold logarithms done in the LMT approach has a particularly poor quality in approximating the exact result. This suggests us that the LMT approach could be improved by upgrading the form of threshold logarithms, and we plan to investigate this in the future.

Appendix A

SCET factorisation formula for double Higgs boson production

Following Refs. [10, 41, 172], we present the calculation of the factorisation formula in position space SCET formalism for the production of two Higgs bosons plus an arbitrary hadronic final state X at hadron collider, expressed as $p\,(p_a)+p\,(p_b) \to H\,(p_1)+H\,(p_2)+X\,(p_X)$. In particular, we consider only the gluonic channel and we work in the centre-of-mass frame, introducing two light-like vectors along the beam directions $n_a^\mu = (1,0,0,1)$ and $n_b^\mu = (1,0,0,-1)$. We define the invariant mass of the Higgs boson pair system as $q^2 = (p_1+p_2)^2$, and employ the decomposition for the four-vector momenta given in Sec. 2.2.1.

The effective Hamiltonian for this process is defined, in position space, as follows

$$\mathcal{H}_{\text{eff}}(x) = \sum_{m=1,2} \int \mathrm{d}r\,\mathrm{d}t\, C_m^{gg}(r,t)\, O_m^{gg}(x,r,t)\,, \tag{A.1}$$

where m represents the two general Lorentz tensor structures given in Ref. [55, 72, 74]. $C_m^{gg}(r,t)$ represents the Wilson coefficient that can be determined through the matching of the effective theory with the full theory. The integrals over r and t are carried out along the two light-cone directions of the initial state gluons. $O_m^{gg}(x,r,t)$ corresponds to the SCET operator and it is defined as

$$O_m^{gg}(x,r,t) = \delta_{ab}\, \mathcal{A}^a_{\bar{c}\nu\perp}(x+rn_a)\, \mathcal{A}^b_{c\mu\perp}(x+tn_b)\, \mathcal{R}_m^{\mu\nu}\, h(x)\, h(x)\,. \tag{A.2}$$

Here $\mathcal{A}_{c\mu\perp}$ is the collinear gauge-invariant field ($\bar{c}$ refers to the anticollinear field), defined as

$$\mathcal{A}_{c\mu\perp} = \frac{1}{g_s} W_c^+(x)(iD_\perp^\mu W_c(x))\,, \tag{A.3}$$

where W_c is the collinear Wilson line, g_s the coupling and D^μ is the covariant derivative, given by

$$i\,D_\perp^{\mu,c} = i\,\partial^\mu + g_s\,\mathcal{A}_\perp^{\mu,c}\,. \tag{A.4}$$

Furthermore, $\mathcal{R}_m^{\mu\nu}$ defines the general tensor structures for this process. The real scalar Higgs boson field is defined by h, derived from the Higgs boson doublet field $\Phi = \frac{1}{\sqrt{2}} \binom{0}{v+h}$, with v the vacuum expectation value. The structure $\mathcal{R}_m^{\mu\nu}$ is given is momentum space [72, 74] and depends on symmetric and antisymmetric combinations of $g^{\mu\nu}$ and the momenta of the particles. The same dependence will be translated in position space as a combination of the partial derivatives $\partial^{\mu,\nu}$. In Eq. (A.2) a and b are the colour indices of the initial state gluons.

When employing the BPS decoupling transformation [173] to decouple the interactions involving soft gluons, we obtain the following result

$$O_m^{gg}(x,r,t) = \mathcal{R}_m^{\mu\nu}\, h(x)\, h(x)\, [O^c(x,r,t)]_{\mu\nu}\, [O^s(x)]\,, \tag{A.5}$$

where c and s stand for collinear and soft, respectively. In particular

$$\begin{aligned} [O^c(x,r,t)]_{\mu\nu} &= \delta_{ab}\, \mathcal{A}^a_{\bar{c}\nu\perp}(x + rn_a)\, \mathcal{A}^b_{c\mu\perp}(x + tn_b)\,, \\ [O^s(x)] &= [Y^{\mathrm{adj}\dagger}_{n_b}(x)]\, [Y^{\mathrm{adj}}_{n_a}(x)]\,, \end{aligned} \tag{A.6}$$

with $Y^{\mathrm{adj}}_{n_{a,b}}$ being the soft Wilson line defined as

$$[Y^{\mathrm{adj}}_{n_{a,b}}(x)] = \mathcal{P} \exp\left[ig_s \int_{-\infty}^{0} dt\, n_{a,b} \cdot \mathcal{A}^e_s(x + tn_{a,b})\, (-if^{ecd}) \right], \tag{A.7}$$

where $\mathcal{P}$ takes care of the path ordering of the colour indices. Note that the soft operator contains the soft Wilson lines Y_i.

We consider the total final state hadronic momenta in the two hemispheres a and b as B_a^μ and B_b^μ. To analyze the differential cross section in terms of these two variables, we define the two components $B_a^+ = n_a \cdot B_a$, $B_b^+ = n_b \cdot B_b$. In the limit where the radiation is soft or collinear to the beam directions, the cross section is

$$\begin{aligned} \frac{\mathrm{d}\sigma}{\mathrm{d}B_a^+\, \mathrm{d}B_b^+} = \frac{1}{2S} \frac{1}{2(N_c^2-1)^2} \int \frac{\mathrm{d}^3\vec{p_1}}{(2\pi)^3 2E_1} \int \frac{\mathrm{d}^3\vec{p_2}}{(2\pi)^3 2E_2} \\ \times \sum_X (2\pi)^4\, \delta^{(4)}(p_a + p_b - p_1 - p_2 - p_X) |\, \langle H(p_1) H(p_2) X(p_X) |\, \mathcal{H}_{\mathrm{eff}}(0)\, |p(p_a) p(p_b)\rangle\, |^2 \\ \times\, \delta(B_a^+ - n_a \cdot B_a(X))\, \delta(B_b^+ - n_b \cdot B_b(X))\,, \end{aligned} \tag{A.8}$$

where the sum over X runs over all possible radiation states and includes their respective phase space integrals, the factor $1/(2(N_c^2-1))$ is given by the average over the gluons colour and the symmetry factor, the average over initial state polarization is already included in the $\mathcal{R}^{\mu\nu}$ term. The hemisphere momentum operator $\hat{p}^\mu_{a,b}$ acts on the radiation state as $p^\mu_{a,b}\, |X\rangle = B^\mu_{a,b}\, |X\rangle$. Inserting the following identity in Eq. (A.8)

$$1 = \int \mathrm{d}M^2\, \mathrm{d}^4 q\, \delta^{(4)}(q - p_1 - p_2)\, \delta(M^2 - q^2)\,, \tag{A.9}$$

we get

$$\frac{\mathrm{d}\sigma}{\mathrm{d}B_a^+\,\mathrm{d}B_b^+} = \frac{1}{16S}\frac{1}{2(N_c^2-1)^2}\frac{1}{(2\pi)^2}\int \mathrm{d}M\,\mathrm{d}y_{HH}\,\mathrm{d}\cos\theta\,\mathrm{d}\phi_H\,M\beta\int\frac{\mathrm{d}^2\vec{q}_\perp}{(2\pi)^4}$$
$$\times\sum\!\!\!\!\!\!\int_X (2\pi)^4\,\delta^{(4)}(p_a+p_b-q-p_X)\Big|\,\langle H(p_1)H(p_2)X(p_X)|\,\mathcal{H}_{\mathrm{eff}}(0)\,|p(p_a)p(p_b)\rangle\,\Big|^2$$
$$\times\,\delta(B_a^+ - n_a\cdot B_a(X))\,\delta(B_b^+ - n_b\cdot B_b(X))\,, \tag{A.10}$$

where y_{HH} is the rapidity of the Higgs boson pair system, ϕ_H is the azimuthal angle of the Higgs boson in the Higgs bosons system rest frame and we define

$$\beta=\sqrt{1-\frac{4m_H^2}{M^2}},\qquad \cos\theta=\frac{1}{\beta}\left(1+2\frac{t_1}{M^2}\right),\qquad t_1=(p_a-p_1)^2-m_H^2\,. \tag{A.11}$$

Using the definition of the delta function and the translation operator acting on the effective Hamiltonian

$$\delta^{(4)}(p_a+p_b-p_1-p_2-p_X)=\int\frac{\mathrm{d}^4x}{(2\pi)^4}e^{i(p_a+p_b-p_1-p_2-p_X)\cdot x},$$
$$\mathcal{H}_{\mathrm{eff}}(x)=e^{i\hat{p}\cdot\hat{x}}\,\mathcal{H}_{\mathrm{eff}}(0)\,e^{-i\hat{p}\cdot\hat{x}}\,, \tag{A.12}$$

we can rewrite the cross section, substituting the hemisphere momentum operator $\hat{p}^\mu_{a,b}$ and solving the integral and the sum over all possibile hadronic states, obtaining

$$\frac{\mathrm{d}\sigma}{\mathrm{d}B_a^+\,\mathrm{d}B_b^+\,\mathrm{d}M\,\mathrm{d}y_{HH}\,\mathrm{d}\cos\theta\,\mathrm{d}\phi_H}=\frac{M\beta}{16S}\frac{1}{(2\pi)^2}\frac{1}{2(N_c^2-1)^2}\int\frac{\mathrm{d}^2\vec{q}_\perp}{(2\pi)^4}$$
$$\times\int d^4x\;\langle p(p_a)p(p_b)|\,\mathcal{H}^\dagger_{\mathrm{eff}}(x)\,|H(p_1)H(p_2)\rangle$$
$$\times\,\delta(B_a^+-n_a\cdot\hat{p}_a)\,\delta(B_b^+-n_b\cdot\hat{p}_b)\;\langle H(p_1)H(p_2)|\,\mathcal{H}_{\mathrm{eff}}(0)\,|p(p_a)p(p_b)\rangle\;. \tag{A.13}$$

We can now replace Eqs. (A.1) and (A.5), and the cross section gives

$$\frac{\mathrm{d}\sigma}{\mathrm{d}B_a^+\,\mathrm{d}B_b^+\,\mathrm{d}M\,\mathrm{d}y_{HH}\,\mathrm{d}\cos\theta\,\mathrm{d}\phi_H}=\frac{M\beta}{32S}\frac{1}{(2\pi)^4}\frac{1}{2(N_c^2-1)^2}\int\mathrm{d}x^+\,\mathrm{d}x^-\int\mathrm{d}^2\vec{x}_\perp\delta^{(2)}(\vec{x}_\perp)$$
$$\times\int\mathrm{d}r'\,\mathrm{d}t'\,\mathrm{d}r\,\mathrm{d}t\,C^{gg*}(r',t')\,C^{gg}(r,t)$$
$$\times\langle p(p_a)p(p_b)|\,[\mathcal{R}^{\rho\sigma}\,h(x)\,h(x)]^\dagger\,[O^{c\dagger}(x,r',t')]_{\rho\sigma}\,[O^{s\dagger}(x)]\,|H(p_1)H(p_2)\rangle$$
$$\times\,\delta(B_a^+-n_a\cdot\hat{p}_a)\,\delta(B_b^+-n_b\cdot\hat{p}_b)$$
$$\times\langle H(p_1)H(p_2)|\,\mathcal{R}^{\mu\nu}\,h(0)\,h(0)\,[O^c(0,r,t)]_{\mu\nu}\,[O^s(0)]\,|p(p_a)p(p_b)\rangle\;, \tag{A.14}$$

where we have also used the light-cone decomposition $\mathrm{d}^4x=\frac{1}{2}\mathrm{d}x^+\,\mathrm{d}x^-\,\mathrm{d}^2\vec{q}_\perp$ and manipulated the Dirac deltas. In the third line, the action of the Higgs boson fields $h(x)$ is solely applied

to the Higgs bosons, as when they are applied to the protons the resulting value is zero. Consequently, we can reformulate the bracket expression as follow

$$\begin{aligned}\langle p(p_a)p(p_b)|\,[\mathcal{R}^{\rho\sigma}\,h(x)\,h(x)]^\dagger\,[O^{c\dagger}(x,r',t')]_{\rho\sigma}\,[O^{s\dagger}(x)]\,|H(p_1)H(p_2)\rangle = \\ \langle 0|\,h^\dagger(x)\,h(x)\,|H(p_1)H(p_2)\rangle\;\langle p(p_a)p(p_b)|\,[\mathcal{R}^{\rho\sigma}]^\dagger\,[O^{c\dagger}(x,r',t')]_{\rho\sigma}\,[O^{s\dagger}(x)]\,|H(p_1)H(p_2)\rangle\;.\end{aligned} \tag{A.15}$$

In particular, the first part of the aforementioned equation yields

$$\langle 0|\,h(x)\,h(x)\,|H(p_1)H(p_2)\rangle = e^{-ip_1\cdot x}\,e^{-ip_2\cdot x}\,\langle 0|0\rangle = e^{-iq\cdot x}\,. \tag{A.16}$$

The same operation can be done for the bracket in the last line of Eq. (A.14), but applying the field $h(0)$ computed at zero will correspond to the ground state configuration. So it does not alter the existing state of the Higgs bosons, yielding to zero.

We can now write the differential cross section as

$$\begin{aligned}\frac{\mathrm{d}\sigma}{\mathrm{d}B_a^+\,\mathrm{d}B_b^+\,\mathrm{d}M\,\mathrm{d}y_{HH}\,\mathrm{d}\cos\theta\,\mathrm{d}\phi_H} &= \frac{M\beta}{32S}\frac{1}{(2\pi)^4}\frac{1}{2(N_c^2-1)^2}\int \mathrm{d}x^+\,\mathrm{d}x^-\,e^{-i(q^-x^+ + q^+x^-)/2} \\ &\times \int \mathrm{d}^2\vec{x}_\perp\delta^{(2)}(\vec{x}_\perp)\int \mathrm{d}r'\,\mathrm{d}t'\,\mathrm{d}r\,\mathrm{d}t\,C^{gg*}(r',t')\,C^{gg}(r,t) \\ &\times \langle p(p_a)p(p_b)|\,[\mathcal{R}^{\rho\sigma}]^\dagger\,[O^{c\dagger}(x,r',t')]_{\rho\sigma}\,[O^{s\dagger}(x)]\,|H(p_1)H(p_2)\rangle \\ &\times \delta(B_a^+ - n_a\cdot\hat{p}_a)\,\delta(B_b^+ - n_b\cdot\hat{p}_b) \\ &\times \langle H(p_1)H(p_2)|\,\mathcal{R}^{\mu\nu}\,[O^c(0,r,t)]_{\mu\nu}\,[O^s(0)]\,|p(p_a)p(p_b)\rangle\;.\end{aligned} \tag{A.17}$$

After applying the BPS transformation, the effective Lagrangian is expressed as the sum of independent Lagrangians for the collinear, anticollinear, soft, and Higgs bosons system sectors, which do not interact with each other. Following the same separation, we can write the hemisphere momentum operator $\hat{p}_{a,b}$ as the sum of independent operators that act within the collinear, anticollinear and soft sector

$$\hat{p}_a = \hat{p}_{a,n_a} + \hat{p}_{a,n_b} + \hat{p}_{a,s}, \qquad \hat{p}_b = \hat{p}_{b,n_b} + \hat{p}_{b,n_a} + \hat{p}_{b,s}\,, \tag{A.18}$$

but since the n_a collinear sector cannot contribute to the momentum in the n_b hemisphere and vice versa, $\hat{p}_{a,n_b} = \hat{p}_{b,n_a} = 0$ and for simplicity we define $\hat{p}_{a,n_a} = \hat{p}_{n_a}$ and $\hat{p}_{b,n_b} = \hat{p}_{n_b}$, getting

$$\hat{p}_a = \hat{p}_{n_a} + \hat{p}_{a,s}\,, \qquad \hat{p}_b = \hat{p}_{n_b} + \hat{p}_{b,s}\,. \tag{A.19}$$

The separation between soft and collinear contributions to the single hemisphere can be done exploiting the Dirac delta. Here is the explicit expression for the separation in the hemisphere a (the same is valid for hemisphere b)

$$\delta(B_a^+ - n_a\cdot\hat{p}_a) = \int \mathrm{d}b_a^+\,\mathrm{d}k_a^+\,\delta(B_a^+ - b_a^+ - k_a^+)\,\delta(b_a^+ - n_a\cdot\hat{p}_{n_a})\,\delta(k_a^+ - n_a\cdot p_{a,s}^+)\,, \tag{A.20}$$

where b_a^μ is the contribution of the collinear momenta and k_a^μ the contribution for the soft momenta. We apply the multipole expansion to the argument of collinear and soft field in

x_μ so that the first one is evaluated at x_μ^+, while the anticollinear at x_μ^- and the soft one at the origin. In order to include the integration over the $x_{a,b}^-$ components, we rewrite the delta function constraints on the collinear fields as

$$1 = e^{ix_b^- n_b\cdot\hat{p}_{n_b}/2}\, e^{-ix_b^- n_b\cdot\hat{p}_{n_b}/2}, \qquad 1 = (a \leftrightarrow b)\,. \tag{A.21}$$

In addition we use the fact that the momentum operator acts on the proton states as

$$n_a\cdot\hat{p}_{n_a}\,|p_a\rangle = 0, \qquad n_b\cdot\hat{p}_{n_b}\,|p_b\rangle = 0\,. \tag{A.22}$$

We get

$$\begin{aligned}
\frac{\mathrm{d}\sigma}{\mathrm{d}B_a^+\,\mathrm{d}B_b^+\,\mathrm{d}M\,\mathrm{d}y_{HH}\,\mathrm{d}\cos\theta\,\mathrm{d}\phi_H} &= \frac{M\beta}{32S}\frac{1}{(2\pi)^4}\frac{1}{2(N_c^2-1)^2}\int \mathrm{d}k_a^+\,\mathrm{d}k_b^+\,\mathrm{d}b_a^+\,\mathrm{d}b_b^+\,\delta(B_a^+ - b_a^+ - k_a^+)\\
&\times \delta(B_b^+ - b_b^+ - k_b^+)\int \mathrm{d}x^+\,\mathrm{d}x^-\,e^{-i(q^-x^+ + q^+x^-)/2}\int \mathrm{d}r'\,\mathrm{d}t'\,\mathrm{d}r\,\mathrm{d}t\,C^{gg*}(r',t')\,C^{gg}(r,t)\\
&\quad\times\langle p(p_a)p(p_b)|\,[\mathcal{R}^{\rho\sigma}]^\dagger\,|0\rangle\,\langle 0|\,\mathcal{R}^{\mu\nu}\,|p(p_a)p(p_b)\rangle\\
&\quad\times\langle p_a|\,\mathcal{A}_{c\rho\perp}(x^+n_b/2 + t'n_b)\,\delta(b_a^+ - n_a\cdot\hat{p}_{n_a})\,\mathcal{A}_{c\mu\perp}(tn_b)\,|p_a\rangle\\
&\quad\times\langle p_b|\,\mathcal{A}_{\bar{c}\sigma\perp}(x^-n_a/2 + r'n_a)\,\delta(b_b^+ - n_b\cdot\hat{p}_{n_b})\,\mathcal{A}_{\bar{c}\nu\perp}(rn_a)\,|p_b\rangle\\
&\quad\times\langle 0|\,\bar{\mathrm{T}}[O^{s\dagger}(0)]\,\delta(k_a^+ - n_a\cdot\hat{p}_{a,s})\,\delta(k_b^+ - n_b\cdot\hat{p}_{b,s})\,\mathrm{T}[O^s(0)]\,|0\rangle
\end{aligned} \tag{A.23}$$

$$\begin{aligned}
&= \frac{M\beta}{32S}\frac{1}{(2\pi)^4}\frac{1}{2(N_c^2-1)^2}\int \mathrm{d}k_a^+\,\mathrm{d}k_b^+\,\mathrm{d}b_a^+\,\mathrm{d}b_b^+\,\delta(B_a^+ - b_a^+ - k_a^+)\\
&\quad\times\delta(B_b^+ - b_b^+ - k_b^+)\int \mathrm{d}x^+\,\mathrm{d}x^-\,e^{-i(q^-x^+ + q^+x^-)/2}\\
&\quad\times\int \mathrm{d}r'\,\mathrm{d}t'\,\mathrm{d}r\,\mathrm{d}t\,C^{gg*}(r',t')\,C^{gg}(r,t)\,\langle p(p_a)p(p_b)|\,[\mathcal{R}^{\rho\sigma}]^\dagger\,|0\rangle\,\langle 0|\,\mathcal{R}^{\mu\nu}\,|p(p_a)p(p_b)\rangle\\
&\quad\times\int\frac{\mathrm{d}x_a^-}{4\pi}e^{ix_a^-b_a^+/2}\,\langle p_a|\,\mathcal{A}_{c\rho\perp}(x^+n_b/2 + x_a^-n_a/2 + t'n_b)\,\mathcal{A}_{c\mu\perp}(tn_b)\,|p_a\rangle\\
&\quad\times\int\frac{\mathrm{d}x_b^-}{4\pi}e^{ix_b^-b_b^+/2}\,\langle p_b|\,\mathcal{A}_{\bar{c}\sigma\perp}(x^-n_a/2 + x_b^-n_b/2 + r'n_a)\,\mathcal{A}_{\bar{c}\nu\perp}(rn_a)\,|p_b\rangle\\
&\quad\times\sum\!\!\!\!\!\!\int_{X_S}\langle 0|\,\bar{\mathrm{T}}[O^{s\dagger}(0)]\,|X_S\rangle\,\langle X_S|\,\mathrm{T}[O^s(0)]\,|0\rangle\,\delta(k_a^+ - k_a^+(X_S))\,\delta(k_b^+ - k_b^+(X_S))\,,
\end{aligned} \tag{A.24}$$

where T and $\bar{\mathrm{T}}$ are the time and anti-time ordering operators. In the equation above we have introduced the eigenvalues $k_i^+(X_S)$ of the projection of the momentum operator on a soft state $|X_S\rangle$.

We give the operatorial definition of the gluon beam function B_{g/p_a} (the formula for p_b is equivalent)

$$\begin{aligned}
&\langle p_a|\mathcal{A}_{c\rho\perp}(x^+\bar{n}_a/2 + x_a^-n_a/2 + t'\bar{n}_a)\,\mathcal{A}_{c\mu\perp}(t\bar{n}_a)\,|p_a\rangle = (-g_{\rho\mu\perp})\,\delta^{ab}\,(\bar{n}_a\cdot p_a)\\
&\quad\times\int_0^1 \mathrm{d}z_a\,e^{iz_a(x^+\bar{n}_a/2 + (t'-t)\bar{n}_a)p_a}\int \mathrm{d}b_a^{+\prime}\,e^{-i(x_a^-b_a^{+\prime})/2}\,B_{g/p_a}\big(z_a(\bar{n}_a\cdot p_a)b_a^{+\prime}, z_a, \mu\big)\,.
\end{aligned} \tag{A.25}$$

Similarly, we define the soft function

$$S_{gg}(k_a^+, k_b^+, \beta, \theta, \mu) = \frac{1}{N_c^2 - 1} \sum\!\!\!\!\!\!\int_{X_S} \langle 0 | \, \bar{\mathrm{T}}[O^{s\dagger}(0)] \, | X_S \rangle \, \langle X_S | \, \mathrm{T}[O^s(0)] \, | 0 \rangle \\ \times \delta(k_a^+ - k_a^+(X_S)) \, \delta(k_b^+ - k_b^+(X_S)) \,, \tag{A.26}$$

and the hard function

$$H_{gg}^{\mu\nu\rho\sigma}(M, \beta, \theta, \mu) = \frac{1}{(4\pi)^2} \frac{1}{2(N_c^2 - 1)} \int \mathrm{d}r' \, \mathrm{d}t' \, e^{iz_a t' n_b \cdot p_a} \, e^{iz_b r' n_a \cdot p_b} \, C^{gg*}(r', t') \\ \times \int \mathrm{d}r \, \mathrm{d}t \, e^{-iz_a t n_b \cdot p_a} \, e^{-iz_b r n_a \cdot p_b} \, C^{gg}(r, t) \\ \times \langle p(p_a) p(p_b) | \, [\mathcal{R}^{\rho\sigma}]^\dagger \, | 0 \rangle \, \langle 0 | \, \mathcal{R}^{\mu\nu} \, | p(p_a) p(p_b) \rangle \,. \tag{A.27}$$

We can define a scalar hard function, contracting the Lorentz indices in Eq. (A.27) with the terms proportional to $g_{\rho\mu\perp}$ (and $g_{\sigma\nu\perp}$) coming from Eq. (A.25)

$$H_{gg}(M, \beta, \theta, \mu) = (-g_{\rho\mu\perp}) \, (-g_{\sigma\nu\perp}) \, H_{gg}^{\mu\nu\rho\sigma}(M, \beta, \theta, \mu) \,. \tag{A.28}$$

Integrating over $x_{a,b}^-$, the differential cross section becomes

$$\frac{\mathrm{d}\sigma}{\mathrm{d}B_a^+ \, \mathrm{d}B_b^+ \, \mathrm{d}M \, \mathrm{d}y_{HH} \, \mathrm{d}\cos\theta \, \mathrm{d}\phi_H} = \frac{\pi M \beta}{S} \int \mathrm{d}k_a^+ \, \mathrm{d}k_b^+ \, \mathrm{d}b_a^+ \, \mathrm{d}b_b^+ \, \delta(B_a^+ - b_a^+ - k_a^+) \\ \times \delta(B_b^+ - b_b^+ - k_b^+) \int \mathrm{d}z_a \, \mathrm{d}z_b \, \delta\!\left(z_a - \frac{q^-}{n_b \cdot p_a}\right) \delta\!\left(z_b - \frac{q^+}{n_a \cdot p_b}\right) \\ \times [B_{g/p_a}\big(z_a(n_b \cdot p_a) b_a^+, z_a, \mu\big) B_{g/p_b}\big(z_b(n_a \cdot p_b) b_b^+, z_b, \mu\big)] \\ \times [H_{gg}(M, \beta, \theta, \mu) \, S_{gg}(k_a^+, k_b^+, \beta, \theta, \mu)] \\ = \frac{\pi \beta M}{S} \int \mathrm{d}\, k_a^+ \, \mathrm{d}k_b^+ \, [H_{gg}(M, \beta, \theta, \mu) \, S_{gg}(k_a^+, k_b^+, \beta, \theta, \mu)] \\ \times [B_{g/p_a}\big(q^-(B_a^+ - k_a^+), q^-/n_b \cdot p_a, \mu\big) B_{g/p_b}\big(q^+(B_b^+ - k_b^+), q^+/n_a \cdot p_b, \mu\big)] \,. \tag{A.29}$$

Here $q^\mp = M \, e^{\pm y_{HH}}$, and the trace over the product of the soft and hard functions arises from the Kronecker deltas δ^{ab} in the beam functions.

In order to constrain the a and b hemisphere simultaneously, we can define

$$\hat{B} = \frac{B_a^+ + B_b^+}{M} \,, \tag{A.30}$$

which can be used when the two hemispheres are equal in size, for example when the rapidity of the Higgs bosons system y_{HH} is zero. We can express the cross section in Eq. (A.29) to be

differential in $\hat{B}$, integrating over $B^+_{a,b}$, using $B^+_{a,b} = k^+_{a,b} + b^+_{a,b}$ and $t_{a,b} = q^{\mp} b^+_{a,b}$, resulting in

$$\begin{aligned}\frac{\mathrm{d}\sigma}{\mathrm{d}M\,\mathrm{d}y_{HH}\,\mathrm{d}\cos\theta\,\mathrm{d}\phi_H\,\mathrm{d}\hat{B}} &= \frac{\pi M\beta}{S}\int \mathrm{d}k_a^+\,\mathrm{d}k_b^+\,\mathrm{d}B_a^+\,\mathrm{d}B_b^+\,\delta(M\hat{B} - B_a^+ - B_b^+)\\ &\quad\times\left[B_{g/p_a}\big(q^-(B_a^+ - k_a^+), q^-/n_b\cdot p_a, \mu\big) B_{g/p_b}\big(q^+(B_b^+ - k_b^+), q^+/n_a\cdot p_b, \mu\big)\right]\\ &\quad\times\left[H_{gg}(M,\beta,\theta,\mu)\, S_{gg}(k_a^+, k_b^+, \beta, \theta, \mu)\right]\\ &= \frac{\pi\beta}{MS}\int \mathrm{d}t_a\,\mathrm{d}t_b\,[B_{g/p_a}(t_a, z_a, \mu) B_{g/p_b}(t_b, z_b, \mu)]\\ &\quad\times\left[H_{gg}(M,\beta,\theta,\mu) S_{B,gg}\left(M\hat{B} - \frac{t_a}{q^-} - \frac{t_b}{q^+}, \beta, \theta, \mu\right)\right]. \end{aligned} \tag{A.31}$$

This result is only valid in the frame where $y_{HH} = 0$. If we were to boost the Higgs bosons system to a different rapidity, the definition of the hemispheres would be altered. Hence, when considering rapidity-dependent hemispheres denoted as a for $y > y_{HH}$ and b for $y < y_{HH}$, we define the boost-invariant combination as follows

$$\tau_B = \frac{q^- B_a^+(y_{HH}) + q^+ B_b^+(y_{HH})}{M^2}\,. \tag{A.32}$$

Only in the partonic centre-of-mass frame the definition of τ_B coincides with the one of $\hat{B}$, consequently $\hat{B}$ can be replaced with τ_B. In Ref. [41], it is shown that the soft function and its arguments for the τ_B case is the same as for $\hat{B}$. The soft function is boost-invariant up to the hemisphere definition, linked to the arguments $k^+_{a,b}$. Moreover, when boosting to a frame at a nonzero rapidity y_{HH}, the beam functions remain unaffected. Thus, we can express the factorisation theorem for the double Higgs boson production as

$$\begin{aligned}\frac{\mathrm{d}\sigma}{\mathrm{d}M\,\mathrm{d}y_{HH}\,\mathrm{d}\cos\theta\,\mathrm{d}\phi_H\,\mathrm{d}\tau_B} &= \frac{\pi\beta}{MS}\int \mathrm{d}t_a\,\mathrm{d}t_b\,[B_{g/p_a}(t_a, z_a, \mu) B_{g/p_2}(t_b, z_b, \mu)]\\ &\quad\times\left[H_{gg}(M,\beta,\theta,\mu)\, S_{B,gg}\left(M\tau_B - \frac{t_a + t_b}{M}, \beta, \theta, \mu\right)\right]. \end{aligned} \tag{A.33}$$

Appendix B

Hard function for $gg \to HH$ in the $\overline{\text{MS}}$ scheme

In this appendix we provide the necessary ingredients to derive the hard function for the double Higgs boson production in the $\overline{\text{MS}}$ scheme.

In order to achieve the NNLL$'$ accuracy, the hard function must be computed up to order $\mathcal{O}(\alpha_S^4)$ in perturbation theory. Regardless of the chosen subtraction scheme (referred to as X), its perturbative expansion can be expressed as

$$H_X = \left(\frac{\alpha_S}{4\pi}\right)^2 \left[H^{(0)} + \frac{\alpha_S}{4\pi} H_X^{(1)} + \left(\frac{\alpha_S}{4\pi}\right)^2 H_X^{(2)} + \mathcal{O}(\alpha_S^3)\right] , \tag{B.1}$$

with α_S the strong coupling. The first contribution, $H^{(0)}$, is independent of the scheme, which explains the absence of the subscript X. Indeed, it is given by the cross section at leading order. The remaining two contributions, the one-loop $H^{(1)}$ and two-loop coefficients $H^{(2)}$, are provided in the Catani scheme ($X = C$) in Refs. [70, 101]. To extract the results needed for the implementation in GENEVA, we have to convert these expressions to be differential in the usual phase space with two particles, denoted as Φ_2, instead of using the Mandelstam variable t as it is done in those references. In particular, we define

$$H_C^{(i)} = \frac{\mathrm{d}\sigma_{\text{fin}}^{(i)}}{\mathrm{d}s\,\mathrm{d}t} \frac{\mathrm{d}t}{\mathrm{d}\Phi_2}, \tag{B.2}$$

where

$$t = -\frac{1}{2}\left[Q^2 - 2m_H^2 - \sqrt{Q^2(Q^2 - 4m_H^2)}\cos\theta\right] \tag{B.3}$$

with $Q^2 = s$ the invariant mass of the final state, m_H the mass of the Higgs boson and θ the angle between one of the two Higgs bosons and the initial partons. The Jacobian needed for our conversion is given by

$$\frac{\mathrm{d}\Phi_2}{\mathrm{d}t} = \frac{1}{8\pi s} \frac{1}{\Gamma(1-\epsilon)} \left[\frac{s(s - 4m_H^2) - (t-u)^2}{16\pi s}\right]^{-\epsilon}, \tag{B.4}$$

where ϵ is the dimensional regularisation parameter appearing in the d-dimensional two-particles phase space of Refs. [70, 101].

To give the explicit values of $H_C^{(i)}$, we introduce the following quantities

$$C_{\mathrm{LO}} = \frac{6\lambda v^2}{s - m_H^2} - 1, \qquad 2\lambda v^2 = m_H^2, \qquad v^4 = \frac{1}{2G_F^2}, \tag{B.5}$$

where v is the vacuum expectation value, λ the Higgs trilinear coupling and G_F the Fermi constant. Expanding in powers of ϵ and taking the limit $\epsilon \to 0$, the hard function coefficients in the Catani scheme are

$$\begin{aligned}
H^{(0)}(s) &= \frac{s\, C_{\mathrm{LO}}^2}{144\, v^4}, \\
H_C^{(1)}(s) &= \left(5\, C_A - 3\, C_F + \frac{4}{3}\frac{1}{C_{\mathrm{LO}}}\right) H^{(0)}(s), \\
H_C^{(2)}(s,t,u) &= \left(\mathcal{F}^{(2)} + \frac{1}{C_{\mathrm{LO}}}\mathcal{R}^{(2)}(s,t,u) + \frac{1}{C_{\mathrm{LO}}^2}\mathcal{V}^{(2)}(s,t,u)\right) H^{(0)}(s),
\end{aligned} \tag{B.6}$$

where $C_A = 3$ and $C_F = 4/3$. Defining for brevity

$$L_m = \log\left(\frac{s}{m_t^2}\right), \qquad L_u = \log\left(\frac{s}{-u}\right), \qquad L_t = \log\left(\frac{s}{-t}\right), \tag{B.7}$$

where m_t is the mass of the top quark, and setting the energy scale μ^2 to the partonic centre-of-mass, the coefficients in Eq. (B.6) are given as

$$\begin{aligned}
\mathcal{F}^{(2)} &= C_A^2\left(\frac{23827}{648} - \frac{83}{6}\zeta_2 - \frac{253}{36}\zeta_3 + \frac{5}{8}\zeta_4 + \frac{7}{2}L_m\right) + C_A C_F\left(-\frac{145}{6} - \frac{11}{2}L_m\right) \\
&\quad + 9C_F^2 - \frac{22}{9}\zeta_2 n_f^2 T_F^2 - \frac{5}{24}C_A - \frac{1}{3}C_F - \frac{1}{3}n_f T_F C_A\left(\frac{2255}{54} - \frac{217}{6}\zeta_2 + \frac{49}{3}\zeta_3\right) \\
&\quad - \frac{1}{3}n_f T_F C_F\left(41 - 12L_m - 24\zeta_3\right), \\
\mathcal{R}^{(2)}(s,t,u) &= -7C_A^2 + 11C_A C_F - 8n_f C_F T_F + \frac{1}{3}C_A\left(\frac{476}{9} + \frac{11}{3}(L_t + L_u) + \frac{4m_H^2}{s}\right) \\
&\quad - 8C_F - \frac{4}{9}T_F n_f\left(\frac{10}{3} + L_t + L_u\right) - \frac{1}{3}C_A\left(1 + \frac{2m_H^4}{s^2}\right)\left[2\mathrm{Li}_2\left(1 - \frac{m_H^4}{tu}\right)\right. \\
&\quad + 4\mathrm{Li}_2\left(\frac{m_H^2}{t}\right) + 4\mathrm{Li}_2\left(\frac{m_H^2}{u}\right) + 4\log\left(1 - \frac{m_H^2}{t}\right)\log\left(-\frac{m_H^2}{t}\right) \\
&\quad \left. + 4\log\left(1 - \frac{m_H^2}{u}\right)\log\left(-\frac{m_H^2}{u}\right) - 8\zeta_2 - \log^2\left(\frac{t}{u}\right)\right], \\
\mathcal{V}^{(2)}(s,t,u) &= \frac{1}{(3\,s\,t\,u)^2}\left[m_H^8(t+u)^2 - 2\,m_H^4\,t\,u(t+u)^2 + t^2u^2(4s^2 + (t+u)^2)\right],
\end{aligned} \tag{B.8}$$

where n_f is the number of flavours and $T_F = 1/2$.

As a first step, we have to convert Eq. (B.6) in the $\overline{\rm MS}$ scheme exploiting the following relations

$$
\begin{aligned}
H^{(1)}_{\overline{\rm MS}}(s,\mu) &= H^{(1)}_C(s) + \lim_{\epsilon\to 0} 2\,{\rm Re}\left[2\,\mathcal{I}^{(1)}(\epsilon,\mu) + \mathcal{Z}^{(1)}(\epsilon,\mu)\right] H^{(0)}(s),\\
H^{(2)}_{\overline{\rm MS}}(s,t,u,\mu) &= H^{(2)}_C(s,t,u,\mu) + \lim_{\epsilon\to 0}\left\{2\,{\rm Re}\left[2\,\mathcal{I}^{(1)}(\epsilon,\mu) + \mathcal{Z}^{(1)}(\epsilon,\mu)\right]\right\} H^{(1)}_C(s)\\
&\quad + \left\{ |\lim_{\epsilon\to 0}[2\,\mathcal{I}^{(1)}(\epsilon,\mu) + \mathcal{Z}^{(1)}(\epsilon,\mu)]|^2 + 2{\rm Re}\lim_{\epsilon\to 0}\Big(4\,\mathcal{I}^{(2)}(\epsilon,\mu)\right.\\
&\quad \left.+ 2\,\mathcal{I}^{(1)}(\epsilon,\mu)[2\,\mathcal{I}^{(1)}(\epsilon,\mu) + \mathcal{Z}^{(1)}(\epsilon,\mu)] + \mathcal{Z}^{(2)}(\epsilon,\mu)\Big)\right\} H^{(0)}(s)\,. \qquad \text{(B.9)}
\end{aligned}
$$

The $\mathcal{I}^{(i)}(\epsilon,\mu)$ are the perturbative coefficients of the $\mathcal{I}(\epsilon,\mu)$ operator defined as [159]

$$
\mathcal{I}(\epsilon,\mu) = 1 + \left(\frac{\alpha_S}{2\pi}\right)\mathcal{I}^{(1)}(\epsilon,\mu) + \left(\frac{\alpha_S}{2\pi}\right)^2\mathcal{I}^{(2)}(\epsilon,\mu) + \mathcal{O}(\alpha_S^3)\,. \qquad \text{(B.10)}
$$

We give the definition of the first two coefficients

$$
\begin{aligned}
\mathcal{I}^{(1)}(\epsilon,\mu) &= -\left(\frac{\mu^2}{-s}\right)^{\epsilon}\frac{\exp(\epsilon\,\gamma_E)}{\Gamma(1-\epsilon)}\left(C_g\frac{1}{\epsilon^2} + \gamma_g\frac{1}{\epsilon}\right),\\
\mathcal{I}^{(2)}(\epsilon,\mu) &= \left(\frac{\mu^2}{-s}\right)^{\epsilon}\frac{\exp(\epsilon\gamma_E)}{72\,\Gamma(1-\epsilon)\epsilon^4}\Big\{12\epsilon(C_g+\epsilon\gamma_g)(11C_A - 2n_f)\\
&\quad - \frac{36\exp(\epsilon\gamma_E)}{(\Gamma(1-\epsilon)}\left(\frac{\mu^2}{-s}\right)^{\epsilon}(C_g+\epsilon\gamma_g)^2 \;+\epsilon\left(\frac{\mu^2}{-s}\right)^{\epsilon}\Big[36\epsilon^2 H_g\\
&\quad + 2(3+5\epsilon)(C_g+2\epsilon\gamma_g)n_f + C_A(C_g+2\epsilon\gamma_g)(-33-67\epsilon+3\epsilon\pi^2)\Big]\Big\}\,, \qquad \text{(B.11)}
\end{aligned}
$$

since the process considered is gluon-initiated, all the factors appearing in Eq. (B.11) are given by

$$
\begin{aligned}
C_g &= C_A, \qquad \gamma_g = \frac{\beta_0}{2} = \frac{11}{6}C_A - \frac{4}{6}T_F n_f,\\
H_g &= C_A^2\left(\frac{1}{2}\zeta_3 + \frac{5}{12} + \frac{11\pi^2}{144}\right) - C_A n_f\left(\frac{29}{27} + \frac{\pi^2}{72}\right) + \frac{1}{2}C_F n_f + \frac{5}{27}n_f^2\,. \qquad \text{(B.12)}
\end{aligned}
$$

The $\mathcal{Z}^{(i)}(\epsilon,\mu)$ in Eq. (B.9) are obtained from the following expansion of the $\mathcal{Z}(\epsilon,\mu)$ factor [174],

$$
\mathcal{Z}^{-1}(\epsilon,\mu) = 1 + \left(\frac{\alpha_S}{4\pi}\right)\mathcal{Z}^{(1)}(\epsilon,\mu) + \left(\frac{\alpha_S}{4\pi}\right)^2\mathcal{Z}^{(2)}(\epsilon,\mu) + \mathcal{O}(\alpha_S^3)\,, \qquad \text{(B.13)}
$$

where

$$
\begin{aligned}
\mathcal{Z}^{(1)}(\epsilon,\mu) &= -\frac{\Gamma_0'}{4\epsilon^2} - \frac{\mathbf{\Gamma}_0(\mu)}{2\epsilon},\\
\mathcal{Z}^{(2)}(\epsilon,\mu) &= \frac{(\Gamma_0')^2}{32\epsilon^4} + \frac{3\beta_0\Gamma_0' + 2\Gamma_0'\mathbf{\Gamma}_0(\mu)}{16\epsilon^3} + \frac{4\beta_0\mathbf{\Gamma}_0(\mu) + 2\mathbf{\Gamma}_0^2(\mu) - \Gamma_1'}{16\epsilon^2} - \frac{\mathbf{\Gamma}_1(\mu)}{4\epsilon}\,, \qquad \text{(B.14)}
\end{aligned}
$$

and

$$\begin{aligned}
\mathbf{\Gamma}_i(\mu) &= -C_A\Gamma_i \log\left(\frac{\mu^2}{-s}\right) + 2\gamma_i^g, \qquad \Gamma_i' = -2C_A\Gamma_i\,,\\
\Gamma_0 &= 4, \qquad \Gamma_1 = \left(\frac{268}{9} - \frac{4}{3}\pi^2\right) C_A - \frac{80}{9} T_F n_f\,,\\
\gamma_1^g &= C_A^2\left(-\frac{692}{27} + \frac{11\pi^2}{18} + 2\zeta_3\right) + C_A T_F n_f\left(\frac{256}{27} - \frac{2\pi^2}{9}\right) + 4C_F T_F n_f\,.
\end{aligned} \tag{B.15}$$

Setting $\mu^2 = s$, we find the following results for the translation to the $\overline{\text{MS}}$ scheme of the hard function coefficients

$$\begin{aligned}
H^{(1)}_{\overline{\text{MS}}}(s) &= H^{(1)}_C(s) + \frac{7C_A\pi^2}{3} H^{(0)}(s),\\
H^{(2)}_{\overline{\text{MS}}}(s,t,u) &= H^{(2)}_C(s,t,u) + \frac{7C_A\pi^2}{3} H^{(1)}_C(s) + \left(\frac{167}{6} C_A^2\pi^2 - \frac{367}{54} C_A n_f \pi^2\right.\\
&\quad \left. + \frac{11 n_f^2\pi^2}{27} + \frac{73}{36} C_A^2\pi^4 - \frac{11}{3} C_A^2\zeta_3 + \frac{2}{3} C_A n_f \zeta_3\right) H^{(0)}(s).
\end{aligned} \tag{B.16}$$

As a last step, we have to restore the exact μ dependence of the hard function. This is done using the renormalisation group equations (RGE)

$$\frac{\mathrm{d}}{\mathrm{d}\log(\mu^2)} H(\mu^2) = \mathrm{Re}[\mathbf{\Gamma}(\mu^2)]\, H(\mu^2). \tag{B.17}$$

The first order of the expansion, $\mathcal{O}(\alpha_S^3)$, is given by

$$\frac{\mathrm{d}}{\mathrm{d}\log(\mu^2)} H^{(1)}(s,\mu^2) - 2\beta_0 H^{(0)}(s) = \mathrm{Re}[\mathbf{\Gamma}_0(\mu^2)] H^{(0)}(s)\,, \tag{B.18}$$

having used

$$\frac{1}{4\pi}\frac{\mathrm{d}}{\mathrm{d}\log(\mu^2)}\alpha_S = -\left(\frac{\alpha_S}{4\pi}\right)^2 \sum_{n=0}\left(\frac{\alpha_S}{4\pi}\right)^n \beta_n. \tag{B.19}$$

with $\beta_0 = \frac{11}{3}C_A - \frac{4}{3}T_F n_f$. The second order of the expansion, $\mathcal{O}(\alpha_S^4)$ in Eq. (B.17), gives

$$\begin{aligned}
\frac{\mathrm{d}}{\mathrm{d}\log(\mu^2)} H^{(2)}(s,t,u,\mu^2) - 2\beta_1 H^{(0)}(s) - 3\beta_0 H^{(1)}(s,\mu^2) &= \mathrm{Re}[\mathbf{\Gamma}_0(\mu^2)] H^{(1)}(s,\mu^2)\\
&\quad + \mathrm{Re}[\mathbf{\Gamma}_1(\mu^2)] H^{(0)}(s)\,,
\end{aligned} \tag{B.20}$$

where $\beta_1 = \frac{34}{3}C_A^2 - \frac{10}{3}C_A n_f - 2C_F n_f$.

To summarize, the hard function in the $\overline{\text{MS}}$ scheme is given by

$$H_{\overline{\text{MS}}}(s,\mu^2) = \left(\frac{\alpha_S}{4\pi}\right)^2 \left[H^{(0)}(s,\mu^2) + \left(\frac{\alpha_S}{4\pi}\right) H^{(1)}_{\overline{\text{MS}}}(s,\mu^2) + \left(\frac{\alpha_S}{4\pi}\right)^2 H^{(2)}_{\overline{\text{MS}}}(s,t,u,\mu^2) + \mathcal{O}(\alpha_S^3)\right], \tag{B.21}$$

where

$$
\begin{aligned}
H^{(0)}(s,\mu^2) &= H^{(0)}(s),\\
H^{(1)}_{\overline{\rm MS}}(s,\mu^2) &= H^{(1)}_{\overline{\rm MS}}(s) - 2C_A \log^2\left(\frac{\mu^2}{s}\right) H^{(0)}(s),\\
H^{(2)}_{\overline{\rm MS}}(s,t,u,\mu^2) &= H^{(2)}_{\overline{\rm MS}}(s,t,u) - H^{(1)}_{\overline{\rm MS}}(s)\left[2C_A \log^2\left(\frac{\mu^2}{s}\right) - \frac{11}{3}C_A \log\left(\frac{\mu^2}{s}\right) + \frac{2}{3}n_f \log\left(\frac{\mu^2}{s}\right)\right]\\
&\quad + H^{(0)}(s)\Bigg[\log\left(\frac{\mu^2}{s}\right)\left(-\frac{772}{27}C_A^2 + \frac{76}{27}C_A n_f + \frac{11}{9}C_A^2\pi^2 - \frac{2}{9}C_A n_f \pi^2 + 4C_A^2\zeta_3\right)\\
&\quad + \log^2\left(\frac{\mu^2}{s}\right)\left(-\frac{134}{9}C_A^2 + \frac{20}{9}C_A n_f + \frac{2}{3}C_A^2\pi^2\right)\\
&\quad + \log^3\left(\frac{\mu^2}{s}\right)\left(-\frac{22}{9}C_A^2 + \frac{4}{9}C_A n_f\right) + 2C_A^2 \log^4\left(\frac{\mu^2}{s}\right)\Bigg]. \qquad \text{(B.22)}
\end{aligned}
$$

Appendix C

Distribution identities

In this appendix we present the distribution identities between the z, u and z_a, z_b variables, using the coefficient function up to next-to-leading order as an example.

Starting from the perturbative expansion of the $q\bar{q}$ coefficient function for rapidity distribution, given by

$$C(z,u,\alpha_S) = \delta(1-z) + \frac{\alpha_S}{\pi} C^{(1)}(z,u) + \left(\frac{\alpha_S}{\pi}\right)^2 C^{(2)}(z,u) + \mathcal{O}(\alpha_S^3)\,, \tag{C.1}$$

the NLO coefficient $C_1(z,u)$ is defined, omitting for semplicity the dependence on α_S, as

$$\begin{aligned}\frac{C^{(1)}(z,u)}{C_F} =& \frac{\delta(1-u)+\delta(u)}{2}\left[(2\zeta_2-4)\delta(1-z) + 2(1+z^2)\left(\frac{\log(1-z)}{1-z}\right)_+ + \log\frac{Q^2}{\mu^2}\left(\frac{1+z^2}{1-z}\right)_+\right.\\ &\left. - \frac{1+z^2}{1-z}\log(z) + 1 - z\right] + \frac{1}{2}\frac{1+z^2}{1-z}\left[\left(\frac{1}{u}\right)_+ + \left(\frac{1}{1-u}\right)_+\right] - (1-z)\,.\end{aligned} \tag{C.2}$$

Note that the term $\frac{1}{1-z}\left[\left(\frac{1}{u}\right)_+ + \left(\frac{1}{1-u}\right)_+\right]$ does not need the plus distribution for the z singularity, as it is already regularised by the plus distribution in the u variable. This can easily be seen using the definition of the plus distribution and the fact that the luminosity, when $z = 1$, is independent on the value of u (see Eq. (8.12)). Integrating in z and u, indeed, we get

$$\begin{aligned}&\int_0^1 \mathrm{d}z \int_0^1 \mathrm{d}u \left(\frac{1}{1-z}\right)_+ \left[\left(\frac{1}{u}\right)_+ + \left(\frac{1}{1-u}\right)_+\right]\mathscr{L}(z,u) =\\ &\qquad \int_0^1 \mathrm{d}z \int_0^1 \mathrm{d}u \frac{1}{u(1-z)}\left[\mathscr{L}(z,u) - \mathscr{L}(z,0) \cancel{- \mathscr{L}(1,u) + \mathscr{L}(1,0)}\right]\\ &\qquad + \int_0^1 \mathrm{d}z \int_0^1 \mathrm{d}u \frac{1}{(1-u)(1-z)}\left[\mathscr{L}(z,u) - \mathscr{L}(z,1) \cancel{- \mathscr{L}(1,u) + \mathscr{L}(1,1)}\right]\\ &\qquad = \int_0^1 \mathrm{d}z \int_0^1 \mathrm{d}u \frac{1}{1-z}\left[\left(\frac{1}{u}\right)_+ + \left(\frac{1}{1-u}\right)_+\right]\mathscr{L}(z,u)\,.\end{aligned} \tag{C.3}$$

$\mathrm{d}z\,\mathrm{d}u$ LHS	$\mathrm{d}z_a\,\mathrm{d}z_b$ RHS
$\delta(1-z)$	$\delta(1-z_a)\,\delta(1-z_b)$
$g(z)\,\delta(1-u)$	$g(z_a)\,\delta(1-z_b)$
$g(z)\,\delta(u)$	$g(z_b)\,\delta(1-z_a)$
$\left(\frac{1}{1-z}\right)_+\left[\left(\frac{1}{u}\right)_+ + \left(\frac{1}{1-u}\right)_+\right]$	$\left(\frac{1}{1-z_a}\right)_+\left(\frac{1}{1-z_b}\right)_+ + \frac{1}{(1+z_a)(1+z_b)} + \zeta_2\delta(1-z_a)\delta(1-z_b)$
	$-\left[\left(\frac{\log(1-z_a)}{1-z_a}\right)_+ + \frac{\log\frac{1+z_a}{2z_a}}{1-z_a}\right]\delta(1-z_b)$
	$-\left[\left(\frac{\log(1-z_b)}{1-z_b}\right)_+ + \frac{\log\frac{1+z_b}{2z_b}}{1-z_b}\right]\delta(1-z_a)$

Table C.1: Conversion of two-dimensional plus distributions between the z, u and z_a, z_b sets of variables. In this case, $g(z)$ can be either a function or a distribution.

Using the relations in Eq. (8.18), we can compute the same coefficient but in the z_a, z_b variables through Eq. (8.21). First, we express the z, u variables in function of z_a, z_b, yielding to

$$z = z_a z_b\,, \qquad u = \frac{z_b(1-z_a^2)}{(1-z_a z_b)(z_a+z_b)}\,. \tag{C.4}$$

The Jacobian associated with this change of variables is given by

$$\frac{\mathrm{d}z\,\mathrm{d}u}{\mathrm{d}z_a\,\mathrm{d}z_b} = \frac{2[1-u(1-z)][1-(1-u)(1-z)]}{1-z^2} = \frac{2z(1+z)}{(1-z)(z_a+z_b)^2}\,. \tag{C.5}$$

In order to compute $\tilde{C}^{(1)}(z_a, z_b)$, the functional form of each term can be computed directly with the change of variables, for distributional terms, such as the plus distributions, the boundary terms at $z_{a,b} = 1$ are determined by comparing the integrals over the integration region in z, u and z_a, z_b.

In table C.1, we show the conversion for all the distributional terms appearing in Eq. (C.2). The first relation is straightfoward, as $z = z_a z_b$ and the delta functions on the $z_{a,b}$ variables. The validity of such calculation can be proven comparing the integral over the whole domain of both sets of variables

$$\int_0^1 \mathrm{d}z \int_0^1 \mathrm{d}u\, \frac{1}{\frac{\mathrm{d}z_a\mathrm{d}z_b}{\mathrm{d}z\mathrm{d}u}} \cdot \frac{\mathrm{d}z_a\mathrm{d}z_b}{\mathrm{d}z\mathrm{d}u} = \int_0^1 \mathrm{d}z_a \int_0^1 \mathrm{d}z_b\, \delta(1-z_a)\delta(1-z_b) = 1\,, \tag{C.6}$$

having used the property of the delta function. The second and third line of the table follow from the definitions in Eqs. (C.4) and (8.18), and can be proven using again the comparison of the integral in the two sets of variables (which we do not report here since it is as trivial as for the first line of the table). The $\delta(1-u)$ condition corresponds to $z_b = 1$ and $z_a = z$, leading to $g(z)\delta(1-u) \to g(z_a)\delta(1-z_b)$. Equally, the $\delta(u)$ condition corresponds to $z_a = 1$ and $z_b = z$, giving $g(z)\delta(u) \to g(z_b)\delta(1-z_a)$. For the last line of the table, we perform the conversion away from the endpoints of these distributions, restoring the singularities after the

calculation. In particular we have

$$\frac{1}{1-z}\left(\frac{1}{u}+\frac{1}{1-u}\right)\to\frac{2z(1+z)}{(1-z)(z_a+z_b)^2}\cdot\frac{1}{1-z}\cdot\frac{(1-z)^2(z_a+z_b)^2}{(1-z_a^2)(1-z_b^2)}$$
$$=\frac{1}{(1-z_a)(1-z_b)}+\frac{1}{(1+z_a)(1+z_b)}\,. \tag{C.7}$$

Restoring the distributions, we get

$$\left(\frac{1}{1-z}\right)_+\left[\left(\frac{1}{u}\right)_+ +\left(\frac{1}{1-u}\right)_+\right]\to\left(\frac{1}{1-z_a}\right)_+\left(\frac{1}{1-z_b}\right)_+ +\frac{1}{(1+z_a)(1+z_b)}$$
$$+f(z_a)\,\delta(1-z_b)+f(z_b)\,\delta(1-z_a)\,, \tag{C.8}$$

where f can be any function or distribution. By symmetry, it will be the same for the two delta terms. In order to determine the function f, we can use the fact that the LHS of Eq. (C.8) vanishes upon integration over u, as reported in section 9.3. To integrate over u on the RHS, we can use the projector $\int \mathrm{d}z_a\,\mathrm{d}z_b\,\delta(z-z_az_b)$. Therefore, we get

$$0=\int_0^1\mathrm{d}z_a\int_0^1\mathrm{d}z_b\,\delta(z-z_az_b)\bigg[\left(\frac{1}{1-z_a}\right)_+\left(\frac{1}{1-z_b}\right)_+ +\frac{1}{(1+z_a)(1+z_b)}+f(z_a)\delta(1-z_b)$$
$$+f(z_b)\delta(1-z_a)\bigg]\,,$$
$$=2\left(\frac{\log(1-z)}{1-z}\right)_+ -\zeta_2\delta(1-z)-\frac{\log z}{1-z}+\frac{\log\frac{(1+z)^2}{4z}}{1-z}+2f(z)\,. \tag{C.9}$$

The nontrivial projection integral required in this formula is

$$(f\otimes g)(z)=\int_0^1\mathrm{d}z_a\int_0^1\mathrm{d}z_b\,\delta(z-z_az_b)\left(\frac{1}{1-z_a}\right)_+\left(\frac{1}{1-z_b}\right)_+ \tag{C.10}$$

which computation is reported in section C.1. From Eq. (C.9), we determine the value of f as

$$f(z)=-\left(\frac{\log(1-z)}{1-z}\right)_+-\frac{\log\frac{1+z}{2z}}{1-z}\,. \tag{C.11}$$

The term $\zeta_2\,\delta(1-z_a)\delta(1-z_b)$ in Eq. (C.9) is a double distributional term, and it has to be counted directly in the conversion of the $\delta(1-z)$. Replacing this result in Eq. (C.8), the last line of the table becomes

$$\left(\frac{1}{1-z}\right)_+\left[\left(\frac{1}{u}\right)_+ +\left(\frac{1}{1-u}\right)_+\right]\to\left(\frac{1}{1-z_a}\right)_+\left(\frac{1}{1-z_b}\right)_+ +\frac{1}{(1+z_a)(1+z_b)}$$
$$+\zeta_2\delta(1-z_a)\delta(1-z_b)-\left[\left(\frac{\log(1-z_a)}{1-z_a}\right)_+ +\frac{\log\frac{1+z_a}{2z_a}}{1-z_a}\right]\delta(1-z_b)$$
$$-\left[\left(\frac{\log(1-z_b)}{1-z_b}\right)_+ +\frac{\log\frac{1+z_b}{2z_b}}{1-z_b}\right]\delta(1-z_a)\,. \tag{C.12}$$

Finally, using the relations in Tab. C.1 and applying the change of variables to the finite terms in Eq. (C.2), the NLO coefficient function in the z_a, z_b variables reads

$$\begin{aligned}\frac{\tilde{C}^{(1)}(z_a,z_b)}{C_F} &= \left(3\zeta_2 - 4 + \frac{3}{2}\log\frac{Q^2}{\mu^2}\right)\delta(1-z_a)\delta(1-z_b)\\ &+ \left(\frac{\log(1-z_a)}{1-z_a}\right)_+\delta(1-z_b) + \delta(1-z_a)\left(\frac{\log(1-z_b)}{1-z_b}\right)_+ + \left(\frac{1}{1-z_a}\right)_+\left(\frac{1}{1-z_b}\right)_+\\ &+ \left(\frac{1}{1-z_a}\right)_+\left[\log\frac{Q^2}{\mu^2}\delta(1-z_b) - \frac{1+z_b}{2}\right] + \left[\log\frac{Q^2}{\mu^2}\delta(1-z_a) - \frac{1+z_a}{2}\right]\left(\frac{1}{1-z_b}\right)_+\\ &+ \delta(1-z_a)\left[\frac{1-z_b}{2} - \frac{1+z_b}{2}\log(1-z_b) + \frac{1}{2}\frac{1+z_b^2}{1-z_b}\log\frac{2}{1+z_b} - \frac{1+z_b}{2}\log\frac{Q^2}{\mu^2}\right]\\ &+ \delta(1-z_b)\left[\frac{1-z_a}{2} - \frac{1+z_a}{2}\log(1-z_a) + \frac{1}{2}\frac{1+z_a^2}{1-z_a}\log\frac{2}{1+z_a} - \frac{1+z_a}{2}\log\frac{Q^2}{\mu^2}\right]\\ &+ \frac{(z_a^2+z_b^2)[(1+z_a)^2+(1+z_b)^2+2z_az_b(3+z_a+z_b+z_az_b)]}{2(1+z_a)(1+z_b)(z_a+z_b)^2}\,, \end{aligned} \tag{C.13}$$

where we have used the following properties of the plus distribution

$$\begin{aligned}[g(z)f(z)]_+ &= g(z)[f(z)]_+ - \delta(1-z)\int_0^1 \mathrm{d}y\, g(y)[f(y)]_+\,,\\ g(z)[f(z)]_+ &= g(1)[f(z)]_+ + [g(z)-g(1)]f(z)\,. \end{aligned} \tag{C.14}$$

C.1 Convolutions in Mellin space

For functions defined in the range $0 < x < 1$, the Mellin transform is defined as

$$\tilde{f}(N) \equiv \mathcal{M}[f](N) \equiv \int_0^1 \mathrm{d}x\, x^{N-1} f(x)\,, \tag{C.15}$$

and the inverse Mellin transform is given as

$$f(x) \equiv \mathcal{M}[f](N) \equiv \int_0^1 x^{N-1} f(x)\,\mathrm{d}x\,. \tag{C.16}$$

The convolution between two functions f and g is given by

$$\begin{aligned}(f\otimes g)(x) &= \int_0^1\int_0^1 f(y)g(z)\,\delta(x-yz)\,\mathrm{d}y\,\mathrm{d}z\\ &= \int_x^1 f(y)\,g\left(\frac{x}{y}\right)\frac{\mathrm{d}y}{y}\,. \end{aligned} \tag{C.17}$$

In Mellin space, the convolution of two functions diagonalizes, giving

$$\begin{aligned}\mathcal{M}[f\otimes g](N) &= \int_0^1 \mathrm{d}z\, z^{N-1}\int_0^1 \mathrm{d}z_a\int_0^1 \mathrm{d}z_b\, f(z_a)g(z_b)\delta(z-z_az_b)\\ &= \int_0^1 \mathrm{d}z_a\, z_a^{N-1} f(z_a)\int_0^1 \mathrm{d}z_b\, z_b^{N-1} g(z_b) = \tilde{f}(N)\tilde{g}(N)\,. \end{aligned} \tag{C.18}$$

For some convolutions, such as Eq. (C.10), the computation is much simpler in Mellin space. In order to do that, using again the results of appendix B.4 of Ref. [156], we observe that

$$\mathcal{M}\left[\left(\frac{1}{1-z}\right)_+\right](N) = \mathcal{D}_0(N) = -L\,, \tag{C.19a}$$

$$\mathcal{M}\left[\left(\frac{\log(1-z)}{1-z}\right)_+\right](N) = \mathcal{D}_1(N) = \frac{1}{2}\left[L^2 + \zeta_2 - \psi_1(N)\right], \tag{C.19b}$$

defining $L = \gamma + \psi_0(N)$, with γ the Euler gamma. In the large-N limit, corresponding to the threshold limit $z \to 1$, $\psi_0(N) \sim \log(N)$. Eq. (C.10) in Mellin space becomes

$$\mathcal{D}_0(N)\mathcal{D}_0(N) = L^2 = 2\mathcal{D}_1(N) - \zeta_2 + \psi_1(N)\,, \tag{C.20}$$

having determined the value of L^2 from Eq. (C.19b). Knowing that

$$\mathcal{M}\left[\frac{\log^k(z)}{1-z}\right] = -\psi_k(N)\,, \tag{C.21}$$

the inverse Mellin transform gives

$$\mathcal{M}^{-1}\left(\mathcal{D}_0\mathcal{D}_0\right)(z) = \mathcal{M}^{-1}\left[L^2\right] = 2\mathcal{D}_1(z) - \zeta_2\delta(1-z) - \frac{\log(z)}{1-z}\,, \tag{C.22}$$

which is the result of the projection in Eq. (C.10).

Appendix D

Analytical expressions for threshold resummation approaches

In this appendix, we provide first the explicit expressions for the approximations based on the BNX and BFR approaches for all the three choices of threshold logarithms discussed, and then the expressions for BDDR, AMRST and LMT, both at NLO and NNLO which are used in the text.

D.1 Coefficient function for BNX/BFR approximations

In the BNX and BFR approaches the threshold approximation of rapidity distributions is obtained from the threshold approximation of the rapidity-integrated coefficient function. For simplicity we define

$$\ell = \log \frac{Q^2}{\mu^2}\,, \tag{D.1}$$

with μ the factorization scale, assumed to be equal to the renormalization scale and the logarithmically enhanced contributions are given by Eq. (10.5). The only relevant channel at threshold for the Drell-Yan process is the $q\bar{q}$ channel, its coefficient function at threshold Eq. (10.4) at NLO is given by

$$C^{(1)}_{\rm thr}(z) = C_F\left[4\mathcal{D}_1(z) + 2\ell\mathcal{D}_0(z) + \left(2\zeta_2 - 4 + \frac{3}{2}\ell\right)\delta(1-z)\right]. \tag{D.2}$$

At NNLO, instead, it is defined as

$$\begin{aligned} C^{(2)}_{\rm thr}(z) &= 8C_F^2\mathcal{D}_3(z) \\ &+ \left[12C_F^2\ell - \frac{11C_A - 2n_f}{3}C_F\right]\mathcal{D}_2(z) \\ &+ \left[\left(4\ell^2 + 6\ell - 16 - 8\zeta_2\right)C_F^2 - \frac{11C_A - 2n_f}{3}C_F\ell + \frac{67C_A - 10n_f}{9}C_F - 2\zeta_2 C_A C_F\right]\mathcal{D}_1(z) \end{aligned}$$

$$
\begin{aligned}
&+\Bigg[\left(3\ell^2-(8+4\zeta_2)\ell+16\zeta_3\right)C_F^2+\left(-\frac{11}{12}\ell^2+\left(\frac{67}{18}-\zeta_2\right)\ell+\frac{7}{2}\zeta_3+\frac{11}{3}\zeta_2-\frac{101}{27}\right)C_AC_F\\
&\quad+\left(\frac{1}{6}\ell^2-\frac{5}{9}\ell+\frac{14}{27}-\frac{2}{3}\zeta_2\right)n_fC_F\Bigg]\mathcal{D}_0(z)\\
&+\Bigg[\left(\left(\frac{9}{8}-2\zeta_2\right)\ell^2+\left(\frac{3}{2}\zeta_2+11\zeta_3-\frac{93}{16}\right)\ell+\frac{1}{10}\zeta_2^2-\frac{35}{8}\zeta_2-\frac{15}{4}\zeta_3+\frac{511}{64}\right)C_F^2\\
&\quad+\left(-\frac{11}{16}\ell^2+\left(\frac{193}{48}-\frac{3}{2}\zeta_3\right)\ell-\frac{3}{20}\zeta_2^2+\frac{37}{9}\zeta_2+\frac{7}{4}\zeta_3-\frac{1535}{192}\right)C_AC_F\\
&\quad+\left(\frac{1}{8}\ell^2-\frac{17}{24}\ell+\frac{1}{2}\zeta_3-\frac{7}{9}\zeta_2+\frac{127}{96}\right)n_fC_F\Bigg]\delta(1-z)\,.
\end{aligned}
\tag{D.3}
$$

For the N-soft approximation, using Eq. (10.7), the coefficient function at NLO is given by

$$
C_{\rm thr}^{(1),N}(z)=C_F\left[4\mathcal{D}_1^{\log}(z)+2\ell\mathcal{D}_0^{\log}(z)+\left(4\zeta_2-4+\frac{3}{2}\ell+2\gamma^2-2\gamma\ell\right)\delta(1-z)\right],
\tag{D.4}
$$

while the NNLO

$$
\begin{aligned}
C_{\rm thr}^{(2),N}(z)&=8C_F^2\mathcal{D}_3^{\log}(z)\\
&+\left[12C_F^2\ell-\frac{11C_A-2n_f}{3}C_F\right]\mathcal{D}_2^{\log}(z)\\
&+\left[\left(4\ell^2+6\ell-16-8\zeta_2\right)C_F^2-\frac{11C_A-2n_f}{3}C_F\ell+\frac{67C_A-10n_f}{9}C_F-2\zeta_2C_AC_F\right]\mathcal{D}_1^{\log}(z)\\
&+\Bigg[\left(3\ell^2-(8+4\zeta_2)\ell+16\zeta_3\right)C_F^2+\left(-\frac{11}{12}\ell^2+\left(\frac{67}{18}-\zeta_2\right)\ell+\frac{7}{2}\zeta_3+\frac{11}{3}\zeta_2-\frac{101}{27}\right)C_AC_F\\
&\quad+\left(\frac{1}{6}\ell^2-\frac{5}{9}\ell+\frac{14}{27}-\frac{2}{3}\zeta_2\right)n_fC_F\Bigg]\mathcal{D}_0^{\log}(z)\\
&+\Bigg[\left(\left(\frac{9}{8}-3\gamma+2\gamma^2\right)\ell^2+\left(-\frac{93}{16}+8\gamma+3\gamma^2-4\gamma^3+\frac{9}{2}\zeta_2-8\gamma\zeta_2+3\zeta_3\right)\ell\right.\\
&\quad\left.+\frac{511}{64}-8\gamma^2+2\gamma^4-\frac{99}{8}\zeta_2+8\gamma^2\zeta_2+\frac{21}{10}\zeta_2^2-\frac{15}{4}\zeta_3+12\zeta_4\right)C_F^2\\
&\quad+\left(\left(-\frac{11}{16}+\frac{11}{12}\gamma\right)\ell^2+\left(\frac{193}{48}-\frac{67}{18}\gamma-\frac{11}{6}\gamma^2-\frac{11}{6}\zeta_2+\gamma\zeta_2-\frac{3}{2}\zeta_3\right)\ell\right.\\
&\quad\left.-\frac{1535}{192}+\frac{101}{27}\gamma+\frac{67}{18}\gamma^2+\frac{11}{9}\gamma^3+\frac{47}{6}\zeta_2-\gamma^2\zeta_2-\frac{23}{20}\zeta_2^2+\frac{151}{36}\zeta_3-\frac{7}{2}\gamma\zeta_3\right)C_AC_F\\
&\quad+\left(\left(\frac{1}{8}-\frac{1}{6}\gamma\right)\ell^2+\left(-\frac{17}{24}+\frac{5}{9}\gamma+\frac{1}{3}\gamma^2+\frac{1}{3}\zeta_2\right)\ell\right.\\
&\quad\left.+\frac{127}{96}-\frac{14}{27}\gamma-\frac{5}{9}\gamma^2-\frac{2}{9}\gamma^3-\frac{4}{3}\zeta_2+\frac{1}{18}\zeta_3\right)n_fC_F\Bigg]\delta(1-z)\,.
\end{aligned}
\tag{D.5}
$$

Lastly, the coefficient functions for the $\psi_{\rm soft_1}$ approximation are given by

$$
C_{\rm thr}^{(1),\psi}(z)=C_F\left[4z\mathcal{D}_1(z)+2z\ell\mathcal{D}_0(z)+\left(2\zeta_2-4+\frac{3}{2}\ell\right)\delta(1-z)-\frac{2z\log(z)}{1-z}\right],
\tag{D.6}
$$

and

$$
\begin{aligned}
C_{\rm thr}^{(2),\psi}(z) &= 8C_F^2 z\,\mathcal{D}_3(z) \\
&+ \left[12C_F^2\ell - \frac{11C_A-2n_f}{3}C_F\right] z\,\mathcal{D}_2(z) \\
&+ \left[\left(4\ell^2+6\ell-16-8\zeta_2\right)C_F^2 - \frac{11C_A-2n_f}{3}C_F\ell + \frac{67C_A-10n_f}{9}C_F - 2\zeta_2 C_A C_F\right] z\,\mathcal{D}_1(z) \\
&+ \Bigg[\left(3\ell^2-(8+4\zeta_2)\ell+16\zeta_3\right)C_F^2 + \left(-\frac{11}{12}\ell^2+\left(\frac{67}{18}-\zeta_2\right)\ell+\frac{7}{2}\zeta_3+\frac{11}{3}\zeta_2-\frac{101}{27}\right)C_A C_F \\
&\quad + \left(\frac{1}{6}\ell^2-\frac{5}{9}\ell+\frac{14}{27}-\frac{2}{3}\zeta_2\right)n_f C_F\Bigg] z\,\mathcal{D}_0(z) \\
&+ \Bigg[\left(\left(\frac{9}{8}-3\gamma+2\gamma^2\right)\ell^2+\left(-\frac{93}{16}+8\gamma+3\gamma^2-4\gamma^3+\frac{9}{2}\zeta_2-8\gamma\zeta_2+3\zeta_3\right)\ell\right. \\
&\quad \left.+\frac{511}{64}-8\gamma^2+2\gamma^4-\frac{99}{8}\zeta_2+8\gamma^2\zeta_2+\frac{21}{10}\zeta_2^2-\frac{15}{4}\zeta_3+12\zeta_4\right)C_F^2 \\
&\quad + \left(\left(-\frac{11}{16}+\frac{11}{12}\gamma\right)\ell^2+\left(\frac{193}{48}-\frac{67}{18}\gamma-\frac{11}{6}\gamma^2-\frac{11}{6}\zeta_2+\gamma\zeta_2-\frac{3}{2}\zeta_3\right)\ell\right. \\
&\quad \left.-\frac{1535}{192}+\frac{101}{27}\gamma+\frac{67}{18}\gamma^2+\frac{11}{9}\gamma^3+\frac{47}{6}\zeta_2-\gamma^2\zeta_2-\frac{23}{20}\zeta_2^2+\frac{151}{36}\zeta_3-\frac{7}{2}\gamma\zeta_3\right)C_A C_F \\
&\quad + \left(\left(\frac{1}{8}-\frac{1}{6}\gamma\right)\ell^2+\left(-\frac{17}{24}+\frac{5}{9}\gamma+\frac{1}{3}\gamma^2+\frac{1}{3}\zeta_2\right)\ell\right. \\
&\quad \left.+\frac{127}{96}-\frac{14}{27}\gamma-\frac{5}{9}\gamma^2-\frac{2}{9}\gamma^3-\frac{4}{3}\zeta_2+\frac{1}{18}\zeta_3\right)n_f C_F\Bigg]\delta(1-z) \\
&+ \Bigg[\left(-\frac{2z\log(z)}{1-z}\ell^2+\left(-\frac{3z\log(z)}{1-z}-\frac{12z\log(1-z)\log(z)}{1-z}+\frac{2z\log^2(z)}{1-z}\right)\ell\right. \\
&\quad + \frac{8z\mathrm{Li}_3(z)}{1-z}-\frac{8z\zeta_3}{1-z}+\frac{8z\log(z)}{1-z}-\frac{4z\mathrm{Li}_2(z)\log(z)}{1-z}-\frac{12z\log^2(1-z)\log(z)}{1-z} \\
&\quad \left.+\frac{4z\log(1-z)\log^2(z)}{1-z}-\frac{z\log^3(z)}{3(1-z)}\right)C_F^2 \\
&\quad + \left(\frac{11z\log(z)}{6(1-z)}\ell-\frac{67z\log(z)}{18(1-z)}+\frac{z\zeta_2\log(z)}{1-z}+\frac{11z\log(1-z)\log(z)}{3(1-z)}-\frac{11z\log^2(z)}{18(1-z)}\right)C_A C_F \\
&\quad + \left(-\frac{z\log(z)}{3(1-z)}\ell+\frac{5z\log(z)}{9(1-z)}-\frac{2z\log(1-z)\log(z)}{3(1-z)}+\frac{z\log^2(z)}{9(1-z)}\right)C_F n_f\Bigg]. \qquad \text{(D.7)}
\end{aligned}
$$

D.2 Coefficient function for BDDR/AMRST approximations

The expansion of the resummed result of BDDR [128] (at leading power) and AMRST [135] (at next-to-leading power) in N space is given at NLO by (setting $\mu_F = \mu_R = Q$)

$$
\tilde{C}_1(N_a, N_b) = C_F\left[\frac{\bar{L}^2}{2}+4\zeta_2-4+\frac{\bar{L}}{2\bar{N}}+\mathcal{O}\left(\frac{1}{\bar{N}^2}\right)\right] \qquad \text{(D.8)}
$$

and at NNLO by

$$\begin{aligned}\tilde{C}_2(N_a,N_b) = {}& \frac{C_F^2}{8}\bar{L}^4 + C_F\frac{11C_A-2n_f}{72}\bar{L}^3 + \left[C_F^2(2\zeta_2-2) + C_FC_A\left(\frac{67}{72}-\frac{\zeta_2}{4}\right) - C_Fn_f\frac{5}{36}\right]\bar{L}^2 \\ & + \left[C_FC_A\left(\frac{101}{54}-\frac{7}{4}\zeta_3\right) - C_Fn_f\frac{7}{27}\right]\bar{L} + C_F^2\left(\frac{511}{64}-\frac{99}{8}\zeta_2+\frac{69}{10}\zeta_2^2-\frac{15}{4}\zeta_3\right) \\ & + C_FC_A\left(-\frac{1535}{192}+\frac{47}{6}\zeta_2-\frac{23}{20}\zeta_2^2+\frac{151}{36}\zeta_3\right) + C_Fn_f\left(\frac{127}{96}-\frac{4}{3}\zeta_2+\frac{\zeta_3}{18}\right) \\ & + \frac{C_F^2}{4}\frac{\bar{L}^3}{\bar{N}} + \left[\frac{C_F^2}{8}\frac{1}{\bar{N}} + C_F\frac{11C_A-2n_f}{48}\right]\frac{\bar{L}^2}{\bar{N}} + C_F^2\left(\frac{\bar{L}_a}{N_a}+\frac{\bar{L}_b}{N_b}\right)\bar{L} - \frac{C_F^2}{4}\left(\frac{\bar{L}_a^2}{N_a}+\frac{\bar{L}_b^2}{N_b}\right) \\ & + \left[C_F^2\left(2\zeta_2-\frac{11}{4}\right) + C_FC_A\left(\frac{133}{72}-\frac{\zeta_2}{4}\right) - C_Fn_f\frac{11}{36}\right]\frac{\bar{L}}{\bar{N}} \\ & + \left[C_F^2\frac{5}{8} - C_FC_A\frac{5}{8}\right]\left(\frac{\bar{L}_a}{N_a}+\frac{\bar{L}_b}{N_b}\right) \\ & + \left[-C_F^2\frac{\zeta_2}{4} - C_Fn_f\frac{19}{54} + C_FC_A\left(\frac{97}{216}-\frac{7}{8}\zeta_3\right)\right]\frac{1}{\bar{N}} + \mathcal{O}\left(\frac{1}{\bar{N}^2}\right) \end{aligned} \tag{D.9}$$

with

$$\frac{1}{\bar{N}} \equiv \frac{1}{N_a}+\frac{1}{N_b} \qquad \bar{L}_{a,b} \equiv \log N_{a,b} + \gamma \qquad \bar{L} \equiv \log(N_aN_b) + 2\gamma = \bar{L}_a + \bar{L}_b\,, \tag{D.10}$$

with γ the Euler-Mascheroni constant. To convert these results to z space, we can invert Eq. (10.8) for the leading power terms, while for the next-to leading power contributions we further need the relation

$$\int_0^1 \mathrm{d}z\, z^{N-1}\, \log^p\frac{1}{z}\, \log^k \log\frac{1}{z} = \frac{1}{N^{1+p}}\sum_{j=0}^{k}\binom{k}{j}\Gamma^{(j)}(1+p)\log^{k-j}\frac{1}{N}\,, \qquad k,p\geq 0\,, \tag{D.11}$$

which can be derived from the generating function $\log^\xi \frac{1}{z}$ deriving k times with respect to ξ in $\xi = p$. Using these results we get at NLO

$$\begin{aligned}\tilde{C}_1(z_a,z_b) = {}& C_F\Big[\left(\mathcal{D}_1^{\log}(z_a) - \gamma\mathcal{D}_0^{\log}(z_a)\right)\delta(1-z_b) + \delta(1-z_a)\left(\mathcal{D}_1^{\log}(z_b) - \gamma\mathcal{D}_0^{\log}(z_b)\right) \\ & \quad + \mathcal{D}_0^{\log}(z_a)\mathcal{D}_0^{\log}(z_b) + \left(4\zeta_2 - 4 + 2\gamma^2\right)\delta(1-z_a)\delta(1-z_b)\Big] \\ & + \frac{C_F}{2}\left[\left(\gamma - \log\log\frac{1}{z_b}\right)\delta(1-z_a) + \left(\gamma-\log\log\frac{1}{z_a}\right)\delta(1-z_b) - \mathcal{D}_0^{\log}(z_a) - \mathcal{D}_0^{\log}(z_b)\right] \end{aligned} \tag{D.12}$$

and at NNLO

$$\tilde{C}_2(z_a,z_b) = \left[C_F^2\left(\frac{511}{64}-\frac{99}{8}\zeta_2+\frac{69}{10}\zeta_2^2-\frac{15}{4}\zeta_3+8\zeta_2\gamma^2-8\gamma^2+2\gamma^4\right)\right.$$

$$
\begin{aligned}
&+ C_F C_A \left(-\frac{1535}{192} + \frac{47}{6}\zeta_2 - \frac{23}{20}\zeta_2^2 + \frac{151}{36}\zeta_3 - \zeta_2\gamma^2 - \frac{7}{2}\zeta_3\gamma + \frac{101}{27}\gamma + \frac{67}{18}\gamma^2 + \frac{11}{9}\gamma^3 \right) \\
&+ C_F n_f \left(\frac{127}{96} - \frac{4}{3}\zeta_2 + \frac{\zeta_3}{18} - \frac{14}{27}\gamma - \frac{5}{9}\gamma^2 - \frac{2}{9}\gamma^3 \right) \Big] \delta(1-z_a)\delta(1-z_b) \\
&+ \frac{C_F^2}{2} \Big[\mathcal{D}_3^{\log}(z_a)\delta(1-z_b) + \delta(1-z_a)\mathcal{D}_3^{\log}(z_b) \Big] \\
&+ \frac{3}{2} C_F^2 \Big[\mathcal{D}_2^{\log}(z_a)\mathcal{D}_0^{\log}(z_b) + \mathcal{D}_0^{\log}(z_a)\mathcal{D}_2^{\log}(z_b) \Big] \\
&+ 3 C_F^2 \mathcal{D}_1^{\log}(z_a)\mathcal{D}_1^{\log}(z_b) \\
&+ \left[-\frac{3}{2} C_F^2 \gamma - C_F \frac{11 C_A - 2 n_f}{24} \right] \Big[\mathcal{D}_2^{\log}(z_a)\delta(1-z_b) + \delta(1-z_a)\mathcal{D}_2^{\log}(z_b) \Big] \\
&- C_F \frac{11 C_A - 2 n_f}{12} \Big[\mathcal{D}_1^{\log}(z_a)\mathcal{D}_0^{\log}(z_b) + \mathcal{D}_0^{\log}(z_a)\mathcal{D}_1^{\log}(z_b) \Big] \\
&+ \left[C_F^2 \left(\frac{5}{2}\zeta_2 - 4 + \frac{3}{2}\gamma^2 \right) + C_F C_A \left(\frac{67}{36} - \frac{\zeta_2}{2} + \frac{11}{12}\gamma \right) + C_F n_f \left(-\frac{5}{18} - \frac{\gamma}{6} \right) \right] \\
&\quad \times \Big[\mathcal{D}_1^{\log}(z_a)\delta(1-z_b) + \delta(1-z_a)\mathcal{D}_1^{\log}(z_b) \Big] \\
&+ \left[C_F^2 \left(\zeta_2 - 4 \right) + C_F C_A \left(\frac{67}{36} - \frac{\zeta_2}{2} \right) - \frac{5}{18} C_F n_f \right] \mathcal{D}_0^{\log}(z_a)\mathcal{D}_0^{\log}(z_b) \\
&+ \left[C_F^2 \left(\zeta_3 - \frac{5}{2}\zeta_2\gamma + 4\gamma - \frac{\gamma^3}{2} \right) + C_F C_A \left(\frac{11}{24}\zeta_2 + \frac{7}{4}\zeta_3 - \frac{101}{54} + \frac{\gamma}{2}\zeta_2 - \frac{11}{24}\gamma^2 - \frac{67}{36}\gamma \right) \right. \\
&\qquad \left. + C_F n_f \left(\frac{7}{27} - \frac{\zeta_2}{12} + \frac{\gamma^2}{12} + \frac{5}{18}\gamma \right) \right] \Big[\mathcal{D}_0^{\log}(z_a)\delta(1-z_b) + \delta(1-z_a)\mathcal{D}_0^{\log}(z_b) \Big] \\
&+ \Bigg\{ \mathcal{D}_2^{\log}(z_a) \left[-\frac{3}{4} C_F^2 \right] \\
&\qquad + \mathcal{D}_1^{\log}(z_a) \left[-\frac{3}{2} C_F^2 \log\log\frac{1}{z_b} + C_F \frac{11 C_A - 2 n_f}{24} + \frac{C_F^2}{4} \log\frac{1}{z_b} \right] \\
&\qquad + \mathcal{D}_0^{\log}(z_a) \left[-\frac{3}{4} C_F^2 \log^2\log\frac{1}{z_b} + \left(C_F^2 + C_F \frac{11 C_A - 2 n_f}{24} \right) \log\log\frac{1}{z_b} \right. \\
&\qquad\qquad + C_F^2 \left(\frac{11}{4} - \frac{\zeta_2}{2} \right) + C_F C_A \left(-\frac{133}{72} + \frac{\zeta_2}{4} \right) + C_F n_f \frac{11}{36} \\
&\qquad\qquad \left. + \frac{C_F^2}{4} \log\frac{1}{z_b} \left(\log\log\frac{1}{z_b} - 1 \right) \right] \\
&\qquad + \delta(1-z_a) \left[-\frac{1}{4} C_F^2 \log^3\log\frac{1}{z_b} + \left(\frac{3}{4} C_F^2 (1+\gamma) + C_F \frac{11 C_A - 2 n_f}{48} \right) \log^2\log\frac{1}{z_b} \right. \\
&\qquad\qquad + \left(C_F^2 \left(\frac{17}{8} - \frac{5}{4}\zeta_2 - \gamma - \frac{3}{4}\gamma^2 \right) + C_F C_A \left(-\frac{11}{9} + \frac{\zeta_2}{4} - \frac{11}{24}\gamma \right) \right. \\
&\qquad\qquad\qquad \left. \left. + C_F n_f \left(\frac{11}{36} + \frac{\gamma}{12} \right) \right) \log\log\frac{1}{z_b}
\end{aligned}
$$

$$
\begin{aligned}
&+ C_F^2 \left(-\zeta_2 - \frac{1}{2}\zeta_3 + \frac{5}{4}\zeta_2\gamma - \frac{11}{4}\gamma + \frac{1}{4}\gamma^3 \right) \\
&+ C_F C_A \left(\frac{97}{216} - \frac{11}{48}\zeta_2 - \frac{7}{8}\zeta_3 - \frac{\zeta_2}{4}\gamma + \frac{133}{72}\gamma + \frac{11}{48}\gamma^2 \right) \\
&+ C_F n_f \left(-\frac{19}{54} + \frac{\zeta_2}{24} - \frac{11}{36}\gamma - \frac{\gamma^2}{24} \right) \\
&+ \frac{C_F^2}{8} \log\frac{1}{z_b} \left(\log^2 \log\frac{1}{z_b} - 2\log\log\frac{1}{z_b} + 2 - \zeta_2 + \gamma^2 \right) \Bigg] \\
&+ (z_a \leftrightarrow z_b) \Bigg\} \\
&+ \frac{C_F^2}{4} \left[\left(\log\log\frac{1}{z_a} + \log\log\frac{1}{z_b} \right)^2 - 2\zeta_2 \right], \qquad \text{(D.13)}
\end{aligned}
$$

having used the $\mathcal{D}_k^{\log}(z)$ distributions defined in Eq. (10.7).

D.3 Coefficient function for LMT approximation

In the generalized threshold expansion of LMT, the expansion of the resummed result can be obtained from the expression

$$
\tilde{C}_{ij}^{\mathrm{LMT}}(z_a, z_b, \alpha_S) = H_{kr}(\alpha_S) \Big[\delta_{ki} \hat{\mathcal{I}}_{rj}(z_a, z_b, \alpha_S) + \hat{\mathcal{I}}_{ki}(z_b, z_a, \alpha_S)\delta_{rj} - \hat{S}(z_a, z_b, \alpha_S) \Big], \qquad \text{(D.14)}
$$

in terms of the functions defined in the LMT paper [124]. Focussing on the $q\bar{q}$ channel and expanding in powers of α_S, we obtain at NLO at central scales

$$
\begin{aligned}
\frac{\tilde{C}_1^{\mathrm{LMT}}(z_a, z_b)}{C_F} &= (3\zeta_2 - 4)\delta(1-z_a)\delta(1-z_b) + \mathcal{D}_1(z_a)\delta(1-z_b) + \delta(1-z_a)\mathcal{D}_1(z_b) \\
&+ \mathcal{D}_0(z_a)\mathcal{D}_0(z_b) + \Bigg\{ \delta(1-z_a) \left[\frac{1-z_b}{2} - \frac{1+z_b}{2}\log(1-z_b) + \frac{1}{2}\frac{1+z_b^2}{1-z_b}\log\frac{2}{1+z_b} \right] \\
&- \mathcal{D}_0(z_a)\frac{1+z_b}{2} + (z_a \leftrightarrow z_b) \Bigg\}, \qquad \text{(D.15)}
\end{aligned}
$$

corresponding to the distributional part of Eq. (C.13), and at NNLO we get

$$
\begin{aligned}
\tilde{C}_2^{\mathrm{LMT}}(z_a, z_b) = &\left[C_F^2 \left(\frac{511}{64} - \frac{67}{8}\zeta_2 + \frac{19}{5}\zeta_2^2 - \frac{15}{4}\zeta_3 \right) + C_F C_A \left(-\frac{1535}{192} + \frac{215}{36}\zeta_2 - \frac{13}{20}\zeta_2^2 + \frac{43}{12}\zeta_3 \right) \right. \\
&\left. + C_F n_f \left(\frac{127}{96} - \frac{19}{18}\zeta_2 + \frac{\zeta_3}{6} \right) \right] \delta(1-z_a)\delta(1-z_b) \\
&+ \frac{C_F^2}{2} \Big[\mathcal{D}_3(z_a)\delta(1-z_b) + \delta(1-z_a)\mathcal{D}_3(z_b) \Big] \\
&+ \frac{3}{2} C_F^2 \Big[\mathcal{D}_2(z_a)\mathcal{D}_0(z_b) + \mathcal{D}_0(z_a)\mathcal{D}_2(z_b) \Big]
\end{aligned}
$$

$$
\begin{aligned}
&+ 3C_F^2 \mathcal{D}_1(z_a)\mathcal{D}_1(z_b) \\
&- C_F \frac{11C_A - 2n_f}{24}\Big[\mathcal{D}_2(z_a)\delta(1-z_b) + \delta(1-z_a)\mathcal{D}_2(z_b)\Big] \\
&+ \left[C_F^2\left(\zeta_2 - 4\right) + C_F C_A\left(\frac{67}{36} - \frac{\zeta_2}{2}\right) - \frac{5}{18}C_F n_f\right]\Big[\mathcal{D}_1(z_a)\delta(1-z_b) + \delta(1-z_a)\mathcal{D}_1(z_b)\Big] \\
&+ \left[C_F^2\left(\zeta_2 - 4\right) + C_F C_A\left(\frac{67}{36} - \frac{\zeta_2}{2}\right) - \frac{5}{18}C_F n_f\right]\mathcal{D}_0(z_a)\mathcal{D}_0(z_b) \\
&+ \left[2\zeta_3 C_F^2 + C_F C_A\left(\frac{11}{12}\zeta_2 + \frac{7}{4}\zeta_3 - \frac{101}{54}\right) + C_F n_f\left(\frac{7}{27} - \frac{\zeta_2}{6}\right)\right] \\
&\times \Big[\mathcal{D}_0(z_a)\delta(1-z_b) + \delta(1-z_a)\mathcal{D}_0(z_b)\Big] \\
&+ \Big\{\mathcal{D}_2(z_a)F_2(z_b) + \mathcal{D}_1(z_a)F_1(z_b) + \mathcal{D}_0(z_a)F_0(z_b) + \delta(1-z_a)F_\delta(z_b) \\
&+ (z_a \leftrightarrow z_b)\Big\}, \qquad \text{(D.16)}
\end{aligned}
$$

where the functions $F_i(z)$ are given by

$$F_2(z) = -\frac{3}{4}C_F^2(1+z)\,, \qquad \text{(D.17a)}$$

$$
\begin{aligned}
F_1(z) = {} & C_F^2\left(\frac{1}{2}\frac{1+z^2}{1-z}\log\frac{2}{1+z} + \frac{3}{4}(1+z)\log\frac{z}{(1-z)^2} - \frac{\log z}{1-z}\right) \\
& + C_F\frac{11C_A - 2n_f}{24}(1+z) + \frac{C_F}{4}\left(\frac{1-z}{2} + \frac{2}{3}\frac{1-z^3}{z} + (1+z)\log z\right), \qquad \text{(D.17b)}
\end{aligned}
$$

$$
\begin{aligned}
F_0(z) = {} & C_F^2\Big[-\frac{3}{4}(1+z)\log^2(1-z) + \left(\frac{z^2}{1-z}\log\frac{2}{1+z} - \frac{3+z^2}{2}\frac{\log z}{1-z}\right)\log(1-z) \\
& + \frac{1+15z}{4} + \left(-1 - \frac{z}{2} + \frac{3}{4}z^2\right)\frac{\log z}{1-z} + \frac{3+z^2}{8}\frac{\log^2 z}{1-z} - \frac{1}{4}\frac{1+z^2}{1-z}\log^2\frac{2z}{1+z} \\
& + \frac{1+z}{2}\left(\mathrm{Li}_2\left(\frac{1+z}{2}\right) + \mathrm{Li}_2\left(\frac{z-1}{2z}\right) + \frac{3}{2}\mathrm{Li}_2(-z) - \frac{3}{2}\mathrm{Li}_2(z) + \frac{\zeta_2}{4} + \log 2\log\frac{2z\sqrt{z}}{1+z}\right)\Big] \\
& + C_F C_A\Big[\frac{11}{24}(1+z)\log(1-z) + \frac{5}{18} - \frac{77}{36}z + \frac{\zeta_2}{4}(1+z) + \frac{17+5z^2}{24}\frac{\log z}{1-z} \\
& \qquad + \frac{1+z^2}{8}\frac{\log^2 z}{1-z} - \frac{11}{24}\frac{1+z^2}{1-z}\log\frac{2}{1+z}\Big] \\
& + C_F n_f\Big[-\frac{1}{12}(1+z)\log(1-z) + \frac{1}{18} + \frac{2}{9}z + \frac{1}{12}\frac{1+z^2}{1-z}\left(\log\frac{2}{1+z} - \log z\right)\Big] \\
& + C_F\Big[\frac{25+7z+22z^2}{36z}(1-z) - \frac{1+z}{z}\left(\frac{2}{3} + \frac{5}{24}z + \frac{z^2}{6}\right)\log\frac{2}{1+z} + \left(\frac{1}{8} + \frac{5}{8}z + \frac{z^2}{3}\right)\log z \\
& \qquad + \frac{1+z}{4}\left(\mathrm{Li}_2(1-z) + \mathrm{Li}_2(-z) + \frac{\zeta_2}{2} + \log 2\log z - \frac{1}{2}\log^2 z\right)\Big], \qquad \text{(D.17c)}
\end{aligned}
$$

$$F_\delta(z) = C_F^2\left(\frac{7}{4}\zeta_2 - 2\right)\left(1 - z - (1+z)\log(1-z) + \frac{1+z^2}{1-z}\log\frac{2}{1+z}\right) + \frac{1}{16}\mathrm{reg}\big[\tilde{I}^{(2)}_{qqV}(z) + \tilde{I}^{(2)}_{qqS}(z)\big]\,. \tag{D.17d}$$

In the last function we have kept the dependence on the functions $I^{(2)}_{qqV}(z)$ and $I^{(2)}_{qqS}(z)$ given in equation (S53) of Ref. [124]. Specifically, these functions contain distributional terms in $\mathcal{D}_k(z)$ and $\delta(1-z)$, which are already taken into account explicitly in Eq. (D.16) as they contribute to the double-distributional part of the result, so here only the remaining regular part, denoted by reg[...] in the formula, has to be considered. The factor 1/16 finally fixes the different normalization due to the different expansion parameters (we use α_S/π while LMT use $\alpha_S/(4\pi)$). It is useful to write explicitly the large z expansion of the $F_i(z)$ functions,

$$F_2(z) = -\frac{3}{2}C_F^2\,, \tag{D.18a}$$

$$F_1(z) = -3C_F^2\log(1-z) + \frac{3}{2}C_F^2 + C_F\frac{11C_A - 2n_f}{12}\,, \tag{D.18b}$$

$$F_0(z) = -\frac{3}{2}C_F^2\log^2(1-z) + \left(\frac{5}{2}C_F^2 + C_F\frac{11C_A - 2n_f}{12}\right)\log(1-z) + C_F^2\left(\frac{19}{4} - \zeta_2\right) + C_FC_A\left(-\frac{233}{72} + \frac{\zeta_2}{2}\right) + C_Fn_f\frac{19}{36}\,, \tag{D.18c}$$

$$F_\delta(z) = -\frac{1}{2}C_F^2\log^3(1-z) + \left(\frac{3}{2}C_F^2 + C_F\frac{11C_A - 2n_f}{24}\right)\log^2(1-z) + \left(C_F^2\left(\frac{33}{8} - \zeta_2\right) + C_FC_A\left(-\frac{47}{18} + \frac{\zeta_2}{2}\right) + C_Fn_f\frac{19}{36}\right)\log(1-z) + C_F^2\left(-2 - \frac{\zeta_2}{2} - 2\zeta_3\right) + C_FC_A\left(\frac{125}{54} - \frac{7}{6}\zeta_2 - \frac{7}{4}\zeta_3\right) + C_Fn_f\left(-\frac{67}{108} + \frac{\zeta_2}{6}\right)\,. \tag{D.18d}$$

Bibliography

[1] S. Alioli, G. Billis, A. Broggio, A. Gavardi, S. Kallweit, M. A. Lim et al., *Double Higgs production at NNLO interfaced to parton showers in GENEVA*, *JHEP* **06** (2023) 205 [2212.10489].

[2] M. Bonvini and G. Marinelli, *On the approaches to threshold resummation of rapidity distributions for the Drell-Yan process*, *Eur. Phys. J. C* **83** (2023) 931 [2306.03568].

[3] ATLAS collaboration, *Observation of a new particle in the search for the Standard Model Higgs boson with the ATLAS detector at the LHC*, *Phys. Lett. B* **716** (2012) 1 [1207.7214].

[4] CMS collaboration, *Observation of a New Boson at a Mass of 125 GeV with the CMS Experiment at the LHC*, *Phys. Lett. B* **716** (2012) 30 [1207.7235].

[5] G. F. Sterman, *Summation of Large Corrections to Short Distance Hadronic Cross-Sections*, *Nucl. Phys. B* **281** (1987) 310.

[6] S. Catani and L. Trentadue, *Resummation of the qcd perturbative series for hard processes*, *Nuclear Physics B* **327** (1989) 323.

[7] S. Catani, *Higher order QCD corrections in hadron collisions: Soft gluon resummation and exponentiation*, *Nucl. Phys. B Proc. Suppl.* **54** (1997) 107 [hep-ph/9610413].

[8] S. Forte and G. Ridolfi, *Renormalization group approach to soft gluon resummation*, *Nucl. Phys. B* **650** (2003) 229 [hep-ph/0209154].

[9] C. W. Bauer and I. W. Stewart, *Invariant operators in collinear effective theory*, *Phys. Lett. B* **516** (2001) 134 [hep-ph/0107001].

[10] T. Becher, A. Broggio and A. Ferroglia, *Introduction to Soft-Collinear Effective Theory*, vol. 896. Springer, 2015, 10.1007/978-3-319-14848-9, [1410.1892].

[11] T. Becher, *Soft-Collinear Effective Theory*, 1803.04310.

[12] T. Becher and M. Neubert, *Threshold resummation in momentum space from effective field theory*, *Phys. Rev. Lett.* **97** (2006) 082001 [hep-ph/0605050].

[13] Y. Dokshitzer, D. D'yakonov and S. Troyan, *On the transverse momentum distribution of massive lepton pairs*, *Physics Letters B* **79** (1978) 269.

[14] J. Bellm et al., *Herwig 7.2 release note*, *Eur. Phys. J. C* **80** (2020) 452 [1912.06509].

[15] T. Sjostrand and P. Z. Skands, *Transverse-momentum-ordered showers and interleaved multiple interactions*, *Eur. Phys. J. C* **39** (2005) 129 [hep-ph/0408302].

[16] C. Bierlich et al., *A comprehensive guide to the physics and usage of PYTHIA 8.3*, 2203.11601.

[17] S. Schumann and F. Krauss, *A Parton shower algorithm based on Catani-Seymour dipole factorisation*, *JHEP* **03** (2008) 038 [0709.1027].

[18] T. Gleisberg, S. Hoeche, F. Krauss, M. Schonherr, S. Schumann, F. Siegert et al., *Event generation with SHERPA 1.1*, *JHEP* **02** (2009) 007 [0811.4622].

[19] Sherpa collaboration, *Event Generation with Sherpa 2.2*, *SciPost Phys.* **7** (2019) 034 [1905.09127].

[20] P. Nason, *A New method for combining NLO QCD with shower Monte Carlo algorithms*, *JHEP* **11** (2004) 040 [hep-ph/0409146].

[21] S. Frixione, P. Nason and C. Oleari, *Matching NLO QCD computations with Parton Shower simulations: the POWHEG method*, *JHEP* **11** (2007) 070 [0709.2092].

[22] S. Alioli, P. Nason, C. Oleari and E. Re, *A general framework for implementing NLO calculations in shower Monte Carlo programs: the POWHEG BOX*, *JHEP* **1006** (2010) 043 [1002.2581].

[23] K. Hamilton, P. Nason and G. Zanderighi, *MINLO: Multi-Scale Improved NLO*, *JHEP* **10** (2012) 155 [1206.3572].

[24] K. Hamilton, P. Nason, C. Oleari and G. Zanderighi, *Merging H/W/Z + 0 and 1 jet at NLO with no merging scale: a path to parton shower + NNLO matching*, *JHEP* **05** (2013) 082 [1212.4504].

[25] S. Hoeche, F. Krauss, M. Schonherr and F. Siegert, *QCD matrix elements + parton showers: The NLO case*, *JHEP* **04** (2013) 027 [1207.5030].

[26] C. W. Bauer, F. J. Tackmann and J. Thaler, *GenEvA (II): A phase space generator from a reweighted parton shower*, *JHEP* **12** (2008) 011 [0801.4028].

[27] C. W. Bauer, F. J. Tackmann and J. Thaler, *GenEvA (I): A new framework for event generation*, *JHEP* **12** (2008) 010 [0801.4026].

[28] S. Alioli, C. W. Bauer, C. Berggren, F. J. Tackmann, J. R. Walsh et al., *Matching Fully Differential NNLO Calculations and Parton Showers*, *JHEP* **1406** (2014) 089 [1311.0286].

[29] P. F. Monni, P. Nason, E. Re, M. Wiesemann and G. Zanderighi, *MiNNLO$_{PS}$: a new method to match NNLO QCD to parton showers*, *JHEP* **05** (2020) 143 [1908.06987].

[30] P. F. Monni, E. Re and M. Wiesemann, *MiNNLO$_{PS}$: optimizing $2 \to 1$ hadronic processes*, *Eur. Phys. J. C* **80** (2020) 1075 [2006.04133].

[31] T. Becher, M. Neubert and G. Xu, *Dynamical Threshold Enhancement and Resummation in Drell-Yan Production*, *JHEP* **07** (2008) 030 [0710.0680].

[32] M. Bonvini, S. Forte and G. Ridolfi, *Soft gluon resummation of Drell-Yan rapidity distributions: Theory and phenomenology*, *Nucl. Phys. B* **847** (2011) 93 [1009.5691].

[33] T. Kinoshita, *Mass singularities of Feynman amplitudes*, *J. Math. Phys.* **3** (1962) 650.

[34] T.-D. Lee and M. Nauenberg, *Degenerate systems and mass singularities*, *Physical Review* **133** (1964) B1549.

[35] S. Catani and M. H. Seymour, *A General algorithm for calculating jet cross-sections in NLO QCD*, *Nucl. Phys. B* **485** (1997) 291 [hep-ph/9605323].

[36] S. Frixione, Z. Kunszt and A. Signer, *Three jet cross-sections to next-to-leading order*, *Nucl. Phys. B* **467** (1996) 399 [hep-ph/9512328].

[37] S. Catani, M. L. Mangano, P. Nason and L. Trentadue, *The Resummation of soft gluons in hadronic collisions*, *Nucl. Phys. B* **478** (1996) 273 [hep-ph/9604351].

[38] S. Forte, G. Ridolfi, J. Rojo and M. Ubiali, *Borel resummation of soft gluon radiation and higher twists*, *Phys. Lett. B* **635** (2006) 313 [hep-ph/0601048].

[39] S. Alioli, A. Broggio, A. Gavardi, S. Kallweit, M. A. Lim, R. Nagar et al., *Matching NNLO to parton shower using N^3LL colour-singlet transverse momentum resummation in GENEVA*, 2102.08390.

[40] I. W. Stewart, F. J. Tackmann and W. J. Waalewijn, *N-Jettiness: An Inclusive Event Shape to Veto Jets*, *Phys. Rev. Lett.* **105** (2010) 092002 [1004.2489].

[41] I. W. Stewart, F. J. Tackmann and W. J. Waalewijn, *Factorization at the LHC: From PDFs to Initial State Jets*, *Phys. Rev. D* **81** (2010) 094035 [0910.0467].

[42] I. W. Stewart, F. J. Tackmann and W. J. Waalewijn, *The Beam Thrust Cross Section for Drell-Yan at NNLL Order*, *Phys. Rev. Lett.* **106** (2011) 032001 [1005.4060].

[43] S. Alioli, C. W. Bauer, C. Berggren, F. J. Tackmann and J. R. Walsh, *Drell-Yan production at NNLL'+NNLO matched to parton showers*, *Phys. Rev.* **D92** (2015) 094020 [1508.01475].

[44] S. Alioli, A. Broggio, S. Kallweit, M. A. Lim and L. Rottoli, *Higgsstrahlung at NNLL′+NNLO matched to parton showers in GENEVA*, *Phys. Rev. D* **100** (2019) 096016 [1909.02026].

[45] S. Alioli, A. Broggio, A. Gavardi, S. Kallweit, M. A. Lim, R. Nagar et al., *Precise predictions for photon pair production matched to parton showers in GENEVA*, *JHEP* **04** (2021) 041 [2010.10498].

[46] S. Alioli, A. Broggio, A. Gavardi, S. Kallweit, M. A. Lim, R. Nagar et al., *Next-to-next-to-leading order event generation for Z boson pair production matched to parton shower*, *Phys. Lett. B* **818** (2021) 136380 [2103.01214].

[47] S. Alioli, G. Billis, A. Broggio, A. Gavardi, S. Kallweit, M. A. Lim et al., *Refining the GENEVA method for Higgs boson production via gluon fusion*, *JHEP* **05** (2023) 128 [2301.11875].

[48] A. Gavardi, *Next-to-next-to-leading order predictions for diboson production in hadronic scattering combined with parton showers*, Ph.D. thesis, Milan Bicocca U., 2023.

[49] G. Degrassi, P. P. Giardino, F. Maltoni and D. Pagani, *Probing the Higgs self coupling via single Higgs production at the LHC*, *JHEP* **12** (2016) 080 [1607.04251].

[50] G. Degrassi, M. Fedele and P. P. Giardino, *Constraints on the trilinear Higgs self coupling from precision observables*, *JHEP* **04** (2017) 155 [1702.01737].

[51] F. Maltoni, D. Pagani, A. Shivaji and X. Zhao, *Trilinear Higgs coupling determination via single-Higgs differential measurements at the LHC*, *Eur. Phys. J. C* **77** (2017) 887 [1709.08649].

[52] Particle Data Group collaboration, *Review of Particle Physics*, *PTEP* **2022** (2022) 083C01.

[53] E. W. N. Glover and J. J. van der Bij, *HIGGS BOSON PAIR PRODUCTION VIA GLUON FUSION*, *Nucl. Phys. B* **309** (1988) 282.

[54] O. J. P. Eboli, G. C. Marques, S. F. Novaes and A. A. Natale, *TWIN HIGGS BOSON PRODUCTION*, *Phys. Lett. B* **197** (1987) 269.

[55] T. Plehn, M. Spira and P. M. Zerwas, *Pair production of neutral Higgs particles in gluon-gluon collisions*, *Nucl. Phys. B* **479** (1996) 46 [hep-ph/9603205].

[56] S. Borowka, N. Greiner, G. Heinrich, S. P. Jones, M. Kerner, J. Schlenk et al., *Higgs Boson Pair Production in Gluon Fusion at Next-to-Leading Order with Full Top-Quark Mass Dependence*, *Phys. Rev. Lett.* **117** (2016) 012001 [1604.06447].

[57] S. Borowka, N. Greiner, G. Heinrich, S. P. Jones, M. Kerner, J. Schlenk et al., *Full top quark mass dependence in Higgs boson pair production at NLO*, *JHEP* **10** (2016) 107 [1608.04798].

[58] J. Baglio, F. Campanario, S. Glaus, M. Mühlleitner, M. Spira and J. Streicher, *Gluon fusion into Higgs pairs at NLO QCD and the top mass scheme*, *Eur. Phys. J. C* **79** (2019) 459 [1811.05692].

[59] J. Baglio, F. Campanario, S. Glaus, M. Mühlleitner, J. Ronca, M. Spira et al., *Higgs-Pair Production via Gluon Fusion at Hadron Colliders: NLO QCD Corrections*, *JHEP* **04** (2020) 181 [2003.03227].

[60] R. Mukherjee, S. Joshi, A. Griesmayer, D. Kroening and T. Melham, *Equivalence checking a floating-point unit against a high-level C model (extended version)*, *CoRR* **abs/1609.00169** (2016) [1609.00169].

[61] G. Ferrera and J. Pires, *Transverse-momentum resummation for Higgs boson pair production at the LHC with top-quark mass effects*, *JHEP* **02** (2017) 139 [1609.01691].

[62] D. De Florian and J. Mazzitelli, *Soft gluon resummation for Higgs boson pair production including finite M_t effects*, *JHEP* **08** (2018) 156 [1807.03704].

[63] G. Heinrich, S. P. Jones, M. Kerner, G. Luisoni and E. Vryonidou, *NLO predictions for Higgs boson pair production with full top quark mass dependence matched to parton showers*, *JHEP* **08** (2017) 088 [1703.09252].

[64] S. Jones and S. Kuttimalai, *Parton Shower and NLO-Matching uncertainties in Higgs Boson Pair Production*, *JHEP* **02** (2018) 176 [1711.03319].

[65] G. Heinrich, S. P. Jones, M. Kerner, G. Luisoni and L. Scyboz, *Probing the trilinear Higgs boson coupling in di-Higgs production at NLO QCD including parton shower effects*, *JHEP* **06** (2019) 066 [1903.08137].

[66] R. Frederix, S. Frixione, V. Hirschi, F. Maltoni, O. Mattelaer, P. Torrielli et al., *Higgs pair production at the LHC with NLO and parton-shower effects*, *Phys. Lett. B* **732** (2014) 142 [1401.7340].

[67] F. Maltoni, E. Vryonidou and M. Zaro, *Top-quark mass effects in double and triple Higgs production in gluon-gluon fusion at NLO*, *JHEP* **11** (2014) 079 [1408.6542].

[68] P. Maierhöfer and A. Papaefstathiou, *Higgs Boson pair production merged to one jet*, *JHEP* **03** (2014) 126 [1401.0007].

[69] J. Grigo, J. Hoff, K. Melnikov and M. Steinhauser, *On the Higgs boson pair production at the LHC*, *Nucl. Phys. B* **875** (2013) 1 [1305.7340].

[70] J. Grigo, K. Melnikov and M. Steinhauser, *Virtual corrections to Higgs boson pair production in the large top quark mass limit*, *Nucl. Phys. B* **888** (2014) 17 [1408.2422].

[71] J. Grigo, J. Hoff and M. Steinhauser, *Higgs boson pair production: top quark mass effects at NLO and NNLO*, *Nucl. Phys. B* **900** (2015) 412 [1508.00909].

[72] G. Degrassi, P. P. Giardino and R. Gröber, *On the two-loop virtual QCD corrections to Higgs boson pair production in the Standard Model*, *Eur. Phys. J. C* **76** (2016) 411 [1603.00385].

[73] R. Gröber, A. Maier and T. Rauh, *Reconstruction of top-quark mass effects in Higgs pair production and other gluon-fusion processes*, *JHEP* **03** (2018) 020 [1709.07799].

[74] R. Bonciani, G. Degrassi, P. P. Giardino and R. Gröber, *Analytical Method for Next-to-Leading-Order QCD Corrections to Double-Higgs Production*, *Phys. Rev. Lett.* **121** (2018) 162003 [1806.11564].

[75] J. Davies, G. Mishima, M. Steinhauser and D. Wellmann, *Double Higgs boson production at NLO in the high-energy limit: complete analytic results*, *JHEP* **01** (2019) 176 [1811.05489].

[76] G. Mishima, *High-Energy Expansion of Two-Loop Massive Four-Point Diagrams*, *JHEP* **02** (2019) 080 [1812.04373].

[77] J. Davies, G. Heinrich, S. P. Jones, M. Kerner, G. Mishima, M. Steinhauser et al., *Double Higgs boson production at NLO: combining the exact numerical result and high-energy expansion*, *JHEP* **11** (2019) 024 [1907.06408].

[78] J. Davies and M. Steinhauser, *Three-loop form factors for Higgs boson pair production in the large top mass limit*, *JHEP* **10** (2019) 166 [1909.01361].

[79] J. Davies, F. Herren, G. Mishima and M. Steinhauser, *Real corrections to Higgs boson pair production at NNLO in the large top quark mass limit*, *JHEP* **01** (2022) 049 [2110.03697].

[80] L. Bellafronte, G. Degrassi, P. P. Giardino, R. Gröber and M. Vitti, *Gluon fusion production at NLO: merging the transverse momentum and the high-energy expansions*, *JHEP* **07** (2022) 069 [2202.12157].

[81] S. Dawson, S. Dittmaier and M. Spira, *Neutral Higgs boson pair production at hadron colliders: QCD corrections*, *Phys. Rev. D* **58** (1998) 115012 [hep-ph/9805244].

[82] D. de Florian and J. Mazzitelli, *Higgs Boson Pair Production at Next-to-Next-to-Leading Order in QCD*, *Phys. Rev. Lett.* **111** (2013) 201801 [1309.6594].

[83] D. de Florian, M. Grazzini, C. Hanga, S. Kallweit, J. M. Lindert, P. Maierhöfer et al., *Differential Higgs Boson Pair Production at Next-to-Next-to-Leading Order in QCD*, *JHEP* **09** (2016) 151 [1606.09519].

[84] L.-B. Chen, H. T. Li, H.-S. Shao and J. Wang, *Higgs boson pair production via gluon fusion at N^3LO in QCD*, *Phys. Lett. B* **803** (2020) 135292 [1909.06808].

[85] P. Banerjee, S. Borowka, P. K. Dhani, T. Gehrmann and V. Ravindran, *Two-loop massless QCD corrections to the $g + g \to H + H$ four-point amplitude*, *JHEP* **11** (2018) 130 [1809.05388].

[86] D. Y. Shao, C. S. Li, H. T. Li and J. Wang, *Threshold resummation effects in Higgs boson pair production at the LHC*, *JHEP* **07** (2013) 169 [1301.1245].

[87] D. de Florian and J. Mazzitelli, *Higgs pair production at next-to-next-to-leading logarithmic accuracy at the LHC*, *JHEP* **09** (2015) 053 [1505.07122].

[88] M. Grazzini, G. Heinrich, S. Jones, S. Kallweit, M. Kerner, J. M. Lindert et al., *Higgs boson pair production at NNLO with top quark mass effects*, *JHEP* **05** (2018) 059 [1803.02463].

[89] S. Dawson, S. Dittmaier and M. Spira, *Two loop QCD corrections to Higgs pair production at the LHC*, *Acta Phys. Polon. B* **29** (1998) 2875 [hep-ph/9806304].

[90] J. Davies, R. Gröber, A. Maier, T. Rauh and M. Steinhauser, *Top quark mass dependence of the Higgs boson-gluon form factor at three loops*, *Phys. Rev. D* **100** (2019) 034017 [1906.00982].

[91] R. Grober, M. Muhlleitner, M. Spira and J. Streicher, *NLO QCD Corrections to Higgs Pair Production including Dimension-6 Operators*, *JHEP* **09** (2015) 092 [1504.06577].

[92] G. Buchalla, M. Capozi, A. Celis, G. Heinrich and L. Scyboz, *Higgs boson pair production in non-linear Effective Field Theory with full m_t-dependence at NLO QCD*, *JHEP* **09** (2018) 057 [1806.05162].

[93] D. de Florian, I. Fabre and J. Mazzitelli, *Higgs boson pair production at NNLO in QCD including dimension 6 operators*, *JHEP* **10** (2017) 215 [1704.05700].

[94] D. de Florian, I. Fabre, G. Heinrich, J. Mazzitelli and L. Scyboz, *Anomalous couplings in Higgs-boson pair production at approximate NNLO QCD*, *JHEP* **09** (2021) 161 [2106.14050].

[95] M. Grazzini, S. Kallweit and M. Wiesemann, *Fully differential NNLO computations with MATRIX*, *Eur. Phys. J. C* **78** (2018) 537 [1711.06631].

[96] C. F. Berger, C. Marcantonini, I. W. Stewart, F. J. Tackmann and W. J. Waalewijn, *Higgs Production with a Central Jet Veto at NNLL+NNLO*, *JHEP* **04** (2011) 092 [1012.4480].

[97] R. Kelley, M. D. Schwartz, R. M. Schabinger and H. X. Zhu, *The two-loop hemisphere soft function*, *Phys. Rev.* **D84** (2011) 045022 [1105.3676].

[98] P. F. Monni, T. Gehrmann and G. Luisoni, *Two-Loop Soft Corrections and Resummation of the Thrust Distribution in the Dijet Region*, *JHEP* **08** (2011) 010 [1105.4560].

[99] J. Gaunt, M. Stahlhofen and F. J. Tackmann, *The Gluon Beam Function at Two Loops*, *JHEP* **08** (2014) 020 [1405.1044].

[100] M. A. Ebert, B. Mistlberger and G. Vita, *N-jettiness beam functions at N^3LO*, *JHEP* **09** (2020) 143 [2006.03056].

[101] D. de Florian and J. Mazzitelli, *Two-loop virtual corrections to Higgs pair production*, *Phys. Lett. B* **724** (2013) 306 [1305.5206].

[102] S. Moch, J. A. M. Vermaseren and A. Vogt, *The Three loop splitting functions in QCD: The Nonsinglet case*, *Nucl. Phys. B* **688** (2004) 101 [hep-ph/0403192].

[103] A. Vogt, S. Moch and J. A. M. Vermaseren, *The Three-loop splitting functions in QCD: The Singlet case*, *Nucl. Phys. B* **691** (2004) 129 [hep-ph/0404111].

[104] G. P. Korchemsky and A. V. Radyushkin, *Renormalization of the Wilson Loops Beyond the Leading Order*, *Nucl. Phys. B* **283** (1987) 342.

[105] O. V. Tarasov, A. A. Vladimirov and A. Y. Zharkov, *The Gell-Mann-Low Function of QCD in the Three Loop Approximation*, *Phys. Lett. B* **93** (1980) 429.

[106] S. A. Larin and J. A. M. Vermaseren, *The Three loop QCD Beta function and anomalous dimensions*, *Phys. Lett. B* **303** (1993) 334 [hep-ph/9302208].

[107] T. van Ritbergen, J. A. M. Vermaseren and S. A. Larin, *The Four loop beta function in quantum chromodynamics*, *Phys. Lett. B* **400** (1997) 379 [hep-ph/9701390].

[108] A. von Manteuffel, E. Panzer and R. M. Schabinger, *Cusp and collinear anomalous dimensions in four-loop QCD from form factors*, *Phys. Rev. Lett.* **124** (2020) 162001 [2002.04617].

[109] S. Höche and S. Prestel, *The midpoint between dipole and parton showers*, *Eur. Phys. J. C* **75** (2015) 461 [1506.05057].

[110] J. Butterworth et al., *PDF4LHC recommendations for LHC Run II*, *J. Phys.* **G43** (2016) 023001 [1510.03865].

[111] A. Buckley, J. Ferrando, S. Lloyd, K. Nordström, B. Page, M. Rüfenacht et al., *LHAPDF6: parton density access in the LHC precision era*, *Eur. Phys. J.* **C75** (2015) 132 [1412.7420].

[112] G. Billis, M. A. Ebert, J. K. L. Michel and F. J. Tackmann, *A toolbox for q_T and 0-jettiness subtractions at N^3LO*, *Eur. Phys. J. Plus* **136** (2021) 214 [1909.00811].

[113] M. A. Ebert, J. K. L. Michel, F. J. Tackmann et al., *SCETlib: A C++ Package for Numerical Calculations in QCD and Soft-Collinear Effective Theory*, DESY-17-099 http://scetlib.desy.de.

[114] A. Denner, J.-N. Lang and S. Uccirati, *Recola2: REcursive Computation of One-Loop Amplitudes 2*, *Comput. Phys. Commun.* **224** (2018) 346 [1711.07388].

[115] A. Denner, J.-N. Lang and S. Uccirati, *NLO electroweak corrections in extended Higgs Sectors with RECOLA2*, *JHEP* **07** (2017) 087 [1705.06053].

[116] F. Buccioni, S. Pozzorini and M. Zoller, *On-the-fly reduction of open loops*, *Eur. Phys. J. C* **78** (2018) 70 [1710.11452].

[117] T. Cridge, M. A. Lim and R. Nagar, *$W\gamma$ production at NNLO+PS accuracy in GENEVA*, 2105.13214.

[118] C. Duhr, F. Dulat and B. Mistlberger, *Drell-Yan Cross Section to Third Order in the Strong Coupling Constant*, *Phys. Rev. Lett.* **125** (2020) 172001 [2001.07717].

[119] C. Duhr, F. Dulat and B. Mistlberger, *Charged current Drell-Yan production at N^3LO*, *JHEP* **11** (2020) 143 [2007.13313].

[120] X. Chen, T. Gehrmann, N. Glover, A. Huss, T.-Z. Yang and H. X. Zhu, *Dilepton Rapidity Distribution in Drell-Yan Production to Third Order in QCD*, *Phys. Rev. Lett.* **128** (2022) 052001 [2107.09085].

[121] C. Duhr and B. Mistlberger, *Lepton-pair production at hadron colliders at N^3LO in QCD*, *JHEP* **03** (2022) 116 [2111.10379].

[122] M. Bonvini, S. Forte and G. Ridolfi, *The Threshold region for Higgs production in gluon fusion*, *Phys. Rev. Lett.* **109** (2012) 102002 [1204.5473].

[123] C. Anastasiou, L. J. Dixon, K. Melnikov and F. Petriello, *High precision QCD at hadron colliders: Electroweak gauge boson rapidity distributions at NNLO*, *Phys. Rev. D* **69** (2004) 094008 [hep-ph/0312266].

[124] G. Lustermans, J. K. L. Michel and F. J. Tackmann, *Generalized Threshold Factorization with Full Collinear Dynamics*, 1908.00985.

[125] P. Bolzoni, *Threshold resummation of Drell-Yan rapidity distributions*, *Phys. Lett. B* **643** (2006) 325 [hep-ph/0609073].

[126] E. Laenen and G. F. Sterman, *Resummation for Drell-Yan differential distributions*, in *7th Meeting of the APS Division of Particles Fields*, pp. 987–989, 11, 1992.

[127] R. Bonciani, S. Catani, M. L. Mangano and P. Nason, *Nll resummation of the heavy-quark hadroproduction cross-section*, *Nuclear Physics B* **529** (1998) 424.

[128] P. Banerjee, G. Das, P. K. Dhani and V. Ravindran, *Threshold resummation of the rapidity distribution for Drell-Yan production at NNLO+NNLL*, *Phys. Rev. D* **98** (2018) 054018 [1805.01186].

[129] G. Das, *$Z, W^{\pm}$ rapidity distributions at NNLL and beyond*, 2303.16578.

[130] A. Mukherjee and W. Vogelsang, *Threshold resummation for W-boson production at RHIC*, *Phys. Rev. D* **73** (2006) 074005 [hep-ph/0601162].

[131] V. Ravindran, J. Smith and W. L. van Neerven, *QCD threshold corrections to di-lepton and Higgs rapidity distributions beyond N^2 LO*, *Nucl. Phys. B* **767** (2007) 100 [hep-ph/0608308].

[132] V. Ravindran and J. Smith, *Threshold corrections to rapidity distributions of Z and $W^{\pm}$ bosons beyond N^2 LO at hadron colliders*, *Phys. Rev. D* **76** (2007) 114004 [0708.1689].

[133] D. Westmark and J. F. Owens, *Enhanced threshold resummation formalism for lepton pair production and its effects in the determination of parton distribution functions*, *Phys. Rev. D* **95** (2017) 056024 [1701.06716].

[134] P. Banerjee, G. Das, P. K. Dhani and V. Ravindran, *Threshold resummation of the rapidity distribution for Higgs production at NNLO+NNLL*, *Phys. Rev. D* **97** (2018) 054024 [1708.05706].

[135] A. H. Ajjath, P. Mukherjee, V. Ravindran, A. Sankar and S. Tiwari, *Next-to-soft-virtual resummed rapidity distribution for the Drell-Yan process to NNLO+NNLL^{-}*, *Phys. Rev. D* **106** (2022) 034005 [2112.14094].

[136] T. Ahmed, A. A. H., P. Mukherjee, V. Ravindran and A. Sankar, *Rapidity distribution at soft-virtual and beyond for n-colorless particles to N^4LO in QCD*, *Eur. Phys. J. C* **81** (2021) 943 [2010.02980].

[137] A. H. Ajjath, P. Mukherjee and V. Ravindran, *Going beyond soft plus virtual*, *Phys. Rev. D* **105** (2022) L091503 [2204.09012].

[138] A. H. Ajjath, P. Mukherjee, V. Ravindran, A. Sankar and S. Tiwari, *On next to soft threshold corrections to DIS and SIA processes*, *JHEP* **04** (2021) 131 [2007.12214].

[139] PDF4LHC Working Group collaboration, *The PDF4LHC21 combination of global PDF fits for the LHC Run III*, *J. Phys. G* **49** (2022) 080501 [2203.05506].

[140] C. Anastasiou, L. J. Dixon, K. Melnikov and F. Petriello, *Dilepton rapidity distribution in the Drell-Yan process at NNLO in QCD*, *Phys. Rev. Lett.* **91** (2003) 182002 [hep-ph/0306192].

[141] M. Bonvini, *Small-x phenomenology at the LHC and beyond: HELL 3.0 and the case of the Higgs cross section*, *Eur. Phys. J. C* **78** (2018) 834 [1805.08785].

[142] A. H. Ajjath, P. Mukherjee and V. Ravindran, *Next to soft corrections to Drell-Yan and Higgs boson productions*, *Phys. Rev. D* **105** (2022) 094035 [2006.06726].

[143] A. H. Ajjath, P. Mukherjee, V. Ravindran, A. Sankar and S. Tiwari, *Next-to-soft corrections for Drell-Yan and Higgs boson rapidity distributions beyond N^3LO*, *Phys. Rev. D* **103** (2021) L111502 [2010.00079].

[144] A. H. Ajjath, P. Mukherjee, V. Ravindran, A. Sankar and S. Tiwari, *Next-to SV resummed Drell–Yan cross section beyond leading-logarithm*, *Eur. Phys. J. C* **82** (2022) 234 [2107.09717].

[145] A. H. Ajjath, P. Mukherjee, V. Ravindran, A. Sankar and S. Tiwari, *Resummed Higgs boson cross section at next-to SV to* NNLO + $\overline{\text{NNLL}}$, *Eur. Phys. J. C* **82** (2022) 774 [2109.12657].

[146] A. Bhattacharya, M. C. Kumar, P. Mathews and V. Ravindran, *Next-to-soft-virtual resummed prediction for pseudoscalar Higgs boson production at NNLO+NNLL^{-}*, *Phys. Rev. D* **105** (2022) 116015 [2112.02341].

[147] V. Ravindran, A. Sankar and S. Tiwari, *Resummed next-to-soft corrections to rapidity distribution of Higgs boson to NNLO+NNLL^{-}*, *Phys. Rev. D* **108** (2023) 014012 [2205.11560].

[148] M. Kramer, E. Laenen and M. Spira, *Soft gluon radiation in Higgs boson production at the LHC*, *Nucl. Phys. B* **511** (1998) 523 [hep-ph/9611272].

[149] H. Contopanagos, E. Laenen and G. F. Sterman, *Sudakov factorization and resummation*, *Nucl. Phys. B* **484** (1997) 303 [hep-ph/9604313].

[150] S. Catani, D. de Florian and M. Grazzini, *Higgs production in hadron collisions: Soft and virtual QCD corrections at NNLO*, *JHEP* **05** (2001) 025 [hep-ph/0102227].

[151] R. D. Ball, M. Bonvini, S. Forte, S. Marzani and G. Ridolfi, *Higgs production in gluon fusion beyond NNLO*, *Nucl. Phys. B* **874** (2013) 746 [1303.3590].

[152] M. Bonvini and S. Marzani, *Resummed Higgs cross section at N^3LL*, *JHEP* **09** (2014) 007 [1405.3654].

[153] D. de Florian, J. Mazzitelli, S. Moch and A. Vogt, *Approximate N^3LO Higgs-boson production cross section using physical-kernel constraints*, *JHEP* **10** (2014) 176 [1408.6277].

[154] M. Beneke, A. Broggio, M. Garny, S. Jaskiewicz, R. Szafron, L. Vernazza et al., *Leading-logarithmic threshold resummation of the Drell-Yan process at next-to-leading power*, *JHEP* **03** (2019) 043 [1809.10631].

[155] M. Beneke, M. Garny, S. Jaskiewicz, R. Szafron, L. Vernazza and J. Wang, *Leading-logarithmic threshold resummation of Higgs production in gluon fusion at next-to-leading power*, *JHEP* **01** (2020) 094 [1910.12685].

[156] M. Bonvini, *Resummation of soft and hard gluon radiation in perturbative QCD*, Ph.D. thesis, Genoa U., 2012. 1212.0480.

[157] J. Blumlein and S. Kurth, *Harmonic sums and Mellin transforms up to two loop order*, *Phys. Rev. D* **60** (1999) 014018 [hep-ph/9810241].

[158] S. Catani, D. de Florian, M. Grazzini and P. Nason, *Soft gluon resummation for Higgs boson production at hadron colliders*, *JHEP* **07** (2003) 028 [hep-ph/0306211].

[159] D. de Florian and J. Mazzitelli, *A next-to-next-to-leading order calculation of soft-virtual cross sections*, *JHEP* **12** (2012) 088 [1209.0673].

[160] C. Anastasiou, C. Duhr, F. Dulat, E. Furlan, T. Gehrmann, F. Herzog et al., *Higgs Boson Gluon-Fusion Production Beyond Threshold in N^3LO QCD*, *JHEP* **03** (2015) 091 [1411.3584].

[161] M. Bonvini, S. Marzani, J. Rojo, L. Rottoli, M. Ubiali, R. D. Ball et al., *Parton distributions with threshold resummation*, *JHEP* **09** (2015) 191 [1507.01006].

[162] M. Bonvini, S. Marzani, C. Muselli and L. Rottoli, *On the Higgs cross section at N^3LO+N^3LL and its uncertainty*, *JHEP* **08** (2016) 105 [1603.08000].

[163] S. Moch, J. Vermaseren and A. Vogt, *Higher-order corrections in threshold resummation*, *Nucl.Phys.* **B726** (2005) 317 [hep-ph/0506288].

[164] S. Moch and A. Vogt, *Higher-order soft corrections to lepton pair and Higgs boson production*, *Phys.Lett.* **B631** (2005) 48 [hep-ph/0508265].

[165] E. Laenen and L. Magnea, *Threshold resummation for electroweak annihilation from DIS data*, *Phys.Lett.* **B632** (2006) 270 [hep-ph/0508284].

[166] S. Catani, L. Cieri, D. de Florian, G. Ferrera and M. Grazzini, *Threshold resummation at N^3LL accuracy and soft-virtual cross sections at N^3LO*, *Nucl. Phys. B* **888** (2014) 75 [1405.4827].

[167] J. M. Henn, G. P. Korchemsky and B. Mistlberger, *The full four-loop cusp anomalous dimension in $\mathcal{N} = 4$ super Yang-Mills and QCD*, *JHEP* **04** (2020) 018 [1911.10174].

[168] M. Bonvini, S. Forte, G. Ridolfi and L. Rottoli, *Resummation prescriptions and ambiguities in SCET vs. direct QCD: Higgs production as a case study*, *JHEP* **1501** (2015) 046 [1409.0864].

[169] M. Bonvini and L. Rottoli, *Three loop soft function for N^3LL' gluon fusion Higgs production in soft-collinear effective theory*, *Phys.Rev.* **D91** (2015) 051301 [1412.3791].

[170] V. Ahrens, T. Becher, M. Neubert and L. L. Yang, *Origin of the Large Perturbative Corrections to Higgs Production at Hadron Colliders*, *Phys. Rev.* **D79** (2009) 033013 [0808.3008].

[171] C. Anastasiou, C. Duhr, F. Dulat, E. Furlan, T. Gehrmann, F. Herzog et al., *High precision determination of the gluon fusion Higgs boson cross-section at the LHC*, *JHEP* **05** (2016) 058 [1602.00695].

[172] S. Alioli, A. Broggio and M. A. Lim, *Zero-jettiness resummation for top-quark pair production at the LHC*, *JHEP* **01** (2022) 066 [2111.03632].

[173] C. W. Bauer, D. Pirjol and I. W. Stewart, *Soft collinear factorization in effective field theory*, *Phys. Rev. D* **65** (2002) 054022 [hep-ph/0109045].

[174] T. Becher and M. Neubert, *On the Structure of Infrared Singularities of Gauge-Theory Amplitudes*, *JHEP* **06** (2009) 081 [0903.1126].

Acknowledgements

This thesis and my entire Ph.D. journey have been possible thanks to many persons. A very special thank goes to my supervisor, Simone Alioli, and all the members of the GENEVA collaboration whom I had the privileged of working alongside: Davide, Riccardo, Alessandro G., Alessandro B., Matthew, Georgios and Stefan. I deeply appreciate all the opportunities, guidance, attention, discussions, encouragement, support and time you all generously shared with me during our collaboration. A huge thank also goes to my master thesis supervisor, Marco Bonvini, who has been and still continue to be a role model for me, more than just a master thesis supervisor. I have to thank also my colleagues with whom I shared the office and all the good, bad, funny and desperate moments of a Ph.D.: Giovanni, for having created a harmonious environment where understanding was often achieved with just a glance, and Filippo, who, despite not saying "ciao" for the first three months, eventually recovered quite well.

I want to take the right moment to officially and publicly thank, for the last time, all my lifelong friends who have always made a difference in my life and who are my family, making me feel at home even though we are on opposite sides of the world. Thanks to Alina, whose telepathy continues to amaze me even after seventeen years. Thank you for always being able to put the pieces together with a simple hug (and a bit of wine and ice cream, and some face masks). Thanks to Lorena, for supporting me for more than twenty years, for believing in me even when I refuse to do so, for her determination, and I would even say her stubbornness, for being able to show me all the colours of the world and make me feel special, always. Thanks to Erika, for making me understand that there are people who never stop loving each other, simply because what binds them is stronger than what divides them, and for always being on my side. Thanks to Luca, for making me give my best, and for never giving up, not even on me. Thank you because every time we drift apart, in the end, we find ourselves closer. Thanks to Eleonora, for always being attentive, kind, present, and ready to lend a hand. I still can't believe what a crazy coincidence it was that brought us together, but it was one of the luckiest things in my life. And then, thanks to Federico, for being who he is and for listening to me, for making a difference countless times and for allowing me to enter his heart and make myself comfortable, not realizing that he is the special one between us two. All of you are extremely fundamental, and I will never stop being grateful to all of you.

During this Ph.D., I had the enormous luck to meet and spend a lot of time with crazy and special people who have amazed and enriched me. I feel obligated to thank the entire U5 group for accepting me and for filling my weekends and some of my vacations with beautiful

memories. I also thank you for my gastritis, because you're definitely the culprits. For learning to speak like me, for shouting "Andreeeea" with the right intonation to drive him crazy, and every time I hear you say "Ce senti?" my heart warms.

But among all, there are people I want explicitly thank. Thanks to Stefano for always choosing the wrong path and for showing me how one can remain light even when everything else hits hard. Thanks to Ninni, we all know perfectly well what I thank him for, but it doesn't seem like the right place to write it. His tenacity and constancy are a great inspiration to me, and he has the magical gift of making every burden feel light. Thanks to Ilaria because, let's face it, if someone doesn't want to be a bit like her in life, they're a bit foolish. And then, I thank Fed(t)e and Piera so much. I spent an enormous amount of time with them, and every time I came home, I felt richer. There was never a time when I didn't feel at home, serene, or relieved. For me, Fete and Piera are those people who surround you and with an eraser, they erase every tangled thought and every bad mood. They always manage to make you smile even when you're angry, and if something is wrong, they are the first to step forward. As someone told me during a night in a taxi after a highly questionable number of gin tonics, "I'm really happy to have met you."

Lastly, I want to thank Andrea, especially for figure 8.1, of which he is very proud. I wish you all to find in your life someone who cheers for you as Andrea does for me. Someone who is always there to show you things in a thousand different ways, to discuss, laugh, joke, and be serious. Someone who always pushes you beyond your limits with patience and kindness. Someone willing to eat a kebab at 2 in the morning, scold you because "devi fa attenzione a quello che te magni!" but occasionally lets you do it, then spends the night with you in the bathroom between one bout and another. Someone who shouts, "Ao, vie' qua! Te do 3 secondi!", someone who always softens all your super anger and makes you laugh even after crying. I've never really understood any of it, but in fact, it seems true that we don't exist until someone sees us exist, that we don't truly speak until someone is able to understand us, and therefore, we don't fully live until we are loved. For all of this, and for a thousand other reasons that I seriously stop listing, thank you, Bì.